Mitochondrial structural and functional dynamism in obesity-induced type 2 diabetes; Do exercise and weight loss regimens restore a healthy phenotype?

A thesis submitted to the University of Manchester for the degree of

Doctor of Philosophy

in the Faculty of Biology, Medicine and Health

2021

Hussam Daghistani

School of Medical Sciences

Division of Cardiovascular Science

Table of contents

Contents

Table of contents 2
List of Figures 8
List of Tables 10
Abstract 11
Declaration 12
Copyright Statement 12
Acknowledgment 13
Publications 14
Poster presentations 14
Abbreviation: 15
Chapter 1 General introduction 18
1.1 Obesity and diabetes 18
1.1.1 Obesity 18
1.1.2 Diabetes 18
1.1.3 Cardiovascular complications in obesity and diabetes 19
1.2 Animal models of diabetes 21
1.3 Mitochondrial dysfunction in diabetic cardiomyopathy 24
1.3.1 Mitochondria and energy production 25
1.3.2 Calcium ion uptake, storage and signalling 25
1.4 Mitochondrial subpopulations 27
1.5 Mitochondrial dynamics 28
1.5.1 Mitophagy 29
1.5.2 Fission and fusion 30
1.5.3 Mitochondrial biogenesis 32
1.6 Regulators of fission and fusion 33
1.6.1 Endoplasmic reticulum stress 33
1.6.2 Prohibitins 35
1.6.3 Sirtuins 36
1.7 The effect of exercise on cardiac function and dynamics 37
1.7.1 Mitochondrial function 37
1.7.2 Mitochondrial dynamics 38
1.7.3 Mitochondrial apoptosis 39

1.8 Conclusion 40
Chapter 2 Investigation of cardiac mitochondrial function and dynamics in a mouse 60% high-fat diet (DIO) model 41
2.1 Introduction 41
2.2 Methods 43
2.2.1 Mouse model of obesity 43
2.2.2 Physiological and metabolic parameters measurement 44
2.2.3 Western blotting 47
2.2.4 Gene expression 50
2.2.5 Mitochondrial respiration 54
2.2.6 Histology 57
2.2.7 Statistical analysis 58
2.3 Results 59
2.3.1 Characterisation of the cardiac phenotype after HFD (DIO) 59
2.3.2 Characterisation of the cardiac function 61
2.3.3 Cardiac remodelling of HFD myocardium 62
2.3.4 Assessment of cardiac conduction system 64
2.3.5 Investigation of molecular level changes to mitochondrial dynamic proteins in HFD (DIO) model 65
2.3.6 Measurement of mitochondrial respiration 70
2.3.7 Assessment of cardiac hypertrophy and fibrosis 72
2.3.8 Analysis of apoptosis 74
2.3.9 Summary of results 76
2.4 Discussion 77
2.4.1 Weight gain, hyperglycaemia and insulin resistance and hyperlipidaemia 77
2.4.2 Concentric remodelling in HFD (DIO) mice 78
2.4.3 Diastolic dysfunction in HFD (DIO) mice 78
2.4.4 Increased transcript expression of the fusion protein Opa1 as a result of HFD (DIO) 79
2.4.5 Increased expression of Drp1 and its receptor Fis1 and MID49 as a result of HFD (DIO) 80
2.4.6 Mitophagy and apoptosis and biogenesis 81
2.5 Conclusion 82
Chapter 3 Cardiac mitochondrial remodelling in the high-fat diet mouse model 84
3.1 Introduction 84
3.2 Methods 87

3.2.1 Sample preparation 87
3.2.2 Serial block face scanning electron microscopy 87
3.2.3 Image analysis 88
3.2.4 Statistical analysis 88
3.3 Results 90
3.3.1 PNM of the control mice are the smallest compared to SSM and IFM. 92
3.3.2 Inter-animal variability in mitochondrial size of HFD (DIO) mice. 93
3.3.3 PNM are smaller in the HFD (DIO) compared to control mitochondrial. 96
3.3.4 Summary of results 97
3.4 Discussion 99
3.4.1 Morphological differences in control mitochondrial subpopulations. 99
3.4.2 Mitochondrial ultrastructure in HFD (DIO). 100
3.5 Conclusion 102
Chapter 4 Effects of exercise and/or diet exchange on the HFD (DIO) cardiac and mitochondrial phenotype 103
4.1 Introduction 103
4.2 Method 104
4.2.1 Animal model 104
4.2.2 Physiological and metabolic parameters measurement 105
4.2.3 Gene expression and Western blotting 105
4.2.4 Statistical analysis 105
4.3 Results 106
4.3.1 Weight loss in exercised and/or diet exchanged mice 106
4.3.2 Insulin resistance in the exercise group 107
4.3.3 Cardiac function and structure in exercise and/or diet exchange groups 107
4.3.4 Exercise with sustained high-fat feeding leads to downregulation of transcript levels of Drp1 in myocardium 110
4.3.5 Exercise in obese mice downregulates Mff and upregulate PINK1 in myocardium 113
4.3.6 Summary of results 116
4.4 Discussion 117
4.4.1 Choice of exercise model 117
4.4.2 Exercise combined with diet exchange C57BL/6J mice group had the highest weight loss 118
4.4.3 Exercise group remained insulin resistant. 119

4.4.4 Improvement of diastolic dysfunction in exercise, diet exchange and exercise/diet exchange groups. 119
4.4.5 Eccentric remodelling in exercised groups. 120
4.4.6 Upregulation of fusion protein Mfn2 in exercise group. 121
4.4.7 The fission protein Drp1 was unchanged in exercise, diet exchange and exercise/diet exchange groups. 122
4.4.8 Mitophagy still upregulated in the exercise group. 124
4.5 Conclusion 125
Chapter 5 Mechanistic pathways regulating mitochondrial dynamics and role of Sirt5 126
5.1 Introduction 126
5.2 Methods 128
5.2.1 Cell culture 128
5.2.2 Protein extraction from cells 128
5.2.3 RNA extraction from cells 128
5.2.4 Insulin resistant H9c2 cells 128
5.2.5 siRNA knockdown 130
5.2.6 qPCR and western blotting 130
5.2.7 Reactive oxygen species dihydroethidium assay 131
5.2.8 Mitochondrial membrane potential 131
5.2.9 Statistical analysis 132
5.3 Results 133
5.3.1 Sirtuins and Prohibitins level in the 12-week high-fat diet (DIO) model 133
5.3.2 Endoplasmic reticulum stress in high-fat diet 134
5.3.3 Investigation of the effect of insulin resistance upon expression levels of mitochondrial fission-fusion proteins 135
5.3.5. Expression of mitochondrial fission and fusion proteins following siRNA mediated Sirt5 knockdown in vitro 137
5.3.6 Analysis of mitochondrial fission/fusion proteins following Sirt5 knockdown 137
5.3.7 Assessment of reactive oxygen species levels and membrane potential following Sirt5 siRNA mediated knockdown 142
5.3.8 Summary of results 143
5.4 Discussion 145
5.4.1 ER stress is not activated in HFD (DIO) model (early DCM) 145
5.4.2 Insulin resistance has no effect on mitochondrial fission/fusion axis 146
5.4.3 Prohibitins has no effect on mitochondrial fission/fusion axis in vitro 146

5.4.4 The effect of Sirt5 on mitochondrial fission and fusion proteins 147
5.4.5 The effect of Sirt5 knock out on mitochondrial function 148
5.5 Conclusion 150
Chapter 6 Proteomics analysis for HFD (DIO) model and exercise/weight loss regimens 151
6.1 Introduction 151
6.2 Methods 154
6.2.1 Sample lysis 154
6.2.2 Reduction and alkylation 154
6.2.3 Quantification of extracted proteins 154
6.2.4 S-Trap sample digestion 154
6.2.5 Sample desalting 155
6.2.6 Sample processing 155
6.3 Results 156
6.3.1 Ingenuity Pathway Analysis of canonical pathways altered in the HFD (DIO) model 157
6.3.2 Ingenuity Pathway Analysis of canonical pathways altered in the exercise model 159
6.3.3 Ingenuity Pathway Analysis of canonical pathways altered in the diet exchange model 162
6.3.4 Ingenuity Pathway Analysis of canonical pathways altered in the exercise/diet exchange model 163
6.3.5 Proteomic analysis of metabolism 164
6.3.6 Quantitative mass spectrometry of mitochondrial dynamic proteins 169
6.3.7 Summary of results 170
6.4 Discussion 171
6.4.1 Activation of inflammatory signalling in HFD (DIO) model 171
6.4.2 Increased oxidative stress in HFD (DIO) model by quantitative mass spectrometry analysis 171
6.4.3 Proteomics revealed alteration to cardiac contraction signalling in HFD (DIO) model 173
6.4.4 Proteomics analysis shows changes to energy production pathways in HFD (DIO) 173
6.4.5 Quantitative mass spectrometry analysis of mitochondrial dynamic proteins 177
6.5 Conclusion 178
Chapter 7 General discussion 179
7.1 Main findings 179

7.2 Methodological considerations 181
7.2.1 Model of obesity and exercise 181
7.2.2 Cell culture 182
7.3 Limitations 183
7.3.1 SBF-SEM 183
7.3.2 Mitochondrial oxygen consumption rate 183
7.4 Future direction 183
7.4.1 The age factor 183
7.4.2 Phosphorylation of Drp1 184
7.5 Conclusion 185
Appendices: 187
Appendix 7.1 187
References 188

List of Figures

Figure 1.1: Number of diabetes cases by continent in 2015 and estimated number in 2040. 19
Figure 1.2: Cardiac excitation-contraction coupling. 26
Figure 1.3: Role of mitochondrial dynamics in protection against oxidative stress. 29
Figure 1.4: Mitochondrial fission and fusion processes. 31
Figure 1.5: Role of ER/SR stress in cell survival. 34
Figure 2.1: The posterior view of the mouse heart. 43
Figure 2.2: Echocardiography of control mouse heart. 46
Figure 2.3: Electrocardiography of control mouse heart. 47
Figure 2.4: Total protein normalisation in Western blot analysis. 50
Figure 2.5: Citrate synthase activity reactions. 56
Figure 2.6: high-fat diet (DIO) significantly increased the body weight of mice over 12 weeks. 59
Figure 2.7**:** High-fat diet (DIO) significantly increased fasting blood glucose and insulin. 60
Figure 2.8: High-fat diet (DIO) significantly altered the lipid profile. 60
Figure 2.9: HFD (DIO) myocardium showed early signs of diastolic dysfunction; decreased stroke volume and increased in lung weight. 62
Figure 2.10: Increased RWT indicated concentric remodelling of HFD (DIO) heart. 63
Figure 2.11: HFD (DIO) had no significant effect on heart rate. 64
Figure 2.12: HFD (DIO) myocardium exhibited significantly increased Opa1 transcript expression. 66
Figure 2.13: The heart of 60% HFD (DIO) C57BL/6J mice exhibited a significant increase in Drp1 expression. 67
Figure 2.14: Drp1 receptors showed altered transcript levels and expression in HFD (DIO) model. 68
Figure 2.15: Increased PINK1 and Parkin indicated mitophagy activation in HFD (DIO) heart. 69
Figure 2.16: Increased TFAM (involved in mitochondrial biogenesis) transcript expression was found in in HFD (DIO) model. 70
Figure 2.17: No change was found in mitochondrial complexes activity in HFD (DIO) mice model. 71
Figure 2.18: No change was found in mitochondrial oxygen consumption rate in control and HFD (DIO) mice. 72
Figure 2.19: No change was found in cell size of cardiomyocytes in control and HFD (DIO) mice. 73
Figure 2.20: No evidence of interstitial and perivascular fibrosis was found in HFD (DIO) mice. 74
Figure 2.21: HFD (DIO) mice showed higher apoptotic cardiomyocytes in TUNEL assay. 75
Figure 3.1: The principle of serial block-face scanning electron microscopy. 85
Figure 3.2: Three-dimensional reconstruction of cardiac mitochondrion from a mouse. 88
Figure 3.3: Identification and segmentation of various control sub-populations of mitochondria. 90
Figure 3.4: 3D reconstruction of different mitochondrial subpopulations in the heart of control mouse. 91
Figure 3.5: No inter-animal variability in control mice for morphometric parameters of different subpopulations cardiac mitochondria. 92
Figure 3.6: IFM were the largest in size in control mice compared to other cardiac tissue mitochondrial subpopulation. 93
Figure 3.7: Alteration in inter-animal variability for morphometric parameters of different subpopulations mitochondria in HFD (DIO). 94
Figure 3.8 IFM were the largest in size and PNM the smallest in HFD (DIO) mice. 95
Figure 3.9: The surface area to volume ratio in PNM was the highest in HFD (DIO) mice compared to other subpopulation of cardiac mitochondria. 96
Figure 3.10: PNM were smaller in size in HFD (DIO) mice compared to control. 97
Figure 4.1: Swimming in a tank of water. 104
Figure 4.2: Weight loss in exercise and/or diet exchange mice groups. 106

Figure 4.3: Exercise group remained insulin resistant. 107
Figure 4.4: Normal systolic cardiac function in exercise and/or diet exchange mice groups. 108
Figure 4.5: Eccentric remodelling in exercise and exercise/diet exchange groups. 109
Figure 4.6: No change was found in Opa1 isoforms expression in exercise and/or diet exchange groups. 111
Figure 4.7: Mfn2 involved in mitochondrial fusion was significantly increased in HFD (DIO) mice. 112
Figure 4.8: Drp1 transcript expression was significantly decreased in exercise group. 113
Figure 4.9: Alteration in Drp1 receptors expression in exercise and/or diet exchange groups. 114
Figure 4.10: PINK1 and Parkin transcript expression was significantly increased in exercise group. 115
Figure 4.11: No change in transcript expression of proteins involved in mitochondrial biogenesis in exercise and diet exchange groups. 116
Figure 5.1: Glucose uptake assay chemical interactions. 129
Figure 5.2: The transcript expression of Sirtuin5 was decreased in the HFD (DIO) mice model. 133
Figure 5.3: No change in the transcript expression of prohibitins in the high fat diet (DIO) model. 133
Figure 5.4: Proteins involved in endoplasmic reticulum stress were not changed in the high-fat diet (DIO) model. 134
Figure 5.5: A decrease in 2-DG uptake in H9c2 treated with 100nM insulin. 135
Figure 5.6: Proteins involved in mitochondrial dynamic remain unchanged in insulin resistant H9c2 cells. 136
Figure 5.7: mRNA expression and protein level of Sirt5 decreased after Sirt5 siRNA-mediated knockdown. 137
Figure 5.8: An increase in the total Opa1 and S-opa1 expression following Sirt5 siRNA-mediated knockdown. 138
Figure 5.9: A decrease in Mfn1 transcript expression following Sirt5 siRNA-mediated knockdown. 139
Figure 5.10: A decrease in the phosphorylated Drp1 at S637 following Sirt5 siRNA-mediated knockdown. 140
Figure 5.11: No change in the expression of Drp1 receptors following Sirt5 siRNA-mediated knockdown. 141
Figure 5.12: Level of AMPK protein was not changed in H9c2 cells after Sirt5 siRNA-mediated knockdown. 142
Figure 5.13: Mitochondrial membrane potential and reactive oxygen species level were not changed after Sirt5 siRNA-mediated knockdown. 143
Figure 5.14: Summary of the finding in the HFD (DIO) model and Sirt5 knockdown H9c2 cells. 150
Figure 6.1: Tandem mass spectrometry principle. 151
Figure 6.2: The total ion chromatogram of a control sample. 152
Figure 6.3: Percentage of upregulated and downregulated mitochondrial proteins in the high-fat diet mice and the mechanisms perturbed compared to control by mass spectrometry. 157
Figure 6.4: Alteration of canonical pathways in the high-fat diet (DIO) mice cardiac mitochondria using proteomic analysis. 159
Figure 6.5: Mass spectrometry analysis of exercise, diet exchange and exercise/diet exchange groups compared to control. 160
Figure 6.6: Down regulation of proteins involved in the most common altered canonical pathways in the cardiac mitochondria of the exercise group. 161
Figure 6.7: Alteration of canonical pathways in the cardiac mitochondria of diet exchange group. 162
Figure 6.8: Alteration of canonical pathways in the cardiac mitochondria of exercise/diet exchange group. 163
Figure 6.9: Upregulation of glycolysis in the high-fat diet mice, but not in the exercise, diet exchange and exercise/diet exchange mice. 164
Figure 6.10: Down-regulation of PDK in the high-fat diet (DIO) mice. 165
Figure 6.11: Decrease expression of ACOX1 in the high fat diet (DIO) model 166
Figure 6.12: Proteomic analysis of Complex 1-5 proteins expression. 168

List of Tables

Table 1.1: Type 1 diabetes animal models. 22
Table 1.2: Summary of the most used type 2 diabetes animal models. 24
Table 2.1: Echocardiography parameters formula. 46
Table 2.2: Primary and secondary antibodies list used to assess mitochondrial dynamics. 48
Table 2.3: Reverse transcription master mix. 51
Table 2.4: Thermal cycler set up. 52
Table 2.5: List of primer assay for mitochondrial dynamics. 52
Table 2.6: Composition of qPCR reaction mixture. 53
Table 2.7: Real-time PCR thermal cycling conditions. 53
Table 2.8: in-vivo cardiac function analysis by echocardiography showed no changes in systolic function for high-fat diet (DIO) mice. 61
Table 2.9: In-vivo cardiac structure analysis by echocardiography for high-fat diet (DIO) model. 63
Table 2.10: ECG parameters comparison between control and HFD (DIO) mice. 64
Table 4.1: Echocardiogram readings in exercise, diet exchange and exercise/diet exchange groups. 110
Table 5.1: H9c2 cardiac myoblasts seeding density. 130
Table 5.2: List of primary and secondary antibodies used for ER stress and sirtuin5 pathway. 130
Table 5.3: List of primer assay for ER stress, sirtuin5, prohibitins and mitochondrial dynamics. 131
Table 6.1: Quantitative analysis of mitochondrial dynamic proteins expression changes in HFD (DIO) group, exercise, diet exchange and exercise/diet exchange groups. 169
Table 6.2: Summary of mitochondrial dynamic proteins expression in the HFD (DIO), Exercise, diet exchange and exercise and diet exchange mice models. 170
Table 7.1: Masson’s trichrome staining protocol. 187

Abstract

Obesity is a common precursor to type 2 diabetes (T2DM); both reaching pandemic proportions and are associated with cardiovascular complications such as diabetic cardiomyopathy. Diabetic cardiomyopathy is linked with changes to mitochondrial function and dynamics; regulated by fission and fusion. However, the underlying mechanisms remain unknown. This project aimed to characterise cardiac function and investigate mitochondrial fission/fusion mechanisms in a diet-induced obesity (DIO) murine model. Here I employed eight-week-old C57BL/6J male mice, fed with either a 60% high-fat diet (HFD) or chow (10% fat) (n= 6-8) for 12 weeks to study mitochondrial function and dynamics remodelling that could contribute to the development of diabetic cardiomyopathy. A second trial group incorporated exercise (most common non-pharmacological management of obesity/T2DM) training (a daily swimming regimen) and/or diet exchange for chow after 12 weeks HFD feeding for 5 weeks to determine the reversible impact upon cardiac and mitochondrial function. Therefore, this study assessed the hypothesis that obesity-induced diabetes (DIO) alters mitochondrial dynamics in the heart, promoting changes to mitochondrial function and structure.

HFD feeding led to weight gain, hyperglycaemia, hyperlipidaemia and insulin resistance in DIO mice, and echocardiography revealed signs of diastolic dysfunction. Histology staining showed evidence of apoptosis but no fibrosis or hypertrophy. Western blotting and RT-qPCR showed increased expression of the fission proteins Drp1 and Fis1 with a decreased in the phosphorylation of Drp1 at Ser637 suggest a shift towards fission. There was an upregulation of mitophagy proteins, PINK1 and Parkin. Employing serial block face scanning electron microscopy (SBF-SEM) I determined that there was a decrease in perinuclear mitochondria surface area and volume but with an increase in its surface area to volume ratio in HFD (DIO) compared to control. In addition, perinuclear mitochondria in control and HFD (DIO) were the smallest in size, and the largest surface area to volume ratio compared to subsarcolemmal and interfibrillar mitochondria. Diet exchange and exercise with diet exchange led to improve insulin sensitivity and lipid profile with restoration of normal fission-fusion axis, but the mice that underwent exercise only remained insulin resistant with alterations to the fission-fusion axis.

I identified that HFD (DIO) feeding led to a decrease in sirtuin 5 (Sirt5) and so next investigated whether mechanistically there is a link to increased mitochondrial fission. siRNA-mediated Sirt5 knockdown in H9c2 cardiac myoblast cell line led to a similar alteration in mitochondrial dynamics as seen in HFD (DIO) model (increase in Drp1, decrease in P-Drp1(S637). I further demonstrated that there was no link between changes in mitochondrial dynamics in early-stage diabetic cardiomyopathy and ER stress, Prohibitins (PHB1 and PHB2) and insulin resistance. Finally, proteomic analysis comparing each permutation of exercise and diet showed perturbed inflammatory, cardiac contraction signalling and stress defence network in HFD (DIO) cardiac mitochondria with a shift in the major energy source from fatty acid oxidation to glycolysis. Moreover, PPARA was identified as one of the main inhibitory upstream regulators in HFD (DIO).

Here I have identified changes in mitochondrial fission/fusion axis as a feature of diabetic cardiomyopathy and hence represent an early pathogenesis event, thus providing novel insights that can be incorporated into future therapeutic research. In addition, our studies on the reversible effect of exercise and/or diet highlight the role of healthy lifestyle in managing cardiac mitochondrial function. A putative mechanistic link between Sirt5 and mitochondrial fission/fusion processes has been investigated, providing a novel understanding of the regulation of mitochondrial dynamics. Furthermore, our proteomic data indicates perturbed mitochondrial pathways in HFD (DIO), exercise and/or diet exchange groups and our datasets provide valuable information for future studies for investigating novel therapeutic approaches to combat obesity induced diabetes particularly since patient compliance to lifestyle changes remains generally poor.

Declaration

I declare that no portion of the work referred to in this thesis has been submitted in support of an application for another degree or qualification at this or any other university or other institute of learning.

Copyright Statement

Acknowledgment

I would like to express my sincere gratitude to my inspiring supervisor, Dr Ashraf Kitmitto, a wonderful person, for her continuous support. Many thanks for everything, I could not have finished my PhD without your guidance, kindness, and friendship. I would also extend my thanks to Dr Elizabeth Cartwright for her co-supervision and help in all animal work. I would also like to thank Florence Baudoin for teaching me laboratory skills and for providing positive vibes in the lab. Thanks to Dr Min Zi and Sukhpal Prehar for their help with *in vivo* work. Thanks to Dr Sophie Saxton for providing me samples to practice in my first year and for her help with animal work. Thanks to Dr Sarah Kassab for offering help when I need it and for her help with Mass spectrometry work. Many thanks also to all my lab members for the brilliant working environment, I have enjoyed working with you all. I would also like to thank King Abdulaziz University for funding my project.

I am also so fortunate to have the constant support of my wonderful family. My biggest thanks to my mother Taghreed Memish, and my father Mohammed Daghistani for their love and encouragement. Thanks for everything you have ever done for me, you got me to where I am today. Thanks also to my siblings Rayan, Yassir, Firas, Ghaidaa and Ghadeer for their motivation. Rayan, my eldest brother, Congratulations on your well-deserved promotion at work, you are doing a great job. Yassir, congratulations on your beautiful daughter “Sarah” and for the acceptance in the rheumatology fellowship in Canada, soon to be a rheumatology consultant. Firas, congratulations on the acceptance for the PhD in Australia and getting married! Ghaidaa, you are a senior medical student now, good luck in choosing the speciality and with the rest of your study. Ghadeer, congratulations for getting accepted in the medical school.

The last four years have been very special to me, I have learned a lot and made true friends. I cannot wait to teach what I have learned to my future students. To everyone else at the division of Cardiovascular sciences, University of Manchester, thank you for this amazing experience.

Publications

Daghistani, H. M., Rajab, B. S. & Kitmitto, A. (2019). "Three-dimensional electron microscopy techniques for unravelling mitochondrial dysfunction in heart failure and identification of new pharmacological targets", British Journal of Pharmacology, 176(22):4340-4359.

Poster presentations

Diet induced obesity leads to impaired mitochondrial dynamics in the heart. Presented at the Division of Cardiovascular Sciences Postgraduate showcase; The University of Manchester, UK; 30th April 2018.

Investigation of Cardiac Mitochondrial Structure and Function in Obesity and T2DM. Presented at the 27th Northern Cardiovascular Research Group Meeting; University of Leeds; April 2019.

Investigation of Cardiac Mitochondrial Structure and Function in Obesity and Effects of exercise. Presented at the 48th European Muscle conference; Canterbury; September 2019.

Abbreviation

3D	Three-dimensional
AF	Atrial fibrillation
AGE	Advanced glycosylation end-product
ALDOB	Aldolase B
AMPK	5' adenosine monophosphate-activated protein kinase
ATF6	Activating transcription factor 6
ATP	Adenosine triphosphate
BFA	Bradford assay
BiP	Binding immunoglobulin protein
BMI	Body mass index
BSA	bovine serum albumin
BSA	Bovine serum albumin
BW/TL	Body weight to tibial length
CAD	Coronary artery disease
CM	Cardiomyocytes
CS	Citrate synthase
cTnT	Cardiac troponin T
DAPI	4′,6-diamidino-2-phenylindole
DCM	Diabetic cardiomyopathy
ddH_2O	Double distilled water
DIO	Diet-induced obesity
dIVS	Diastolic Interventricular Septum
dLVD	Diastolic Left Ventricular Diameter
DM	Diabetes mellitus
DMEM	Dulbecco's Modified Eagle Medium
dPW	Diastolic Posterior Wall
DPX	Distryne, plasticizer and xylene
Drp1	Dynamin-related protein 1
DTT	Dithiothreitol
ECG	Electrocardiography
EF%	Ejection fraction
ELISA	Enzyme-linked immunosorbent assay
EM	Electron microscopy
ER	Endoplasmic reticulum
FCCP	Carbonyl cyanide-4-(trifluoromethoxy)phenylhydrazone
FFA	Free fatty acids
FIB-SEM	Focussed ion-beam scanning electron microscopy
Fis1	Fission 1 protein
FS%	Fractional shortening
H&E	Haematoxylin & eosin
HDL	High-density lipoproteins
HEK	Human embryonic kidney
HEPES	4-(2-hydroxyethyl)-1-piperazineethanesulfonic acid
HFD	High-fat diet
HFHS	High fat, high sucrose
HFpEF	Heart failure with preserved ejection fraction
HPLC	High-Quality Liquid Chromatography
HTN	Hypertension
IAM	Iodoacetamide

IFM	Interfibrillar mitochondria
IL	Interleukin
IMM	Inner mitochondrial membrane
IMS	industrial methylated spirit
IPA	Ingenuity pathway analysis
iPSC	Human-induced pluripotent stem cell
IR	Insulin resistance
IRE-1	Inositol-requiring enzyme 1
LDHD	D-lactate dehydrogenase
LDL	Low-density lipoproteins
LVM	Left ventricular mass
LW/TL	Lung weight normalised to tibial length
m/z	Mass-to-charge ratio
Mdivi-1	Mitochondrial division inhibitor 1
MEF	Mouse embryonic fibroblast
Mff	Mitochondrial fission factor
Mfn1	Mitofusin 1
Mfn2	Mitofusin 2
MID 49	Mitochondrial dynamics 49
MID 51	Mitochondrial dynamics 51
mPTP	Mitochondrial permeability transition pore
MS	Mass spectrometry
MS/MS	Tandem mass spectrometry
mtDNA	Mitochondrial DNA
NCM	Non-cardiomyocytes
NHS	National health service
NRCM	Neonatal rat cardiomyocyte
OCR	Oxygen consumption rate
OMM	Outer mitochondrial membrane
OXPHOS	Oxidative phosphorylation
PBS	Phosphate-buffered saline
PDK	Pyruvate dehydrogenase kinase
PERK	Protein kinase R-like endoplasmic reticulum kinase
PFA	paraformaldehyde
PGC-1α	Peroxisome proliferator-activated receptor gamma coactivator 1-alpha
PHB	Prohibitin
PINK1	PTEN-induced kinase protein 1
PNM	Perinuclear mitochondria
PPARA	Peroxisome proliferator-activated receptor alpha
PTM	Post-translational modification
PVDF	Polyvinylidene difluoride
qPCR	Quantitative polymerase chain reaction
rcf	Relative centrifugal force
ROS	Reactive oxygen species
RWT	Relative wall thickness
SA/Vol	Surface area to volume ratio
SBF-SEM	Serial block-face scanning electron microscopy
SDS-PAGE	Sodium dodecyl sulphate-polyacrylamide gel electrophoresis
SEM	Standard error of the mean
siRNA	Small interfering RNA
Sirt	Sirtuin

sIVS	Systolic Interventricular
sLVD	Systolic Left Ventricular Diameter
SR	Sarcoplasmic reticulum
SSM	Subsarcolemmal mitochondria
STZ	Streptozotocin
SV	Stroke volume
T1DM	Type 1 diabetes mellitus
T2DM	Type 2 diabetes mellitus
TBST	Tris-buffered saline and Tween-20
TCA	Tricarboxylic acid
TCH	Thiocarbohydrazide
TEAB	Tetraethylammonium bicarbonate
TEM	Transmission electron microscopy
TFAM	Mitochondrial transcription Factor A
TG	Triglyceride
TMB	Tetramethylbenzidine
TMRE	Tetramethylrhodamine ethyl ester
TNB	5-thio-2-nitrobenzoic acid
TUNEL	Terminal deoxynucleotidyl transferase dUTP nick end labeling
UCP	Uncoupling protein
UPR	Unfolded protein response
VLDL	Very low-density lipoproteins
WT	Wild type
XBP1	X-box binding protein 1

Chapter 1 General introduction

1.1 Obesity and diabetes

1.1.1 Obesity

Obesity and overweight are described as the excess fat in the body that could negatively affect the health. According to World Health Organization (2017), 38.5% of adult global population were overweight, 13% were obese in 2014, highlighting that obesity is reaching pandemic proportions and represents a global healthcare burden. The most common cause of obesity is the increased intake of high energy foods and the lack of physical activity (Lau et al., 2007). However, few cases are caused by medical, psychiatric or genetic diseases (Bleich et al., 2008). Health Survey for England (2015) reported that 27% of England's population are classified as obese. Foresight (2007) predicted that 60% of adult men and 50% of adult women in England will defined as obese by 2050 (Bryony Butland, 2007). Obesity is measured by body mass index (BMI), dividing an individual's body mass in kilograms by the square of the height in meters (kg/m^2). BMI categorises the population into underweight, normal, overweight or obese groups. Normal BMI is from 18.5 kg/m^2 up to 25 kg/m^2, whereas a BMI of 25 kg/m^2 up to 30 kg/m^2 is characterised as overweight and more than or equal to 30 kg/m^2 is described as obese. Obesity is subdivided into different categories, class 1: BMI of 30 to 34.9 kg/m^2, class 2: BMI of 35 kg/m^2 to 39.9 kg/m^2 and class 3: BMI of 40 kg/m^2 or higher. Obesity is a major risk factor for heart disease, stroke, obstructive sleep apnoea, osteoarthritis and type 2 diabetes mellitus (T2DM) (World Health Organization, 2014). Furthermore, there are numerous studies on the association between obesity and T2DM. For example, Resnick et al. (2000) stated that overweight and obesity were associated with increased T2DM risk.

1.1.2 Diabetes

Diabetes mellitus (DM) is a serious health condition characterised by a persistent elevation of blood glucose concentration (≥ 7 mmol/l fasting glucose) and presented with polyuria, polydipsia and weight loss (American Diabetes Association, 2017). Diabetes is a global problem with reports stating that 415 million adults around the world had diabetes in 2015, which equals to 1 in 11. Figure 1.1 shows the number of diabetic patients in each continent in 2015 and the expected number of diabetic patients in 2040 (International Diabetes Federation, 2015). It is estimated that DM accounts for 22,000 deaths per year in the United Kingdom. There are two main types of diabetes: Type 1 DM (T1DM), also known as insulin-dependent diabetes mellitus, and T2DM, also known as non-insulin-dependent diabetes mellitus. Although the exact cause of T1DM is unknown, it is generally thought to result

from autoimmune damage to pancreatic islet cells leading to decrease insulin secretion. T1DM usually occurs during childhood or in youth while T2DM mostly occurs in adults (Harjutsalo et al., 2010). Around 85% of diabetics, globally, are T2DM (World Health Organization, 2004). The cause of T2DM includes lifestyle, genetics and some medical conditions. Although the National Health Service (NHS) spends 9% of its budget annually which equals £8.8 billion on the treatment of T2DM, it is preventable by controlling obesity, which is an important risk factor for T2DM (Awa et al., 2012, Public Health England, 2015). Around 90% of T2DM patients are overweight or obese (World Health Organization, 2004). Overweight and obesity have been assigned to 44% of the diabetes burden around the world (World Health Organization, 2009). It has been found that obesity can cause insulin resistance and eventually inadequate insulin secretion which leads to T2DM (Muoio and Newgard, 2008) (Gardner et al., 2011). Untreated DM can cause several short-term and long-term complications. Short-term complications are hyperosmolar hyperglycaemic state, hyperglycaemic diabetic ketoacidosis and death (Kitabchi et al., 2009), while the long-term complications are neuropathy, nephropathy, retinopathy and cardiovascular disease.

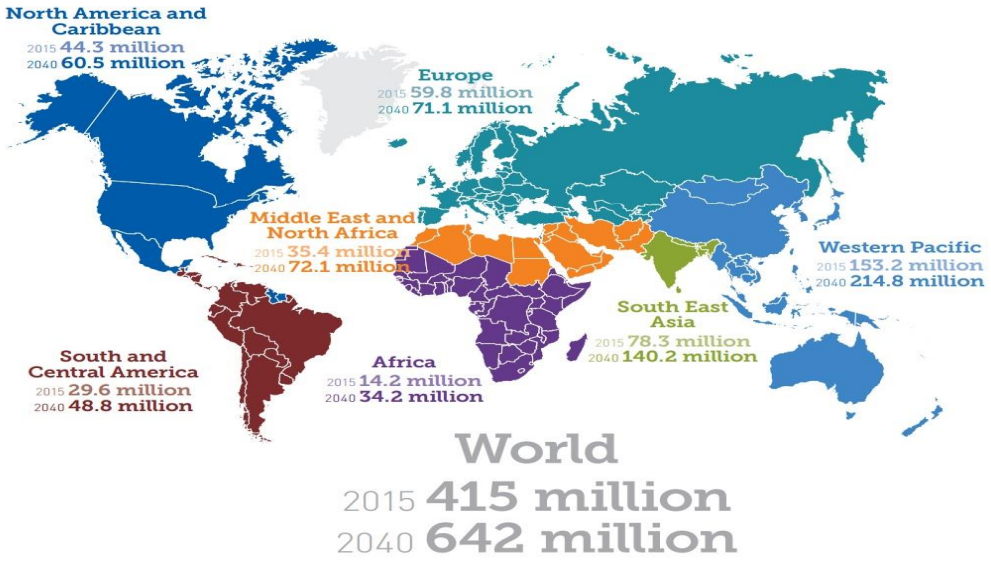

Figure 1.1: Number of diabetes cases by continent in 2015 and estimated number in 2040.
Adapted from International Diabetes Federation (2015).

1.1.3 Cardiovascular complications in obesity and diabetes

It has been found that obesity increases the likelihood of developing hypertension, heart failure and coronary artery disease (CAD) (Lavie et al., 2009). Kenchaiah et al. (2009) reported a doubling in the risk of developing heart failure in obese individuals compared to

normal BMI individuals. Madala et al. (2008) described a strong negative relationship between the BMI and the age of the patient presenting with a non-ST elevation myocardial infarction. In addition, obesity has been linked to ventricular diastolic dysfunction (Pascual et al., 2003), left atrial enlargement (Stritzke et al., 2009) and left ventricular hypertrophy (Lauer et al., 1991) which are considered risk factors for atrial fibrillation (AF). Wanahita et al. (2008) also reported an increased risk of AF by 49% in obese patients in comparison to normal weight patients.

In addition to the association of cardiovascular disease with obesity, cardiovascular complications are common in diabetic patients (Sarwar et al., 2010) and are associated with increased mortality (Di Angelantonio et al., 2015). Diabetes is considered one of the major risk factors for heart failure, which can be caused by CAD and myocardial dysfunction (Aneja et al., 2008). Diabetic patients have a higher risk, greater than three-fold, to develop CAD and are at higher risk for myocardial dysfunction (Avogaro. et al., 2004).

The term diabetic cardiomyopathy (DCM) which was introduced by Rubler et al. (1972) identifies myocardial structural or functional abnormalities that are induced by diabetes which could result in heart failure. DCM is categorized into three stages: early, middle and late stage. In the earliest stage, metabolic and mitochondrial dysfunction is initiated with normal ejection fraction and no obvious functional abnormality. Decreased ejection fraction and diastolic dysfunction is seen in the middle stage. In the late stage, microvascular changes lead to heart failure (Chavali et al., 2013) .

Cardiovascular complications in obesity and diabetes have been proposed to be caused by various mechanisms including hyperglycaemia, lipid toxicity and mitochondrial dysfunction (Duncan et al., 2010). There are four pathogenic mechanisms that are thought to be driven by hyperglycaemia. One of the best characterised mechanisms by which hyperglycaemia leads to organ damage is through accelerating the production of advanced glycosylation end-products (AGEs), which in turn increase reactive oxygen species (ROS). Both AGEs and ROS have been demonstrated to lead to collagen damage and stimulate the inflammatory cascade (Aneja et al., 2008).

The increase in myocardial free fatty acids metabolism is reported to cause systolic and diastolic dysfunction in addition to elevation of mitochondrial ROS level (Bando and Murohara, 2014, Amaral and Okonko, 2015, Wang et al., 2014). These changes could lead to myocardial abnormalities such as fibrosis, hypertrophy, microangiopathy and contraction abnormality (Borbely et al., 2009, Bugger and Abel, 2014). Excessive fatty acids lead to myocardial abnormalities in two mechanisms: increase rates of fatty acid oxidation and

ectopic lipid deposition. The ratio of glucose and fatty acid oxidation by the heart physiologically varies in a dynamic manner to ensure the maximum energy production. Pathological changes in this ratio are seen in obesity and diabetes. Low level of cellular glucose leads to an increase in fatty acid oxidation results in increased ROS production and oxygen consumption, in addition to impaired energy production which could lead to apoptosis (Duncan et al., 2010). For example, human and animal hearts of T1DM showed an increase in fatty acid oxidation, oxygen consumption and decrease in glucose oxidation associated with impaired cardiac function (How et al., 2006, Bugger et al., 2008, Herrero et al., 2006). A similar finding has been reported in an animal model of T2DM (Boudina et al., 2007, Buchanan et al., 2005, Mazumder et al., 2004, Boudina et al., 2005). The second mechanism for myocardial abnormality associated with excessive fatty acid, ectopic lipid deposition, has been reported in human and animal studies (Wende and Abel, 2010) (Sharma et al., 2004). For example, fat accumulation around the animal heart, caused by a high fat diet, lead to systolic and diastolic dysfunction (Montani et al., 2004). In addition, ectopic lipid deposition in the heart associated with diastolic dysfunction has been reported in obese mice model (Christoffersen et al., 2003).

The link between obesity and diabetes association in being major risk factors for cardiovascular complications could be explained by the fact that obesity is a risk factor for insulin resistance and, therefore, T2DM as previously explained. Obesity contributes to T2DM development and can independently cause cardiac dysfunction. Therefore, studies on the link between the possible mechanisms by which obesity and diabetes lead to cardiovascular complications are required, in addition to research on the effects of lifestyle routines in preventing obesity and consequently, diabetes and cardiovascular diseases.

1.2 Animal models of diabetes

Laboratory animals have been used as surrogate of human diseases to facilitate research when it is difficult, harmful, and unethical to be conducted on humans. Laboratory animals have been used due to the similarity of pathophysiology compared to human. Furthermore, it has been determined that the mouse genome is similar to human genome by more than 90% (Waterston et al., 2002). Accordingly, researchers have extensively used small animal models of diabetes and obesity to delineate the molecular cardiovascular complications associated with both DM and obesity.

T1DM rodent models are categorised into different groups depending on the induction mechanism: chemical induction, spontaneous autoimmune, genetically induced and virally induced. Chemical induction models have been used to test new insulin types (Sheshala et al.,

2009, Jederstrom et al., 2005), as well as pancreatic islets transplantation (Makhlouf et al., 2003, Deeds et al., 2011). The downside of this approach is the cytotoxicity of the chemicals used, for example, the streptozotocin (STZ) contributes to increasing free radical formation (Lee et al., 2010). In addition, misinterpretation of data could occur when studying the autoimmunity in STZ models because it has been reported to reduce lymphocyte count and increase suppressor T-cells (Muller et al., 2011). However, the STZ model remains one of the most popular animal models of T1DM as it is relatively cheap and fast to develop with the rats showing symptoms of diabetes at 8 weeks post-injection. Spontaneous autoimmune induction includes the non-obese diabetic (NOD) model, which is the model of choice to study autoimmunity (Yang and Santamaria, 2006). Disadvantages of this model include its high susceptibility to bacterial infection, which could alter the development of DM. Therefore, it is expensive to keep this model in a specific pathogen-free environment (King, 2012). The Akita mouse is an example of a genetically induced model, which has been commonly used to study Endoplasmic reticulum (ER) stress in the pancreatic islets, which could lead to an early death of mouse if left untreated (Chen et al., 2011a). A range of cardiac abnormalities with each of the models have been reported, summarised in Table 1.1 (Moore et al., 2014, Pacher et al., 2002, Bugger and Abel, 2009).

Table 1.1: Type 1 diabetes animal models.
(STZ, streptozotocin; NOD, non-obese diabetic; ER, endoplasmic reticulum).

Mechanism of induction	Model	Uses	Disadvantage	Cardiac features
Chemically induced	STZ	• Appropriate model for testing insulin and islets transplantation • inexpensive	• Cytotoxic. • Lymphopenia • Increase in suppressor T cells	• Diastolic dysfunction • Decrease mitochondrial respiratory capacity • Decrease cardiac efficiency
Spontaneous autoimmune	NOD	• Appropriate model for autoimmunity	• Costly	• Decrease left ventricular systolic pressure
Genetically induced	Akita	• Appropriate model for ER stress in the pancreatic islets	• Short life span	• Decrease cardiac function

Since T2DM is associated with obesity, the majority of T2DM models are obese and so are also often used as models of obesity. Rodent models of T2DM are divided into obese and non-obese models. Obesity is induced by monogenic, polygenic or diet.

Leptin, also known as satiety hormone, inhibits hunger. Dysfunctional leptin lead to obesity by hyperphagia, which is the most common mechanism used in monogenic models. Monogenic models include $Lep^{ob/ob}$, $Lepr^{db/db}$ mice and Zucker fatty rats (ZFR). $Lep^{ob/ob}$ mice have been often used to study metabolic disturbances leading to T2DM, and the association between insulin and leptin (King, 2012). Moreover, hyperlipidaemia was found in $Lep^{ob/ob}$ and ZFR (Lindstrom, 2007), whereas ketosis and short life span were reported in $Lepr^{db/db}$ mice, whereas hypertension and glucose intolerance were reported only in ZFR (Srinivasan and Ramarao, 2007).

Furthermore, polygenic models include Kasukabe (KK), New Zealand Obese (NZO) and TallyHo mice. These models have been used to study oral hypoglycaemic agents (Yoshinari and Igarashi, 2011, Mochizuki et al., 2011) and DM complications (Buck et al., 2011, Lee et al., 2011). Different from monogenic models, these models have no wild-type phenotype, and gender bias is present (Leiter, 2009). KK mice are reported to have signs of diabetic nephropathy (Ikeda, 1994) and they have mild obesity (Clee and Attie, 2007). Non-obese models of T2DM include Goto-Kakizaki (GK) rats. Table 1.2 summarises T2DM models with a range of cardiac abnormalities that have been reported (Bugger and Abel, 2009, Ye et al., 2004, Fang et al., 2008, Daniels et al., 2012, Picatoste et al., 2013). The diet for all mice models in the table is chow diet except for DIO model which is a high-fat diet. High fat diet can be 45% or 60% (calories from fat).

Table 1.2: Summary of the most used type 2 diabetes animal models.
(ZFR: Zucker fatty rats, KK: Kasukabe, NZO: New zealand Obese, GK: Goto-Kakizaki, Lepr: deficient leptin receptor, Lep: leptin deficient, DIO: diet-induced obesity).

Mechanism	Model	Hyper glycaemia	Hyper insulinaemia	Hyper phagia	Specific features	Cardiac features
Obese (monogenic)	$Lep^{ob/ob}$	Yes	Yes	Yes	• Severe obesity • Hyperlipidaemia • Infertile	• Diastolic dysfunction • Decrease mitochondrial respiratory capacity • Decrease cardiac efficiency
	$Lepr^{db/db}$	Yes	Yes	Yes	• Ketosis • Short life span	• Diastolic dysfunction • Decrease mitochondrial respiratory capacity • Decrease cardiac efficiency
	ZFR	Glucose intolerance	Yes	Yes	• Hyperlipidaemia • Hypertensive	• Diastolic dysfunction
Obese (Polygenic)	KK mice	Yes	Yes	Yes	• Mild obesity, • Sign of diabetic nephropathy • Hyperliptinimia	• Contractile dysfunction
	NZO mice	Yes	Yes	Yes	• Hyperliptinimic	
	TallyHo	Yes	Yes	Yes	• Hyperglycaemia is limited to male mouse • Hyperlipidaemia	
Obese (DIO)	HFD (45%, 60% calories from fat)	Glucose intolerance	Yes	No		• Cardiac hypertrophy • Contractile dysfunction
Non-obese	GK rats	yes	No	No		• Diastolic dysfunction

1.3 Mitochondrial dysfunction in diabetic cardiomyopathy

Evidence is converging to indicate that a hallmark of diabetes is altered cardiac metabolism (Lee et al., 2017b, Lee et al., 2015, An and Rodrigues, 2006), a feature that will lead to impaired contractile function (Miki et al., 2013). Central to myocardial metabolism are mitochondria, organelles within the cardiac myocytes. It has been found that aberrant mitochondrial function and morphology occur as a result of obesity and DM, pathophysiological changes that are proposed to contribute towards the development of heart failure (Bugger and Abel, 2010). For this reason, understanding the effect of obesity and its

possible consequence, T2DM, on cardiomyocyte mitochondria is central to research on cardiovascular disease and prevention.

1.3.1 Mitochondria and energy production

Mitochondria are double membrane organelles found in all eukaryotic cells. Mitochondria have an outer (OMM) and inner (IMM) membrane separated by the intermembrane space (IMS). Infolding of the inner membrane forms the cristae. The space within the inner membrane is called the matrix. Mitochondria are a major intracellular organelle that are mainly responsible for energy production and as a regulator for various cellular mechanisms. The main cellular energy source, adenosine triphosphate (ATP), l is produced by the mitochondria. For example, a human heart produces over 30 kg of ATP daily (Mailloux, 2015). Cellular respiration is the process of generating energy, in the form of ATP, from food. This includes glycolysis, the tricarboxylic acid (TCA) cycle, β-oxidation and oxidative phosphorylation (OXPHOS). Glycolysis occurs in the cytosol, while citric acid cycle, OXPHOS and beta-oxidation occurs in the mitochondria. Glycolysis and β-oxidation produce acetyl-CoA which are oxidized in the TCA cycle for energy production. OXPHOS occurs through the electron transport chain (ETC), with the Complexes localised to the inner mitochondrial membrane. ETC is formed from a series of protein complexes that relocate electrons from a reducing agent to an oxidising agent in redox reactions; these electron-transfer reactions generate energy. Electrons are derived from NADH and FADH2 which are produced from glycolysis and TCA cycle. ETC consists of Complex I, II, III, IV, V, ubiquinone Q and cytochrome C.

In obesity and diabetes, mitochondrial energy production is affected due to the alteration of Complex activity, which could lead to cardiac myopathy. For example, Vazquez et al. (2015) reported a decrease in complex I activity resulting in decrease OXPHOS in STZ mice heart (T1DM). Boudina et al. (2007) observed a significant decrease in complex V proteins associated with impaired OXPHOS in $Lepr^{db/db}$ heart mitochondria. In addition, Boudina et al. (2005) reported a decrease in protein levels of complex I, III and V in heart of $Lep^{ob/ob}$ mice. A study of hearts from STZ diabetic rats showed a significant decline in enzymatic activities of complex I and II that were associated with reduction in mitochondrial respiration (Lashin et al., 2006).

1.3.2 Calcium ion uptake, storage and signalling

Calcium (Ca^{2+}) plays an important role in signal transduction and is considered one of the most common intracellular signalling molecules which help in neurotransmitter release and

muscle contraction (Brini et al., 2013). Excitation-contraction coupling (ECC) is a mechanism that regulates cardiomyocyte contractility. Figure 1.2 summarises the main processes in ECC. An action potential from sinoatrial (SA) node depolarizes the sarcolemma. Depolarization of the sarcolemma leads to Ca^{2+} entry into the cytosol via the L-type voltage-gated calcium channels which then binds to the ryanodine receptors (RyR2) triggering a release of a bolus of Ca^{2+} from the sarcoplasmic reticulum by a mechanism known as Ca-induced Ca-release (CICR) (Bers, 2002). CICR leads to an increase to cytosolic Ca^{2+} levels which leads to conformational changes to sarcomeric proteins culminating in cardiomyocyte contraction. Following contraction, relaxation of the sarcomere occurs by decreasing the Ca^{2+} concentration in the cytosol through removal of the Ca^{2+} from the cell predominantly via sarcolemmal Na/Ca exchange (NCX) and with transfer of Ca^{2+} back into the SR via sarcoplasmic reticulum Ca-ATPase (SERCA). The Ca^{2+} released in the CICR stage is also taken up into mitochondria via the voltage dependent anion channel (VDAC) and mitochondrial Ca^{2+} uniporter (MCU). VDAC is located in the OMM, whereas MCU is found in the IMM (Sejersted, 2011). Mitochondrial Ca^{2+} uptake is essential in the cardiac cycle as mitochondrial Ca^{2+} uptake and buffering affect the cytosolic Ca^{2+} concentration which has a role in the contraction. In addition, mitochondrial Ca^{2+} is central for regulating several TCA cycle enzymes and other cellular metabolism such as apoptosis as well as for the production of ATP (Marks, 2003).

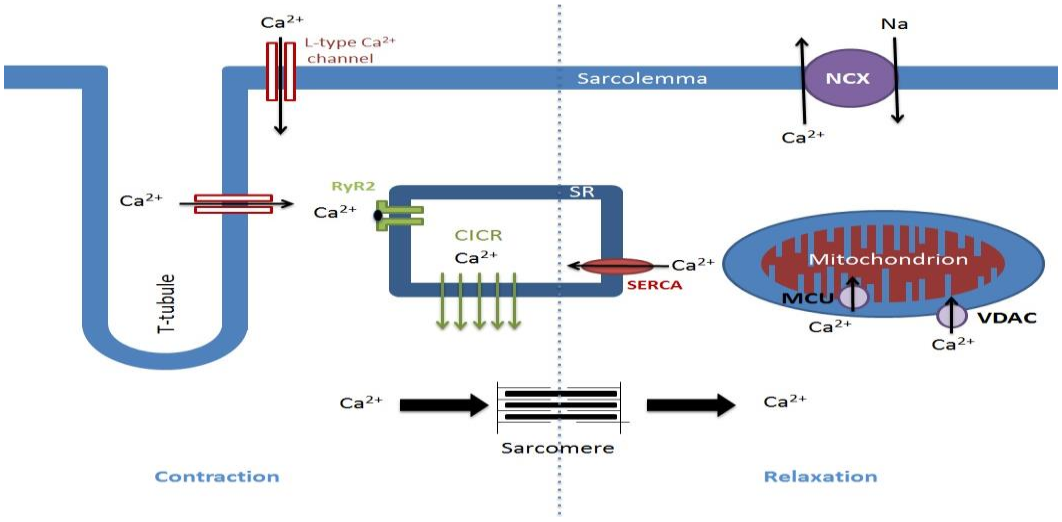

Figure 1.2: Cardiac excitation-contraction coupling.
Calcium ions enter the cytoplasm via the L-type calcium channels which triggers opening of the RyR2, which leads to the release of calcium from the SR into the cytoplasm. High cytoplasmic calcium stimulates proteins of the sarcomere leading to contraction. Relaxation is initiated by decreasing cytoplasmic calcium by removal of calcium via MCU, VDAC, SERCA and NCX. RyR2, ryanodine receptor; CICR, Calcium-induced Calcium-release; SERCA, sarcoplasmic reticulum Ca ATPase; NCX, Na/Ca exchange; MCU, mitochondrial calcium uniporter; VDAC, voltage dependent anion channel.

Cardiomyocyte mitochondrial Ca^{2+} mishandling has been reported in many T1DM animal models (Suarez et al., 2008, Zhao et al., 2006, Ye et al., 2004) as well as in T2DM models. For example, Belke et al. (2004) reported a myocardial contractile dysfunction associated with decrease Ca^{2+} handling by the sarcoplasmic reticulum (SR) in the $Lepr^{db/db}$ diabetic mice. In addition to this, Li et al. (2006) reported Ca^{2+} mishandling in cardiomyocytes in $Lep^{ob/ob}$ obese diabetic mice, manifested as impairment contractility. From these studies and others, there is a growing consensus that impaired calcium signalling in the cardiomyocyte mitochondria in obesity and DM contributes to contractile dysfunction.

1.4 Mitochondrial subpopulations

The cardiomyocyte has a higher number of mitochondria than other cell types (around third of its volume) because of its high energy demand (Ruiz-Meana et al., 2010). Cardiac mitochondria consist of three different structurally, spatially and biochemically separate populations: interfibrillar (IFM), subsarcolemmal (SSM) and perinuclear mitochondria (PNM) (Hollander et al., 2014). SSM are situated underneath the cell membrane (sarcolemma) and have been reported to have lamelliform cristae, whereas IFM are located between the muscle fibrils and mostly have tubular cristae (Riva et al., 2005), whereas perinuclear mitochondria are clustered around the nucleus. In addition, perinuclear mitochondria are smaller, less complicated in structure than other subpopulations and rounded in shape (Lukyanenko et al., 2009). It is believed that perinuclear mitochondria play a role in nuclear transcription (Al-Mehdi et al., 2012). There is evidence that each population may have a different function in the cell. Since IFM are embedded between myofibrils, IFM have been reported to have greater OXPHOS and Ca^{2+} loading, enzymatic activity and energy production which could help in muscle contraction (Hatano et al., 2015, Schwarzer et al., 2013). Although IFM have been reported to have greater OXPHOS, Crochemore et al. (2015) found that ROS level is higher in SSM than IFM in normal condition. Mitochondria subpopulations have been reported to be affected differently in pathological conditions. Aging have been reported to affect IFM negatively. For example, Lesnefsky et al. (2001) stated that aging decrease complex III activity in heart IFM subpopulation only. In addition, Suh et al. (2003) reported a higher oxidative stress and lower complex IV activity in old rats' heart IFM compared to young. Ischemic injury has been reported to have a negative effect on SSM. For example, Holmuhamedov et al. (2012) reported that SSM is more susceptible to

ischemic injury and Ca^{2+} overload than IFM. This could suggest that most cardiomyocyte ischemic damage occurs in SSM.

However, SSM and IFM have been reported to be affected differentially in DM. A study on cardiac myocytes from animal model of T1DM showed a decrease in complex I and III activity with an increase in ROS in IFM and no changes in SSM (Dabkowski et al., 2009). In the same study, mitochondrial size was decreased in SSM but not in IFM. Moreover, Baseler et al. (2011) observed a decrease in complex I, II, III, IV and V proteins in IFM of STZ mice models. Interestingly, multiple mitochondrial respiration proteins were increased in SSM which could be a compensatory protective mechanism. Although the exact mechanism is not clear, this could explain the contractile dysfunction seen in T1DM patients since IFM is near the muscle. However, contractile dysfunction is also seen in T2DM when SSM is affected. For example, decrease in complex I activity in SSM was found in T2DM human heart with no change in IFM (Croston et al., 2014). Taken together, different mitochondrial subpopulation responses to different DM types require further investigation.

1.5 Mitochondrial dynamics

Mitochondria, specifically by OXPHOS in the ETC, are the major cellular source for ROS which include superoxide and hydroxyl anions (Bugger and Abel, 2010). Excessive ROS generation is seen in pathological conditions such as obesity and diabetes that lead to oxidative stress which could induce cellular and mitochondrial DNA damage, and subsequent cell death if unresolved (Betteridge, 2000). A number of studies revealed a correlation between obesity and DM with increase ROS production (Liu et al., 2014).

Mitochondrial defensive mechanisms include antioxidant enzymes, mitochondrial uncoupling and mitochondrial dynamics. Antioxidant enzymes are involved in protecting mitochondria against ROS (Sena and Chandel, 2012). Several studies have also linked mitochondrial membrane potential to ROS production (Suski et al., 2012). DCM contributes to the increase in IMM potential resulting in high ROS production (Brand et al., 2004). Depolarization of IMM and subsequent limitation of the ROS protect mitochondria by a mechanism known as mitochondrial uncoupling (Arsenijevic et al., 2000). This mechanism is controlled by uncoupling proteins (UCPs). UCP2 and UCP3 are the most UCPs in the heart (McLeod et al., 2005). It has been reported that DCM is associated with an increase of UCPs in many animal models (Murray et al., 2005, Gerber et al., 2006). For example, Murray et al. (2005) reported an increase in cardiac UCP2 and UCP3 levels in $Lepr^{db/db}$ mice. Although mitochondrial

uncoupling leads to higher oxygen consumption with less ATP production, it could protect the mitochondria from ROS. For example, Lepr$^{db/db}$ mice showed an increase of myocardial oxygen consumption associated with ventricular dysfunction (Buchanan et al., 2005). Moreover, Boudina et al. (2007) reported an increase of myocardial oxygen consumption associated with impaired cardiac function. Another defensive mechanism is mitochondrial dynamics which include mitophagy, fission, fusion and biogenesis. However, persisted oxidative stress can overcome mitochondrial quality control and cause dysfunction of the mitochondria and heart.

Mitochondrial dynamics maintain mitochondrial physiological function, quality control and cellular homeostasis. Mitochondrial dynamics include the movement of the mitochondria and the alteration in the size and structure by mitophagy, fission, fusion and biogenesis. Figure 1.3 illustrates these processes. These processes require energy and are controlled by certain proteins. Unlike other cells, mitochondrial dynamics in the cardiomyocytes are restricted and relatively slow due to a large quantity of myofilaments. However, most studies suggest a fundamental role of mitochondrial dynamics in physiological and pathological conditions such as DCM (Hwang and Kim, 2013).

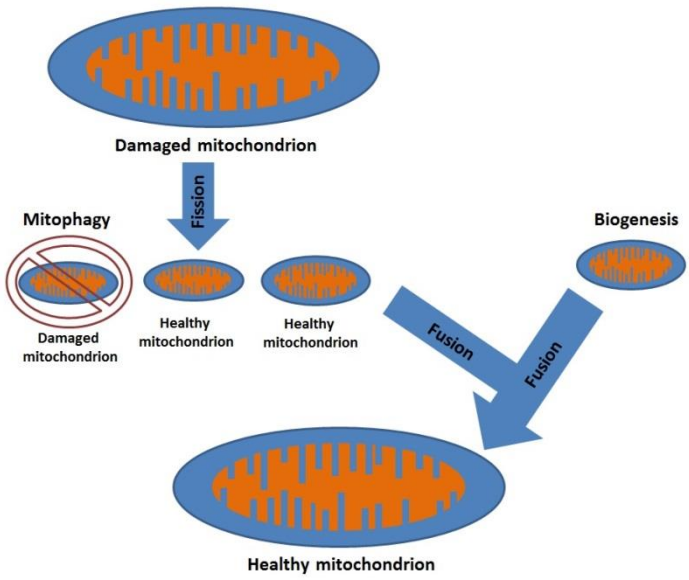

Figure 1.3: Role of mitochondrial dynamics in protection against oxidative stress.
Isolation of damaged mitochondria occurs by fission followed by mitophagy. Healthy mitochondria fuse with a newly synthesized one by fusion.

1.5.1 Mitophagy

Mitophagy is involved with degradation of the damaged mitochondria. PTEN-induced kinase protein 1 (PINK1) and Parkin are believed to regulate mitophagy (Youle and Narendra, 2011,

Okatsu et al., 2012). PINK1 is synthesised in the cytoplasm and is intimately involved with mitophagy (Narendra et al., 2012). The healthy mitochondria import PINK1 into the IMM and cleave it by presenilins-associated rhomboid-like protein (PARL) and other proteases (Jin and Youle, 2012). Depolarized mitochondrial membrane in damaged mitochondria inhibits the import of PINK1. Therefore, accumulation of PINK1 in the OMM phosphorylates OMM proteins which facilitate Parkin recruitment and activation. Parkin activation leads to ubiquitination of the OMM fusion protein, mitofusin 2 (Mfn2) and consequently degradation.

It has been found that Parkin overexpression is associated with amelioration of dysfunctional aged hearts in mice (Hoshino et al., 2013). In addition, Billia et al. (2011) found that swelling of damaged mitochondria was associated with ventricular hypertrophy in PINK1-deficient hearts. However, Parkin-deficient hearts showed an accumulation of disorganized mitochondria without affecting the function in mice (Kubli et al., 2013).

STZ mice showed a decrease in PINK1 and Parkin levels in the heart (Xu et al., 2013). Reduced PINK1 and Parkin could inhibit mitophagy which may contribute to the pathology of DCM. Some medications used in treating heart problem have been reported to initiate mitophagy. For example, Andres et al. (2014) proved that simvastatin provides cardioprotection by triggering Parkin-dependent mitophagy. In addition, both mitophagy and apoptosis are preceded by fission (Westermann, 2010).

1.5.2 Fission and fusion

Mitochondrial quality control includes fission and fusion as fission isolates damaged mitochondria for mitophagy or apoptosis and fusion helps to fuse the mitochondria with a newly synthesised one by biogenesis (Rimbaud et al., 2009). Mitochondrial fusion of the OMM is mediated by mitofusins (Mfn1 and Mfn2) which are present in the OMM, while mitochondrial fusion of the IMM is regulated by optic atrophy 1 (Opa1) which is in the IMM. These proteins contain a GTPase domain, a transmembrane (TM) region and coil-coil (HR1 and HR2) domains. The GTPase domain is responsible for GTP hydrolysis, the TM domain plays a role in tethering proteins to the OMM, and the coil-coil domain is proposed to mediate protein interactions. The HR2 domains of Mfns play a role in tethering before fusion (Koshiba et al., 2004). Mfn1 and Mfn2 have an 80% similar structure (Santel et al., 2003). The GTPase activity in Mfn1 is higher than Mfn2. So, the tethering efficiency is more in Mfn1 (Ishihara et al., 2004). Dilated cardiomyopathy, impaired mitochondrial respiration and marked mitochondrial fragmentation are a feature of murine cardiomyocyte when Mfn1 and

Mfn2 are ablated (Chen et al., 2011b). Mfn2 has other function other than fusion include regulating apoptosis and metabolism (de Brito and Scorrano, 2008). It has been found that Mfn2 plays a role in mitophagy by recruiting Parkin. Mfn2 has to be first phosphorylated by PINK1 for this recruitment to occur (Dorn, 2016). For example, both Parkin recruitment and mitophagy were inhibited in ablated Mfn2 mouse cardiomyocytes with high number of damaged mitochondria (Chen and Dorn, 2013). In addition to the role of Opa1 in fusion, it has a role in preventing apoptosis by inhibiting cytochrome c (Frezza et al., 2006).

Mitochondrial fission is regulated by dynamin-related protein 1 (Drp1), which contains GTPase domain. Drp1 is a cytosolic protein that is recruited to the mitochondria via the cytoskeleton such as microtubules and microfilaments (Varadi et al., 2004, De Vos et al., 2005). Due to the lack of a TM domain in Drp1, it interacts with protein receptors on the OMM that includes fission 1 protein (Fis1), mitochondrial fission factor (Mff) and mitochondrial dynamics protein of 49kDA (MID49) or 51 kDA (MID51). Loson et al. (2013) reported that Fis1, Mff, MID49 and MID51 play a role in Drp1 recruitment. Moreover, MID49 and MID 51 can recruit Drp1 in the absence of Fis1 and Mff. Figure 1.4 illustrates mitochondrial fission and fusion processes.

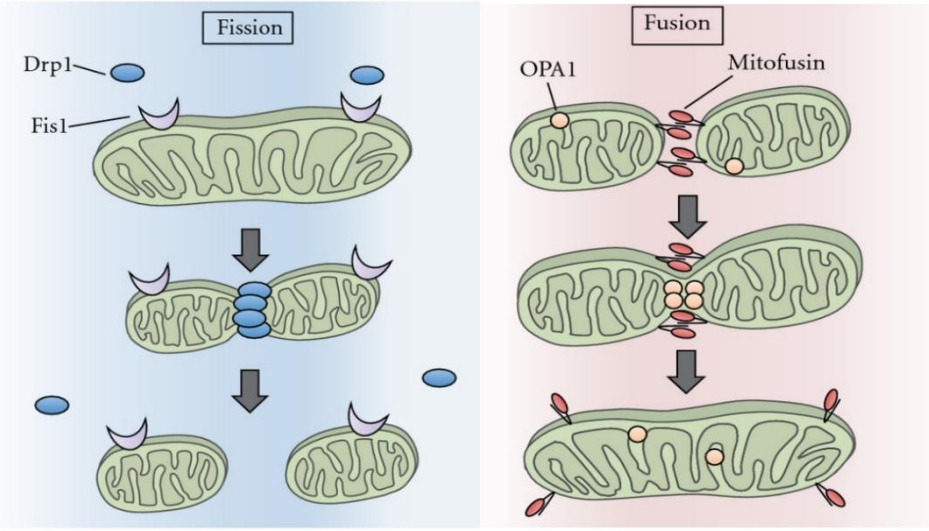

Figure 1.4: Mitochondrial fission and fusion processes.
Mitochondrial fission protein (Drp1) recruited to the mitochondria by different receptors include (Fis1, Mff, MID49 and MID51) resulting in smaller mitochondria. Fusion is mediated by Mfn1, Mfn2 and Opa1 leading to bigger fused mitochondria. Adapted from (Kanamaru et al., 2012).

Alteration in fission and fusion proteins has been associated with mitochondrial dysfunction. For example, *in-vitro* ablation of Opa1 results in impaired mitochondrial respiration and

mitochondrial fragmentation (Song et al., 2009). Watanabe et al. (2014) reported a mitochondrial dysfunction and insulin resistance in overexpressed Drp1 H9C2 myoblasts. Pharmacological inhibitors of Drp1 in murine cardiomyocytes have been reported to be cardioprotective against ischemia/reperfusion injury (Ong et al., 2010). Levels of Opa1 are reported to be decreased in heart failure patients associated with mitochondrial dysfunction (Chen et al., 2009).

Alterations in fission and fusion proteins have been reported in obesity and DM. For example, Montaigne et al. (2014) reported a decrease in the expression of Mfn1 in T2DM human hearts with no alteration of Mfn2, Opa1, Fis1 or Drp1 associated with mitochondrial and contractile dysfunction. Moreover, Mfn1 expression was inversely correlated to glycated haemoglobin (HGBA1C), suggesting that hyperglycaemia is one of the major drivers of mitochondrial dysfunction. In addition, Gao et al. (2012) reported a decrease in the expression of heart Mfn2 in T1DM animal model. In addition, Makino et al. (2010) reported a decreased level of Opa1 and an increased level of Drp1 in diabetic mouse coronary endothelial cells. Reduction in Opa1 levels have been reported in rat neonatal cardiomyocytes treated with high glucose and was associated with mitochondrial dysfunction (Makino et al., 2011). It has been found that some diabetes treatments affect fusion proteins. For example, insulin treatment of rat neonatal cardiomyocytes showed an increase level of Opa1 associated with an improvement in mitochondrial function (Parra et al., 2014). Taken together, impaired fission/fusion in obesity and diabetes could be a cause of cardiovascular complications.

1.5.3 Mitochondrial biogenesis

Mitochondrial homeostasis depends on the balance between mitochondrial biogenesis, fission, fusion and mitophagy (Peng et al., 2016, Palikaras et al., 2015). Mitochondrial biogenesis is a process of synthesising mitochondria and increasing mitochondrial mass resulting in more energy production (Hood, 2009). Assessing mitochondrial biogenesis includes measuring mitochondrial DNA (mtDNA) copy number, Peroxisome proliferator-activated receptor gamma coactivator 1-alpha (PGC-1α) and Mitochondrial transcription Factor A (TFAM) (Medeiros, 2008). PGC-1α is the nuclear transcription factor regulating mitochondrial biogenesis with links to OXPHOS, fission and fusion (Valero, 2014). In addition, expression of antioxidant enzymes have been reported to be increased by PGC-1α upregulation (St-Pierre et al., 2006). Pisano et al. (2016) found a decrease in PGC-1α mtDNA expression that was associated with deranged mitochondrial biogenesis in adult human heart with heart failure. Similarly, Yan et al. (2013) reported a down regulation of PGC-1α and a

decrease in mtDNA copy number in $Lep^{ob/ob}$ mice cardiomyocyte. On the other hand, Boudina and Abel (2006) observed an increase in mtDNA copy number in $Lep^{ob/ob}$ diabetic hearts associated with impaired OXPHOS, suggesting that there is no association between mitochondrial biogenesis and function. In addition, Chandrasekaran et al. (2015) reported an increase in TFAM level associated with an increase of mtDNA in STZ diabetic mice. Taken together, these results could mean that impaired mitochondrial biogenesis in the diabetic heart could contribute to the pathology of DCM.

1.6 Regulators of fission and fusion

1.6.1 Endoplasmic reticulum stress

The endoplasmic reticulum (ER) is an organelle situated in the cytoplasm which supports many functions in human cells. A specialized form of the ER that is called sarcoplasmic reticulum (SR), is present in myocytes (Michalak and Opas, 2009). The SR plays a role in Ca^{2+} storage and transport, therefore, mediating excitation-contraction coupling. The SR may be classified on the basis of structure and function into junctional and longitudinal SR (Rossi et al., 2008). ER/SR both participate in protein-folding that is mediated by specific chaperone proteins (Glembotski, 2012). Accumulation of unfolded proteins causes ER/SR stress, which triggers unfolded protein response (UPR). UPR maintains cell survival by eliminating misfolded proteins, decreasing protein translation and increasing chaperones protein. Pharmacological induction of ER stress was found to be protective against apoptosis by controlling cytosolic Ca^{2+} level (Zhang et al., 2004). Activation of UPR initiates three major signalling pathways: activating transcription factor 6 (ATF6), inositol-requiring enzyme 1 (IRE-1) and protein kinase R-like endoplasmic reticulum kinase (PERK). Normally, Binding immunoglobulin Protein (BiP) is bound to these proteins, which inactivates them. BiP is released in ER stress which activates UPR that in turn activates the three signalling pathways (Xu et al., 2005). Eukaryotic Initiation Factor 2 α (elF2α) is phosphorylated by PERK. This phosphorylation leads to attenuation of mRNA translation and activation of the activating transcription factor 4 (ATF4) to produce more chaperones (Minamino and Kitakaze, 2010). Furthermore, mRNA expressing the x-box binding protein 1 (XBP1) is cleaved by IRE-1, and this produces more chaperones, and degrades misfolded proteins by a mechanism known as endoplasmic reticulum associated protein degradation (ERAD) (Ron and Walter, 2007). There is also the ATF6 pathway whereby ATF6 cleavage regulates transcription of ER chaperones (Minamino and Kitakaze, 2010). These pathways are summarised in Figure 1.5.

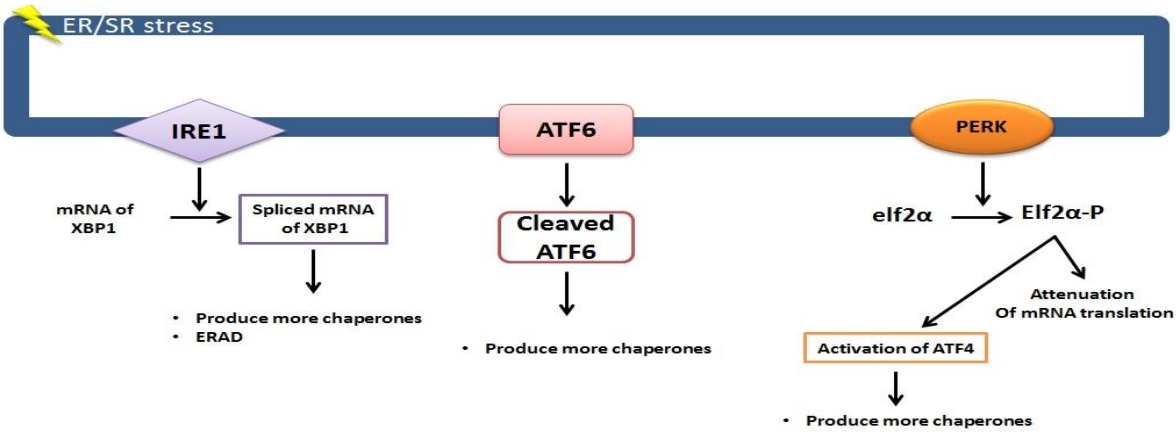

Figure 1.5: Role of ER/SR stress in cell survival.
ER/SR stress activates PERK, ATF6 and IRE1 pathways. The end results of these pathways are decreasing proteins translation, increasing chaperone production and endoplasmic reticulum associated protein degradation (ERAD). (ER/SR, Endoplasmic/Sarcoplasmic; XBP1, x-box binding protein 1).

ER/SR-mitochondria connections mediate crucial processes such as mitochondrial function, Ca^{2+} transfer and mitochondrial fission/fusion (Rowland and Voeltz, 2012). These processes are essential for normal cellular function and survival. The ER/SR has been found to play a role in mitochondrial fission. For example, Friedman et al. (2011) suggested that ER tubules play a significant role in mitochondrial fission by recruiting Drp1 at the ER-mitochondria contact part. Thus, it localizes the site of mitochondrial fission. The role of ER as a site for mitochondrial fission is also supported by Fujioka et al. (2012) who found that SR elements were always related to mitochondrial constrictions sites in rat cardiomyocytes. ER/SR plays a significant role in regulating mitochondrial function and dynamics. Therefore, ER/SR stress could lead to mitochondrial dysfunction.

Obesity has been reported to be an important factor for ER stress and to cause insulin resistance (Boden, 2009). Ozcan et al. (2004) proposed that ER stress associated with obesity and T2DM is the cause for insulin resistance by activation of JNK pathway. In addition, ER stress has been reported to be involved in the pathophysiology of the DCM (Li et al., 2010). Another essential point is that ER stress is considered an early event in the development of cardiac dysfunction in obesity and DM (Yang et al., 2015). ER stress and UPR activation are associated with DCM by three main triggers: hyperglycaemia, free fatty acids (FFA) and inflammation. Hyperglycaemia is responsible for ER stress in DCM by activating PERK and ATF6 pathways (Lakshmanan et al., 2013). Multiple studies have reported saturated fatty acids to cause ER stress (Camacho et al., 2012, Kim et al., 2011, Mayer and Belsham, 2010).

In addition, FFAs have been found to upregulate CHOP and induce cardiomyocyte apoptosis in T1DM mice model (Pulinilkunnil et al., 2013). Diaz et al. (2015) suggested that saturated fatty acids cause Mfn2 downregulation which cause ER stress and lead to insulin resistance. This means that the association of hyperglycaemia and hyperlipidaemia with obesity and T2DM is the main contributor to cardiomyocyte ER stress. In diabetic type 2 rat model, ER stress inhibition by tauroursodeoxycholic acid (TUDCA) prevented heart damage (Miki et al., 2009). This shows the important role of ER stress in the pathogenesis of cardiac complication of obese and T2DM patients.

There is some evidence linking ER stress pathway to mitochondrial fission and fusion proteins. For example, Leboucher et al. (2012) suggested that JNK activation leads to phosphorylation of Mfn2. This results in recruitment of ubiquitin ligase (E3) Huwe1, which degrades Mfn2 resulting in mitochondrial fragmentation and apoptosis. Ablation of Mfn2 in mouse cardiomyocyte has been reported to be associated with ER stress (Ngoh et al., 2012). In the same study, induction of ER stress was associated with overexpression of Mfn2 in mouse embryonic fibroblasts (MEF) while other fission and fusion proteins including Opa1, Mfn1, Fis1 and Drp1 remained the same. These data suggest that there is a link between Mfn2 and ER stress in regulating ER homeostasis. It has been reported that ER stress is associated with mitochondrial dysfunction. For example, Yu et al. (2007) reported that activation of JNK pathway led to mitochondrial respiratory chain damage and mitochondrial dysfunction. Understanding the exact mechanism of how ER stress affects mitochondrial function and dynamics is important to prevent progression of DCM. Therefore, this study will investigate the potential link of ER stress to mitochondrial dynamics.

Taken together, obesity and T2DM is associated with ER/SR stress and mitochondrial dysfunction in the heart. ER/SR stress and mitochondrial dysfunction are considered early events in DCM which could lead to cardiac cell death and subsequent dysfunction. ER/SR stress appears to cause mitochondrial dysfunction by affecting mitochondrial fission and fusion. Another potential regulator of mitochondrial dynamics is prohibitin.

1.6.2 Prohibitins

Prohibitins (PHBs) have received a lot of attention in recent years because of their many functions in the mitochondria, including energy metabolism, apoptosis and proliferation (Signorile et al., 2019). Both PHB1 and 2 form a ring-shaped structure, composed of around 16-20 subunits, located at the inner mitochondrial membrane (Nijtmans et al., 2000). PHB

protein dysfunctions were linked to aging (Artal-Sanz and Tavernarakis, 2009) and metabolic diseases (Supale et al., 2013). The PHBs are associated with the OXPHOS activity regulation. In the absence of PHB1, mitochondrial coded subunits of the respiratory chain were found to be unstable (Bayot et al., 2010).

Loss of Prohibitins is reported to impact upon mitochondrial morphology. For example, Prohibitins ablation in mouse embryonic fibroblasts (MEFs) caused enhanced mitochondrial fission (Merkwirth et al., 2008). A study recently conducted in isolated primary cardiomyocytes showed that miR-361 triggers mitochondrial fission with consequent apoptosis by suppressing PHB1 translation (Wang et al., 2015b). It has been reported that PHB2 stabilizes L-Opa1, and its loss impaired the stability of L-Opa1, which may inhibit mitochondrial fusion process (Merkwirth et al., 2012). Mitochondrial dynamics could also be regulated by sirtuins.

1.6.3 Sirtuins

Sirtuins are a type of signalling proteins that are involved in the regulation of metabolism. Seven sirtuins have been reported in mammals (Sirt1-7). The location of Sirt1, 6 and 7 is in the nucleus, whereas Sirt2 if found in the cytoplasm. Sirt3-5 are located in the mitochondria and are primarily involved in the regulatory processes of energy metabolism (Ye et al., 2017). Sirtuins have deacylase activity, which requires NAD^+, for deacetylation, demalonylation, desuccinylation, deglutarylation, and delipoylation (Mathias et al., 2014, Tan et al., 2014, Hirschey and Zhao, 2015, Du et al., 2011). As the sirtuin function depends mostly on the NAD^+/NADH ratio, it is assumed that this protein family are sensors of the molecular energy status. This could be important within the mitochondria, which have a high number of acylated proteins and contain high amounts of NAD^+ and NADH (Kim et al., 2006, Park et al., 2013).

Sirt5 has been found to deacetylate cytochrome c and peroxiredoxin 1, thus participating in apoptosis, redox regulation and mitochondrial respiration (Schlicker et al., 2008, Fischer et al., 2012, Rauh et al., 2013). Sirt5 functions essentially as a protein lysine desuccinylase (Peng et al., 2011). Rardin et al. (2013) reported that 56% of an identified 1190 succinyllysine sites on 252 proteins were likely targets of Sirt5. Many of these proteins were found in mitochondrial metabolic pathways such as fatty acid oxidation, the TCA cycle, glycolysis and ATP synthesis (Nishida et al., 2015, Park et al., 2013). Sirt5 is highly expressed in the heart (Nishida et al., 2015) and it is downregulated under the condition of

oxidative stress in cardiomyocytes. Knockdown of Sirt5 significantly increases apoptosis of cardiomyocytes (Liu et al., 2013). Taken together, mitochondrial dynamics is potentially regulated by multiple proteins include ER stress, prohibitins and sirtuins.

1.7 The effect of exercise on cardiac function and dynamics

According to World Health Organization (2009) estimation, 27% of diabetes is caused by sedentary lifestyle. Preventing T2DM is achieved by managing obesity by healthy diet and active lifestyle (Lau et al., 2007). One of the most known non-pharmaceutical treatments for this chronic illness is exercise (Nogueira-Ferreira et al., 2016). Exercise has been reported to play a major role in improving cardiac function and, therefore, the extension of life expectancy (Ferreira et al., 2014). Exercise also protects the heart against acute conditions such as myocardial ischemia and infarction (Alleman et al., 2015). In addition, exercise reduces the risk factor for cardiovascular complications associated with obesity and T2DM such as blood pressure, lipid profile, waist circumference, BMI and insulin resistance (Golbidi and Laher, 2012). Obesity and T2DM related cardiovascular complications are preventable. Exercise has been suggested one of the most effective measures to manage obesity, DM and the associated DCM. Whether exercise prevents DCM by affecting the possible mechanisms involved in mitochondrial dysfunction remains to be determined.

1.7.1 Mitochondrial function

Exercise has been found to improve cardiomyocyte mitochondrial function in healthy individuals. For example, Ferreira et al. (2014) observed an improvement in cardiomyocyte mitochondrial respiration through the activity of enzyme complex IV and V from regularly exercised rats. In addition, cardiac mitochondria from mice that underwent swimming showed an increase in mitochondrial number, density, volume and biogenesis (Vettor et al., 2014). This means that exercise could be beneficial for non-diseased heart health. Studies on the beneficial effect of exercise on damaged mitochondria in the heart have been also reported. For example, Hafstad et al. (2013) observed a systolic and diastolic dysfunction in diet-induced obesity mice model, which was reversed by exercise, as it ameliorates mitochondrial dysfunction associated with reduced fibrosis. They also argued that only high intensity exercise can improve glucose intolerance. In addition, Jiang et al. (2014) found an improvement in complex I, III and IV activities and overexpression of PGC-1α after exercise in post MI rats. Moreover, Wang et al. (2015a) demonstrated that regular to moderate intensity exercise increased mitochondrial biogenesis, prevented cardiomyocyte apoptosis and maintained normal cardiac function in the advanced DCM of $Lepr^{db/db}$ mice

hearts. This means that exercise could be cardioprotective even in the severe late stage of DCM. Exercise is also beneficial in damaged mitochondria in that it prevents further complications or restores normal function in various tissues. Lumini et al. (2008) stated that exercise could prevent mitochondrial dysfunction in skeletal muscle caused by obesity or DM by increase mitochondrial biogenesis and attenuate the reduction in UCP3 expression. Skeletal muscle in mitochondrial myopathy patients showed improved function after chronic exercise (Jeppesen et al., 2006). Taken together, this means that exercise counteract mitochondrial dysfunction caused by obesity and subsequently prevent cardiac complications. These studies advocate the non-pharmaceutical treatment of exercise in dysfunctional obese heart mitochondria.

1.7.2 Mitochondrial dynamics

Enhancement of mitochondrial biogenesis in various tissues has been associated with regular exercise in the literature (Hood, 2001). For example, Sutherland et al. (2009) reported an increase in mRNA expression of PGC-1α in white adipose tissue of exercising rats. Furthermore, Little et al. (2010) reported an increase in PGC-1α expression in skeletal muscle of high intensity trained human. It has been found that intensive exercise for three consecutive days increase the mRNA expression of PGC-1α in human skeletal muscle (Dumke et al., 2009). However, Mille-Hamard et al. (2015) argue that expression of mitochondrial biogenesis (PGC-1α) is negatively correlated with exercise intensities in skeletal muscle.

Mitochondrial dynamics have been reported to be altered in normal individuals with exercise. For example, Perry et al. (2010) found that high-intensity exercise increased Mfn1, Fis1 and Drp1 proteins in skeletal muscle of humans. This could mean that exercise make the mitochondria dynamically active by increasing both fission and fusion. Konopka et al. (2014) reported an increase of Mfn1, Mfn2 and Fis1 proteins level with no change to Opa1 level in skeletal muscle of young and old individuals after regular exercise training associated with better aerobic capacity. In regularly trained cyclists, mRNA expression of Mfn1 and Mfn2 were elevated 24 hours post exercise in human skeletal muscle (Cartoni et al., 2005). However, prolonged intense exercise could be detrimental to mitochondria. For example, It has been shown that a single high intensity exercise increased mRNA expressions of Fis1 after 24 hours of the exercise onset in rats skeletal muscle and decreased mRNA expression of Mfns with a reduction in Mfn1 protein levels associated with an increase in ROS (Ding et

al., 2010). This suggests that extreme exercise could lead to metabolic stress and consequently mitochondrial dysfunction.

While less well studied than skeletal muscle, exercise has also been reported to alter mitochondrial dynamics in different cardiac diseases as a defensive mechanism. For example, dysfunctional mitochondria in the cardiac tissue of post-MI rats showed an increase in Mfn2, Opa1 and a decrease in Drp1 associated with improvement of complex I, III and IV activity after exercise (Jiang et al., 2014). This suggest that exercise could restore mitochondrial function by altering mitochondrial dynamics proteins. Exercise has been demonstrated to ameliorate DCM. For example, Givvimani et al. (2015) observed a decrease in Drp1 expression associated with decrease blood pressure (BP), interstitial fibrosis, apoptosis (decrease cytochrome c leakage) and improvement of left ventricular function in moderately exercised $Lepr^{db/db}$ compared to sedentary $Lepr^{db/db}$. Fealy et al. (2014) provided *in vivo* evidence in the skeletal muscle of obese patients that underwent exercise training, there was a decrease in Drp1 activity and an increase in Mfns activity associated with an improvement of insulin sensitivity. In a study on $Lepr^{db/db}$ mice, moderate intensity exercise prevented a decrease in Mfn2/Drp1 ratio in the heart. Although the blood glucose level did not significantly change, an improvement of the heart function had been noted. There was a decrease in the body weight, BP and cardiac fibrosis and an improvement of ejection fraction and oxygen consumption rate (Veeranki et al., 2016). These results mean that moderate exercise could protect the heart from obesity and diabetes-related cardiovascular complications. However, very little is known about the mechanism that exercise regulate mitochondrial dynamics.

Mitophagy has also been reported to be altered in exercise. For example, it has been shown that during acute exercise there is an activation of mitochondrial autophagy by upregulation of beclin1, LC3 and Bnip3 in heart which reduce cardiac damage (Li et al., 2016). Vainshtein et al. (2015) reported an overexpression of Parkin mRNA levels in skeletal muscles following exercise in wild type (WT) mice. On the other hand, Ju et al. (2016) reported no change to transcript levels of PINK1 and Parkin levels, in skeletal muscle of WT mice swimming regularly.

1.7.3 Mitochondrial apoptosis

Mitochondrial apoptosis has been found to be inhibited by exercise. Fernstrom et al. (2004) reported an increase in mitochondrial resistance to Ca^{2+} overload in human skeletal muscle

after an acute exercise. This resistance might help to maintain cardiac function by preventing apoptosis caused by Ca^{2+} overload. For example, mitochondrial apoptotic pathway has been inhibited in cardiomyocyte of exercised rat models by a decrease expression of Bax, Bak and cytochrome C (Hsu et al., 2010). Susceptibility of opening the mitochondrial permeability transition pore (mPTP) in the heart in response to cardiomyotoxicity has been found to be decreased in exercised rats (Ascensao et al., 2011). Furthermore, Marcil et al. (2006) suggested that mPTP in the heart are more resistant to Ca^{2+} overload which induce mPTP and subsequent apoptosis in treadmill running exercised rats.

Exercise has been found to be cardioprotective in normal and abnormal conditions. For example, Pons et al. (2013) found that regularly exercise WT mice had less induced myocardial infarct size by 60% compared to non-exercised corresponding mice, whereas regularly exercised $Lep^{ob/ob}$ obese mice had less myocardial induced infarct size by 67% compared to the non-exercised corresponding mice group. In addition, they found that exercise improved the resistance of mPTP opening to Ca^{2+} in WT and $Lep^{ob/ob}$. Kavazis et al. (2008) mentioned that SSM and IFM isolated mitochondria from hearts of exercised rats were more resistant to ROS-induced apoptosis than sedentary group. In the same study, SSM mitochondria are more resistant to apoptotic stimuli than IFM.

1.8 Conclusion

In summary, obesity and diabetes are both risk factors for the development of cardiovascular disease, with mitochondrial dysfunction playing a key role. The molecular drivers of mitochondrial impairment, specifically mitochondrial dynamics, still remain to be fully resolved particular in the setting of obesity/diabetes. Understanding early pathological changes is important for identifying novel therapeutic targets to prevent disease progression. Therefore, the overall goals of this Thesis research work are:

1. Investigate the cardiac and mitochondrial phenotype (specifically mitochondrial dynamics) in a high fat feeding mouse model.
2. Investigate whether changes to cardiac and mitochondrial function after a period of high fat feeding are reversed restoring the healthy phenotype.
3. Investigate the putative mechanisms regulating mitochondrial fission-fusion, focussing on Sirt5.
4. Large scale analysis of the mitochondrial phenotype from a number of animal models combining exercise and diet.

Chapter 2 Investigation of cardiac mitochondrial function and dynamics in a mouse 60% high-fat diet (DIO) model

2.1 Introduction

Research into the pathogenesis of cardiac diseases in the human heart is difficult due to a limited number of samples. It is mostly exclusively available for specific operations e.g. heart transplant surgery. Therefore, the differences in the severity of the disease, age, other comorbidities, and medications taken by the patient are an issue. Thus, the use of small and large animal models has been a fundamental step forward in clarifying the mechanisms and pathologies that cause cardiac disorders.

The mouse became the ideal model organism to study human cardiac diseases. One of the reasons for this is the fact that 99% of human genes have direct mouse orthologous genes. Another reason is that they have a short life span, so that the researchers can follow the disease at an accelerated time frame. Additionally, they are easy to handle, house in large numbers and less expensive to maintain compared to large animals (Recchia and Lionetti, 2007).

This thesis research employs a high-fat diet (HFD) (DIO) model since there is no genetic modification in HFD (DIO) models, and it provides an accurate model of the human being situation (King, 2012). Obesity in HFD (DIO) models is caused by high-fat diets. The benefits of this model include being able to have a combination of genetic and dietary influences at the same time. Also, the length of high-fat diet feeding can be controlled. It may also be a fast method to induce obesity and it resembles western diet which is high in fat. Overall, there is a notable similarity to human obesity, and it is cost-effective (Suleiman et al., 2020).

Diet-induced obesity includes 45% and 60% fat by calories. On the 45% fat diet, mice become obese, as well as mice on the 60% fat diet do so faster with more gain-weight. It is convenient because it shortens the time needed to house the animals, thus reducing cage expenses. Takahashi et al. (1999) investigated the linear relationship between dietary fat and glucose tolerance by using C57BL/6J mice which were fed various percentages of fat calories for 15 weeks (10, 20, 30, 40, 50, and 60% of total daily energy). Following a 12-week diet, a noticeable impairment of glucose tolerance was reported in those diets containing more than 40% fat indicating a linear relationship between dietary fat and glucose tolerance.

Hu et al. (2018) assessed several nutritional diets on adiposity. They investigated 29 types of diets ranging from 10 to 80% carbohydrate, 5 to 30% protein and 8 to 80% fat on C57BL/6J mice. The only increased dietary content that was associated with adiposity was the fat with a peak reached at 50-60% fat content. However, some reports have not identified such differences (Mundy et al., 2007, Morrison et al., 2010). One factor for this inconsistency is the age of mice at the beginning of introducing the high-fat diet, as in Hu study the age of mice were 10 weeks old while in Morrison study were 20-months old which is a huge difference.

Another controlling factor is the duration of the high-fat diet. For example, Chen et al. (2018) reported cardiac systolic dysfunction illustrated by a decrease in ejection fraction and fractional shortening which were assessed by transthoracic echocardiography in Sprague-Dawley rats fed 60% HFD (DIO) for 28 weeks in concomitant with cardiac hypertrophy. Also, Fang et al. (2008) fed mice for 6 months 45% HFD (DIO) found a decrease in fractional shortening (systolic dysfunction) with evidence of cardiac hypertrophy. Moreover, Sokolova et al. (2019) found a reduction in systolic function by a decrease in longitudinal strain assessed by cardiac MRI analysis in 60% HFD (DIO) fed C57BL/6J mice for 52 weeks. These studies have reported a middle to late-stage DCM as categorised by Fang et al. (2004). Here we chose a 12-week HFD (DIO) feeding regimen to understand early pathology of DCM.

The aims for this chapter include the following:

1) Characterise the cardiac phenotype after HFD (DIO) feeding.
2) Investigate mitochondrial function and dynamics in the HFD (DIO) mouse myocardium.

2.2 Methods

2.2.1 Mouse model of obesity

The Personal license has been granted by the Home Office in order to perform regulated procedures on laboratory animals. Procedures on animals adhered to the United Kingdom Animals Scientific Procedures Act 1986 and fulfilled guidelines from the University of Manchester Ethics Committee. The project license holder is Elizabeth Cartwright (P3A97F3D1).

7-week-old C57BL/6J male mice were obtained from Envigo. They were left for acclimatization for 1 week prior to the start of the experiment. They were randomized into two dietary groups starting at the age of 8 weeks: high-fat diet (60% calories from fat, 20% calories from protein and 20% calories from carbohydrates) (Special Diet Services, UK, code: 824054) or control diet "chow diet" (13% calories from fat, 22% calories from protein and 65% calories from carbohydrate) for 12 weeks. Mice were housed under designated establishment for animal scientific procedures. Mice were maintained on a constant 12-hour light-dark cycle and a specific pathogen-free environment. The exclusion criteria include all HFD (DIO) mice with a bodyweight increase of under 10% when compared to controls (Hariri and Thibault, 2010). At the end of the experiment, mice were euthanized with cervical dislocation followed by decapitation (Schedule 1). The heart was excised afterwards and chopped for different types of analysis. Figure 2.1 demonstrates the mouse heart anatomy.

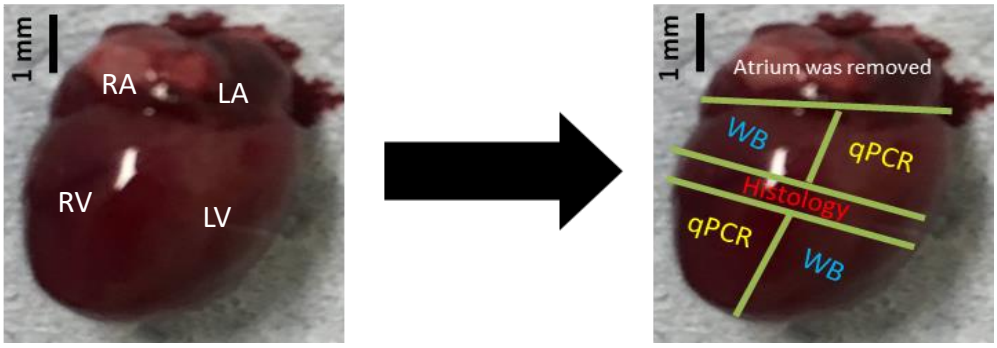

Figure 2.1: The posterior view of the mouse heart.
Heart was separated into sections for the different types of analyses.
Scale bar = 1 mm. RA= right atrium, LA= left atrium, RV= right ventricle, LV= left ventricle.

2.2.2 Physiological and metabolic parameters measurement

Bodyweight was measured at baseline and monthly. Overnight fasted blood glucose was obtained by pricking the lateral tail vein at the end of the experiment (Accu-Chek Aviva). Training in using echocardiography has been received by Dr Min Zi who is gratefully acknowledged for also collecting the echo data. Echocardiography and electrocardiography (ECG) were performed under nonterminal inhalational anaesthesia (isoflurane). Mice were placed on a warming pad (37°C) to maintain body temperature. Blood was collected from the jugular vein by a terminal procedure for lipid profile and insulin level. Blood was left to clot in the fridge for 4 hours and then spun at 5,000 rcf for 10 minutes. The top serum layer was collected and stored at 80°C until further use.

2.2.2.1 Insulin assay kit

Insulin intensity was assessed using a mouse insulin enzyme-linked immunosorbent assay (ELISA) kit manufactured by ALPCO (80-INSMS-E01). The samples, controls and standards were added to a 96-well plate pre-coated with anti-insulin antibodies. After adding the conjugate to each well, the plate was incubated on a microplate shaker for 2 hours at 700-900 rpm. The wells were washed 6 times with a washing buffer. Visualizing reagent 3,3′,5,5′-Tetramethylbenzidine (TMB) was added to each well and then the plate was incubated on a microplate shaker for 15 minutes at 700-900 rpm. After incubation, a stopping solution was added to measure the optical density using a plate reader at 450 nm. The optical density is proportional to the concentration of insulin. The concentration of insulin was extrapolated from a sigmoidal standard curve as per the kit manufacturer's instructions.

2.2.2.2 HDL and LDL/VLDL

Serum was used to quantify high-density lipoproteins (HDL), low-density lipoproteins (LDL) and very-low-density lipoproteins (VLDL) by an assay Kit from Abcam (ab65390). In this experiment, free cholesterol is recognized and quantified by one of its products which generate colour (570 nm) after reacting with a probe. The first step in this process was to separate HDL and LDL/VLDL. The serum was mixed with the same volume of 2X precipitation buffer and incubated for 10 minutes at room temperature. After the incubation, samples were centrifuged at 2,000 rcf for 10 minutes. Supernatant which is the HDL was transferred into a new tube. The precipitate which is the LDL/VLDL fraction was resuspended by 200 µl phosphate-buffered saline (PBS). 50 µl of standards, controls and samples were loaded into 96-well plate with 50 µl of total cholesterol reaction mixture (Cholesterol assay buffer, cholesterol probe, enzyme mix and cholesterol esterase). The plate

was mixed and incubated protected from light for 60 minutes at 37°C prior to measuring absorbance at 570 nm. The cholesterol concentration was extrapolated from a linear standard curve.

2.2.2.3 Triglyceride assay kit

To quantify triglyceride concentration, a Triglyceride Colorimetric Assay Kit was used (Cayman Chemical 10010303). This assay measures triglyceride by a series of reactions as follows.

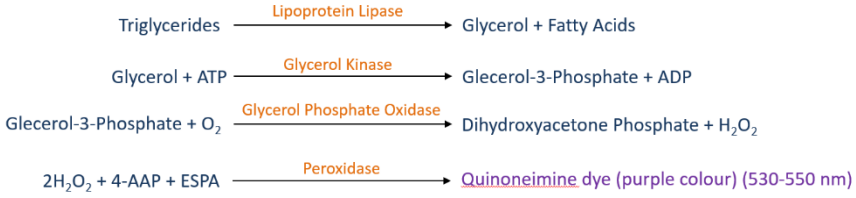

In this assay, 10 µl of serial diluted standards and samples were added to the 96-well plate. To initiate the reaction, 150 µl of diluted enzyme mixture was added to each well. The plate was covered and incubated at room temperature for 15 minutes before reading absorbance at 540 nm. The total cholesterol concentration was calculated by the following Friedewald equation (all concentration unit in mg/dl).

$$\text{Total cholesterol} = [\text{LDL\&VLDL} + \text{HDL} + (\text{Triglyceride} / 5)]$$

2.2.2.4 Echocardiography

Depilatory cream was used to remove the chest hair of the mice. A transthoracic echocardiogram was done using Acuson Sequoia 256 cardiac ultrasound system with 15L8 transducer probe set to 14MHz. Before placing the probe on the thorax, the probe was covered by warm transmission gel (Henleys Medical). Chamber dimensions include Diastolic Left Ventricular Diameter (dLVD), Systolic Left Ventricular Diameter (sLVD), Diastolic Interventricular Septum (dIVS), Systolic Interventricular Septum (sIVS) and Diastolic Posterior Wall (dPW) thickness were measured using M-Mode (Figure 2.2). Formulae listed in Table 2.1 were used to calculate other parameters.

Table 2.1: Echocardiography parameters formula.
dLVD, diastolic left Ventricular Diameter. dPW, diastolic posterior wall. dIVS, diastolic interventricular septum. sLVD, systolic left ventricular diameter.

Parameter	Formula
Ejection fraction (EF%)	[(dVol - sVol)/dVol] x100
Fractional shortening (FS%)	[(dLVD-sLVD)/dLVD] x 100
Relative wall thickness (RWT)	(dIVS+dPW)/dLVD
Left ventricular mass (LVM)	1.055 x [(dLVD+dPW+dIVS)^3 – dLVD^3]

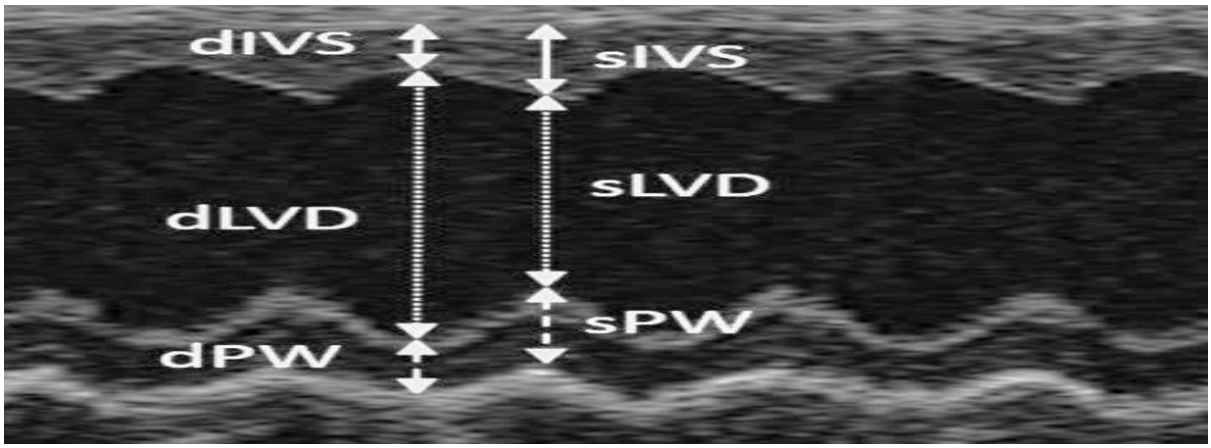

Figure 2.2: Echocardiography of control mouse heart.
Representative image (M-Mode) used for measurement of wall thicknesses. dIVS, diastolic interventricular septum. dLVD, diastolic left ventricular diameter. dPW, diastolic posterior wall. sIVS, systolic interventricular septum. sLVD, systolic left ventricular diameter. sPW, systolic posterior wall.

2.2.2.5 Electrocardiography

During unconscious electrocardiography (ECG), mice were placed on a warm pad after being anaesthetised to maintain the body temperature. Electrodes were inserted into the right and left forelimb muscles, and right hindlimb muscle. After that, ECG traces were recorded for 10 minutes using the PowerLab system (AD Instruments). Non-invasive conscious (without anaesthesia) ECG traces were recorded using ECGenie (Mouse Specifics). LabChart 7 (AD Instruments) was used to analyse both data (Figure 2.3). Corrected QT interval was calculated using Bazett's formula ($QT_c = \frac{QT}{\sqrt{(RR)}}$).

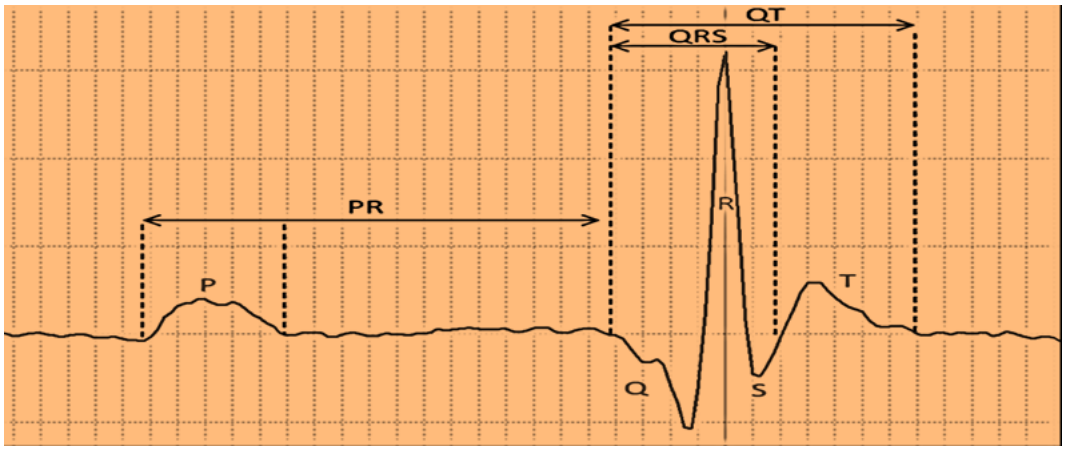

Figure 2.3: Electrocardiography of control mouse heart.
Representative image used to measure waves length. P wave represents atrium depolarization whereas QRS complex represents the ventricular depolarization. PR interval represents the atrioventricular node conduction time.

2.2.3 Western blotting

2.2.3.1 Homogenization and protein extraction

Lysis buffer was prepared by adding one protease inhibitor tablet (Roche) to 10 ml RIPA buffer (Sigma). 2 ml lysis buffer was added to 0.2 - 0.3 g of the mouse ventricles and then added to the metal bead lysing matrix tube (MP Biomedicals). Homogenization was carried out using the FastPrep-24 5G homogenizer (MP Biomedicals). A pre-programmed optimized protocol for mouse heart lysis was used. The homogenate was centrifuged at 8,000 rcf for 10 minutes at 4^{o}C to get rid of cell fragments.

Total protein was quantified using the Bradford assay (Bio-Rad Laboratories) where Coomassie Brilliant Blue G-250 dye binds to the proteins and shifts the absorbance to 595 nm. A spectrophotometer (Jenway 6305) was used to measure the wavelength at 595 nm of the sample after first zeroing the machine with buffer. Typically, 10 µl of tissue lysate was added to 990 µl of Bradford reagent for a total volume of 1 ml. A series of diluted bovine serum albumin (BSA) standard (0-2 mg/ml) were first analysed to generate a standard curve. To determine the concentration of the protein content of the tissue lysate, the standard curve was extrapolated with the reading then adjusted for the appropriate dilution factor.

2.2.3.2 Sodium dodecyl sulphate-polyacrylamide gel electrophoresis and Western blotting

10 μg of the lysed mouse ventricles was diluted with 5x Laemmli buffer [320 mM Tris (PH = 6.8), 5% (w/v) sodium dodecyl sulphate, 25% (v/v) glycerol, 5% (v/v) beta-mercaptoethanol and 0.1% (w/v) bromophenol blue], then heated at 90^{o}C for 10 minutes or 60^{o}C for 20 minutes. Sodium dodecyl sulphate-polyacrylamide gel electrophoresis (SDS-PAGE) was used to separate the proteins according to the molecular weight. 10 μg of each sample was loaded into 10% SDS-polyacrylamide gel and was run electrophoretically in 1x running buffer (25mM Tris, 119mM glycine and 3.5mM SDS). To visualise the protein bands a stain-free image of the gel was taken using the ChemiDoc XRS+ imaging system (Bio-Rad Laboratories). Proteins were then transferred onto low fluorescence polyvinylidene difluoride (PVDF) membrane using a Trans-Blot Turbo Blotting System (Bio-Rad Laboratories). The protein bands transferred were analysed again using a stain-free image of the membrane. The membrane was then blocked to prevent nonspecific binding for an hour with 5% (w/v) non-fat dry milk in Tris-buffered saline and Tween-20 (TBST) [10mM Tris, 150 mM NaCl and 0.1% (v/v) tween 20]. After that, membranes were incubated with primary antibody (Table 2.2) either overnight or 1 hour at 4^{o}C. Following incubation, membranes were washed three times with TBST for 5 minutes each. Membranes were then incubated for 1 hour at room temperature with appropriate secondary antibody listed in Table 2.2.

Table 2.2: Primary and secondary antibodies list.

Primary Antibody	Dilution	Manufacturer	Secondary Antibody	Dilution	Manufacturer
Drp1	1:1000	Santa Cruz	Anti-Rabbit HRP	1:3000	Bio-Rad
Opa1	1:3000	Santa Cruz	Anti-Goat HRP	1:3000	Santa Cruz
Mfn1	1:1000	Abcam	Anti-Mouse HRP	1:3000	Bio-Rad
Mfn2	1:3000	Abcam	Anti-Rabbit HRP	1:3000	Bio-Rad
Phospho-DRP1 (Ser637)	1:2000	Cell Signaling Technology	Anti-Rabbit HRP	1:3000	Bio-Rad
Phospho-DRP1 (Ser616)	1:2000	Cell Signaling Technology	Anti-Rabbit HRP	1:3000	Bio-Rad
Mff	1:2000	Abcam	Anti-Rabbit HRP	1:3000	Bio-Rad
MID49	1:1000	ThermoFisher	Anti-Rabbit HRP	1:3000	Bio-Rad

MID51	1:2000	ThermoFisher	Anti-Rabbit HRP	1:3000	Bio-Rad
Fis1	1:2000	Proteintech	Anti-Rabbit HRP	1:3000	Bio-Rad
PINK1	1:1000	Santa Cruz	Anti-Rabbit HRP	1:3000	Bio-Rad
Parkin	1:5000	Abcam	Anti-Mouse HRP	1:3000	Bio-Rad

Clarity Western ECL Blotting Substrate kit (Bio-Rad Laboratories) was used for chemiluminescent Western blot detection. Briefly, Substrate kit components were mixed in a 1:1 ratio. The membrane was placed in the mixture for 4 minutes in the absence of light. ChemiDoc XRS+ system imaging (Bio-Rad Laboratories) was used to detect chemiluminescent signal. Total protein normalisation, also known as, stain-free technology, was used to accurately compare protein signals (Gurtler et al., 2013). Proteins signals were normalised to total protein loaded. This technique is termed 'total protein Western blotting' and instead of using a single housekeeping protein the total amount of protein loaded and transferred is used to standardise each sample (see Figure 2.4). This technique has the advantage that when comparing protein expression in disease animals the dependency upon one housekeeping protein, which may also change, is removed. Additionally, house-keeping proteins are often highly expressed and upon developing can skew the dynamic range. All gels were run in technical triplicates. Fold change relative to control was used to describe protein expression.

A

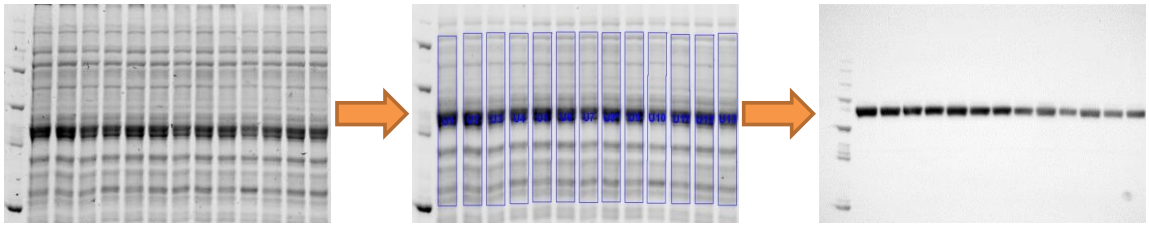

B

Label	Total Protein	Band density	Intensity	Mean	Intensity / Control Mean	Average intensity
HFD						
H1	1.08	7,579,063.20	7028408.481		2.17	1.66
H2	1.08	7,037,118.48	6541829.986		2.02	
H3	0.92	3,749,480.56	4084152.334	HFD	1.26	
H4	0.93	4,920,268.91	5277537.061	5370572.193	1.63	
H5	1.02	5,331,077.33	5209462.433		1.61	
H6	1.03	4,396,097.68	4285723.17		1.32	
H7	0.91	4,691,512.00	5166891.888		1.60	
Control						
L9	1.00	2,614,127.92	2614127.923		0.81	1
L10	0.93	3,494,330.34	3763787.413		1.16	
L11	0.80	2,671,300.75	3341774.294	Control	1.03	
L12	0.92	3,438,440.27	3756766.089	3235785.243	1.16	
L13	0.96	2,386,859.64	2488645.226		0.77	
L14	0.92	3,163,389.43	3449610.512		1.07	

Figure 2.4: Total protein normalisation in Western blot analysis.
A. Steps involved in Western blotting. B. Table illustrating Western blot analysis by total protein normalisation.

2.2.4 Gene expression

2.2.4.1 RNA extraction

500 µl of Trizol was added to two-quarters of frozen heart tissue in a tube and homogenised using electrical tissue grinder (IKA RW 16 basic). Homogenates were incubated at room temperature for 15 minutes. 200 µl of chloroform was added to the homogenate and were shaken for 15 seconds and incubated for 2 minutes at room temperature. The mixture was then centrifuged at 9184 rcf for 15 minutes at 4^{o}C. The supernatant aqueous phase was transferred to a new Eppendorf tube already containing 250 µl isopropanol. The tubes were inverted 30 times and left for 10 minutes at room temperature. Next, tubes were centrifuged 15,521 rcf for 10 minutes at 4^{o}C. The white pellet was then washed with 125 µl 75% (v/v) ethanol and centrifuged again at 15,521 rcf for 10 minutes at 4^{o}C. The pellet was resuspended in 60 µl RNase free water. Quantification of RNA concentration was measured using the Nanodrop 1000 spectrophotometer (ThermoFisher) at a wavelength of 260 nm. RNA purity was assessed by the A260/A280 ratio. Samples were stored at -80^{o}C until further use.

2.2.4.2 DNase treatment

For RNA purification, DNase I, Amplification Grade (Invitrogen^{TM}) was used to degrade DNA. 1 µl DNase I and 1 µl 10X DNase I reaction buffer were added to 1 µg RNA. RNase free water was added to get to the final volume 10 µl. The mixture was incubated for 15 minutes at room temperature prior to stopping the reaction by adding 1 µl 25mM EDTA and another incubating for 10 minutes at 70^{o}C.

2.2.4.3 Reverse transcription

cDNA was synthesised using High-Capacity cDNA Reverse Transcription Kit (Applied Biosystems). Reverse transcription master mix was prepared as illustrated in Table 2.3. RNase free water was added instead of the reverse transcriptase enzyme in the negative reverse transcription control.

Table 2.3: Reverse transcription master mix.

Component	**Volume per reaction (µl)**
RNase free water	4.2
10X Random primers	2
10X RT buffer	2
MultiScribe Reverse Transcriptase	1
25X dNTP Mix	0.8
Total per reaction	10

10 µl of the master mix was added to 1 µg RNA sample in a PCR tube. After that, PCR tubes were loaded to PCR thermal cycler (MJ Research PTC-200). Thermal Cycler was programmed as described in Table 2.4. cDNA was diluted 1 in 5 and then stored at -20°C until further use.

Table 2.4: Thermal cycler set up.

Step	Time (minutes)	Temperature (°C)
1	10	25
2	120	37
3	5	85
4	∞	4

2.2.4.4 Quantitative Polymerase chain Reaction (qPCR)

qPCR was used to determine the transcript expression changes. Amplification of a targeted gene was done by using specific primers, summarized in Table 2.5.

Table 2.5: List of primer assay for mitochondrial dynamics.

Function	Target gene	Primer	Supplier	Catalogue number
Fission	Opa1	Mm_Opa1_1_SG	Qiagen	QT00162085
	Drp1	Mm_Dnm1L_2_SG	Qiagen	QT01166809
Fusion	Mfn1	Mm_Mfn1_1_SG	Qiagen	QT00167839
	Mfn2	Mm_Mfn2_1_SG	Qiagen	QT00134295
Housekeeping	Gapdh	Mm_Gapdh_3_SG	Qiagen	QT01658692
Mitochondrial biogenesis	PGC1- α	Mm_Ppargc1a_1_SG	Qiagen	QT00156303
	TFAM	Mm_Tfam_1_SG	Qiagen	QT00154413
Mitophagy	PINK1	Mm_Pink1_1_SG	Qiagen	QT00111349
	Parkin	Mm_LOC641034_1_SG	Qiagen	QT01278823
Drp1 receptors	MID49	Mm_Mief2_2_SG	Qiagen	QT01077776
	MID51	Mm_Mief1_1_SG	Qiagen	QT00163443
	Mff	Mm_Mff_1_SG	Qiagen	QT00174125

qPCR reactions were prepared using Brilliant III Ultra-Fast SYBR Green qPCR Master Mix (Agilent Technologies) as illustrated in Table 2.6.

Table 2.6 : Composition of qPCR reaction mixture.

Ingredients (composition)	Volume (μl)
2× Brilliant III Ultra-Fast SYBR Green QPCR Master Mix	5
RNase free water	2.85
Primer	1
Reference dye, 1mM (diluted 1:500)	0.15
Total	9

Each reaction has 1 μl cDNA and 9 μl qPCR reaction mix. Samples, negative RT controls and RNase free water were loaded onto 96-well plate in triplicate. Water control was used to exclude primer-dimer amplification. Negative RT controls were analysed to determine DNA contamination. Plates were analysed in duplicate to assess between-run variation. The plates run on a 7500 Fast Real-Time PCR instrument using the amplification cycle are listed in Table 2.7. The Livak method was used for analysis. The housekeeping gene GAPDH was used for normalisation, as previous lab members had evaluated different housekeeping genes and found GAPDH to be most reliable. In addition, Perez et al. (2017) examined the stability of 15 reference genes based on RT-qPCR for obese/diabetic heart and found that GAPDH is one of the most stable reference gene.

Table 2.7: Real-time PCR thermal cycling conditions.

Stage	Number of cycles	Temperature(°C)	Time
Holding	1	95	3 minutes
Cycling	40	95	5 seconds
		60	25 seconds
Melt curve	1	95	15 seconds
		60	1 minutes
		95	15 seconds
		60	15 seconds
Holding		4	∞

2.2.5 Mitochondrial respiration

2.2.5.1 Mitochondrial isolation

Mitochondria were isolated from mice heart using a Mitochondrial Isolation Kit for Tissue (Abcam, ab110168). Typically, 0.2-0.3 g tissue was washed three times with wash buffer. The tissue was then minced and homogenized manually by 40 strokes in pre-chilled Dounce tissue grinder with 2 ml isolation buffer. The homogenate was transferred into 2 ml tube and made up to 2 ml with isolation buffer. The homogenate was then spun down at 1,000 rcf for 15 minutes at 4^{o}C, after which the supernatant was divided between 2 tubes which were again made up to 2 ml with isolation buffer, and then centrifuged at 12,000 rcf for 15 minutes at 4^{o}C. Supernatants were discarded and pellets then washed with 1 ml isolation buffer supplemented with protease inhibitors (Sigma) and then centrifuged at 12,000 rcf for 15 minutes at 4^{o}C. The pellets were collected, resuspended, and centrifuged again. Pellets were then combined and resuspended in 500 µl of isolation buffer supplemented with protease inhibitors. Aliquots were taken immediately for measuring oxygen consumption rates or complexes activity.

2.2.5.2 Mitochondrial oxygen consumption rate

Oxygen consumption rate (OCR) was measured using fibre optic oxygen measurement (Instech). After isolating the mitochondria, 100 µl of the mitochondria [final concentration = 0.25 mg /ml, diluted with OCR buffer (210 mM mannitol, 70 mM sucrose, 5 mM KH2PO4, 0.5 mg/ml BSA and 10 mM MOPS, PH = 7.4)] were added to the chamber, followed by the addition of 5 µl of each substrate, pyruvate, malate, glutamate, ADP and succinate. The stock solutions for the substrates are (2000 mM, 400 mM, 2000 mM, 500 mM and 1000 mM, respectively). The OCR machine was initially calibrated and oxygen consumption recorded until the oxygen reached zero per cent. Readings were done in technical triplicate. Rate was measured after adding all the substrates for 5 minutes by the following equation:

$$\text{Slope}=\frac{\Delta y}{\Delta x}=\frac{Change\ in\ oxygen\ percentage\ (\%)}{Change\ in\ time\ (minutes)}=rate=\frac{(rate\ per\ minute)}{Mitochondrial\ concentration\ (mg)}=\text{ rate/min/mg}$$

3 µl of 10 mM Carbonyl cyanide-4-(trifluoromethoxy)phenylhydrazone (FCCP) “mitochondrial oxidative phosphorylation uncoupler” were added to assess the mitochondrial respiration during stress.

2.2.5.3 Complex I

Mitochondrial respiratory complexes were measured individually by enzymatic colorimetric function assay. Isolated mitochondria (method 2.2.5.1) were used in the following complexes assay (I, II, IV and V).

In this assay (Abcam, ab109721), proteins were extracted by adding 10x detergent solution. Following this, it was incubated for 30 minutes on ice. The mixture was then centrifuged at 16,000 rcf at 4°C for 20 minutes. The supernatant was transferred to a new tube and then protein concentration was measured by BFA (method 2.2.3.1). Samples were then diluted to 0.1mg/ml before loading 200 µl into MaxiSorp™ modular microplate. The plate was then incubated at room temperature for 3 hours. After the incubation, the plate was washed 3 times. 200 µl Assay solution (1x dilution buffer, 20x NADH, 100x dye) was then added to each well. The changes in the optical density at 450 nm for 30 minutes at room temperature was monitored by FLUOstar® Omega microplate reader (BMG Labtech).

2.2.5.4 Complex II

Proteins were extracted from isolated mitochondria and diluted to 0.1 mg/ml as described above (method 2.2.5.3). Samples and background were added to the pre-coated wells (Abcam, ab109908) and were incubated at room temperature for 2 hours in the dark. The plate was then washed 2 times. After the wash, 40 µl of lipid mixture was added to each well and the plate was incubated for 30 minutes. After the incubation, 200 µl of activity solution (Ubiquinone, Succinate, DCPIP and activity buffer) were added on top of lipid mixture. The change in the absorbance in 60 minutes at 600 nm at room temperature was then measured using FLUOstar® Omega microplate reader (BMG Labtech).

2.2.5.6 Complex IV

In this assay (ab109911), the activity of cytochrome c oxidase enzyme is determined. Proteins were extracted from mitochondrial isolation as described above (method 2.2.5.3). Samples were then added to pre-coated wells and incubated for 3 hours at room temperature. Wells were washed twice and then assay solution (Reduced cytochrome c and buffer solution) was added to wells. The changes in the absorbance in 2 hours at 30°C was measured using FLUOstar® Omega microplate reader (BMG Labtech).

2.2.5.7 Complex V

Proteins were extracted from the samples as described above (method 2.2.5.3). Proteins were added to the pre-coated wells (Abcam, ab109716) and left incubating at room temperature for

3 hours. Wells were rinsed twice with water. The plate was incubated again with lipid mix for 45 minutes. After the incubation, the reagent mix was added to each well. The activity was measured by monitoring the change in absorbance at 30°C for 2 hours at 340 nm using FLUOstar® Omega microplate reader (BMG Labtech).

2.2.5.8 Citrate synthase activity

Mitochondrial protein is commonly normalized to citrate synthase activity (CS). MitoCheck® kit (Cayman Chemical) was used to detect citrate synthase activity. To measure CS activity, the production of 5-thio-2-nitrobenzoic acid (TNB) after a coupled reaction, as shown in Figure 2.5, was monitored by measuring the absorbance at 412 nm. TNB is the product of 5, 5'-dithiobis-(2-nitrobenzoic acid (DTNB) reacting with coenzyme A (CoASH). The latter is a product of acetyl CoA reacting with Oxaloacetate regulated by CS.

The first step in this process was to prepare two Mixtures, A and B. Mixture A contains 960 µl of Assay buffer, 20 µl of Developer reagent and 20 µl of Acetyl-CoA and Mixture B contains 480 µl of Assay buffer and 20 µl of Oxaloacetate reagent. 50 µl of Mixture A were added to each well followed by adding 20 µl of diluted isolated mitochondria (1:200). Once the mitochondrial isolations were added, the plate was centrifuged quickly to remove bubbles. To start the reaction, 20 µl of mixture B was added to each well. The plate was placed immediately on a plate reader to monitor the reaction for 20 minutes at 25°C by measuring absorbance at 412 nm.

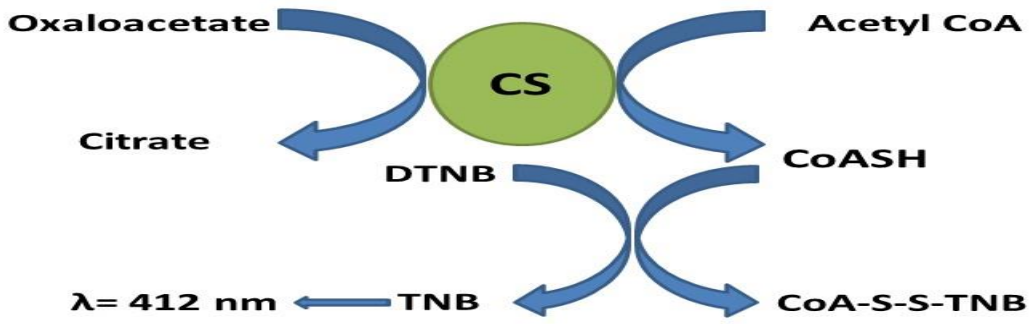

Figure 2.5: Citrate synthase activity reactions.

TNB, 5-thio-2-nitrobenzoic acid. DTNB, 5, 5'-dithiobis-(2-nitrobenzoic acid). CoASH, coenzyme A.

2.2.6 Histology

Fixation of the ventricle is to preserve cells and morphology. This was done by immersion in 4% (v/v) paraformaldehyde (PFA) and incubation for 24 hours at 4°C followed by immersion in 70% (v/v) ethanol for 24-72 hours at 4°C. The routine overnight run in the enclosed tissue processor (Leica ASP300S) was used to infiltrate paraffin wax overnight by removing PFA and a process of dehydration. Tissues were then embedded vertically in paraffin wax into histology cassettes.

For sectioning, Leica RM2155 microtome was used to cross-section 5-micron paraffin ribbon which was transferred to float on a water bath at 37°C. This is followed by transferring ribbon sections to polysine adhesion slides (ThermoFisher). The slides were left to dry in the oven 37°C overnight and then stored at room temperature until further use.

2.2.6.1 Haematoxylin and eosin satin

Haematoxylin & eosin (H&E) staining is used to measure cardiomyocyte size. Slides were stained by H&E using Leica ST5010-CV5030. Slides were dewaxed by heating and then immersed in xylene to remove melted wax. For rehydration, descending dilutions of IMS was used (100%, 90% and 75%) (v/v) respectively prior to washing with distilled water. Harris' haematoxylin was used to stain cell nuclei for 5 minutes and then washed with distilled water. After that, slides were immersed in acid alcohol for 10 seconds and then rinsed in distilled water. Slides were then immersed in Eosin for 2 minutes to stain cytoplasm and then rinsed with distilled water. For dehydration, ascending solutions of IMS were used (90%, 95% and 100%) (v/v) respectively before immersion in xylene for 30 minutes. Sections were then mounted with DPX (Distryne, plasticizer and xylene). To image the slides, Panoramic 250 Flash II slide scanner (3D Histech) was used. Average cell size was calculated after randomly measuring surface area for 100 cells in the cross-section of ventricles using Case viewer software (version 2.3, 3D Histech).

2.2.6.2 Masson's trichrome stain

Interstitial and perivascular fibrosis was assessed by using Masson's trichrome staining to detect collagen fibres deposition. Slides were dewaxed on a heat block. The steps of staining are summarised in Table 7.1 (Appendix 1).

Slides were then mounted using DPX mountant and covered with coverslips. Panoramic 250 Flash II slide scanner (3D Histech) was used to image sections and then the percentage of fibrosis was calculated using case viewer (version 2.3, 3D Histech).

2.2.6.3 TUNEL assay

Terminal deoxynucleotidyl transferase dUTP nick end labelling (TUNEL) assay is used to detect apoptotic DNA fragmentation by a specific dye labelling DNA strand break. Initially, the slides were dewaxed and then rehydrated by xylene and descending dilution of IMS (100%, 75% and 50%) (v/v). Following this, it was placed in 3% (v/v) H_2O_2 for 15 minutes and then washed once with distilled water and twice with PBS for 5 minutes each. For permeabilization, each section was incubated in 40 µl of proteinase K (20 µg/ml) at 37°C for 15 minutes. It was permeabilised for the second time by 0.1% (v/v) Triton X and 0.1% (v/v) Sodium citrate at room temperature for 8 minutes and then washed twice with PBS. After that, it was placed in the enzyme solution mixed with label solution (Roche) for an hour at 37°C. 1% (v/v) bovine serum albumin (BSA) was used to block the sections at room temperature for an hour. It was then incubated in a primary antibody cardiac troponin T (cTnT) (Sigma) (1:100 dilution) overnight at 4°C covered from the light. The following day, it was washed with PBS for 10 minutes followed by incubation in the secondary Alexa Fluor 647-conjugated anti-mouse at room temperature for an hour covered from light. It was then washed 3 times with PBS for 5 minutes each. 4′, 6-diamidino-2-phenylindole (DAPI) was then added to the sections and incubated for 1 minute at room temperature followed by washing 3 times in PBS for 5 minutes each. It was then cover slipped with VECTASHIELD mounting medium. Zeiss Fluorescence snapshot microscope was used for imaging all areas of the heart at 10X magnification. It was then analysed by ImageJ software to detect TUNEL-positive cardiomyocytes and non-cardiomyocytes. The total number of apoptotic cells in a sample was normalised to a total of 10,000 cells.

2.2.7 Statistical analysis

All results are presented as the mean ± standard error of the mean (Mean ± SEM). Data were analysed using GraphPad Prism (version 7, California, USA). Data were assessed for normality using Shapiro-Wilk test. An unpaired t-test was used to compare readings between the control (chow) and high-fat-fed mice. Pearson correlation coefficient was used for linear correlation. Data were considered statistically significant when $P<0.05$.

2.3 Results

A high-fat diet feeding regimen was set up as described in the Methods section. In brief, phenotypic changes were studied by in-vivo analysis echocardiography and ECG as well as metabolic changes. Fission and fusion mitochondrial proteins were analysed by western blotting and qPCR. Finally, the complex activity and oxygen consumption rate of the mitochondria was analysed for each group.

2.3.1 Characterisation of the cardiac phenotype after HFD (DIO)

We first investigated the effects of a HFD (DIO) upon physical parameters and blood glucose. HFD-fed mice (DIO) for 12 weeks showed a significant weight gain compared to age-matched controls (Figure 2.6A). Normalised body weight to tibial length (BW/TL) was significantly higher in the HFD (DIO) group (Figure 2.6B) an indicator of obesity.

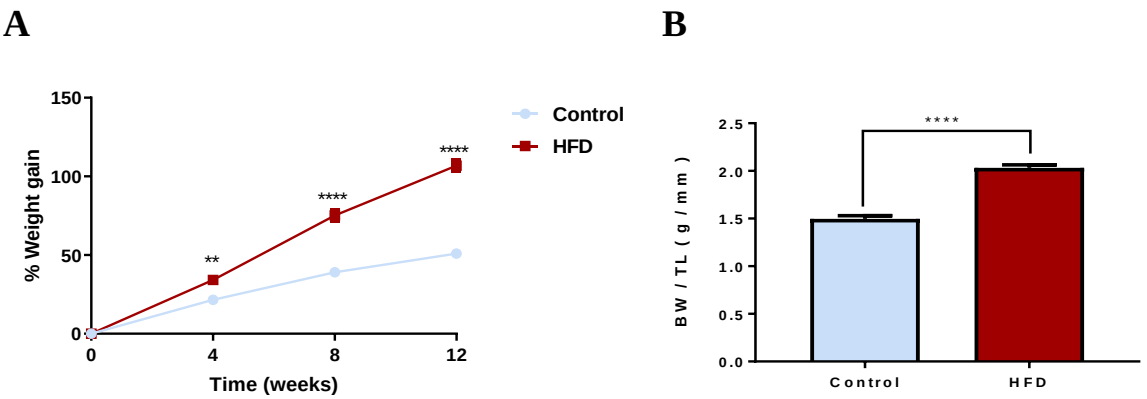

Figure 2.6: high-fat diet (DIO) significantly increased the body weight of mice over 12 weeks.

A. Body weight gain over time between control (n=7) and 60%HFD-fed (DIO) C57BL/6J mice (n=8). B. Body weight normalised to tibial length in control (n=14) and 60%HFD (DIO) fed C57BL/6J mice (n=16). Data are expressed as mean ± SEM. **P≤0.01, ****P≤0.0001.

Using tail vein sampling we determined that the mice on the HFD (DIO) showed a significant increase in fasting blood glucose (Figure 2.7A). Plotting body weight against blood glucose levels revealed a strong positive significant linear relationship between fasting blood glucose level and body weight (Figure 2.7B) (Spearman correlation = 0.74, p= 0.0017). There was a significant 4-fold increase in insulin levels in the HFD (DIO) group (1.6 ± 0.5 ng/ml) compared to control (0.4 ± 0.5 ng/ml) indicating insulin resistance.

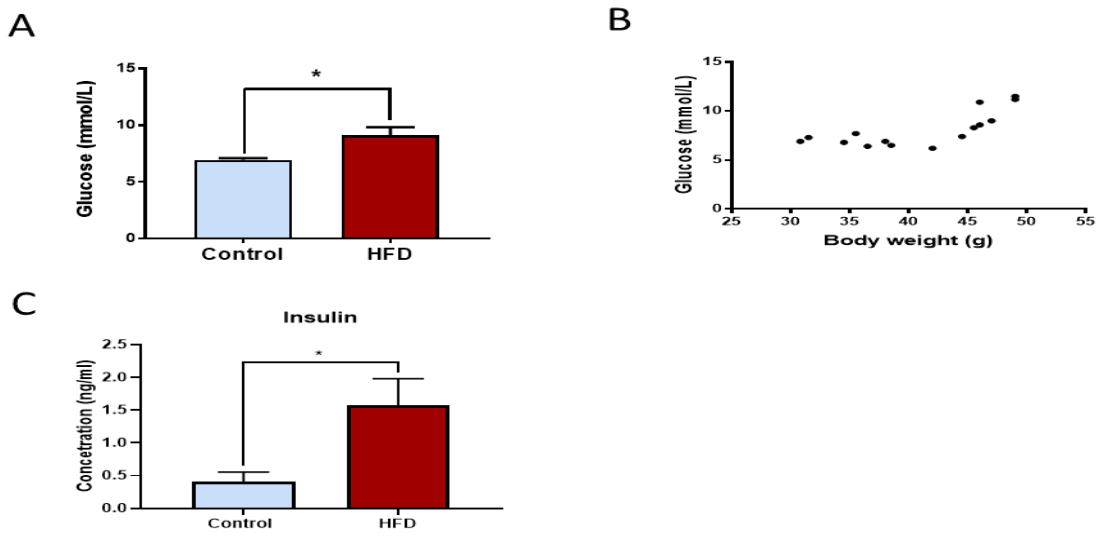

Figure 2.7: High-fat diet (DIO) significantly increased fasting blood glucose and insulin.
A. Fasting blood glucose level in control (n=7) and 60%HFD-fed (DIO) C57BL/6J mice (n=8). B. Scatter plot of fasting blood glucose level and body weight (spearman correlation = 0.74, p≤0.01, n=15). C. Insulin level in 60%HFD (DIO) was significantly higher than control. Data are expressed as mean ± SEM. *P≤0.05

cardiomyopathies. Therefore, the effects of HFD (DIO) on serum lipid profile were next investigated (Figure 2.8). Triglyceride, HDL, LDL/VLDL, total cholesterol and total cholesterol/HDL ratio were all significantly higher in HFD (DIO) mice compared to control.

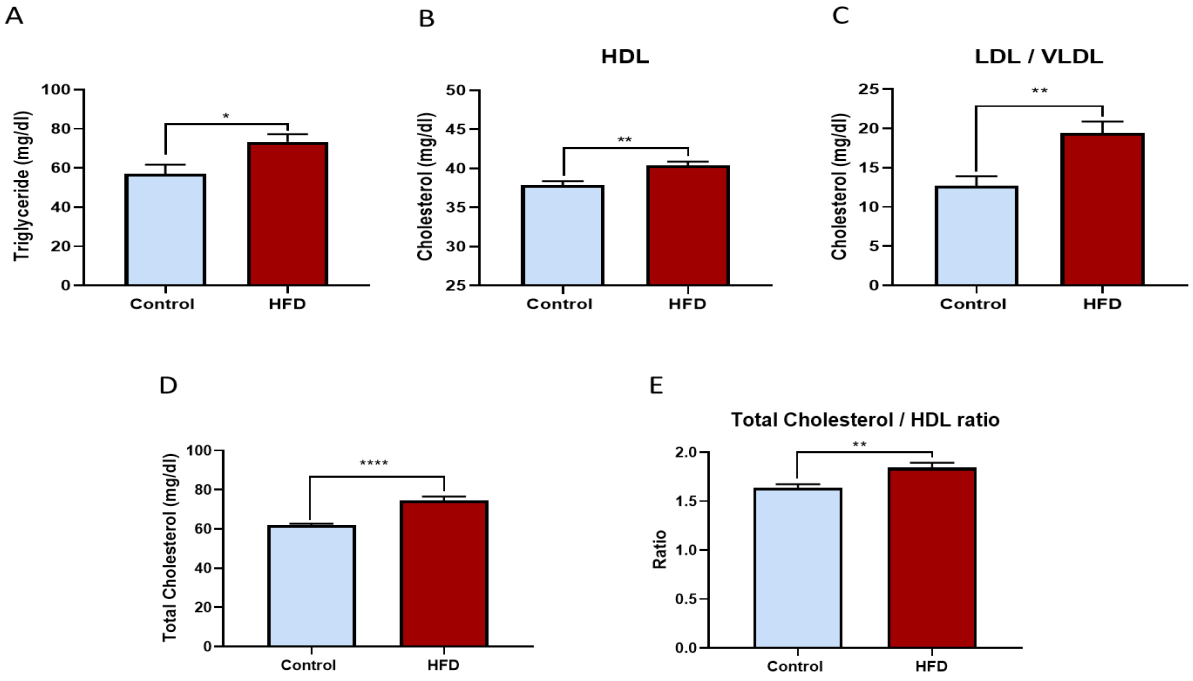

Figure 2.8: High-fat diet (DIO) significantly altered the lipid profile.
A. Triglyceride level was significantly increased in HFD (DIO) compared to control. B. High density lipoproteins (HDL) was increased as well as LDL/VLDL (C) in 60%HFD-fed C57BL/6J mice compared to control. D. Total cholesterol was significant in 60%HFD-fed C57BL/6J mice compared to control. E. The ratio of total cholesterol / HDL ratio was elevated after 60% HFD. Data are expressed as mean ± SEM (n=7). *P≤0.05 **P≤0.01 ****P≤0.0001

2.3.2 Characterisation of the cardiac function

Whilst other groups in the division have employed this HFD (DIO) feeding model for vascular studies reporting that the mice become hypertensive (Saxton, 2017), there had been no robust characterisation of the cardiac phenotype. Therefore, here we employed both echocardiography and ECG to determine whether there is structural and electrical remodelling. Echocardiography revealed that the systolic function has not been changed in HFD (DIO) mice, as EF and FS showed no significant differences between groups (Table 2.8). EF% refers to the percentage of the blood volume pumped out from a contracted ventricle, while FS% represents the percentage of the reduction in the diastolic dimension length in systole.

Table 2.8: in-vivo cardiac function analysis by echocardiography showed no changes in systolic function for high-fat diet (DIO) mice.

Ejection fraction and fractional shortening parameters in 60%HFD-fed (DIO) C57BL/6J mice and control. EF: ejection fraction, FS: fractional shortening, SV: stroke volume.

Parameters	Control (n=7)	DIO (n=8)	P value
	mean ± SEM	mean ± SEM	
EF%	78.7 ± 1.99	78.16 ± 1.73	0.840
FS%	40.62 ± 1.85	40.1 ± 1.65	0.840

On the other hand, HFD (DIO) mice showed a decrease in cardiac output illustrated by a significant decrease in stroke volume (SV) (Figure **2.9**A); the amount of ejected blood by left ventricle per beat. As well as a sign of pulmonary congestion explained by a significant increase in gross lung weight normalised to tibial length (LW/TL) (Figure 2.9B). In diastolic dysfunction, blood flows back to the lung and leads to elevated hydrostatic pressure which causes congestion.

A B

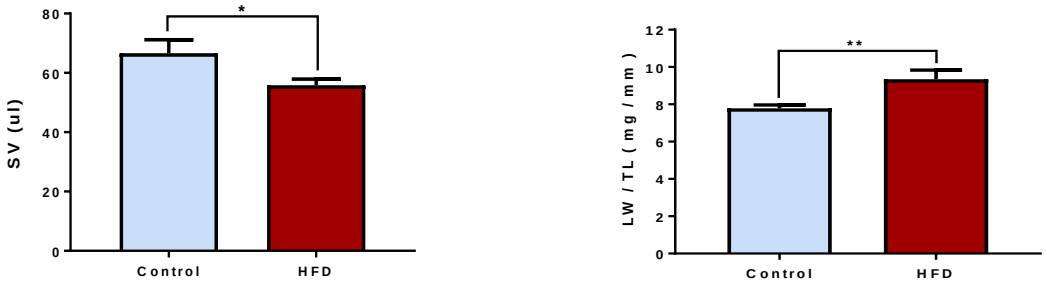

Figure 2.9: HFD (DIO) myocardium showed early signs of diastolic dysfunction; decreased stroke volume and increased in lung weight.

A. Stroke volume in control (n=7) and 60%HFD-fed (DIO) C57BL/6J mice (n=8). B. Normalised lung weight to tibial length in control (n=14) and HFD (DIO) mice (n=16). Data are expressed as mean ± SEM. *P≤0.05 **P≤0.01.

Echocardiographic analysis of cardiac structure revealed a significant increase in the relative wall thickness (RWT) in the HFD (DIO) heart compared to control (P≤0.001, n=8, 7 respectively). RWT is used to classify LV geometric changes. This increase in RWT was not associated with an increase in LV mass estimation by echocardiography (p=0.48) or gross heart weight normalised to tibial length (HW/TL) (P value=0.7) implying concentric remodelling (Figure 2.10). Also, there was a significant decrease in dLVD in HFD (DIO) myocardium associated with a significant increase in dIVS and sPW (P≤0.05).

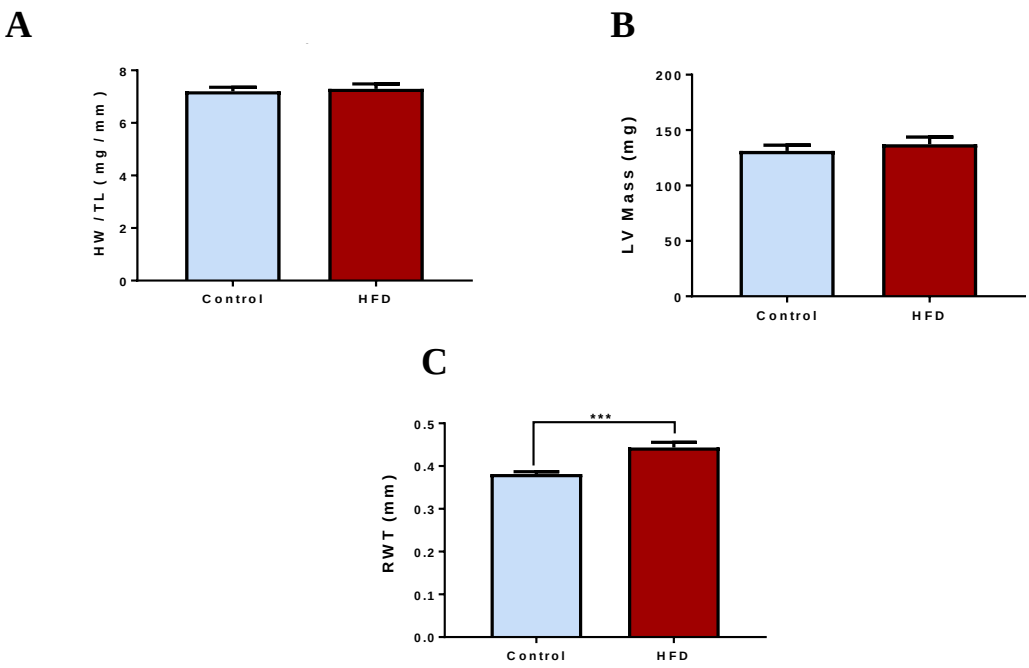

Figure 2.10: Increased RWT indicated concentric remodelling of HFD (DIO) heart.
A. Normalised gross heart weight to tibial length in control (n=14) and 60%HFD-fed C57BL/6J mice (n=16) (p=0.7). B. Echocardiographic estimation of left ventricular mass in control (n=7) and HFD mice (n=8) (p=0.49). C. Relative wall thickness in control (n=7) and HFD (n=8) mice. Data are expressed as mean ± SEM. ***P≤0.001.

Table 2.9 presents the summary statistics for other wall thickness measurements and left ventricular dimensions.

Table 2.9: In-vivo cardiac structure analysis by echocardiography for high-fat diet (DIO) model. s: systolic, d: diastolic, LVD: left ventricular diameter, IVS: interventricular septum, PW: posterior wall, RWT: relative wall thickness. * P≤0.05

Parameters	Control (n=7)	DIO (n=8)	P value
	mean ± SEM	mean ± SEM	
Left Ventricular Dimensions			
sLVD (mm)	2.56 ± 0.06	2.45 ± 0.08	0.321
dLVD (mm)	4.31 ± 0.07	4.08 ± 0.05	0.018*
Wall Thickness			
sIVS (mm)	1.47 ± 0.05	1.53 ± 0.05	0.366
dIVS (mm)	0.87 ± 0.01	1.04 ± 0.06	0.017 *

sPW (mm)	1.21 ± 0.04	1.32 ± 0.03	0.048 *
dPW (mm)	0.77 ± 0.01	0.77 ± 0.01	0.899

2.3.4 Assessment of cardiac conduction system

To determine the effect of the HFD (DIO) on the electrical activity of the heart, parameters were recorded by ECG in both groups. Table 2.10 summarises ECG parameters analysed in HFD (DIO) and control mice. None of these parameters were statistically significant but there is a trending of a prolonged PR interval in HFD (DIO) group (P value=0.072).

Table 2.10: ECG parameters comparison between control and HFD (DIO) mice.

QT_c: corrected QT interval, ms: milliseconds, mV: millivolts.

Parameters	Control (n=7) mean ± SEM	DIO (n=8) mean ± SEM	P value
RR Interval (ms)	146.2 ± 4.11	151 ± 4.92	0.476
PR Interval (ms)	39.99 ± 1.18	43.33 ± 1.22	0.072
P Duration (ms)	10.13 ± 0.7	10.62 ± 0.34	0.519
QRS Interval (ms)	10.4 ± 0.33	9.2 ± 0.76	0.192
QT Interval (ms)	17.66 ± 0.71	16.24 ± 0.8	0.211
QT_c (ms)	46.33 ± 2.11	41.94 ± 2.2	0.177
ST Height (mV)	0.01 ± 0.01	0.01 ± 0.01	0.498

There was no evidence that HFD (DIO) has an influence on heart rate (Figure 2.11). The next goal was to focus upon cellular level changes, specifically mitochondrial fission and fusion.

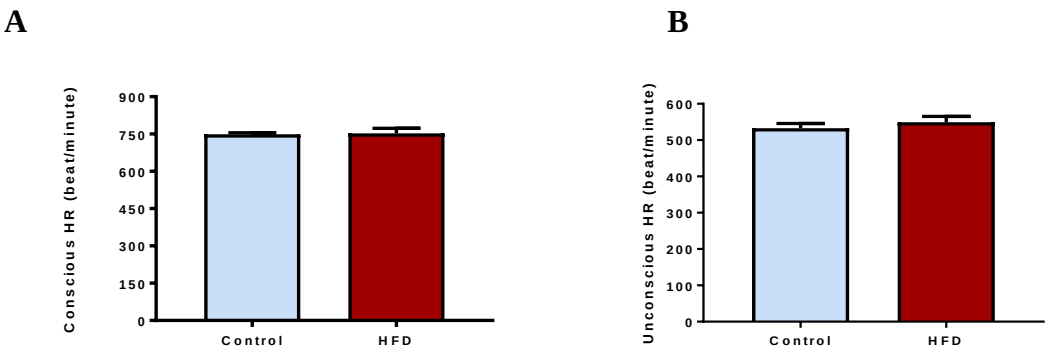

Figure 2.11: HFD (DIO) had no significant effect on heart rate.
A. Conscious heart rate in control and 60%HFD-fed (DIO) C57BL/6J mice (P value=0.88). B. Unconscious heart rate in control and HFD (DIO) mice (p=0.43). Data are expressed as mean ± SEM (n=7, 8 respectively).

2.3.5 Investigation of molecular level changes to mitochondrial dynamic proteins in HFD (DIO) model

Employing RT-qPCR methods the transcript levels of the four principal proteins regulating fusion, Mfn1, Mfn2, Opa1 and fission, Drp1 were probed. Western blotting methods were employed to investigate changes to protein expression levels with protein levels quantified using the total protein method as described in the Material and Methods section.

For proteins involved in mitochondrial fusion, there was an increase in Opa1 transcript expression in HFD (DIO) myocardium ($p \leq 0.05$). Other fusion proteins e.g. Mfn1 and Mfn2 showed no significant differences. Expression level of fusion proteins Mfn1, Mfn2 and Opa1 showed no differences in HFD (DIO) myocardium compared to control (Figure 2.12).

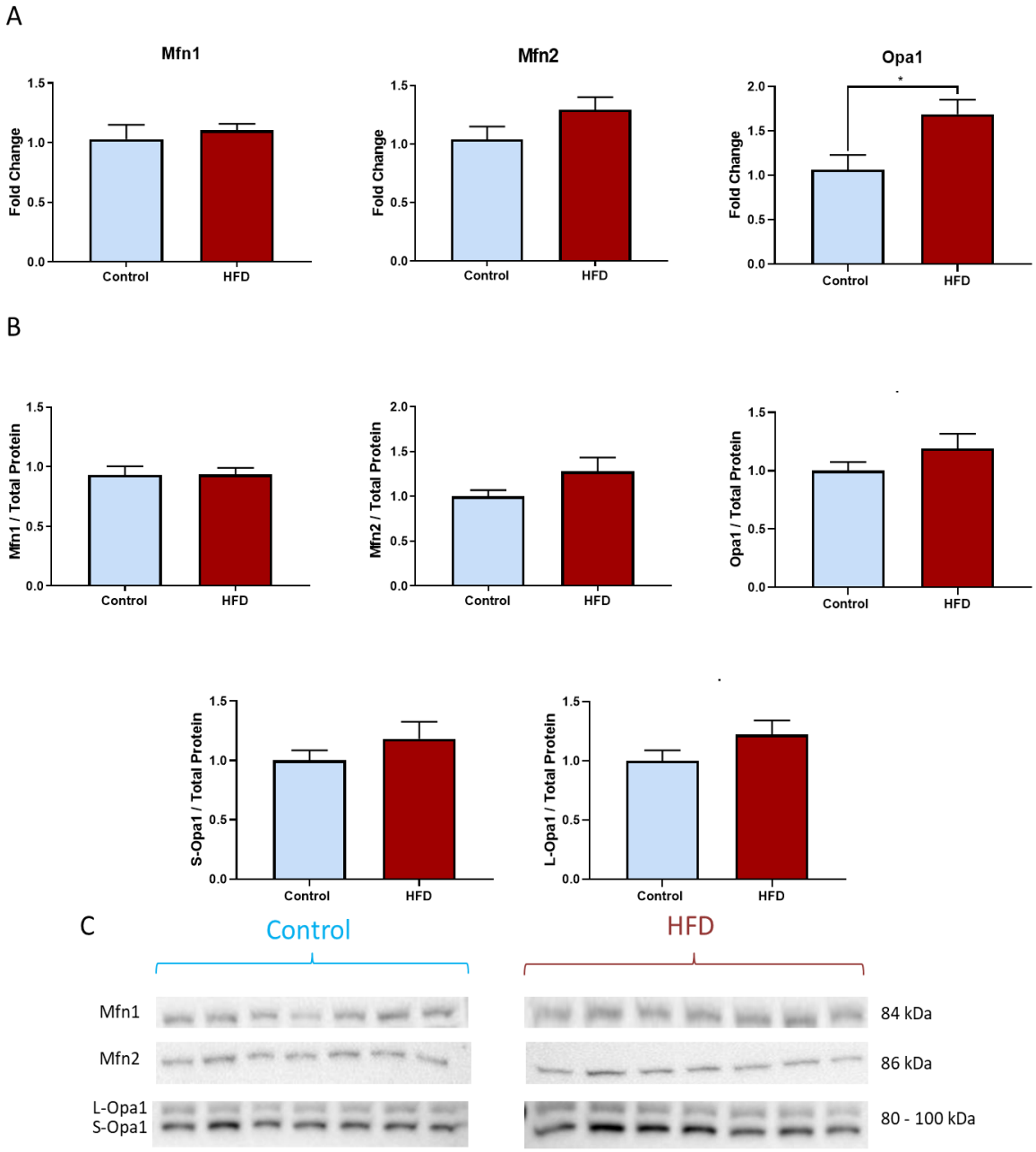

Figure 2.12: HFD (DIO) myocardium exhibited significantly increased Opa1 transcript expression. A. There was a significant increase in Opa1 transcript expression in the HFD (DIO) myocardium. There were no significant differences in other proteins involved in mitochondrial fusion (Mfn1 and Mfn2). B. Western blot analysis for control and HFD myocardium showed no significant differences in proteins involved in mitochondrial fusion (Opa1, Mfn1 and Mfn2). C. Representative blot showing proteins involved in mitochondrial fusion expression (Mfn1, Mfn2, L-Opa1 and S-Opa1). An image for the membrane after the transfer of proteins showing the total protein has been taken by ChemiDoc machine. Total protein normalisation, also known as, stain-free technology, was used to compare protein signals (Gurtler et al., 2013). Proteins signals were normalised to total protein loaded. This technique is termed 'total protein Western blotting' and instead of using a single housekeeping protein the total amount of protein loaded and transferred is used to standardise each sample. Data are expressed as mean ± SEM (n=7). *p≤0.05

Drp1 transcript expression was decreased in HFD (DIO) myocardium compared to control (P≤0.01). However, protein levels of Drp1 were significantly increased in HFD (DIO) myocardium (P≤0.01). Elevated levels of Drp1 may suggest that the processes leading to protein turnover/degradation are impaired leading to accumulation in the heart. As post-translational modification, namely phosphorylation is known to regulate Drp1 activity, the expression of two sites of Drp1 phosphorylation at Serine 616 (pro-fission) and Serine 637 (inhibit fission) was measured. P-Drp1(S637) to total Drp1 ratio was decreased in HFD (DIO) myocardium compared to control while P-Drp1(S616) to total Drp1 ratio showed no differences between control and HFD (DIO) (Figure 2.13).

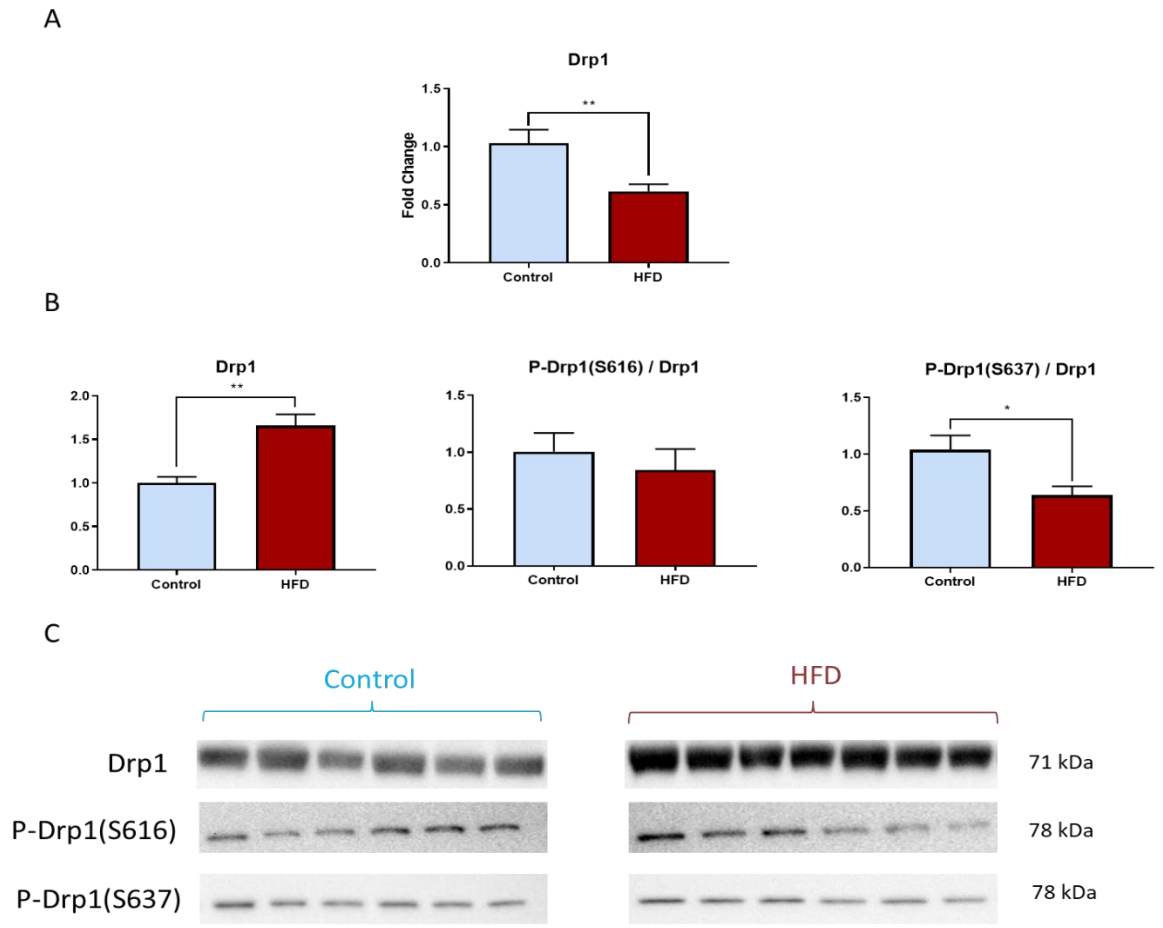

Figure 2.13: The heart of 60% HFD (DIO) C57BL/6J mice exhibited a significant increase in Drp1 expression.

A. There was a significant decrease in Drp1 transcript expression in the 60%HFD (DIO) myocardium of C57BL/6J using RT-qPCR. B. Upregulation of Drp1 expression in 60%HFD mice with a significant decrease in P-Drp1 (S637) compared to control using western blotting. C. Expression of proteins in western blot in control and HFD (DIO). An image for the membrane after the transfer of proteins showing the total protein has been taken by chimidoc machine. Total protein normalisation, also known as, stain-free technology, was used to compare protein signals. Proteins signals were normalised to total protein loaded. Data are expressed as mean ± SEM (n=6). *P≤0.05 **P≤0.01.

Transcript expression of MID49 and MID51 showed no significant difference between groups. There was a significant decrease in Mff transcript expression in HFD (DIO) myocardium compared to control (P≤0.05). Western blot revealed an increase expression of MID49 and Fis1 in HFD (DIO) myocardium compared to control and a decrease in Mff expression (Figure 2.14).

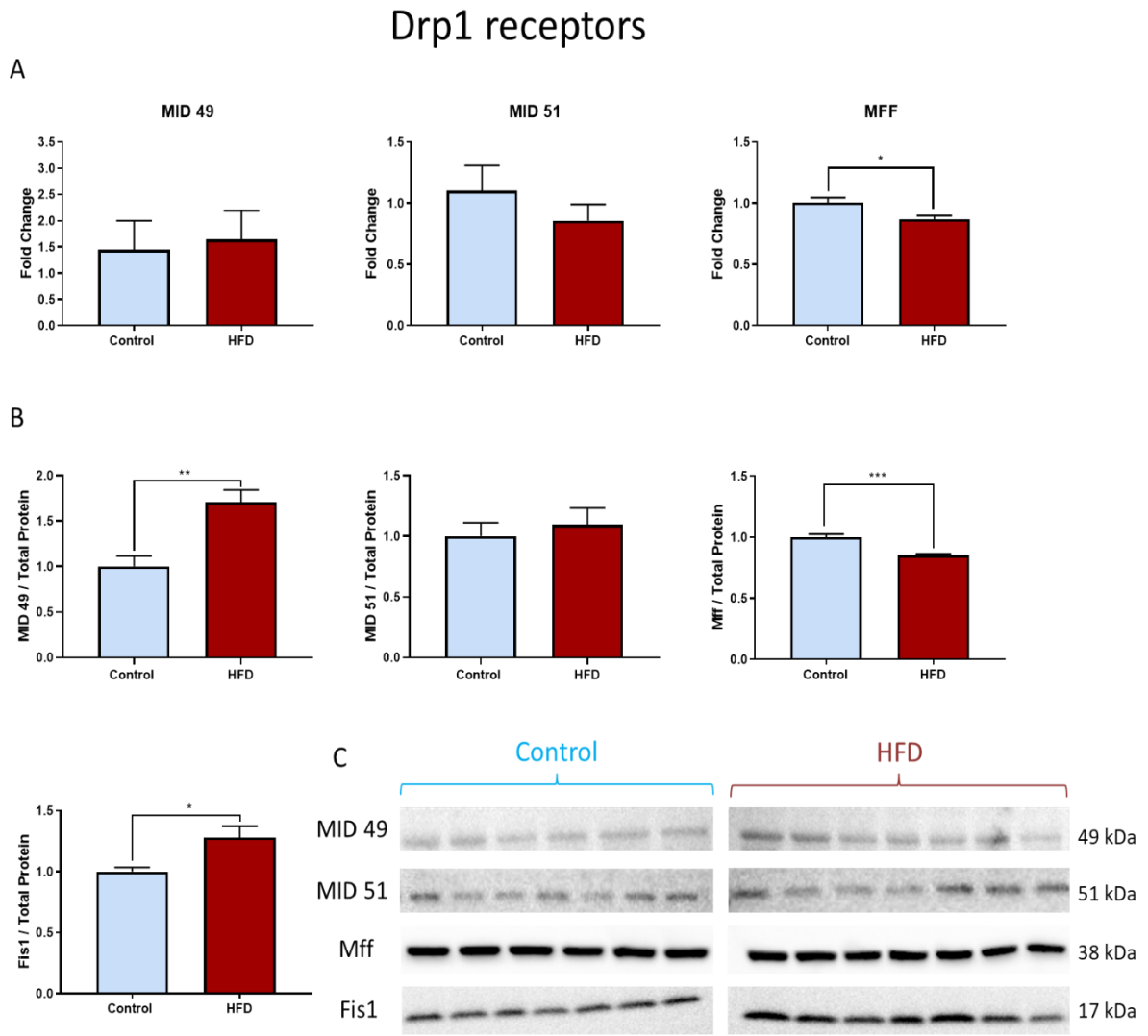

Figure 2.14: Drp1 receptors showed altered transcript levels and expression in HFD (DIO) model.
A. There was a decrease in Mff transcript expression in HFD (DIO) myocardium compared to control. B. Western blot analysis showing an increase of MID49 and Fis1 expression and a decrease in Mff expression in HFD (DIO) myocardium compared to control. C. Representative blot showing Drp1 receptors protein expression. Data are expressed as mean ± SEM (n=6, 7 respectively). *P≤0.05 **P≤0.01 ***P≤0.001

PINK1 and Parkin are the key regulators of mitophagy. PINK1 recruits Parkin to ubiquitinate damaged mitochondria. There was a significant increase in PINK1 and Parkin level at both

transcript and protein expression in HFD compared to control (Figure 2.15). Therefore, it may be inferred that mitophagy is activated in response to the high fat feeding.

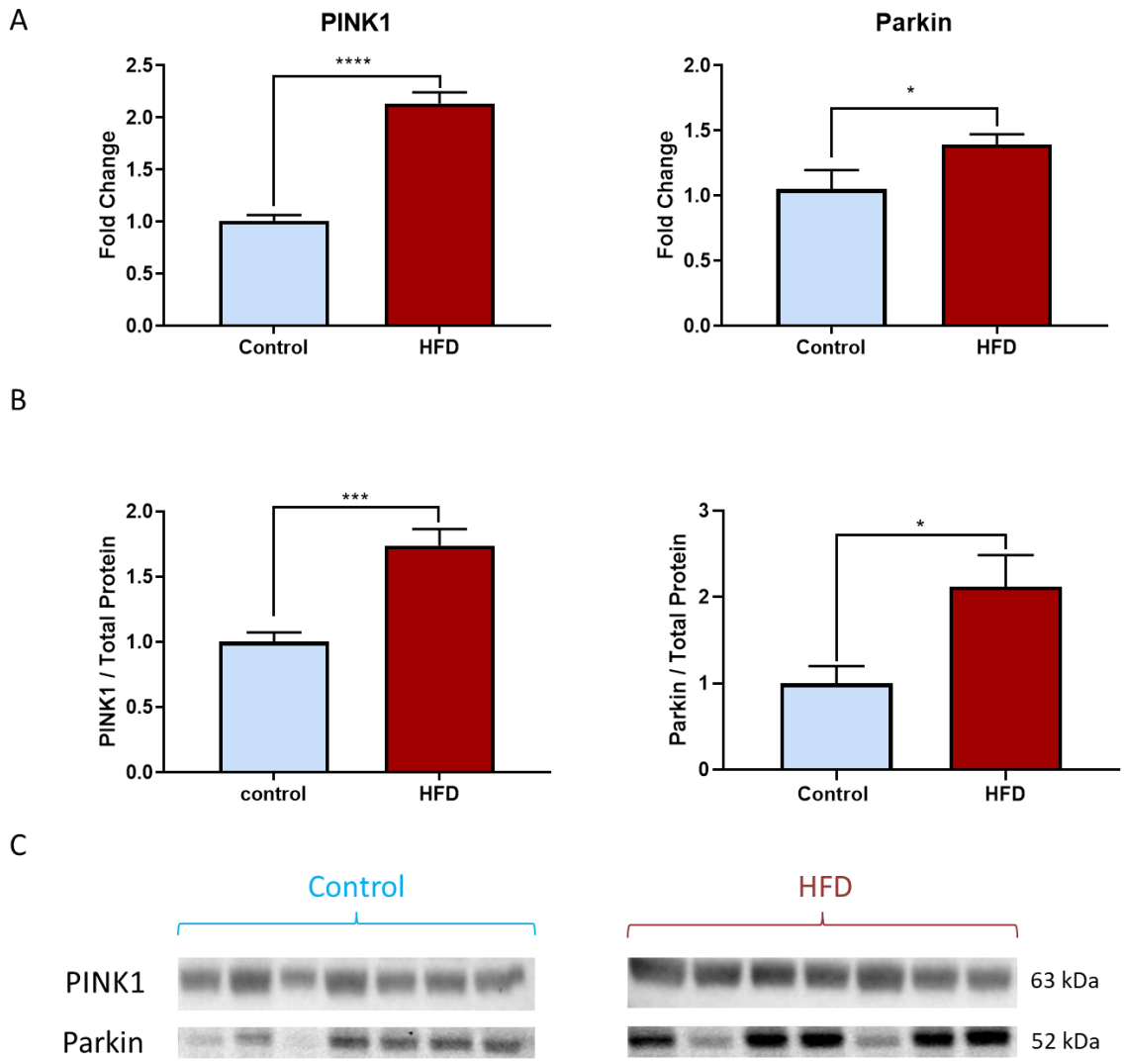

Figure 2.15: Increased PINK1 and Parkin indicated mitophagy activation in HFD (DIO) heart.
A. Transcript level of PINK1 and Parkin are significantly increased in HFD (DIO) compared to control. B. PINK1 and Parkin level expression in increased in HFD (DIO) myocardium. C. Representative blot showing protein expression of PINK1 and Parkin. Data are expressed as mean ± SEM (n=7) *P≤0.05 ***P≤0.001****P≤0.0001.

The transcript expression of TFAM and PGC-1α proteins regulating mitochondrial biogenesis were analysed. TFAM transcript levels were significantly increased in HFD (DIO) mice compared to control, while PGC-1α showed no significant differences between groups (Figure 2.16).

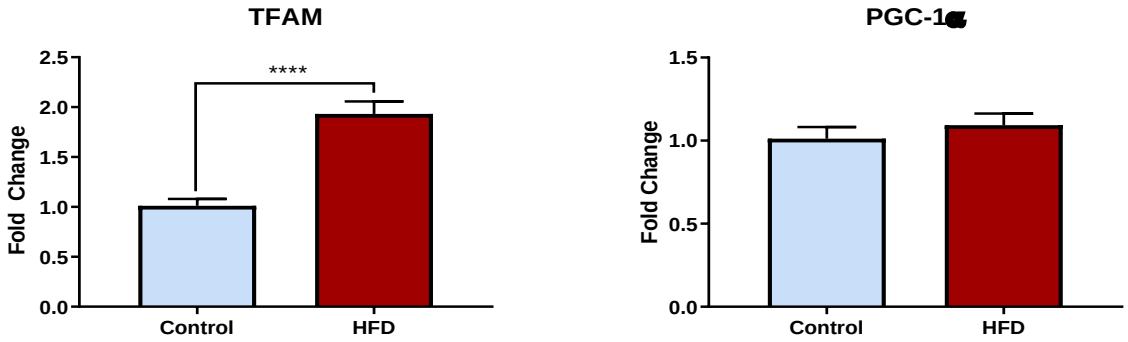

Figure 2.16: Increased TFAM (involved in mitochondrial biogenesis) transcript expression was found in in HFD (DIO) model.

There was a significant difference in the transcript expression of TFAM and no difference in PGC-1α in HFD (DIO) model compared to control. Data are expressed as mean ± SEM (n=6,8 respectively). ****P≤0.0001.

2.3.6 Measurement of mitochondrial respiration

Mitochondrial function was next investigated to identify whether the changes in Drp1 were associated with a change in mitochondrial function. The activity of respiratory chain complexes of isolated mitochondria from control and HFD (DIO) was assessed. There were no significant changes between groups. Citrate synthase activity assay was used to check whether the results of mitochondrial function were altered due to changes in mitochondrial content. It showed no changes in citrate synthase activity between groups which means there was no variation in mitochondrial content (Figure 2.17).

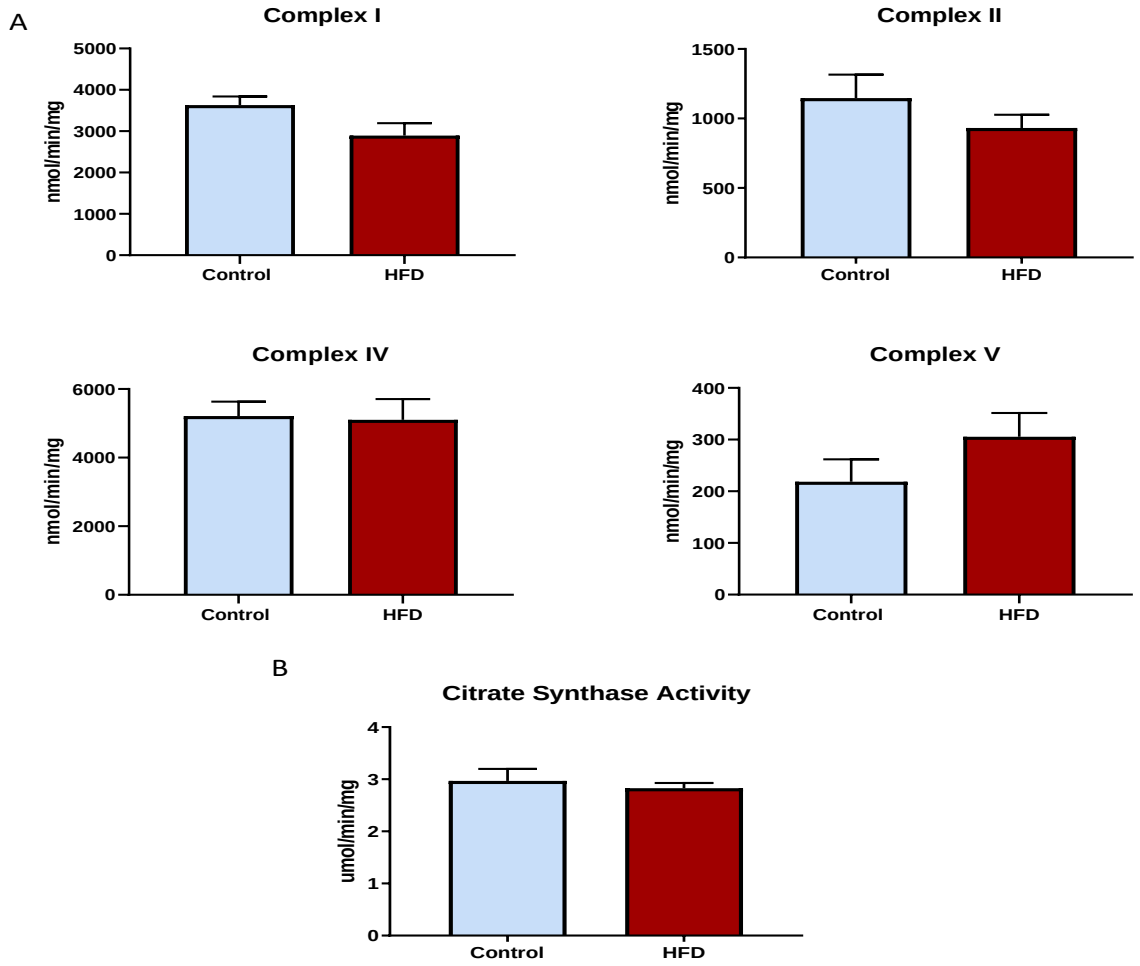

Figure 2.17 : No change was found in mitochondrial complexes activity in HFD (DIO).
A. Mitochondrial complexes activity in control and HFD (DIO) (n= 6, 8 respectively). B. Citrate synthase activity. Data are expressed as mean ± SEM (n=5)

In another approach to investigate mitochondrial function, we employed an Instech (based upon the fibre optics) to measure the rate of oxygen consumption (OCR). The first step involved isolating mitochondria using centrifugation techniques as described in Methods section 2.2.5.1. Mitochondria from mice on chow and HFD (DIO) (n=5) were investigated. As can be seen in Figure 2.18C, the oxygen percentage declines as ADP is consumed. There was no significant difference between the groups (Figure 2.18). FCCP is a mitochondrial uncoupler and the addition led to a noticeable increase in the oxygen consumption rate in both control and HFD (DIO) with no significant changes between the groups (Figure 2.18B, D).

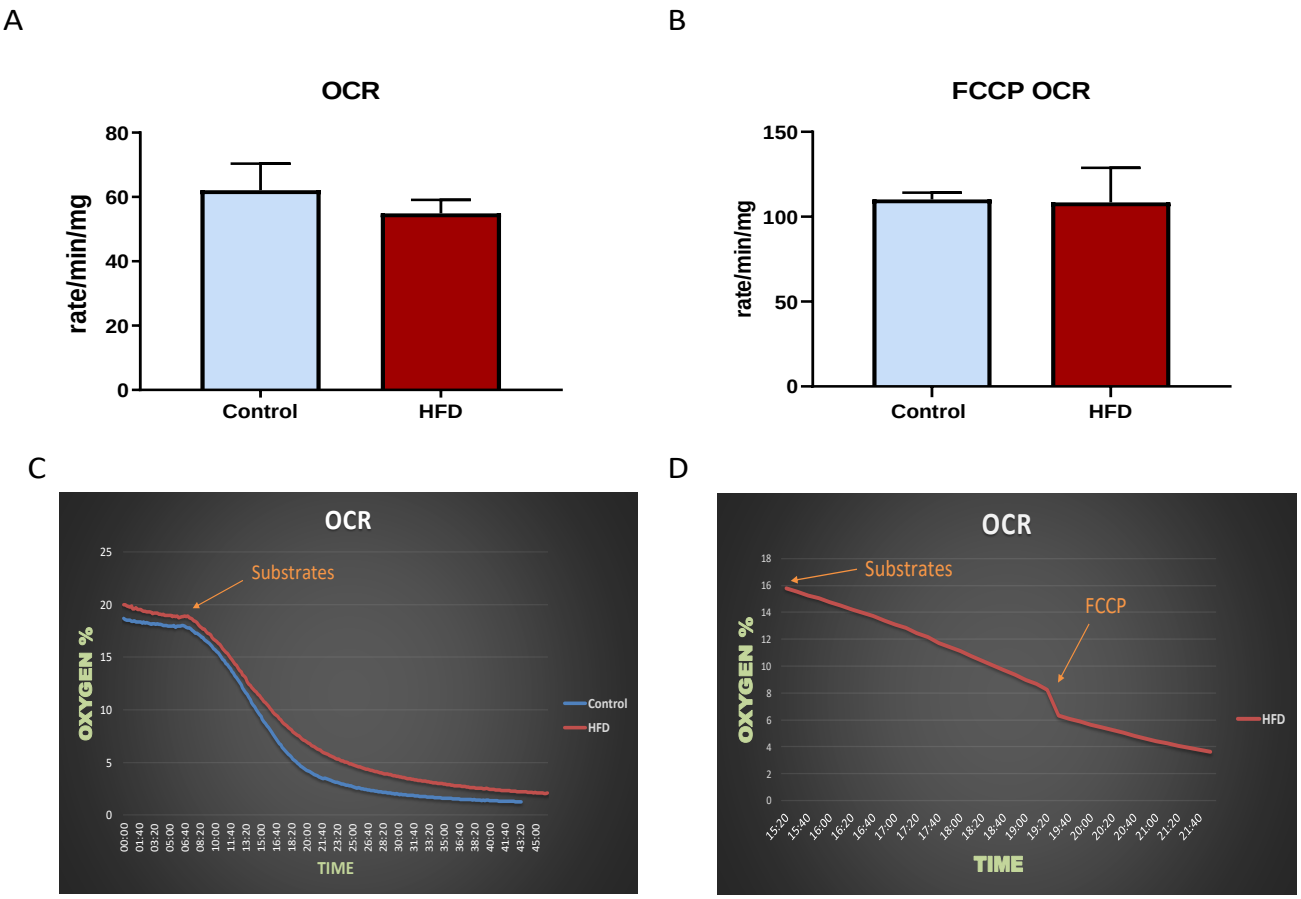

Figure 2.18: No change was found in mitochondrial oxygen consumption rate in control and HFD (DIO) mice.
A. Oxygen consumption rate (OCR) in control and HFD (DIO) mice. B. Oxygen consumption rate after mitochondrial uncoupler FCCP. C. Representative plot for control and HFD samples. D. Representative plot when add mitochondrial uncoupler FCCP. Data are expressed as mean ± SEM

2.3.7 Assessment of cardiac hypertrophy and fibrosis

To determine whether there were any underlying changes in the heart structure, the size of the cardiomyocyte cells and cardiac fibrosis were assessed. Changes in the size of cardiomyocyte cells may be an indication for cardiac hypertrophy. To study the cell size of the cardiomyocytes, H&E staining was used on both control and HFD (DIO). After cell size analysis, there was no statistical difference in cardiomyocyte size between control and HFD (DIO) mice (Figure 2.19).

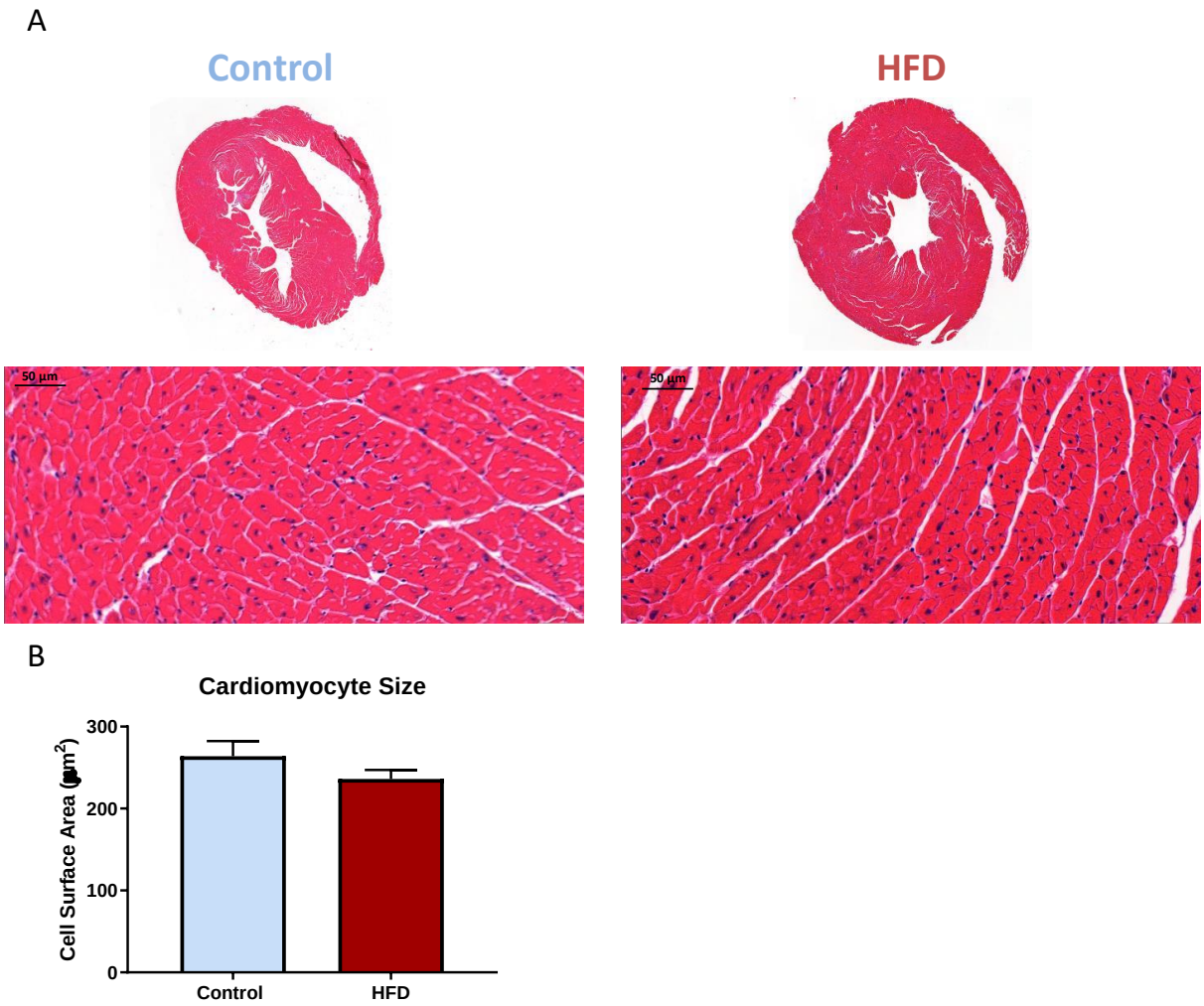

Figure 2.19: No change was found in cell size of cardiomyocytes in control and HFD (DIO) mice.
A. Representative H&E sections from a control and HFD (DIO) mice. Scale bar = 50 µm. B. There was no significant change between groups. 100 random cardiomyocytes evaluated per sample. Data are expressed as mean ± SEM (n=6).

Since heart function may be impaired by collagen deposition in the left ventricle, we next investigated whether fibrosis was present in the myocardium of HFD (DIO) mice using Masson's trichrome staining was performed. Masson's trichrome stains muscle fibres red and collagen fibres blue. The analysis of these sections showed less than 0.1% interstitial and perivascular fibrosis in both control and HFD (DIO) mice (Figure 2.20).

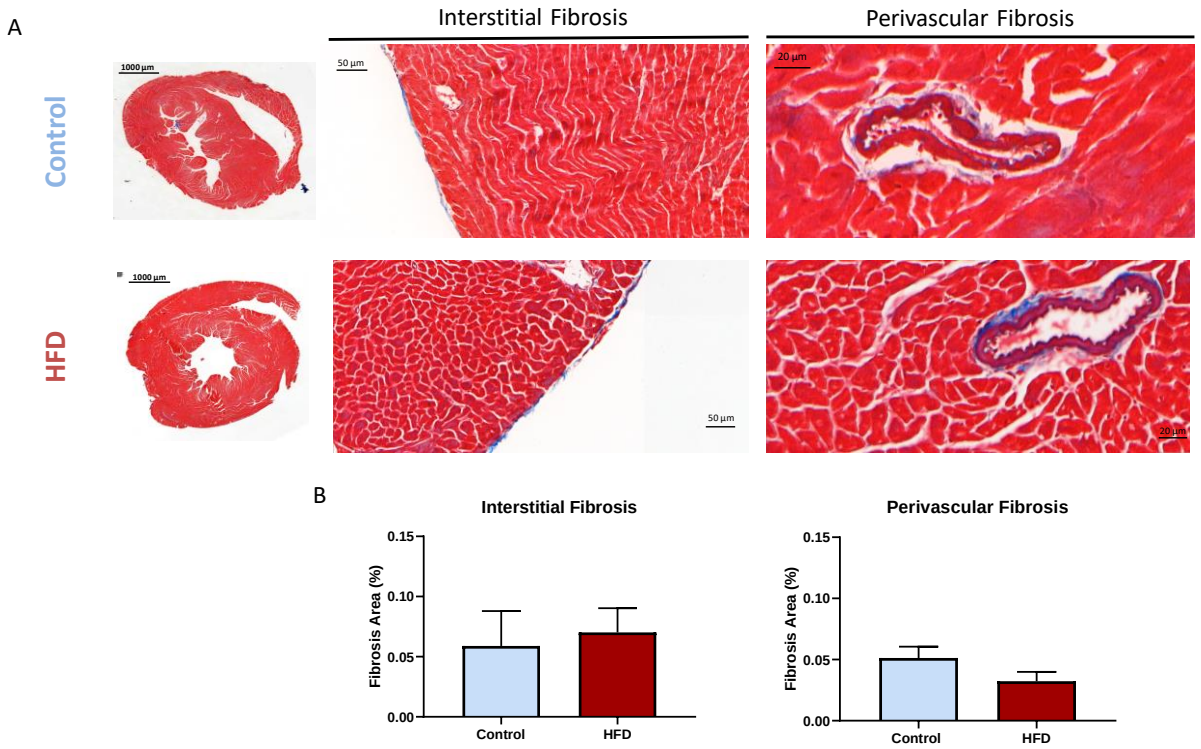

Figure 2.20: No evidence of interstitial and perivascular fibrosis was found in HFD (DIO) mice.

A. The levels of fibrosis were measured following staining with Masson's trichrome in control and HFD (DIO) mice. B. There was no significant difference in interstitial and perivascular fibrosis in both groups. Scale bar: whole heart (left) = 1000 µm, interstitial (middle) = 50 µm, perivascular (right) = 20 µm. Data are expressed as mean ± SEM (n=7).

2.3.8 Analysis of apoptosis

To further assess the effect of HFD (DIO) on cardiomyocytes (CM) and non-cardiomyocytes (NCM) apoptosis in the heart, the TUNEL assay was performed. The TUNEL staining of paraffin-fixed cardiac sections showed a significant increase in the number of apoptotic cardiomyocytes (CM) per 10,000 cells in the HFD (DIO) group compared to control and no statistical difference in non-cardiomyocytes (NCM) (Figure 2.22).

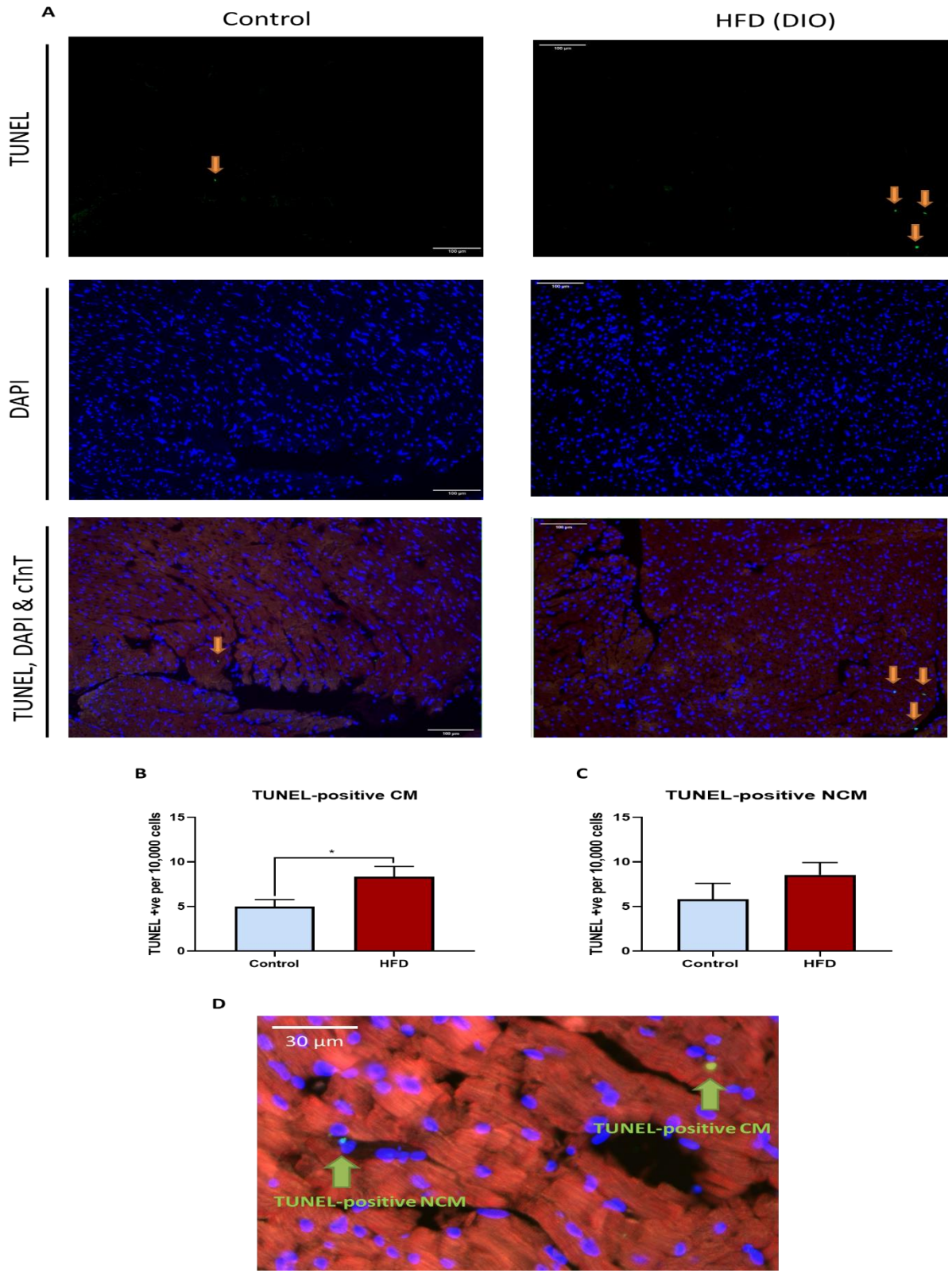

Figure 2.22: HFD (DIO) mice showed higher apoptotic cardiomyocytes in TUNEL assay.
A. Immunofluorescent images of HFD (DIO) hearts and their control showing DAPI staining for nuclei (blue) and TUNEL staining for apoptotic cells (green) with co-staining of cardiac troponin T (red). Scale bar = 100 µm. B. Quantification of apoptotic cardiomyocytes per 10,000 cells showed significantly increased apoptosis (TUNEL-positive CM). C. Quantification of apoptotic non-cardiomyocytes per 10,000 cells was not significant (TUNEL-positive NCM). D. The difference between TUNEL-positive cardiomyocyte (CM); nuclei position within the cells, TUNEL-positive noncardiomyocyte (NCM); located outside the cells. Scale bar = 30 µm. Data are expressed as mean ± SEM (n=5). *P≤0.05

2.3.9 Summary of results

Chapter two focused on the study of the effects of obesity on cardiac function and at the cellular level changes to cardiac mitochondrial fission/fusion proteins. The key findings were:

- Obesity led to a change in the cardiac phenotype with cardiac concentric remodelling
- A significant increase in body weight concomitant with hyperglycaemia.
- At the protein level the mitochondrial proteins Drp1, MID49, Fis1, PINK1 and Parkin were significantly upregulated but Mff and P-Drp1 (S637) were decreased in the HFD (DIO) myocardium.
- At the transcript level there was an increase in Opa1, PINK1 and Parkin expression in the HFD (DIO) but a decrease in Drp1 and Mff.

2.4 Discussion

2.4.1 Weight gain, hyperglycaemia and insulin resistance and hyperlipidaemia

Obesity and T2DM have been associated with numerous cardiac complications. A range of different animal models for obesity/T2DM have been employed to investigate the underlying mechanism of DCM. The HFD (DIO) model has been used in this study because it mimics obesity in humans without genetic modification. Besides, the severity of obesity can be controlled by changing the HFD (DIO) percentage and feeding duration. To study the early changes in obesity/T2DM, a duration of only 12 weeks of HFD (DIO) has been chosen. In this study, the HFD (DIO) model showed a weight gain concomitant with hyperglycaemia and hyperinsulinemia, which agrees with previous studies (Cao et al., 2017, Antonioli et al., 2017, Kothari et al., 2017). We did not find a definitive categorisation of glucose or insulin limits for classification of diabetes in C57BL/6J mice in the literature; using a diagnostic criterion for diabetes in human (fasting blood glucose ≥ 7 mmol/l) is not applicable since some of the control mice had a fasting blood glucose level > 7 mmol/l. However, after a HFD (DIO) feeding the mice in this study were significantly hyperglycaemic, combined with 4-fold increase in insulin in the HFD (DIO) group and so we suggest that this group can be considered analogous to early stage T2DM.

The triglyceride (TG) level in the blood is increased by the high caloric consumption, while the cholesterol level in the blood is increased by the total fat consumption. In our model, both TG and cholesterol were increased. All types of cholesterol HDL, LDL and VLDL were increased as well. This finding is consistent with that of Podrini et al. (2013) who found a significant increase in both HDL and LDL/VLDL in C57BL/6NTac mice after just 2 weeks of HFD (DIO). Most of the fat in our model is from lard which contains around 43% total saturated and 57% total unsaturated fats. Saturated fat consumption elevates LDL cholesterol (Siri-Tarino et al., 2010a) and also HDL (Siri-Tarino et al., 2010b), whereas unsaturated fat increases HDL (Morton et al., 2019) which can explain the elevation in both types of cholesterol. Total cholesterol / HDL ratio is used as a risk marker for cardiovascular diseases (Arsenault et al., 2009) and there is an increase in this ratio in our model. Jeppesen et al. (1998) found individuals with high total cholesterol/HDL ratios are insulin resistant. This study supports the insulin resistance seen in the HFD (DIO) group. On the other hand, Eisinger et al. (2014) showed no significant increase to TG nor total cholesterol in 14 weeks of HFD (DIO) feeding mice model. The difference between the Eisinger study and here is the

fat percentage was 60% in our model while they used 45% which could explain the unchanged level of TG and cholesterol.

2.4.2 Concentric remodelling in HFD (DIO) mice

To determine whether cardiac remodelling occurred after the HFD (DIO), echocardiography was used to determine any changes in the myocardial wall thickness in vivo followed by histological H&E and Masson's Trichrome stains in vitro to detect hypertrophy and fibrosis.

An increase in the RWT without change in estimated LV mass suggests concentric remodelling (Drazner, 2011). In agreement with echocardiogram data, H&E stains showed no hypertrophy is present with no significant difference in cell size in HFD (DIO) myocardium compared to control. Concentric remodelling in the HFD (DIO) myocardium is consistent with a study which describing concentric remodelling in HFD-fed (DIO) mice for 9 weeks (Hafstad et al., 2013). One explanation for the remodelling is excessive afterload which could be caused by hypertension (HTN) (Mihl et al., 2008). The same strain used in our study has been found to develop HTN when fed HFD (DIO) (Chaar et al., 2016, Saxton, 2017). However, pressure overload in our study was not sufficient to cause hypertrophy. These data agree with another study which found that 45% HFD (DIO) for 20 weeks was not enough to induce hypertrophy in C57BL/6J mice (Littlejohns et al., 2014). However, increasing the duration of HFD (DIO) and quantity was sufficient to induce hypertrophy. For example, Wang et al. (2015c) found that chronic 60% HFD (DIO) feeding for 11 months induced hypertrophy but not remodelling. This suggests that concentric remodelling is one of the early signs of DCM.

As one of the causes of concentric remodelling is extracellular fibrosis, we excluded the presence of fibrosis by Masson's trichrome stain as it showed no significant interstitial or perivascular fibrosis in HFD (DIO). A study of longer duration 18-24 weeks 60% HFD (DIO) showed a significant interstitial fibrosis but not perivascular fibrosis (Naresh et al., 2016).

2.4.3 Diastolic dysfunction in HFD (DIO) mice

The function of the heart was studied by echocardiogram. There were no changes to systolic function as assessed by EF% and FS%, parameters that were not significantly different when compared to control. These results are in agreement with a previous study of HFD-fed (DIO) C57BL/6J mice (Naresh et al., 2016) (Littlejohns et al., 2014). In contrast, Louwe et al. (2012) reported a significant decrease in systolic function illustrated by a decrease in EF% in 40% HFD-fed (DIO) mice. This decrease in systolic function may be due to age. It has been

found that the HFD (DIO) effects are different in different age groups (de Castro et al., 2013). Louwe et al. (2012) started the HFD (DIO) on mice aged 12 to 16 weeks, whereas the HFD was started at 8 weeks in our study.

We found a decrease in SV and an increase in LW/TL which might suggest diastolic dysfunction. This finding agrees with Nilsson et al. (2016), who found a decreased SV in female C57BL/6J mice fed 75% HFD (DIO) for 4 weeks compared to controls. Our data is also supported by other studies in the literature (Abdurrachim et al., 2014, Kang et al., 2015).

Electrocardiogram was performed to assess the electrical function of the heart. There were no significant differences in conscious and unconscious heart rate between HFD (DIO) mice and controls consistent with reports from Higa TS et al. (2014) and Naresh et al. (2016). Although there is one report where HFD (DIO) feeding for a duration up to 20 weeks made a significant difference in the heart rate compared to control (Aizawa et al., 2013). A difference in the heart rate could suggest a severe DCM phenotype. The reason for this is that severe DCM will lead to compensated fast heart rate. Therefore, we suggest that our model represents early-stage DCM.

There was a statistical trend of prolonged PR interval in HFD (DIO) mice studied here. Interestingly, Sun et al. (2013) found that obesity is associated with prolonged PR interval in humans. Long-term prolonged PR interval has been reported to increase the risk of atrial fibrillation (Cheng et al., 2009). In contrast to our finding, Zhang et al. (2016a) found a shortened PR interval in 8 weeks HFD-fed (DIO) male ICR mice with widening of QRS complex interval compared to control. The differences in ECG parameters could be due to the difference in animal strain and HFD (DIO) feeding duration. As previously mentioned, the difference in age results in different HFD (DIO) effects (de Castro et al., 2013). Zhang et al. (2016a) did not mention the age of the mice at the beginning of the experiment.

In summary, the characterisation of the cardiac phenotype suggests that the mouse model of HFD (DIO) feeding exhibits diastolic dysfunction with a normal systolic function, heart rate and ECG and therefore could be classified as early-stage DCM (Fang et al., 2004).

2.4.4 Increased transcript expression of the fusion protein Opa1 as a result of HFD (DIO)

In this study it was shown that at the transcript level Opa1 was increased in HFD (DIO) mice compared to control but there were no significant changes in expression of L-Opa1 and S-Opa1. It should be noted that there are at least eight-transcript variant for Opa1 gene due to

alternative splicing (Delettre et al., 2001) and so possibly the primer we used may not detect all the variants. These variants could be categorised as long isoforms (L-Opa1) and short isoforms (S-Opa1). Anand et al. (2014) suggested that long Opa1 (L-Opa1) regulates fusion, whereas short Opa1 (S-Opa1) was associated with mitochondrial fragmentation and fission. Different molecular weights for S-Opa1 and L-Opa1 have been reported in the literature (80 kDa and 100 kDa respectively) (Lang et al., 2017) (Lee et al., 2017a). Opa1 also undergoes proteolytic cleavage to regulate mitochondrial morphology (Ishihara et al., 2006).

Since OMM fusion proteins Mfns were not changed then although the IMM fusion protein Opa1 transcript level is increased this would not likely lead to increased fusion since IMM fusion is dependent on OMM fusion. Cipolat et al. (2004) showed that Opa1 needs Mfn1 to initiate mitochondrial fusion. Therefore, the increase in Opa1 transcript expression could have a non-canonical role, which is to prevent apoptosis. It has been found that Opa1 has a role in cardio-protection by stabilizing the cristae (Patten et al., 2014). Stabilizing the cristae could prevent mitochondrial dysfunction and consequently apoptosis (Varanita et al., 2015). It has been found that Opa1 prevents apoptosis by inhibiting cytochrome c (Frezza et al., 2006). So, Opa1 transcript level increases might be a protective mechanism against cellular apoptosis in mild stage DCM.

2.4.5 Increased expression of Drp1 and its receptor Fis1 and MID49 as a result of HFD (DIO)

HFD (DIO) mice showed an increased expression of Drp1 protein compared to age-matched control. Increased Drp1 will shift the balance towards smaller, fragmented mitochondria (Karbowski et al. (2006). Littlejohns et al. (2014), also reported a significant increase in Drp1 expression in C57BL/6J mice heart fed 45% HFD (DIO) for 20 weeks relative to control. Lionetti et al. (2014) showed an increase in Drp1 expression in the liver of HFD-fed (DIO) rats suggesting that obesity triggers dysregulation. Drp1 over-expressed in H9c2 cells is detrimental to mitochondrial function as it causes mitochondrial fragmentation associated with mitochondrial dysfunction and insulin resistance (Watanabe et al., 2014). Inhibition of Drp1 in murine cardiomyocytes by mitochondrial division inhibitor-1 (Mdivi-1) protects the heart from reperfusion injury (Ong et al., 2010). This could suggest that targeting Drp1 protein in obesity/T2DM prevents developing DCM. The effect of Drp1 inhibition in obesity and T2DM is still to be determined.

Interestingly, increased expression of Drp1 was associated with a decrease in transcriptional level of Drp1, which could be a cardioprotective mechanism of Drp1 to reduce fission, but

then offset by Drp1 not being turned over at the protein level. Reported post-translational modifications of Drp1 include phosphorylation, S-nitrosylation, ubiquitination and sumoylation (Chang and Blackstone, 2010). A possible inhibition of these post-translational modifications in HFD (DIO) group could explain the overexpression of Drp1 in contrast to its transcriptional level, which was decreased. There was a decrease in P-Drp1 (S637) in our model which suggests a shift towards fission as phosphorylation at S637 inhibits fission. These results are in agreement with Tsushima et al. (2018) showing a decrease in phosphorylated Drp1-S637 in a study of lipid overload in a transgenic model of cardiac lipotoxicity in postnatal hearts. Ni et al. (2020) also showed a decrease in P-Drp1 (S637) after 18 weeks 60% HFD (DIO) in mice but an increase in P-Drp1 (S616).

Drp1 receptors Fis1 and MID49 were significantly increased while Mff was significantly decreased. A decrease in Mff could be explained by the fact that Parkin ubiquitinates Mff under non-stressed conditions (Lee et al., 2019) and Parkin levels were increased in our model. Another explanation for that could be the interaction between Drp1 and Mff creating Drp1-Mff complex which was not detected by western blot. Liu and Chan (2015) confirmed that a Drp1-Mff complex forms and migrates to a higher molecular weight using a pull-down assay.

Drp1 receptors can all recruit Drp1 but it is still unclear about their function. A study found that Mff and Fis1 can work independently in mouse embryonic fibroblasts (MEFs) to regulate mitochondrial fission (Loson et al., 2013). They also found that MID49 and MID51 are capable of stimulating mitochondrial fission in the absence of both Fis1 and Mff. On the other hand, Palmer et al. (2011) proposed that MID49 and MID51 recruit inactive forms of Drp1.

2.4.6 Mitophagy and apoptosis and biogenesis

The PINK1-Parkin interaction is the most characterised pathway enabling mitophagy. An increase in both proteins suggests an activation of mitophagy in our model. Tong et al. (2019) found an increase in mitophagy using Mito-Keima at week 3 after 60% HFD (DIO) in mice which persisted after 2 months. They concluded that mitophagy was initiated at week 3 of a HFD (DIO) but was not adequate to maintain mitochondrial functionality during the early stages of DCM. Too many damaged mitochondria will lead to apoptosis. The induction of apoptosis in our model due to mitochondrial dysfunction is demonstrated by elevated TUNEL staining. Cardiomyocyte apoptosis was seen in 24 weeks of HFD (DIO) mice (Hsu et al.,

2016). Cai et al. (2002) showed an increase in apoptosis characterized by the release of cytochrome C and activation of caspase-3 in cardiomyocytes of diabetic mice caused by hyperglycaemia. It has been reported that mitochondrial diabetic heart has an increase propensity for mitochondrial permeability transition pore opening in human (Anderson et al., 2011) and diabetic animal models (Oliveira et al., 2003, Bhamra et al., 2008, Williamson et al., 2010). Moreover, Zhang et al. (2016b) reported a high expression of Bax and low level of Bcl-2 in STZ mice associated with left ventricular dysfunction. These finding suggest that cardiomyocyte apoptosis can occur in diabetic patients which could be caused by dysfunctional mitochondria and alteration in mitochondrial dynamics.

The balance between mitophagy and biogenesis is required for maintaining mitochondrial quality control (Andres et al., 2015). As a compensatory mechanism to mitochondrial loss, mitochondrial biogenesis will increase mitochondrial production which could explain the increase in TFAM level in our model. To assess mitochondrial number, citrate synthase activity, a marker for intact mitochondria, was measured but showed no significant difference. This suggests that the change in molecular analysis and functional studies is not due to changes in mitochondrial number.

Therefore, an increase in mitophagy/apoptosis and biogenesis was expected as a quality control mechanism to prevent further cardiac dysfunction, which could explain why OCR as well as respiratory chain complex activity was unchanged between groups. This finding was also reported by Littlejohns et al. (2014) who found no change in mitochondrial respiration after 20 weeks of HFD (DIO) In C57BL/6J mice. Delineating the mechanisms involved in regulating mitochondrial dynamics is important to develop strategies to effectively target the fission and fusion processes to attenuate mitochondrial dysfunction in obesity and in the early stages of DCM.

2.5 Conclusion

In summary, the HFD (DIO) leads to a cardiac phenotype that recapitulates symptoms seen in patients with early-stage DCM. The results of this chapter demonstrate an upregulation of Drp1, Fis1 and MID49 in the HFD (DIO) myocardium concomitant with a downregulation of P-Drp1(S637)/total Drp1 and Mff. Mitophagy is activated by an increased in both PINK1 and Parkin expression as well as apoptosis analysed by TUNEL assay. These protein changes correlate with an alteration in lipid profile, hyperglycaemia, insulin resistance, diastolic dysfunction and concentric remodelling. It is still unclear whether the changes in Drp1

protein are an adaptive cardioprotective response or represent the early stages of the pathogenesis of DCM. Most studies around Drp1 are non-cardiac and currently there is an incomplete understanding of the regulatory pathways involved. Similarly, the effect of this protein change on mitochondrial structure remains to be established. Therefore, in the next chapter, it will be investigated whether the elevation of fission proteins correlates with an increase in mitochondrial fission by electron microscopy.

Chapter 3 Cardiac mitochondrial remodelling in the high-fat diet mouse model

3.1 Introduction

The characterisation of the cardiac phenotype of HFD (DIO) was described in Chapter 2 by assessing heart function and other physiological measurements, which identified the development of early diastolic dysfunction. On a molecular level, proteins involved in mitochondrial dynamics and biogenesis have been altered. Therefore, it will be further investigated in this chapter whether the changes in mitochondrial dynamic proteins are reflected in a change in mitochondrial structure using serial block-face scanning electron microscopy (SBF-SEM).

Two common types of electron microscopy (EM) include Transmission electron microscopy (TEM) and scanning electron microscopy (SEM). TEM was used for the first time by Claude and Fullam (1945) to reveal a new understanding of the morphology of mitochondria. TEM uses a high-voltage electron beam to interact with the specimen's atom and produce a 2D image, while SEM is characterised by the detection of the backscattered electrons from the specimen after the exposure to the electron beam. Consequently, TEM provides details about the internal structure of the sample, while SEM presents details of the sample surface. Both techniques use an electron source that is in a high vacuum chamber. There are TEM studies that have shown that cristae morphology differs between cardiac mitochondrial populations. For example, it has been reported that SSM show lamellar cristae (Hollander et al., 2014), while PNM and IFM show tubular cristae (Riva et al., 2005). Even though TEM and SEM have both been used to produce a wide range of images to promote understanding of the structure of the mitochondria, the importance of understanding the three-dimensional (3D) features of the mitochondria and other biological characteristics is still to be fully recognised.

Through the new development of serial block-face scanning electron microscopy (SBF-SEM) by Denk and Horstmann (2004) the 3D reconstruction of a tissue's nanostructure has become possible at nm resolutions. SBF-SEM houses a microtome and SEM with low-vacuum operation and backscattering contrast. In short, the tissue (or cells) are chemically fixed (for full details and a review of the technique see Pinali and Kitmitto (2014)) and the sample is mounted on a pin in the microscope. The top of the block is imaged and then the microtome removes a thin slice, which in the case here was 50 nm thick. After that, the newly exposed block face is imaged. This process is iterative leading to the collection of serial images through the tissue block that are in register (Figure 3.1). SBF-SEM has been applied

successfully by Kitmitto's group to reconstruct the t-tubule network within sheep heart myocytes (Pinali et al., 2013) and the intercalated disc (Pinali et al., 2015). This thesis used SBF-SEM for the first time to investigate potential differences in mitochondrial subpopulations morphology between control and obesity-induced type 2 diabetes that is characterized by a significant increase in Drp1 expression. The putative differences in the mitochondrial subpopulations, SSM, IFM and PNM, are discussed in detail in the main Introduction, section 1.4.

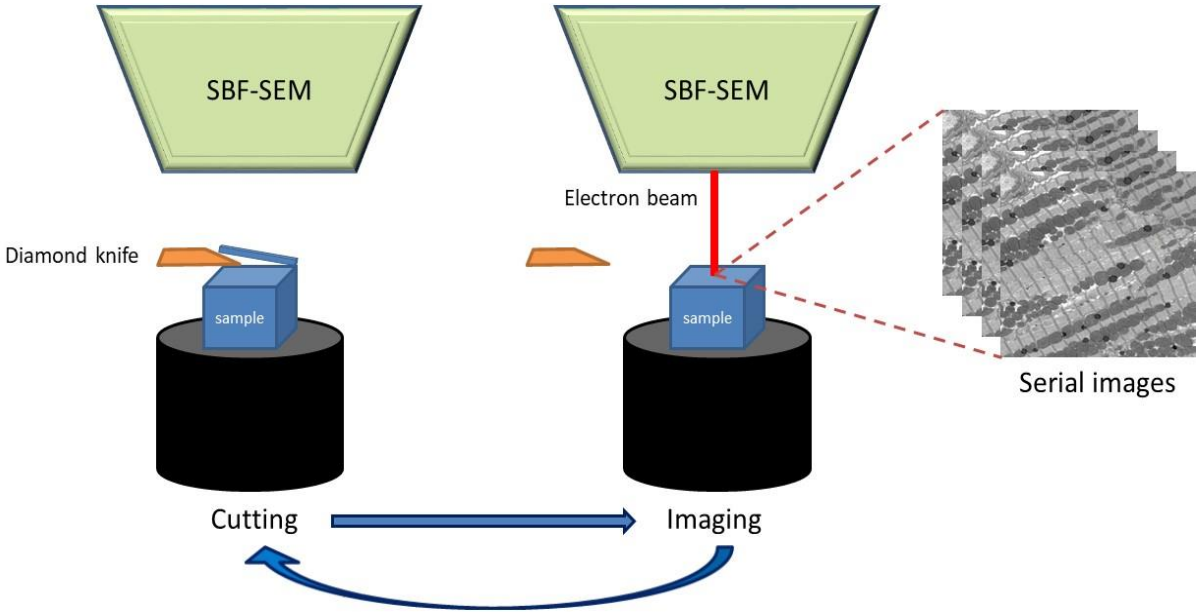

Figure 3.1: The principle of serial block-face scanning electron microscopy.
This is an illustration of a serial block-face scanning electron microscopy (SBF-SEM) technique showing the repetitive process of cutting and imaging to collect serial images from a sample forming a stack. The SBF-SEM consists of a scanning electron microscope (SEM) and an ultra-microtome mounted in the SEM specimen chamber which employs a diamond knife to cut the sections. It is used in this project to characterize the three-dimensional (3D) nanostructure of cardiac mitochondria at medium-high resolution. Images of block surface are collected by backscatter detection of electrons deflected from the electron beam scanning the surface of the block face.

One of the early events in the pathogenesis of diabetic cardiomyopathy is mitochondrial dysfunction. Kelley et al. (2002) found smaller mitochondria of the skeletal muscle in obese and type 2 diabetic patients. Using TEM, a significant decrease in subsarcolemmal mitochondria in obese and type 2 diabetes individuals has been reported (Ritov et al., 2005). Additionally, Dabkowski et al. (2010) showed a significant decrease in SSM size from the cardiac tissue of type 2 diabetic *db/db* mice compared to control. However, none of these studies employed 3D EM methods. The limitation of using 2D images is that the

interpretation can be misleading due to the factors of mitochondrial orientation in the specimen and the intersection of the cut angle.

Aims of this chapter include:

1) Collection of SBF-SEM datasets for the control (chow) and obese (high fat fed) apex; followed by segmentation of mitochondrial subpopulations SSM, IFM and PNM manually with IMOD software to measure the surface area and volume of each mitochondrial subtypes.
2) Assess the variance between SSM, IFM and PNM in control.
3) Evaluate the difference in surface area and volume of each mitochondrial subpopulation between control and HFD (DIO) model.

3.2 Methods

3.2.1 Sample preparation

At the end of the HFD (DIO) experiment, four obese and four control mice were euthanized. After heart excision, left ventricles (≈ 2mm^3) were fixed immediately in a fixative buffer containing 4% (v/v) formaldehyde, 2.5% (v/v) glutaraldehyde and 0.1M 4-(2-hydroxyethyl)-1-piperazineethanesulfonic acid (HEPES) and placed at room temperature for 2 hours prior to incubate it overnight at 4°C. Tissues were then washed 5 times with HEPES for 3 minutes each and then immersed in 2% (w/v) osmium tetroxide and 1.5% (w/v) potassium ferrocyanide in 0.2 M cacodylate buffer with 2 mM calcium chloride at room temperature for 1 hour. Tissues were then washed 5 times with double distilled water (ddH_2O) for 3 minutes each. Tissues were then incubated in a prepared thiocarbohydrazide solution (TCH) at room temperature for 20 minutes. TCH solution was prepared by preparing 94 mM of TCH in ddH_2O and heat it in the oven at 60°C for an hour. The tissues were then washed again with ddH_2O 5 times 3 minutes each. After the wash, tissues were then immersed for 30 minutes at room temperature in 2% (w/v) osmium tetroxide covered with foil. After another 5 washes with ddH_2O, Tissues were incubated overnight in an aqueous 1% (w/v) uranyl acetate at 4°C.

The tissues were then washed the following day 5 times with ddH_2O for 3 minutes each then incubated in Walton's (Walton, 1979) lead aspartate staining (0.02 M of lead nitrate in 0.03 M aspartic acid, pH=5.5) and for 30 minutes in a 60°C oven. It was washed again with ddH2O 5 times 3 minutes each. For dehydration, tissues were placed in ice-cold 20%, 50%, 70%, 80%, 90%, 100% and 100% (v/v) ethanol for 10 minutes each and then placed in acetone at room temperature for 20 minutes. It was then infiltrated with 25%, 50% and 75% (v/v) resin in acetone for 2 hours each. After that, it was infiltrated in 100% (v/v) resin for 2 hours, this was repeated 3 times. Tissues were next embedded in a 100% resin in a mould and were baked in a 60°C oven for 48 hours into resin capsules. The tissue pieces were then mounted on aluminium pins. A glass knife was used to trim blocks to squares (≈1 mm3). After that, it was coated with gold for imaging.

3.2.2 Serial block face scanning electron microscopy

FEI Quanta 250 Scanning EM supplemented by 3View ultramicrotome (Gatan) was used to image the samples. The vacuum was set to 0.3-0.5 torr and the operating voltage to 3.8 kV. A diamond knife was used to cut a serial 50 nm sections. Each section was imaged producing a stack of images with a voxel size 13.3:13.3:50 nm (X, Y, Z).

3.2.3 Image analysis

Datasets of 1000 images were collected for each sample. IMOD software (Kremer et al., 1996) was used to segment approximately 30 mitochondria for each different population of mitochondria i.e. SSM, IFM and PNM in three different cells of one sample. Each mitochondrion was segmented manually using closed contour by drawing around the surface of it as shown in Figure 3.2, a published review by our group (Daghistani et al., 2019).

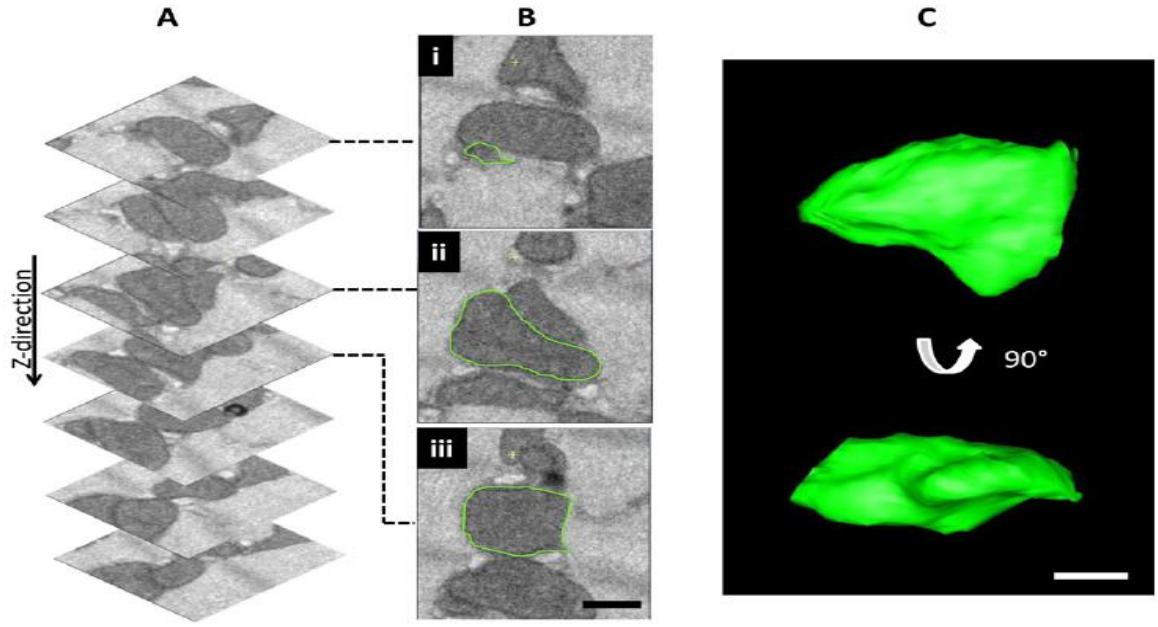

Figure 3.2: Three-dimensional reconstruction of cardiac mitochondrion from a mouse. Each mitochondrion was segmented manually through the stack to generate 3D image. A. The stack of images collected by serial block-face scanning electron microscopy of murine cardiac tissue (the cut-depth in Z-direction = 50 nm). B. A mitochondrion segmented (outlined) in green. (B, i) The mitochondrion when it becomes visible for the first time in the stack. (B, ii) A tubular shape after of the mitochondrion after around 300 nm deeper. (B, iii) Approximately a square shape mitochondrion after a further 100 nm deeper. C. 3D structure of the mitochondria using IMOD after segmentation of the highlighted mitochondrion. Scale bars = 500 nm. (Daghistani et al., 2019).

3.2.4 Statistical analysis

Following the identification of the distinct subpopulations of mitochondria based on their location, about 90 for each SSM, IFM and PNM from 3 different cells were segmented by the IMOD software (Kremer et al., 1996) from each sample (Control n=4 and HFD (DIO) n=4 mice). One-way ANOVA (with post-hoc test) was used to assess inter-animal variation in each experimental group. The mean ± SEM (n=4) was then calculated for SSM, IFM and PNM for each sample and were compared together by one-way ANOVA (with post-hoc test). The comparison between control and HFD (DIO) were analysed using unpaired t-test. Data were assessed for normality using Shapiro-Wilk test. All statistical tests were conducted

using GraphPad Prism (version 7, California, USA). Data were considered statistically significant when $P<0.05$.

3.3 Results

To understand how changes in obesity affect mitochondrial structure, SBF-SEM was employed to investigate different subpopulations. The first task was to define the spatial location of the three mitochondrial subtypes. Figure 3.3 illustrates the definition of the three different spatial subpopulations in a control cardiac tissue employed here. It is clear from the figure that SSM are located under the cell membrane (sarcolemma). IFM are positioned between the muscle fibrils, whereas PNM are around the nucleus. As can be seen from the figure below, PNM formed clusters around the two poles of the nucleus. SSM as well tend to form clusters underneath the sarcolemma, whereas IFM reside between contractile myofibrils forming longitudinal rows.

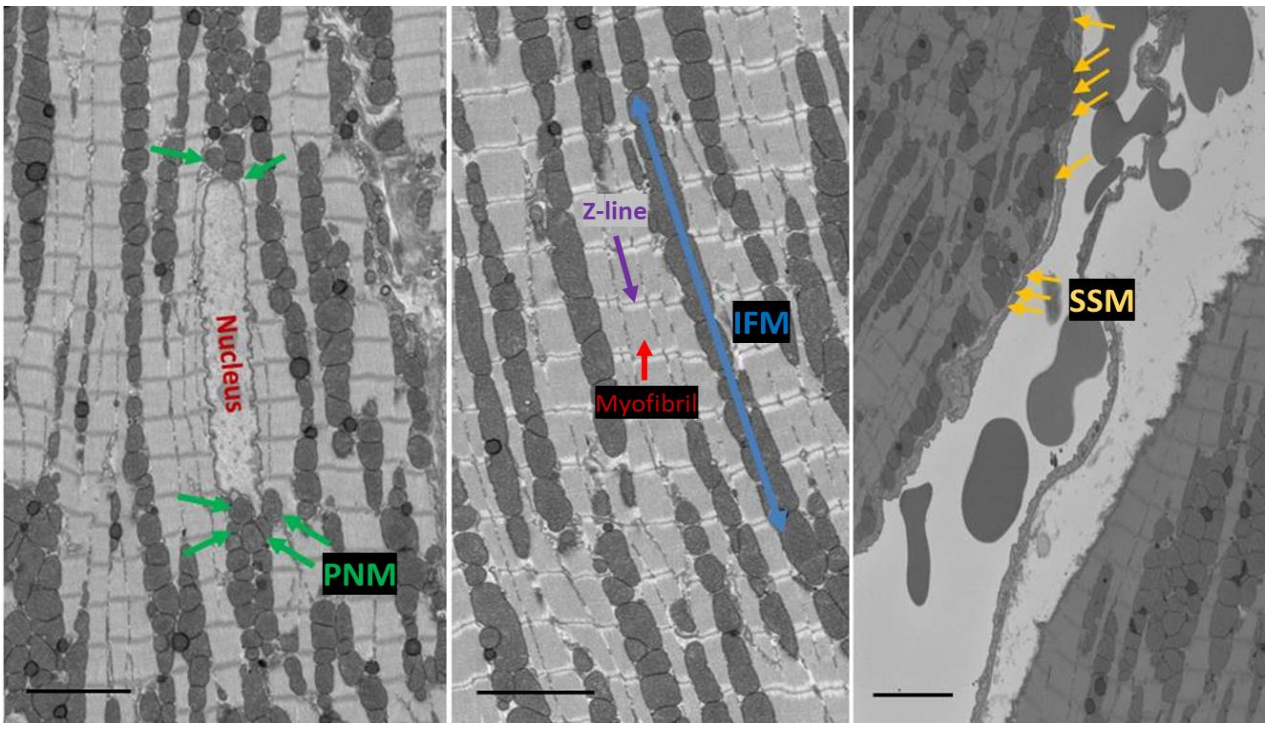

Figure 3.3: Identification and segmentation of various control sub-populations of mitochondria.
Green arrows highlight perinuclear mitochondria (PNM) which were selected only if they were touching the nuclear envelope. Yellow arrows indicate subsarcolemmal mitochondria (SSM) which were only selected if they were touching or immediately adjacent to the cell membrane. The long blue arrow points out how the interfibrillar mitochondria (IFM) form a longitudinal row which only those flanked by myofibrils (red arrow) were selected. The purple arrow highlights the z-line. Scale bar = 5 µm.

Therefore, for consistency of analyses we only segmented those SSM that were in direct contact (or immediately juxtaposed) to the sarcolemma, those IFM that were flanked on either side by myofibrils and PNM that were touching or immediately adjacent to the nuclear envelope. Figure 3.4 illustrates how the different spatial populations can be manually reconstructed in 3D using the IMOD software. Similarly, other features such as the sarcolemma and nucleus can be segmented to illustrate the inter-organelle relationships. This figure shows how the SSM cluster below the sarcolemma and the longitudinal row nature of IFM and the distribution of PNM around the nucleus.

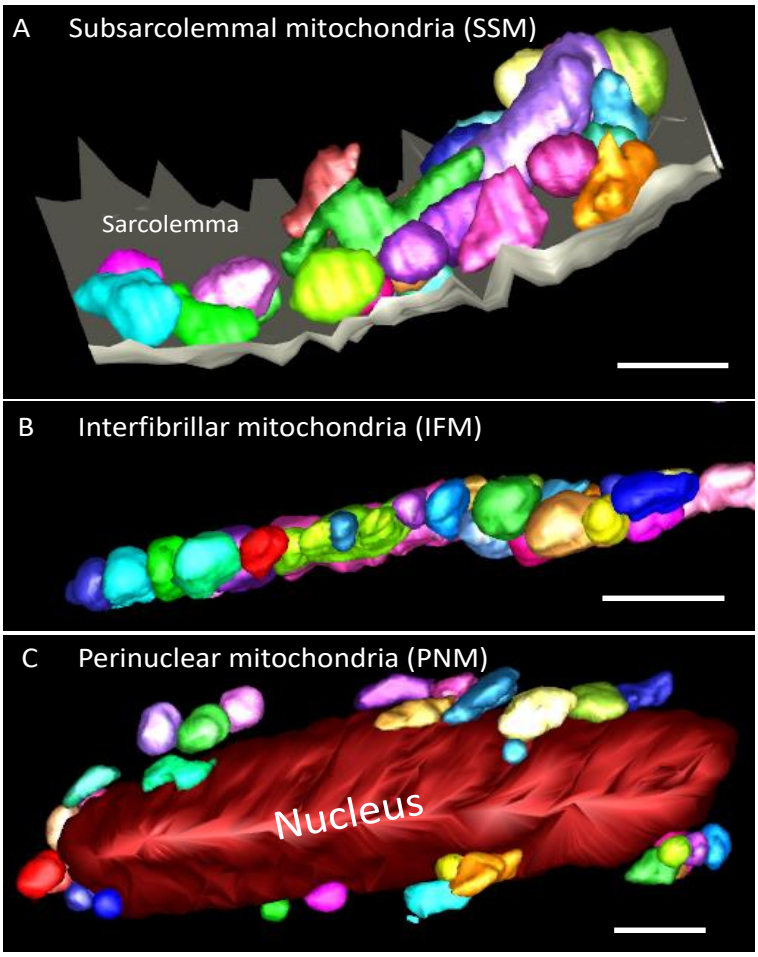

Figure 3.4: 3D reconstruction of different mitochondrial subpopulations in the heart of control mouse.
A. 3D segmentation of subsarcolemmal mitochondria adjacent to the sarcolemma (Grey). B. Longitudinal rows of interfibrillar mitochondria. C. Perinuclear mitochondria around the nucleus (red). Scale bar = 2 µm.

3.3.1 PNM of the control mice are the smallest compared to SSM and IFM.

To investigate inter-animal variability, one-way ANOVA was applied between control mice for SSM, IFM and PNM for each of the surface area, volume and surface area/volume ratio (SA/Vol) (Figure 3.5). There were no variations in these parameters between the control animals for the different mitochondrial subpopulations.

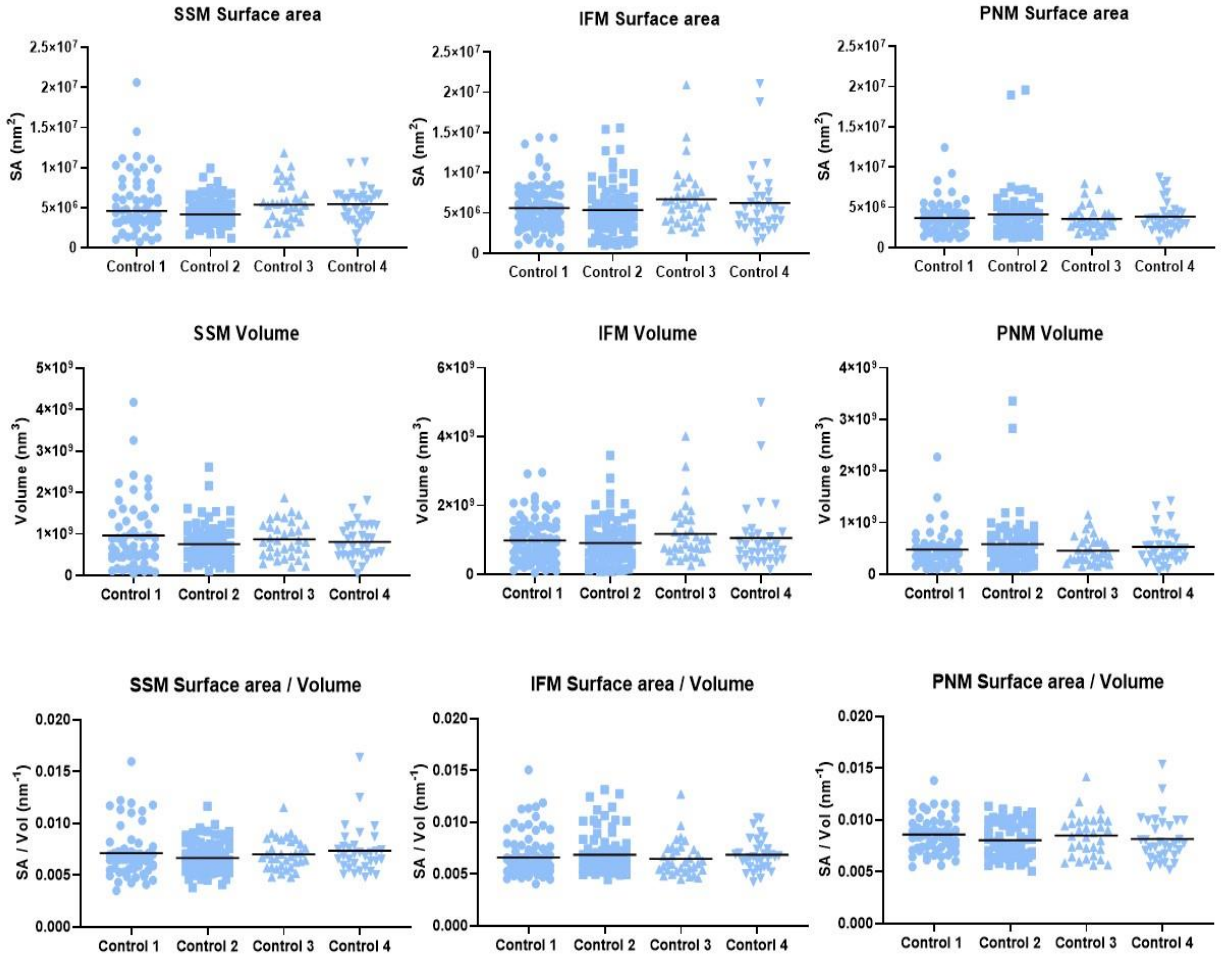

Figure 3.5: No inter-animal variability in control mice for morphometric parameters of different subpopulations cardiac mitochondria.
There was no significant difference for each mitochondrial subset (SSM, IFM and PNM) surface area, volume and surface area/volume ratio. Data represented as scatter plot where each dot represents one mitochondrion reading. Horizontal lines represent mean value.

As there was no inter-animal variability in control, the average for the surface area and volume for SSM, IFM and PNM were as follows: 5.2 ± 0.26 x10^6 (SSM) 6 ± 0.3 x10^6 (IFM) 3.8 ± 0.1 x10^6 (PNM) (nm^2); 8.4 ± 0.5 (SSM) 9.8 ± 0.3 (IFM) 5.2 ± 0.2 x10^8 (PNM) (nm^3).

The surface area and volume comparison between the SSM, IFM and PNM has shown that in both parameters there was no significant change between SSM and IFM, while the PNM were significantly smaller than SSM and IFM (Figure 3.6A and 4B). Interestingly, the surface area to volume ratio (SA/Vol) of PNM was significantly higher than IFM and SSM in control mice (Figure 3.6C), which may be related to function, i.e. juxtaposition to the nucleus to improve diffusional properties.

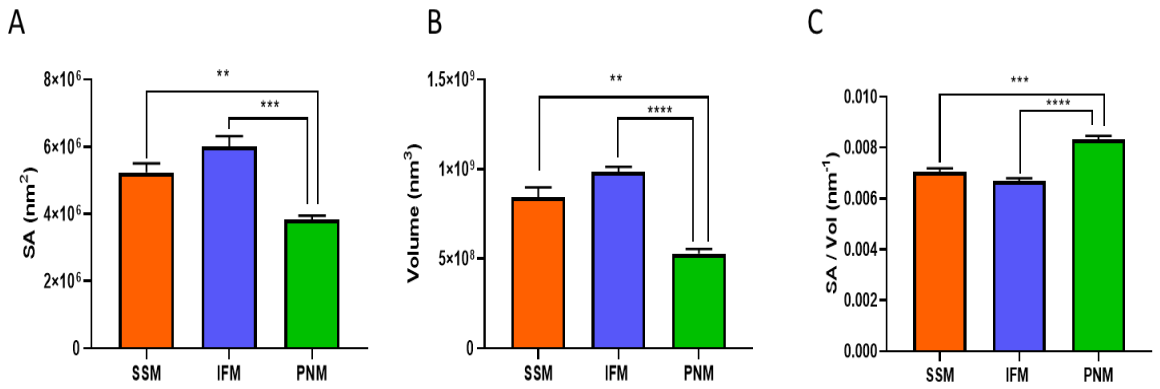

Figure 3.6: IFM were the largest in size in control mice compared to other cardiac tissue mitochondrial subpopulation.
A. Comparison of the surface area showed that PNM are significantly smaller than SSM and IFM. B. The volume of the PNM is significantly smaller than that of SSM and IFM. C. Surface area/volume ratio of PNM is significantly larger than SSM and IFM. No significant difference between SSM and IFM surface are, volume and surface area/volume. Data are expressed as mean ± SEM. n=4 animals. **P≤0.01 ***P≤0.001 ****P≤0.0001.

3.3.2 Inter-animal variability in mitochondrial size of HFD (DIO) mice.

Next, the variation of each HFD (DIO) mouse morphometric parameters of its mitochondrial subpopulations were studied using one-way ANOVA. As shown in Figure 3.7, unlike control mitochondria, there was a significant inter-animal variation in HFD (DIO) mitochondria.

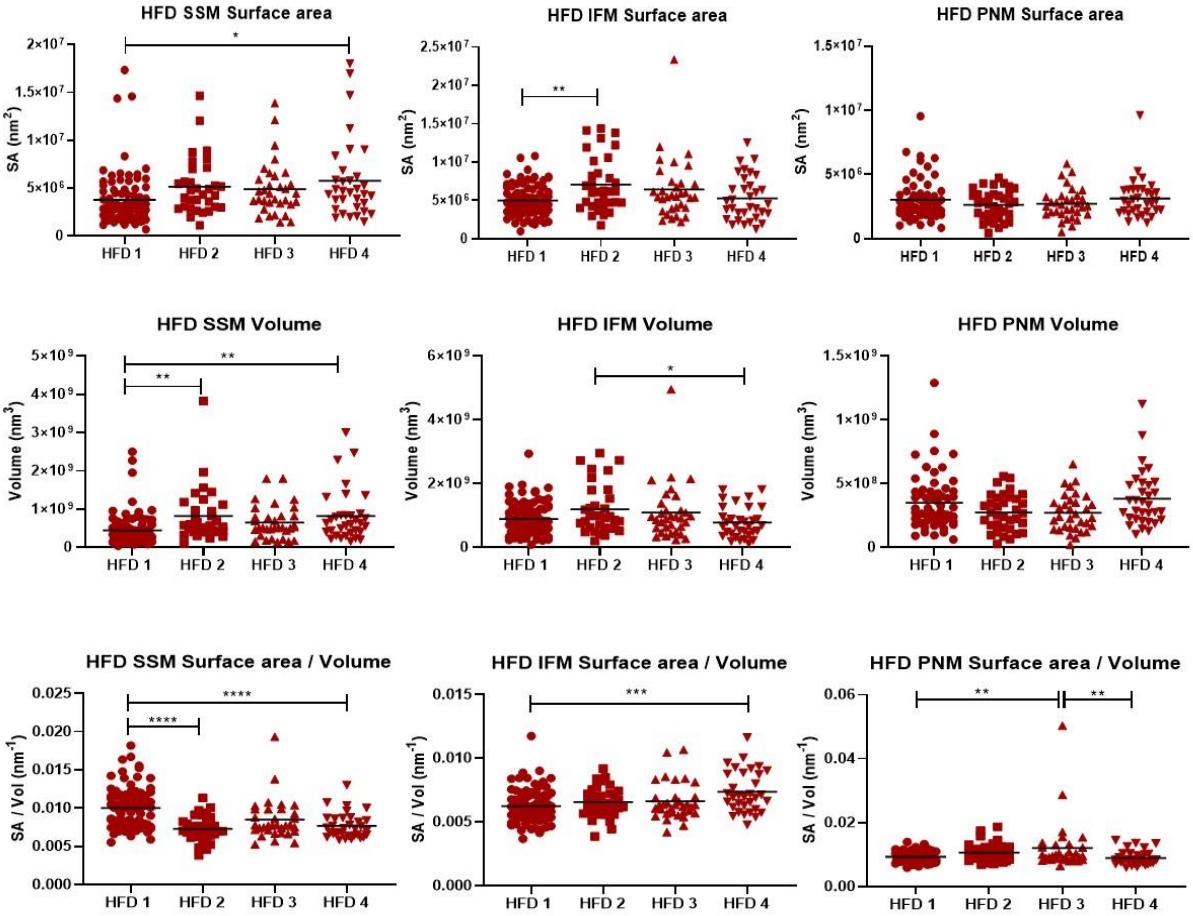

Figure 3.7: Alteration in inter-animal variability for morphometric parameters of different subpopulations mitochondria in HFD (DIO).
Raw data from cardiac tissue taken from HFD (DIO) mice. Using one-way ANOVA, it showed inter-animal variability between morphometric parameters of SSM, IFM and PNM. *P≤0.05 **P≤0.01 ***P≤0.001 ****P≤0.0001.

Due to the inter-animal variation in HFD (DIO), the analysis of morphometric parameters of mitochondrial subpopulations for each HFD (DIO) animal was done separately (Figure 3.8). There was a pattern of increasing size PNM < SSM < IFM, which was consistent for at least three HFD (DIO) mice. Taken the average values of the surface area (Figure 3.8B), PNM was significantly smaller than SSM and IFM. However, despite the inter-animal variation calculation of the average (n=4) for each parameter showed a similar profile to surface area with PNM being the smallest (Figure 3.9D). In addition, IFM were significantly larger than SSM.

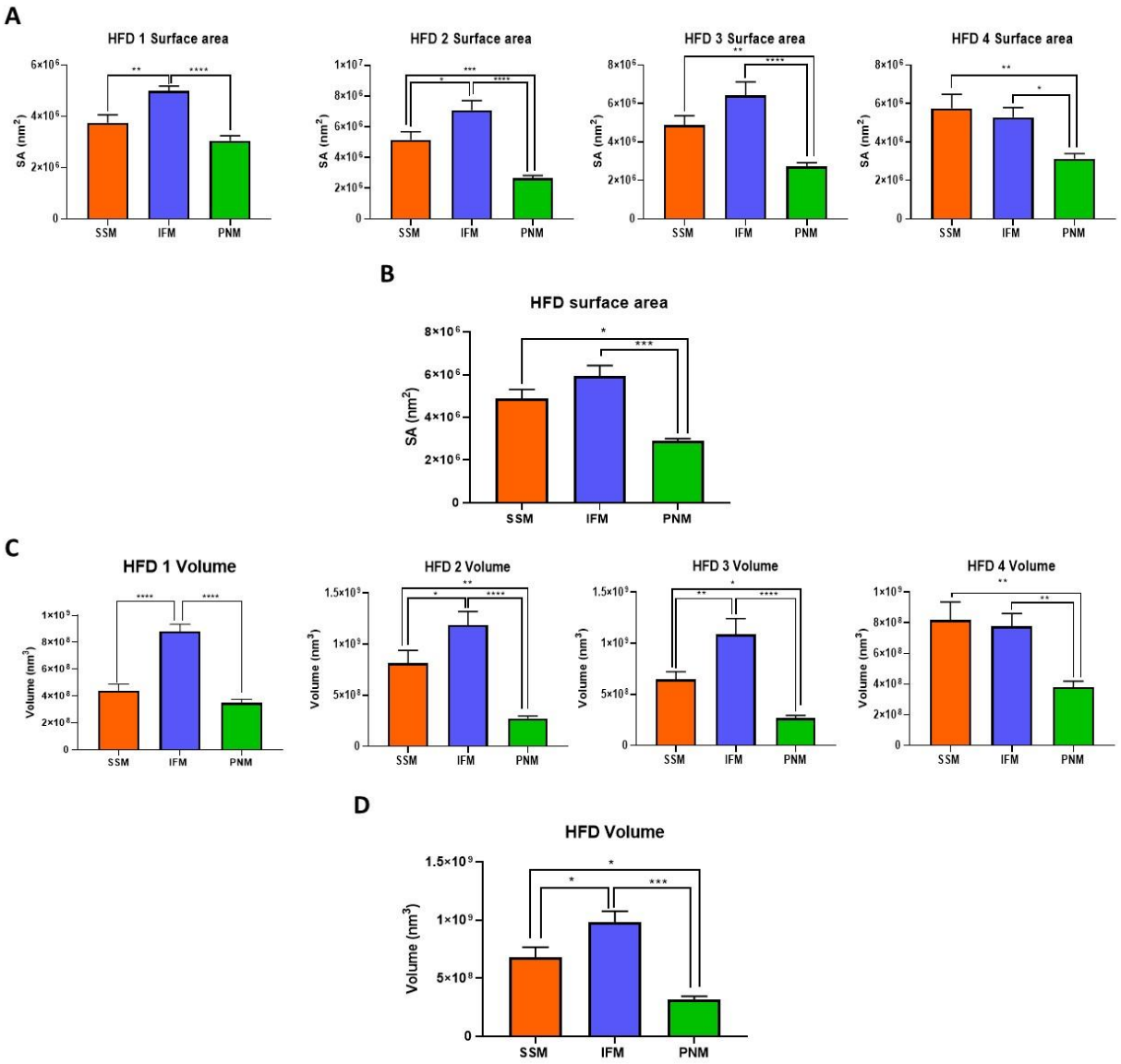

Figure 3.8: IFM were the largest in size and PNM the smallest in HFD (DIO) mice.
A. Analysis of the surface area for each HFD (DIO) mice separately. B. Analysis of the surface area of the average values for each HFD (DIO) mouse. C. The volume of different mitochondrial subpopulation of each HFD (DIO) mouse. D. The average volume of SSM, IFM and PNM of each HFD mouse. Data are expressed as mean ± SEM. n=4 animals *P≤0.05 **P≤0.01 ***P≤0.001 ****P≤0.0001.

The same analysis was applied for SA/Vol of each HFD (DIO) mouse. A common pattern of PNM having the largest SA/Vol is consistent with the control data (Figure 3.10A). Calculating the average of all animals the PNM surface area to volume ratio was also shown to be the largest (Figure 3.10B).

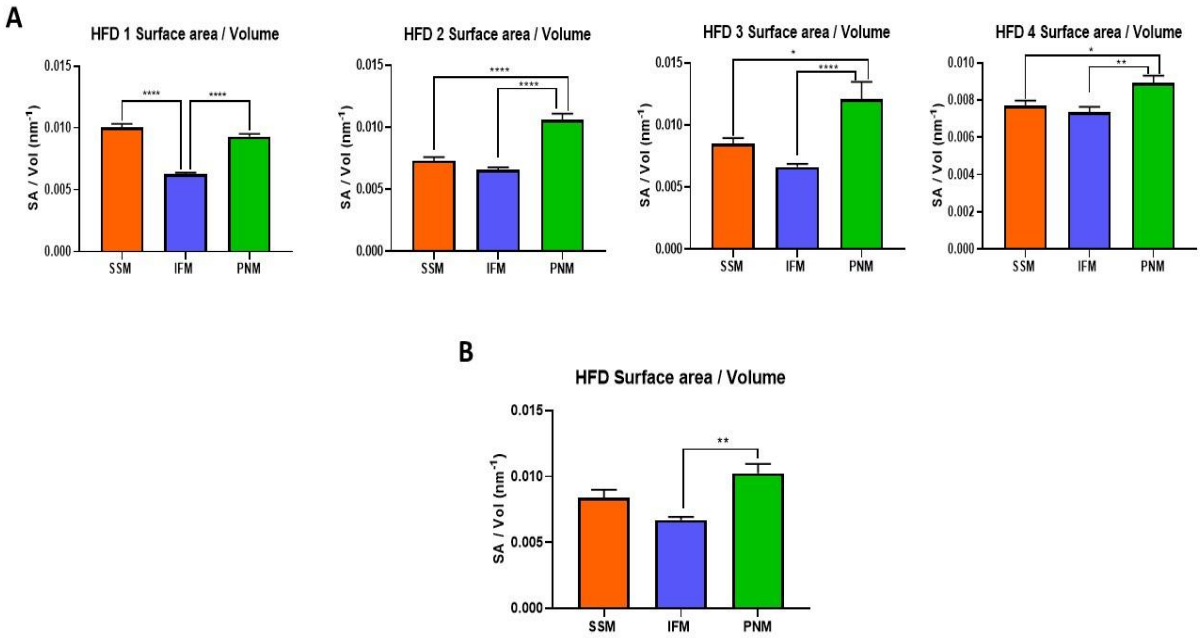

Figure 3.9: The surface area to volume ratio in PNM was the highest in HFD (DIO) mice compared to other subpopulation of cardiac mitochondria.
A. The surface area to volume ratio of each HFD (DIO) of each mitochondrial subpopulation. B. A comparison of surface area to volume ratio of SSM, IFM and PNM of the average values of each HFD (DIO) mouse. Data are expressed as mean ± SEM. *P≤0.05 **P≤0.01 ****P≤0.0001

3.3.3 PNM are smaller in the HFD (DIO) model compared to control.

As shown in Figure 3.10A, SSM morphometric parameters were not changed in HFD (DIO) compared to control. The same profile was for IFM (Figure 3.10B). Interestingly, both PNM surface area and volume were significantly decreased in HFD (DIO) compared to control. The HFD (DIO) PNM volume are at around 0.6x smaller than control PNM. The mean ± SEM of HFD (DIO) PNM volume is 3.1 ± 0.2 $x10^8$ nm3 compared to age-matched control 5.1 ± 0.2 $x10^8$ nm^3; n=4 per group. On the contrary, the surface area/volume ratio was significantly increased in HFD (DIO) compared to control (Figure 3.10C).

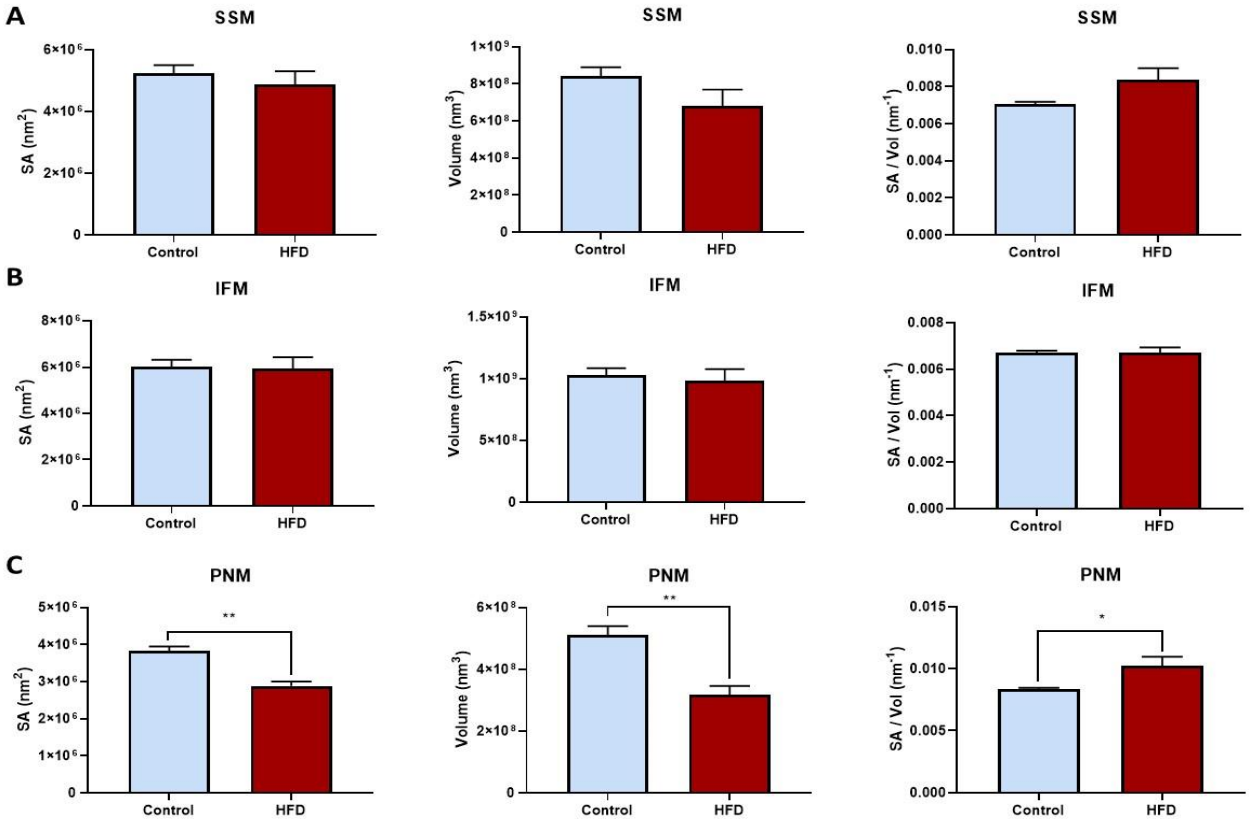

Figure 3.10: PNM were smaller in size in HFD (DIO) mice compared to control.
A. SSM in the HFD model showed no significant difference in surface area, volume and surface area to volume ratio compared to control. B. all morphometric parameters were not significantly changed in IFM in the HFD model compared to control. C. PNM in the HFD model showed a significant decrease in surface area and volume, while surface area to volume ratio was significantly increased compared to control. Data are expressed as mean ± SEM. n=4 mice. *P≤0.05 **P≤0.01.

3.3.4 Summary of results

The present study explored by SBF-SEM the mitochondrial structure in the cardiac tissue and how these are modulated in the HFD (DIO) diabetic mouse. The key results of this chapter were:

- PNM were significantly smaller in size compared to SSM and IFM in control heart, with no difference between the sizes of SSM and IFM.
- PNM from the control heart had the largest surface area to volume ratio among other subpopulations.
- Although there is an inter-animal variability in the HFD (DIO) heart, there was a consistent pattern of different mitochondrial subtypes size, IFM>SSM>PNM.
- As reported for control, the surface area/volume ratio of PNM was the largest in HFD (DIO) heart as well.

- A comparison of control and HFD (DIO) identified that PNM were significantly smaller in HFD (DIO), but that the SA/volume ratio was significantly larger in HFD (DIO) compared to age-matched control.

These novel results report mitochondrial morphological remodelling/adaptation to obesity/T2DM stress on the heart that are in line with molecular changes identified in Chapter 2, indicating an increase in mitochondrial fission in the HFD (DIO).

3.4 Discussion

3.4.1 Morphological differences in control mitochondrial subpopulations.

Interestingly, we determined that the PNM in the cardiac tissue of control mice were smaller than SSM and IFM in size, in agreement by an independent study in our group using a different mouse strain and genetic model of type 2 diabetes at 6 months of age (Bodour Rajab, PhD Thesis). We suggest that this may be explained by the different mitochondrial subtypes having distinct roles in the cell (as described in the general introduction (Chapter1), physiological differences in structure therefore would be expected. Lukyanenko et al. (2009) showed by using immunofluorescent labelling that PNM were smaller in size compared to IFM in rat ventricular myocyte. They also noted that PNM has a round shape, whereas IFM is more oval shape. It is worth noting that the immunofluorescence is limited by the quality of staining that is targeted specifically to the protein of interest and only provides a 2D visualization of the model at low-resolution (200-300 nm in the lateral axis and 500-700 nm in the axial axis) (Huang et al., 2009). Here, we have advanced this earlier study by measuring at a higher resolution using SBF-SEM that volume and surface area of PNM were smaller than IFM and SSM. We have not noticed a difference in the shape between PNM and IFM e.g. PNM rounder than IFM as mentioned in previous studies. These findings may be biased due to the limitation of 2D images. Importantly, the study here allowed calculation of the surface area to volume ratio (SA/Vol) showing that PNM in the control heart had a larger SA/Vol compared to SSM and IFM. We propose that this parameter may aid diffusion properties that are beneficial for mitochondria in close contact to the nucleus are important for the efficiency of energy production may therefore be improved (Dzeja et al., 2002). Like control, PNM of the HFD (DIO) were also the smallest among other mitochondrial subtypes and its surface area to volume ratio was the largest.

Cristae morphology has been reported to be varied between different mitochondrial subtypes. The resolution limitation of SBF-SEM (~13 nm: X-Y plane and 50 nm: Z plane) made it difficult to study the cristae structures in these specimens. Cristae morphology would be useful to study as future work. It could be valuable for future work as well to increase the number of PNM and include the entire clusters around the nucleus, not just those that touch the nucleus to determine if the larger SA/Vol is only a feature of those mitochondria directly in contact with the nucleus. It is also worth comparing different types of PNM as well e.g. PNM in the poles of the nucleus with PNM on the sides of the nucleus.

3.4.2 Mitochondrial ultrastructure in HFD (DIO).

Smaller fragmented mitochondria have been widely described in a variety of cardiac diseases, as reviewed in (Daghistani et al., 2019). For example, Boudina et al. (2007) concluded that in a *db/db* mouse heart, a model of T2DM, there are smaller mitochondria, and that the mitochondrial density is increased by 50%. Chen et al. (2009) found small and fragmented mitochondria in failing hearts of a coronary ligation rat model using TEM. On the other hand, cardiac samples from UCP-DTA transgenic mice, a model of obesity, showed larger mitochondria than control by TEM. The variations noted in the previous studies could be a consequence of the technique used. The interpretation of 2D images can be influenced by the section angle or the area of the cell analysed which may be misleading.

Interestingly, the size of the PNM decreased in HFD (DIO) compared to control. This is consistent with the molecular results reported in Chapter 2, showing an increase in fission protein (Drp1) which intuitively would suggest smaller mitochondria. On the other hand, IFM and SSM of HFD (DIO) was not changed in size compared to control. These data may suggest that some subpopulations are more vulnerable than others to stress conditions. For example, Dabkowski et al. (2009) reported a decrease in size in IFM but not SSM in the heart tissue of STZ type 1 diabetic mice. The decrease in IFM size coincided with a reduction in IFM complex activity. They suggested that IFM is more vulnerable to T1DM stress. In a comparison of IFM and PNM in adult cardiac myocyte, Lu et al. (2019) suggested that IFM are more sensitive to oxidative stress. They also showed translocation of IFM to the perinuclear region for undergoing mitophagy under conditions of starvation in cardiac myocytes (using photoactivatable mtPA-GFP), with disruption of the microtubule network using nocodazole shown to prevent IFM movement to the perinuclear region. Significantly, the study also showed that the fission/fusion rate of PNM is faster than that of IFM. Hence, the perinuclear region may be the primary location for mitochondrial turnover for all mitochondria subtypes. The damaged mitochondria of IFM in our model might be translocated to the perinuclear region for mitophagy as a part of quality control. This could explain the change in size of the HFD (DIO) model occurred only in the PNM. In previous studies, the size of IFM were changed in some diabetic models. It may be the case that translocation of damaged mitochondria to the perinuclear space occurs as a quality control process only at the early stage of diabetic cardiomyopathy. Long-term uncontrolled stress might affect mitochondrial motility so that damaged IFM will remain in their location, which could eventually lead to systolic dysfunction, as IFM is the energy provider for contractile

myofibrils of the heart. This can be further supported by our previous results, which showed no systolic dysfunction in HFD (DIO) compared to control, illustrated by normal ejection fraction. Since microtubules are crucial for the translocation of damaged mitochondria to the perinuclear region for mitophagy, which is activated in our HFD (DIO) model (increased in PINK1 and Parkin expression), future research could be undertaken to investigate changes in mitochondrial motility e.g. Miro1 and Miro2 with disease progression.

Although PNM were fragmented in HFD (DIO), mitochondrial function assessed by complexes activity and oxygen consumption rate in section 2.3 was not affected. Early changes in the structure could prevent further damage to the mitochondria and consequent dysfunction. Ritov et al. (2005) found a decrease in Complex activity only in the SSM in the skeletal muscle of T2DM individuals, while the overall activity was normal. They also found SSM were significantly smaller in T2DM subjects compared to control. It may be useful for future work to assess the function of each mitochondrial subtypes separately by isolation of mitochondrial fraction. Ritov and his colleagues reported that mtDNA was lower in T2DM volunteers than that of control. It might be informative as well to measure mtDNA in our model in future work.

Surprisingly, the SA/Vol of the fragmented PNM of the HFD (DIO) was significantly higher than that of the control despite being smaller in size. This could be a compensatory response as higher SA/volume means more contact to the nucleus as a compensation of the small size. Better diffusional properties are needed in the PNM of HFD (DIO) due to an increased energy demand caused by smaller mitochondria. The contact of the PNM to the nucleus might be important in crosstalk. A defective communication between these two organelles is reported to lead to calcium overload, metabolism disorders and DNA damage (Xia et al., 2019). Employing a higher resolution technique e.g. focused ion beam with scanning electron microscopy (FIB-SEM) which is similar to SBF-SEM but employs a laser to remove the top layer of the block, with resolutions up to typically <10 nm: X-Y plane and 20 nm: Z plane (Xiao et al., 2018) or electron tomography (resolutions < 5nm) might also be useful for studying the SA/volume ratio of the cristae in which the Complexes are organised for optimising OXPHOS (Davies et al., 2014).

PNM are believed to be involved in providing energy to the nucleus for transcription (Ong et al., 2017). Given the fact that HFD (DIO) PNM were fragmented, metabolic pathways that take place entirely inside mitochondria e.g. Krebs cycle and fatty acid oxidation or partially

e.g. urea cycle might be affected in the HFD (DIO). These pathways investigated by LC-MS/MS in Chapter 6. In this project, the implementation of SBF-SEM gives for the first time a global picture of the *in situ* mitochondrial structure and the 3D reconstruction provides an evaluation of the morphological parameters.

3.5 Conclusion

Taken together, these results illustrate that changes to mitochondrial structure in cardiac tissue is an early sign of diabetic cardiomyopathy concomitant with changes to fission protein expression (See Section 2.3). We found that PNM are more vulnerable to obesity/T2DM with almost no impact on IFM and SSM. A further study with more focus on PNM may form the basis of future work. These morphological changes may be a result of there being increased damaged mitochondria due to increasing mitochondrial fragmentation but with defective mitophagy. These conclusions support increases in fission protein (Drp1) and mitophagy proteins (PINK1 and Parkin) expression, indicating a potential adaptive response to obesity/diabetic insult. Given that functionally we have shown no change to Complex activity or OCR we speculate that either fission is initially a cardioprotective response to the obesity/diabetic stimuli or that there is a limited number of damaged mitochondria; however, these remodelling events may be pathological under long-term exposure to the stress conditions. There are still many unanswered questions around obesity and whether for example lifestyle changes can bring about a reverse in the remodelling events at the level of cardiac function and at the molecular level. The following Chapter will study the effect of exercise, diet exchange and exercise/diet exchange to reverse molecular changes seen in HFD (DIO) model.

Chapter 4 Effects of exercise and/or diet exchange on the HFD (DIO) cardiac and mitochondrial phenotype

4.1 Introduction

Although the National Health Service (NHS) spends 9% of its budget annually which equals £8.8 billion on the treatment of T2DM, it is preventable by controlling obesity, which is an important risk factor for T2DM (Awa et al., 2012, Public Health England, 2015). Preventing T2DM is achieved by managing obesity by diet and activity (Lau et al., 2007). One of the most recommended non-pharmaceutical treatments for obesity/T2DM is exercise (Nogueira-Ferreira et al., 2016). Exercise has been reported to play a major role in cardiac function improvement in DCM (Seo et al., 2019). Veeranki et al. (2016) found an amelioration of cardiac dysfunction seen in obese-diabetic (*db/db*) mice through restoration of mitochondrial function. Exercise reduces the risk factor for cardiovascular complications associated with obesity and T2DM such as blood pressure, lipid profile, waist circumference, BMI and insulin resistance (Golbidi and Laher, 2012). Reduced-calorie diets are also associated with an amelioration of systolic and diastolic dysfunction in obese individuals (de las Fuentes et al., 2009). However, a lack of patient compliance to exercise and healthy diet highlights the need for a detailed understanding of cardiac mitochondrial function through molecular level changes. There have been no detailed studies on the effects of exercise and diet on cardiac mitochondrial function in obesity, particularly in the context of mitochondrial dynamics. The following are the specific objectives of this chapter:

- To establish an exercise regimen in obese mice using a daily swim training protocol.
- To investigate using obese mice the potential effects of exercise, diet exchange (replacement of the HF diet with normal chow) and exercise/diet exchange in reversing diastolic dysfunction in obesity.
- Study the effects of exercise, diet exchange and the combination of both exercise and diet exchange on mitochondrial dynamics alteration due to obesity.

4.2 Method

4.2.1 Animal model

Chapter 2 characterised the molecular and structural changes and dysfunction in the heart of obese/T2DM mice. This Chapter has established a second HFD (DIO) group incorporating exercise training and/or diet exchange starting at week 12 for 5 weeks to determine if the 'healthy' cardiac phenotype at the physiological and mitochondrial level is restored.

Mice were acclimatised for 1 week before the start of the experiment and then randomized into 4 groups at the age of 8 weeks (n= 4-5 mice per group). Group 1 (age-matched control) was fed a chow diet for 17 weeks. Group 2 - the exercise group (E) was fed a high-fat diet for 17 weeks and then exposed at week 13 to swimming exercise for 5 weeks. Group 3 - the diet exchange group (D) was fed for 12 weeks on a HFD (DIO) then replaced with a chow diet for 5 weeks. Group 4 - the exercise/diet exchange group (E+D) was fed a high-fat diet for 12 weeks, with the HF diet exchanged for chow and daily swimming for 5 weeks.

Mice were initially swim trained for 10 minutes on the first day. The training length was increased daily by 10 minutes for 5 days to a final duration of 50 minutes at the end of the first week. The following week, mice exercised five days per week for 1 hour once a day. Mice were pen marked on the tail for identification. The tank was filled to an appropriate level with water at a temperature of 29-32◦C. The surface area of the tank was 2500 cm^2 and the depth was around 35 cm (Figure 4.1)

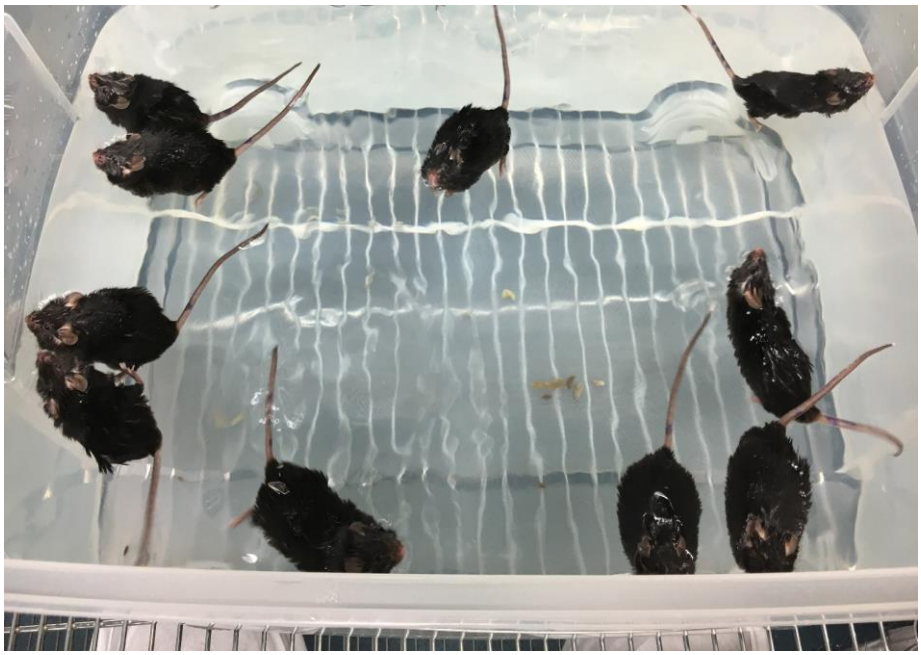

Figure 4.1: Swimming in a tank of water.
A maximum of 10 mice in the tank at the same time. The mice tails were labelled for identification. The surface area of the tank is 2500 cm^2 and the depth is 35 cm.

Mice were observed for the whole swimming time for any signs of stress. One mouse from the exercise/diet exchange group was withdrawn from the study because he was unable to swim comfortably and appeared distressed more than one time. Mice were scooped in and out of the tank. At the end of each session, mice were thoroughly towel-dried and transferred to a warming cabinet for a minimum of 1 hour and a maximum of 2 hours to ensure they are dry. A maximum number of 10 mice were allowed in the tank at the same time.

4.2.2 Physiological and metabolic parameters measurement

The weights of mice were measured at baseline and at regular intervals during the trial. Random blood glucose was assessed using Accu-Chek Aviva after restraining the mouse and prick the lateral tail vein at the end of the experiment. Insulin levels were measured using an ELISA kit by ALPCO (80-INSMS-E01) previously described in 2.2.2.1. TG level was measured using a Colorimetric Assay Kit (Cayman Chemical 10010303) as described in section 2.2.2.3. To assess cardiac function and wall thicknesses, echocardiography was performed for all groups (See Chapter 2.2.2.4). In addition, non-invasive ECG was performed to assess the heart rate (See Chapter 2.2.2.5).

4.2.3 Gene expression and Western blotting

Mice cardiac tissue harvested as described in section 2.2.1. Tissue harvesting Quantitative RT-PCR (qPCR) for exercise, diet exchange and exercise/diet exchange groups were performed to determine changes in mitochondrial dynamics protein transcript level. RNA extraction, DNase treatment, reverse transcription and qPCR were described in Method section 2.2.4. Changes to protein expression levels in each experimental model were carried using Western blotting as described earlier in section 2.2.3.

4.2.4 Statistical analysis

All results are shown as mean ± standard error of the mean (Mean ± SEM). The data were analysed with GraphPad Prism (Version 7, California, USA). Data were assessed for normality using Shapiro-Wilk test. A one-way ANOVA followed by Dunnett's test was used to compare each mean to the mean of the control group. The data were considered statistically significant if $P<0.05$.

4.3 Results

4.3.1 Weight loss in exercised and/or diet exchanged mice

A comparison of the weight gain between the experimental groups and control mice showed that the percentage of weight gain in the first 12 weeks were significantly increased in exercise, diet exchange and exercise/diet exchange groups compared to control (Figure 4.2A, B and C). From the graphs below it can see that from week 12 (red arrow) mice start to lose weight with the introduction of the new treatment regimen. The percentage of weight loss from week 12 until week 17 was significantly increased in all groups with a maximum weight loss in the exercise combined with diet exchange group followed by diet exchange only. The exercise group still receiving a high-fat diet showed the lowest weight loss between the groups (less than 6%) (Figure 4.2D).

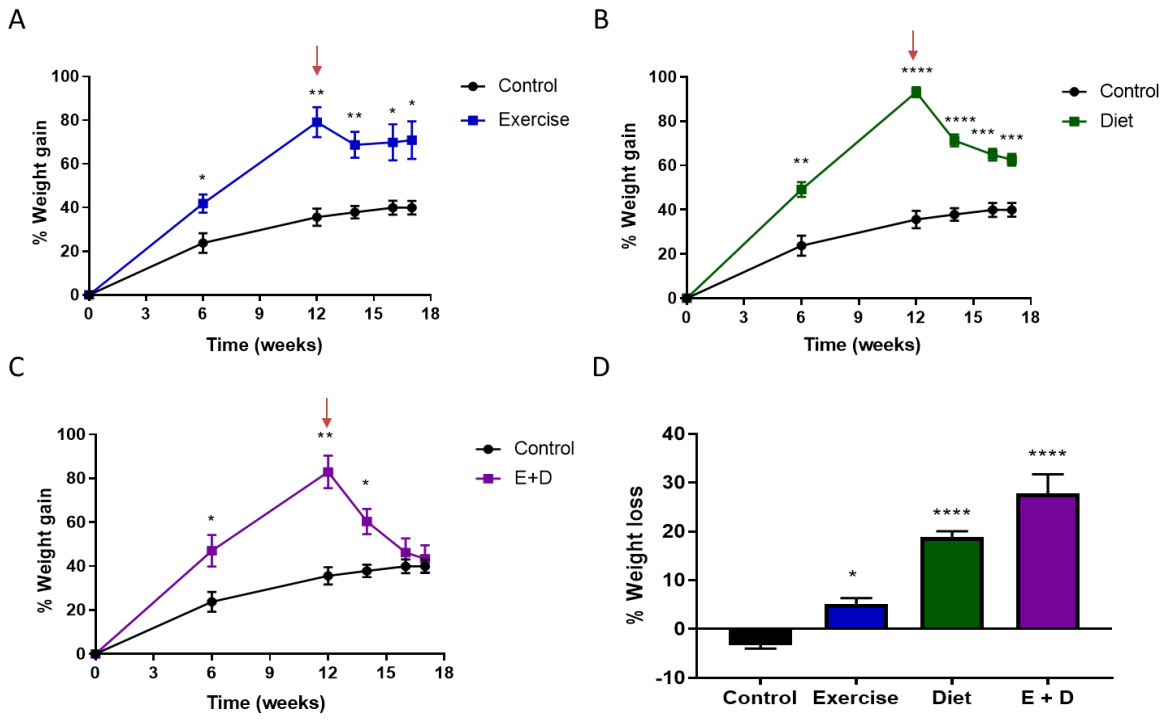

Figure 4.2: Weight loss in exercise and/or diet exchange mice groups.
A. Percentage of weight loss in all groups were significant with biggest %weight loss in combined exercise and diet exchange and smallest in exercise only group. B. Percentage of weight gain over time in exercise group, exercise started at week 12 (red arrow). C. Percentage of weight gain over time in diet exchange group, diet exchanged to chow at week 12 (red arrow). D. Percentage of weight gain over time in exercise/diet exchange group, (Exercise and diet exchange started at week 12 (red arrow). Data are expressed as mean ± SEM. *P≤0.05, **P≤0.01, ***P≤0.001, ****P≤0.0001.

4.3.2 Insulin resistance in the exercise group

As reported in Chapter 2, 12 weeks high fat feeding led to hyperglycaemia, hyperlipidaemia and insulin resistance. After exercise and/or diet exchange trials, blood glucose and triglyceride level returned to control level in all groups as shown in Figure 4.3A and B. Additionally, insulin level returned to control level in diet exchange group (P=0.07) and exercise/diet exchange group (P=0.5). However, the exercise group showed a significant increase (P=0.02) in serum insulin level (insulin resistance) revealing that abnormalities in the exercise group persists compared to control (Figure 4.3C).

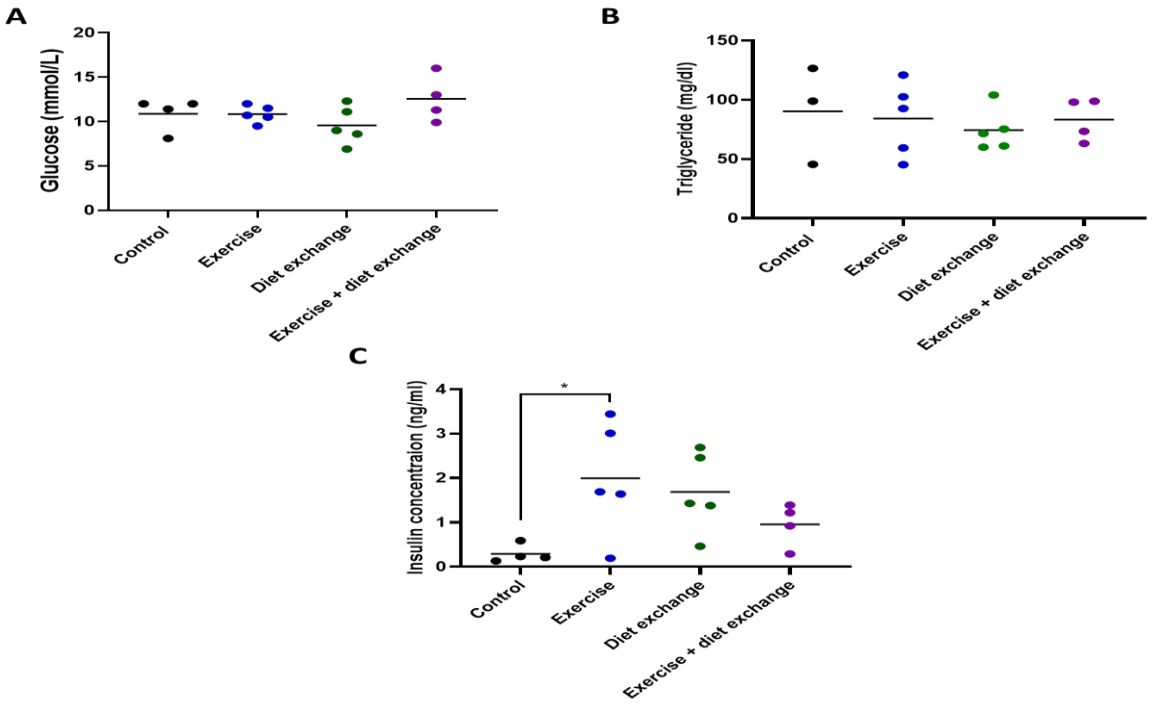

Figure 4.3: Exercise group remained insulin resistant.
A. Random blood glucose showed no significant differences between exercise, diet exchange and exercise + diet exchange groups compared to control. B. Insulin level showed a significant increase in exercise only group. C. There were no significant differences in triglyceride level in all groups. Data are represented by Column Scatter chart with the mean line (n=4-5). *P≤0.05.

4.3.3 Cardiac function and structure in exercise and/or diet exchange groups

In Chapter 2, it was shown that at 12 weeks of HFD (DIO) feeding the mice had developed signs of diastolic dysfunction illustrated by a significant decrease in stroke volume and a significant increase in gross lung weight normalised to tibial length (LW/TL) with normal ejection fraction. These experiments show that in each of the experimental groups at 17 weeks cardiac parameters of ejection fraction remained normal and the stroke volume as well

as LW/TL had returned to normal levels suggesting restoration of a normal diastolic function Figure 4.4.

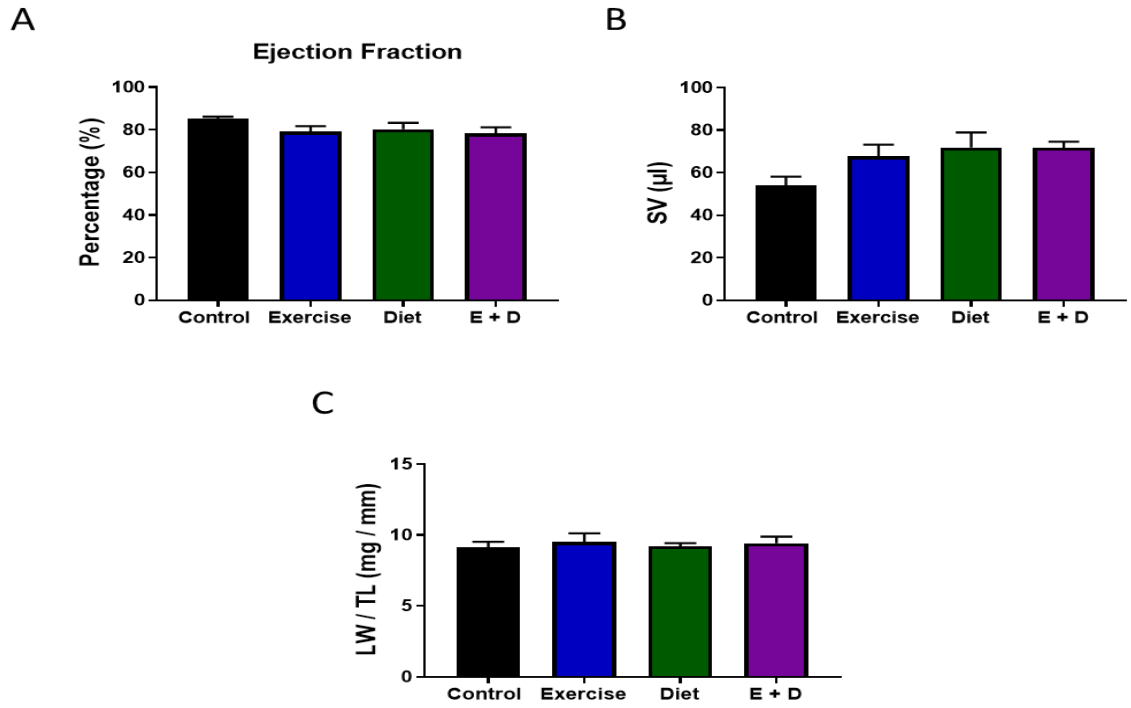

Figure 4.4: Normal systolic cardiac function in exercise and/or diet exchange mice groups.
A. There was no significant difference in ejection fraction between groups as well as stroke volume in panel B. C. Lung weight normalised to tibial length (LW/TL) showed no difference between groups. Data are expressed as mean ± SEM.

As with the 12-week HFD (DIO) model, there were no significant differences in gross heart weight normalised to tibial length and left ventricular mass estimated by echocardiography between all groups (Figure 4.5A). The diastolic left ventricular diameter was significantly decreased in our HFD (DIO) model, as shown before, which was reversed in all experimental groups. Systolic left ventricular diameter, which was unchanged in HFD (DIO), was significantly increased in groups that underwent swimming (exercise group and exercise/diet exchange group), with restoration to normal diameter in diet exchange group (Figure 4.5B). The HFD (DIO) group showed a significant increase in RWT compared to the control, which had returned to a normal level in all groups. These changes seen in exercise and exercise/diet exchange groups suggest an eccentric remodelling as a compensatory response to the increased blood flow in exercise. As shown in Figure 4.5C, there was a significant decrease in resting heart rate in both exercise and exercise/diet exchange groups which were within

normal levels in HFD (DIO). The table below shows other echocardiography readings (Table 4.1).

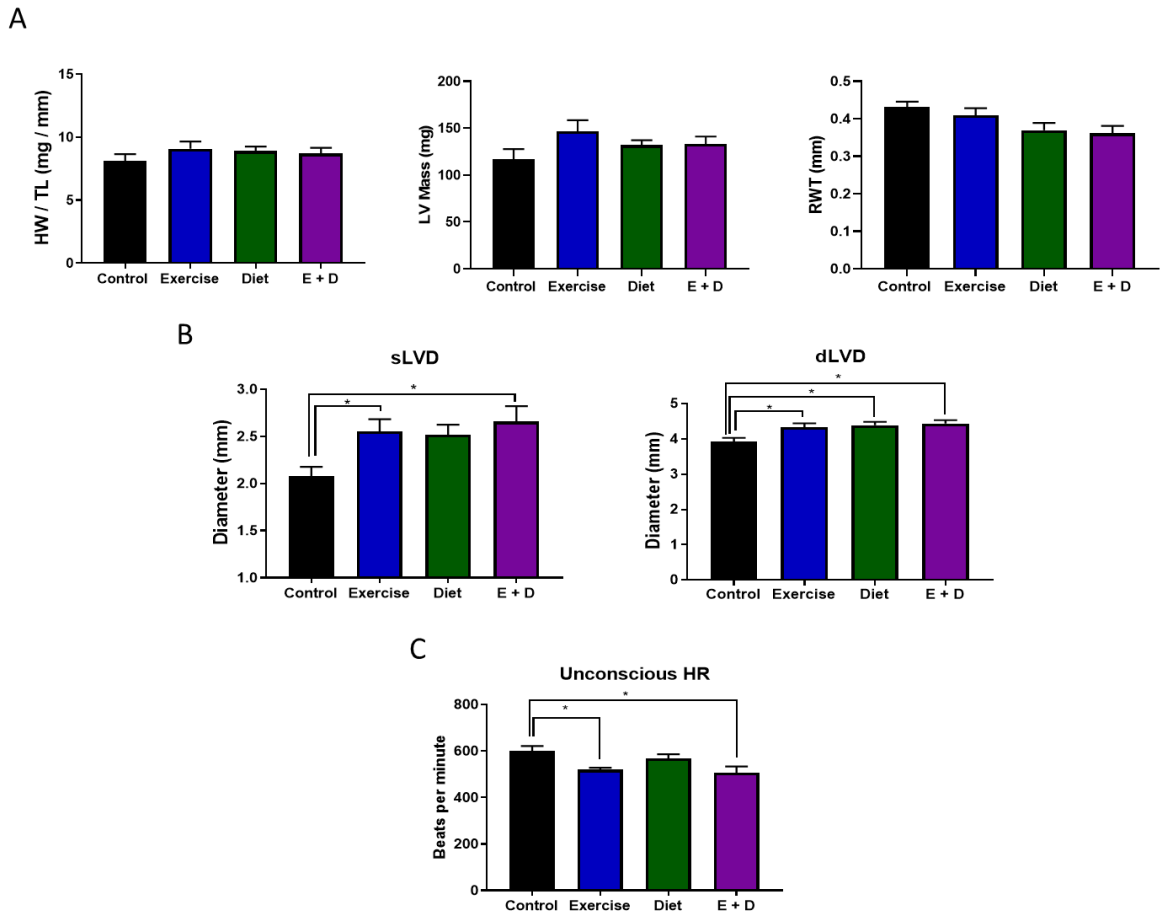

Figure 4.5: Eccentric remodelling in exercise and exercise/diet exchange groups.
A. No signs of hypertrophy as gross heart weight normalised to tibial length (HW/TL), left ventricular mass estimated by echocardiography and relative wall thickness showed no significant differences in all groups compared to control. B. Systolic left ventricular diameter (sLVD) was significantly increased in exercise and exercise/diet exchange groups while diastolic left ventricular diameter (dLVD) was increased in all groups compared to control. C. Exercise and exercise/diet exchange groups showed a significant decrease in unconscious heart rate. Data are expressed as mean ± SEM. *P≤0.05.

Table 4.1: Echocardiogram readings in exercise, diet exchange and exercise/diet exchange groups.

sLVD: systolic left ventricular diameter, dLVD: diastolic left ventricular diameter, sIVS: systolic interventricular septum, dIVS, diastolic interventricular septum, sPW: systolic posterior wall, dPW, diastolic posterior wall, RWT: relative wall thickness, EF: ejection fraction, FS: fractional shortening, SV: stroke volume, HR: heart rate. Data are expressed as mean ± SEM.

Parameters	Control (n=4) mean ± SEM	Exercise (n=5) mean ± SEM	Diet exchange (n=5) mean ± SEM	Exercise + diet exchange (n=4) mean ± SEM	P value
Left Ventricular Dimensions					
sLVD (mm)	2.075 ± 0.1	*2.554 ± 0.1	2.518 ± 0.1	*2.655 ± 0.2	P ≤ 0.05
dLVD (mm)	3.918 ± 0.1	*4.332 ± 0.1	*4.388 ± 0.1	*4.44 ± 0.09	P ≤ 0.05
Wall Thickness					
sIVS (mm)	1.655 ± 0.08	1.466 ± 0.06	1.558 ± 0.06	1.488 ± 0.04	ns
dIVS (mm)	0.8825 ± 0.04	0.974 ± 0.02	0.88 ± 0.03	0.8675 ± 0.03	ns
sPW (mm)	1.418 ± 0.07	1.426 ± 0.05	1.308 ± 0.04	1.47 ± 0.1	ns
dPW (mm)	0.8075 ± 0.03	0.796 ± 0.03	0.736 ± 0.05	0.735 ± 0.08	ns
RWT (mm)	0.4315 ± 0.01	0.4094 ± 0.02	0.3696 ± 0.02	0.3615 ± 0.02	ns
LV mass (mg)	117.1 ± 10.7	146.8 ± 11.6	131.9 ± 5.2	133.3 ± 7.8	ns

Parameters	Control (n=4) mean ± SEM	Exercise (n=5) mean ± SEM	Diet exchange (n=5) mean ± SEM	Exercise + diet exchange (n=4) mean ± SEM	P value
EF%	85.13 ± 1.1	79.13 ± 2.6	80.27 ± 3.1	78.34 ± 2.9	ns
FS%	47.1 ± 1.3	41.06 ± 2.4	42.42 ± 3.1	40.3 ± 2.7	ns
SV (µl)	53.86 ± 4.3	67.81 ± 5.4	71.9 ± 7.02	71.7 ± 2.96	ns
HR (bpm)	601.8 ± 19.9	*519.6 ± 8.72	567.4 ± 18.93	*506.5 ± 27.23	P ≤ 0.05

4.3.4 Exercise with sustained high-fat feeding leads to downregulation of transcript levels of Drp1 in myocardium

The high-fat feeding model developed in Chapter 2 showed alterations to the expression level of several proteins regulating mitochondrial dynamics. Similar to the 12-week HFD (DIO) model there was no change in the fusion protein Opa1 and its isoforms expression in the myocardium of all experimental groups were detected (Figure 4.6).

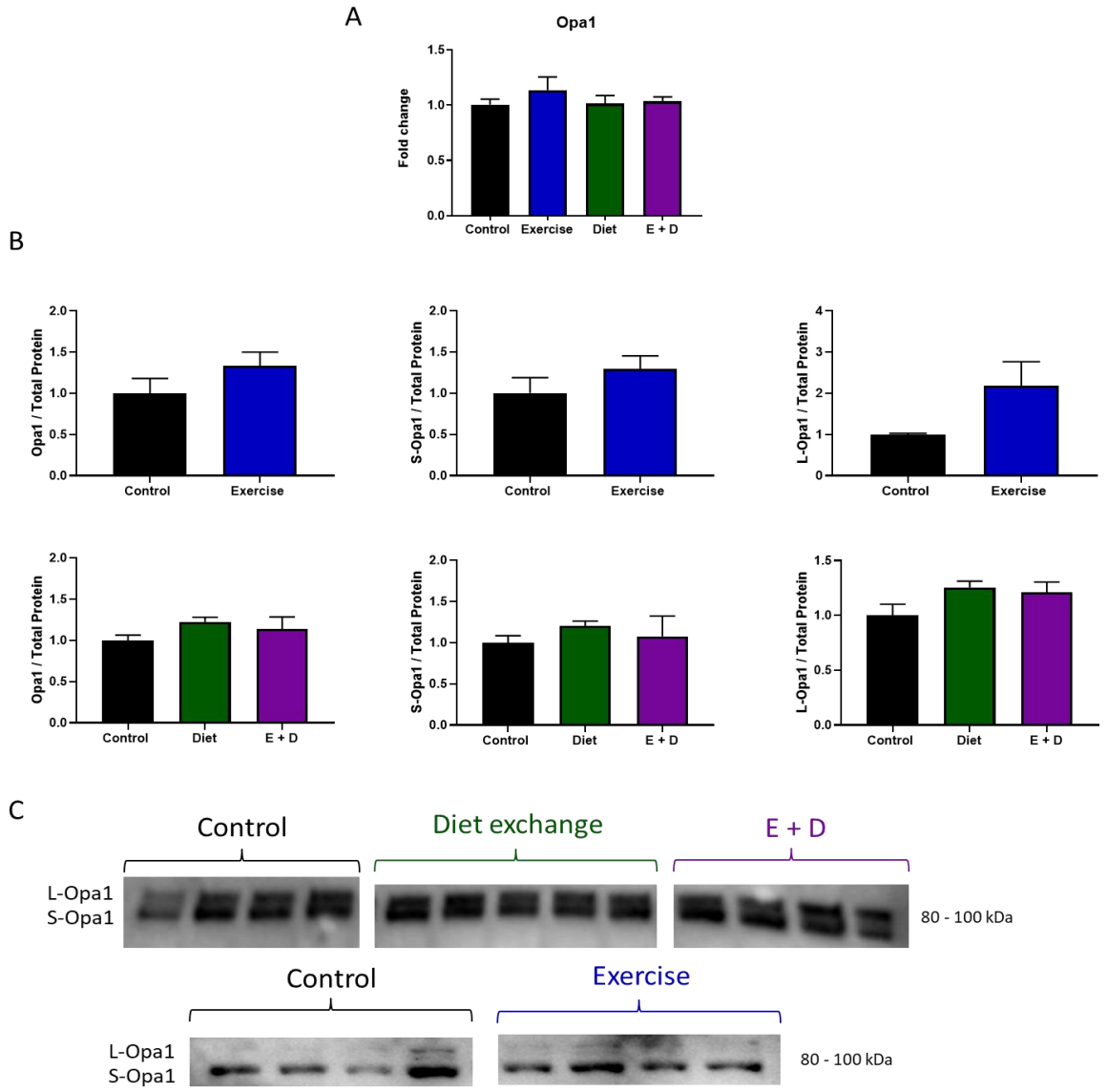

Figure 4.6: No change was found in Opa1 isoforms expression in exercise and/or diet exchange groups.

A. No change to Opa1 transcript expression in all groups. B. No difference in opa1 isoforms were seen in all groups compared to control. C. Representative blots showing S-Opa1 and L-Opa1 expression. Data are expressed as mean ± SEM (n=4-5).

Additionally, there was no significant changes to transcript expression of Mfn1 and Mfn2, in all experimental groups in this Chapter. Similar to the 12-week HFD (DIO) model, Mfn1 protein expression level in the myocardium was not changed in any of the experimental groups. However, levels of Mfn2 level unchanged in HFD (DIO) were increased in exercise group but with no changes in diet exchange group and exercise/diet exchange group (Figure 4.7).

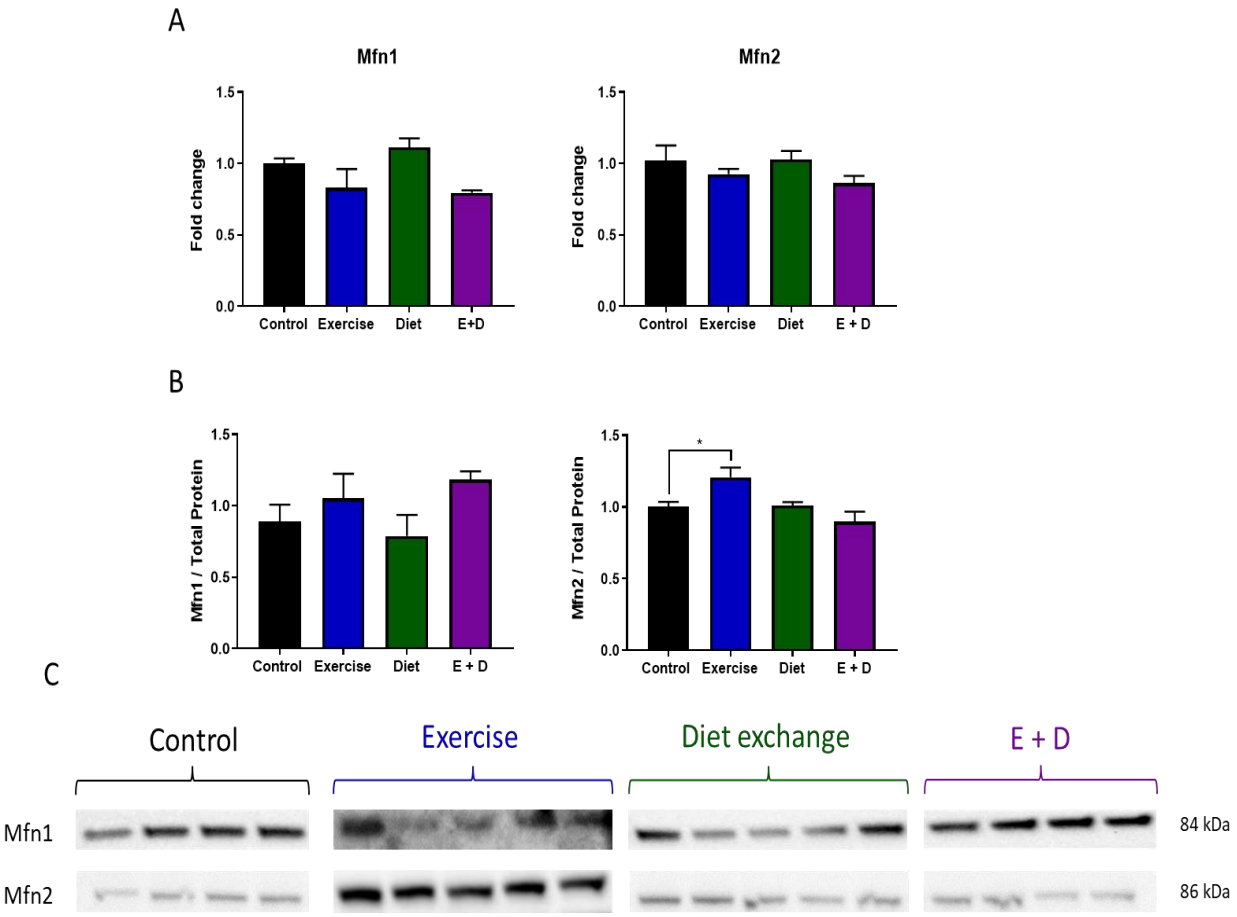

Figure 4.7: Mfn2 involved in mitochondrial fusion was significantly increased in HFD (DIO) mice.
A. There was no changes to Mfn1 and Mfn2 transcript expressions. B. There was a significant increase in Mfn2 expression in exercise group, while Mfn1 showed no significant changes. Data are expressed as mean ± SEM (n=4-5). *P≤0.05.

As reported for the 12-week HFD (DIO) model, the exercise group showed a significant decrease in Drp1 transcript expression which returned to normal level in diet exchange and exercise/diet exchange groups (Figure 4.8A). However, the high level of Drp1 expression identified in the myocardium of the HFD (DIO) model returned to normal in all groups as compared to the 17-week control as shown below in Figure 4.8B. Since the activity of Drp1 is linked to the phosphorylation state, P-Drp1 (S616) and P-Drp1 (S637) levels were assessed. P-Drp1(S616) to the total Drp1 ratio, promoting fission, was unchanged in HFD (DIO) model and remained the same in all experimental groups. However, the significant decrease in P-Drp1 (S637)/total Drp1, suggesting fission, seen in HFD (DIO) model had returned to normal levels in exercise, diet exchange and exercise/diet exchange groups (Figure 4.8B).

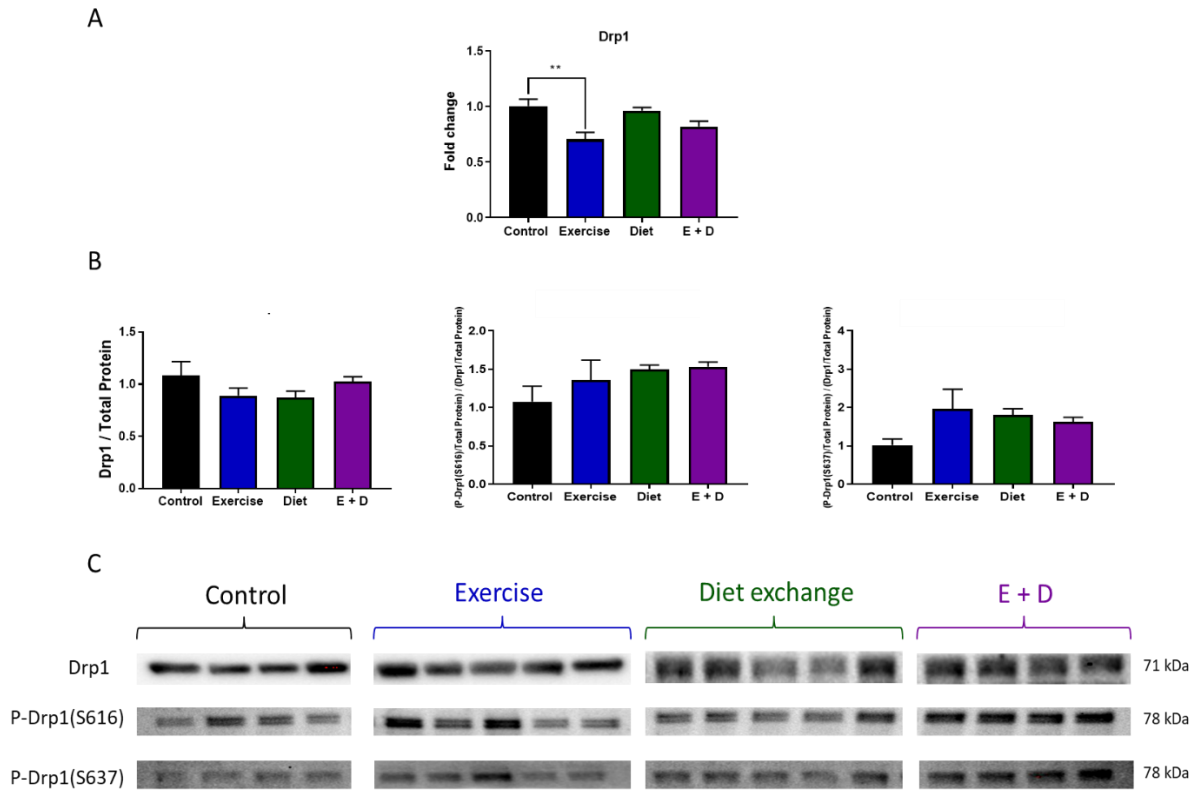

Figure 4.8: Drp1 transcript expression was significantly decreased in exercise group.
A. There was a significant decrease in Drp1 transcript expression. B. There was no change in Drp1 and its phosphorylated forms (S616) and (S637) in all groups. C. Representative blots showing Drp1 and phosphorylated Serine 616 and 637 in all groups. Data are expressed as mean ± SEM (n=4-5). **P≤0.01

4.3.5 Exercise in obese mice downregulates Mff and upregulate PINK1 in myocardium

Since Drp1 is a cytosolic protein recruited to the outer mitochondrial membrane by its receptors Fis1, Mff, MID49 and MID51, receptor expressions were investigated. A normal level of MID51 in HFD (DIO) remained the same in all exercise and/or diet exchange groups. The upregulation of Fis1 in HFD (DIO) had returned to normal in all groups. Similar to the HFD (DIO) model, there was a significant decrease in Mff level in the exercise group ($p \leq 0.01$), unlike diet exchange and exercise/diet exchange groups. A significant increase in MID49 level in HFD (DIO) remained the same in diet exchange and exercise/diet exchange groups ($P \leq 0.0001$) and had returned to normal in exercise group (Figure 4.9B). Figure 4.9 presents the transcript and myocardium expressions summary for Drp1 receptors in exercise and/or diet exchange groups. Therefore, while the fission-fusion protein profile has returned to normal in all the experimental groups, the expression of the receptors has not all returned to basal levels.

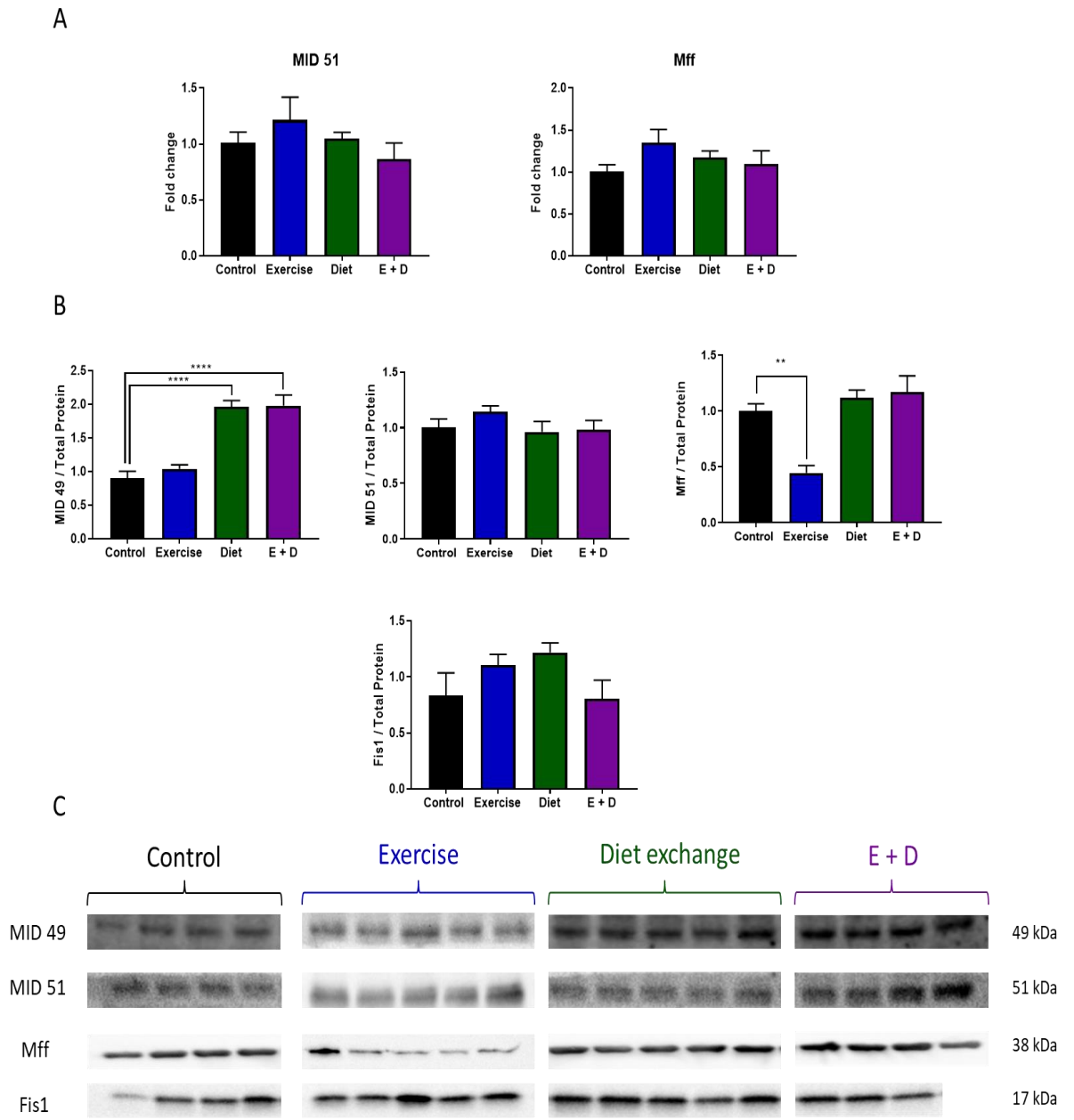

Figure 4.9: Alteration in Drp1 receptors expression in exercise and/or diet exchange groups.

A. There was no difference in MID51 and Mff transcript expression in all groups compared to control. B. There was a significant increase in MID49 expression in diet exchange and exercise/diet exchange groups and a significant decrease in Mff expression in exercise group while in HFD (DIO) compared to control. C. Representative blot showing protein expression of MID49, MID51, Mff and Fis1. Data are expressed as mean ± SEM (n=3-5). **P≤0.01, ****P≤0.0001.

The mRNA levels of the main mitophagy proteins PINK1 and Parkin were significantly increased in our HFD (DIO) model, both proteins remained elevated in exercise group only and returned to normal in diet exchange and exercise/diet exchange groups (Figure 4.10A). Similarly, PINK1 protein levels in the myocardium were remained upregulated in the

exercise group only (P≤0.001) but returned to normal level in diet exchange group and exercise/diet exchange groups. However, the elevated level of Parkin in HFD (DIO) model reversed to control levels in all groups (Figure 4.10B). These results suggest that diet exchange and the combination of exercise with diet exchanged reduces mitophagy which was activated in response to 12 weeks HFD (DIO) feeding. However, exercise, while on HFD (DIO), group showed an increase in only one of the two main proteins associated with mitophagy pathway, which might induce mitophagy independently or could be involved in another canonical pathway.

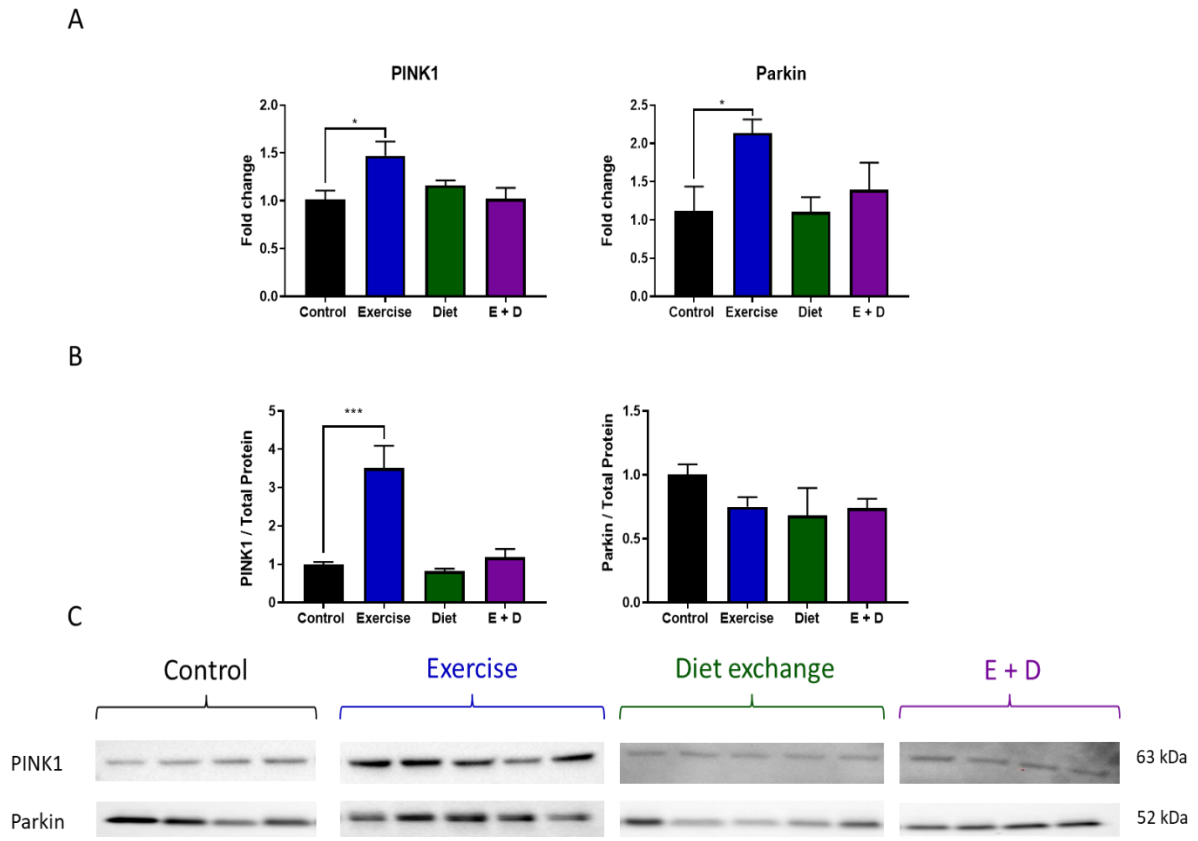

Figure 4.10: PINK1 and Parkin transcript expression was significantly increased in exercise group.
A. PINK1 and Parkin transcript expression was significantly increased in exercise while on HFD compared to control. B. PINK1 protein expression was significantly increased in exercise group as well with no difference in Parkin level. C. Representative blot showing PINK1 and Parkin expression. Data are expressed as mean ± SEM (n=4-5). *P≤0.05, ***P≤0.001.

The master regulator of mitochondrial biogenesis PGC-1α transcript expression was unchanged in HFD (DIO) model and remained the same in exercise, diet exchange and exercise/diet exchange groups (Figure 4.11). Another activator of mitochondrial transcription is TFAM which was significantly upregulated in HFD (DIO) model and had returned to

normal after exercise and/or diet regimes in all groups, suggesting inactivation of mitochondrial biogenesis.

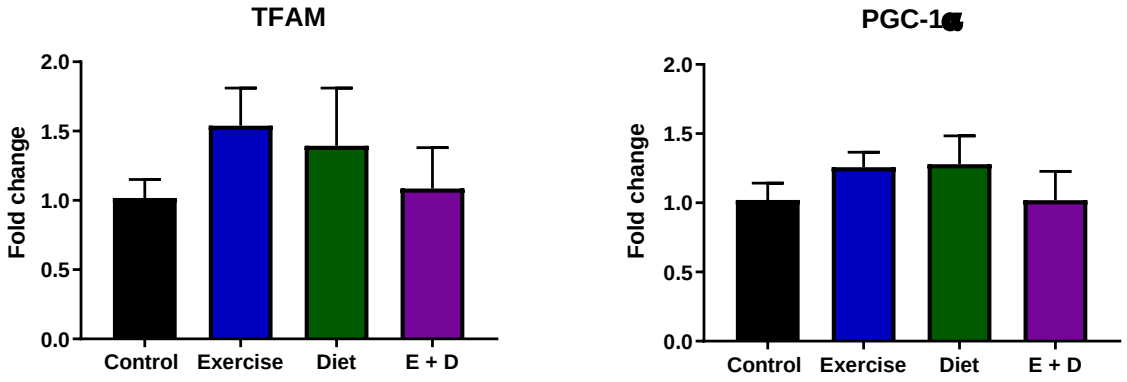

Figure 4.11: No change in transcript expression of proteins involved in mitochondrial biogenesis in exercise and diet exchange groups.
Unchanged mRNA level of mitochondrial biogenesis TFAM and PGC-1α in all groups. Data are expressed as mean ± SEM. n= 4-5 per group.

4.3.6 Summary of results

Exercise and a healthy diet are the main non-pharmacological management for obesity/T2DM. In this chapter, the exercise and diet exchange potential for reversing diabetic cardiomyopathy was examined. The primary results of this chapter were:

- There is reversal of TG and blood glucose levels in exercise, diet exchange and exercise/diet exchange groups.
- Diet exchange and exercise/diet exchange, but not exercise with a sustained HFD (DIO), restored insulin sensitivity.
- Reversal of diastolic dysfunction occurs in all groups with eccentric remodelling in exercise and exercise/diet exchange groups.
- Restoration of the fission-fusion axis in all groups except the exercise group.

4.4 Discussion

4.4.1 Choice of exercise model

Exercise models are categorised based on the type, intensity, and duration of the training. Different types of exercise will have a different outcome. For example, dynamic exercise is known to prevent cardiovascular disease (Guo et al., 2020). The intensity of exercise is described by low, moderate and vigorous. Vigorous physical activity increases the risk for acute cardiovascular events in particular acute myocardial infarction in physically unfit people with an underlying cardiac condition (Franklin et al., 2020). The lifespan of mice is different from human; therefore, the exercise time relative to the lifespan has been introduced to differentiate short, medium and long-term exercise. Less than 4 weeks is considered a short-term, 4-8 weeks exercise is considered a medium-term, and more than 8 weeks is a long-term exercise (Feng et al., 2019).

Swimming is a type of dynamic exercise, which involves the participation of many muscle groups and an increase in heart output and is, therefore, considered effective aerobic training (Kaplan et al., 1994). Swimming intensity is determined by the length of the swimming session daily. Based on studies using swimming as model of exercise in mice, 60 – 90 minutes per day is considered a moderate-intensity, while 20 – 59 minutes per day is considered a low intensity and more than 90 minutes is a high intensity (Guo et al., 2020). The advantage of swimming is that it doesn't focus on one part of the body but the whole-body muscles. However, one disadvantage of this model is that it needs an observer to watch the whole swimming session for floating or drowning mice. There are critics of swimming with claims that swimming induces stress and increases the cortisol level. Studies which found the increase in cortisol aimed to induce stress; for example, Gong et al. (2015) who reported an increase in mice forced to swim in a cold water 23°C (thermal stress) for the whole 2 hours at the first time. However, generally a swimming as a model of exercise is well-established through several studies. For example, D'Souza et al. (2014) used swimming training to study the bradycardia induced by exercise in mice. Mice were exercised twice daily for an hour for 4 weeks. The authors reported a persistence of bradycardia after blockage of the autonomous nervous system. They also found a decrease in HCN4, which contributes to the pacemaker currents in the heart, explained by an increase in both Neuron-Restrictive Silencer Factor (NRSF) and miR-1. Nogueira et al. (2017) studied the physiological variables caused by swimming with weight load in mice fed a HFD (DIO); swimming training for an hour daily for 8 weeks (5 days/week) was efficient to control the

weight and glucose levels. However, the study did not address molecular level changes. Moreover, Soares et al. (2019) analysed the effect of intense exercise on the cardiovascular system by mice swim trained three times daily for 90 minutes with weight overload for 6 weeks. Mice developed cardiac hypertrophy with improved oxidative capacity. Also, unchanged levels of angiotensin peptides and β-isoform myosin heavy chain to α-isoform ratio was reported.

Another commonly used method is treadmill running. An advantage of this approach is the ability to control the exercise intensity by increasing the treadmill pace. A limitation of this technique is the possibility that mice refuse to run, when sometimes an electric shock is used to force mice to run, which is considered inhumane. Svensson et al. (2016) found that forced treadmill exercise for mice induced stress and anxiety associated with a high level of corticosterone. Additionally, Tang et al. (2008) found that forced strenuous running in rats on a treadmill induced osteoarthritis. This inflammation might have a systemic effect that might interfere with molecular data obtained from the heart.

Each method has advantages and disadvantages. Here, to investigate the reversible effect of exercise on mitochondrial dysfunction caused by HFD (DIO), swimming has been chosen as a model of exercise primarily due to the ease and cost-effectiveness. Mice have been acclimatised to swimming for one week followed by another 4 weeks of swimming sessions, 5 days a week, 1 hour per day, which is considered a dynamic moderate-intensity exercise for a medium-term (Guo et al., 2020, Feng et al., 2019).

4.4.2 Exercise combined with diet exchange C57BL/6J mice group had the highest weight loss

In the current study, all groups showed weight loss with the maximum loss occurring in the exercise/diet exchange group. There was a decrease in weight in the exercise group in the first 2 weeks after beginning the exercise protocol, after which the weight stabilised. One reason for this might be an increase in skeletal muscle mass due to physical activity. Kemi et al. (2002) observed an increase in skeletal muscle mass by 12-18% in treadmill running mice. Another reason is that the exercise group was still on HFD (DIO), the highest calories among the others which explain the lowest weight loss in this group. A systematic evaluation of studies with a minimum of one-year monitoring suggested that individuals who used exercise alone for reducing weight experienced only minor weight loss (Franz et al., 2007). Thomas et

al. (2012) reviewed 15 studies and suggested that the low levels of weight loss in exercise is because there is a subsequent increase in calorie intake.

4.4.3 Exercise group remained insulin resistant.

In our HFD (DIO) model, there was an increase in glucose, insulin and TG levels. However, after exercise, diet exchange and exercise/diet exchange, glucose and TG returned to normal levels at the end of the trial. Aerobic exercise is effective in lowering triglyceride levels (Wang et al., 2019). Obese individuals with T2DM were introduced to a low-fat diet for 4 weeks showed a decrease in TG level (Papakonstantinou et al., 2010). Therefore, in agreement with human studies, this mouse model of obesity showed that exercise, diet exchange and exercise/diet exchange similarly reduced TG to the control levels.

Insulin levels remained high in the exercise group but not in the diet exchange and exercise/diet exchange groups which returned to normal levels. It has been found that exercise improves insulin sensitivity and therefore controls blood glucose in obese individuals (Damaso et al., 2014, Suh et al., 2011, AbouAssi et al., 2015). Exercise improves insulin sensitivity in T2DM; it is still not clear the exercise itself or the weight loss accompanied exercise is the cause (Whillier, 2020). A decrease in pro-inflammatory cytokines in skeletal muscle after weight loss is one of the causes for insulin sensitivity improvement (Schenk et al., 2009). Our results suggest that weight loss which occurred in both diet exchange groups (diet exchange and exercise/diet exchange) has a strong link in insulin sensitivity improvement. A decrease in pro-inflammatory cytokines in skeletal muscle after weight loss is one of the causes for insulin sensitivity improvement (Bradley et al., 2009). Thus, features of the mouse HFD (DIO) model used here appears to mimic well obesity in humans.

4.4.4 Improvement of diastolic dysfunction in exercise, diet exchange and exercise/diet exchange groups.

Systolic function represented by EF% and FS% was unchanged in HFD (DIO) model and remained the same in all exercise and/or diet exchange groups. Diastolic dysfunction was reported in our HFD (DIO) model represented by a decrease in stroke volume associated with an increase in lung weight normalised to tibial length (LW/TL); these parameters returned to normal across all experimental groups. These results are consistent with those of Schuster et al. (2012) who found an improvement in diastolic dysfunction include the E/A ratio after 8 weeks of dynamic exercise 3 times per week in obese nondiabetics patients. Moreover,

weight reduction in obese individuals by 12 weeks of low-calorie diet was sufficient to improve diastolic function and restore partially normal diastolic function (Karimian et al., 2017). However, Hare et al. (2011) investigating the effect of an exercise-based lifestyle on the progression of diastolic dysfunction in T2DM patients did not observe a positive effect of exercise on the progression of diastolic dysfunction. The exercise was based in the gym, twice a week for 4 weeks under full supervision followed by telephone counselling for 3 years. This rather contradictory result may be due to different exercise types and intensity, and the severity of diastolic dysfunction. It can therefore be assumed that a moderate-intensity aerobic exercise can attenuate diastolic dysfunction in the early stage of DCM. Further work is required to establish the variable effect of different exercise intensity and types on different stages of diabetic cardiomyopathy.

4.4.5 Eccentric remodelling in exercised groups.

There was a concentric remodelling in our HFD (DIO) model due to pathological stress (pressure overload) as discussed in Chapter 2. During exercise, the heart is exposed to intermittent hemodynamic stress. To normalise this stress and to cope with the systemic demand for increased blood flow, the heart is morphologically adapted to exercise. Eccentric remodelling in exercise and exercise/diet exchange groups is likely therefore due to physiological stimuli (volume overload). In accordance with these results, Vega et al. (2017) have demonstrated that eccentric remodelling represented by an increase in left ventricular diameters with no change to RWT is physiological remodelling rather than pathological. A study on human long-term swimmers ≥ 5 years training with 1 hour 4 times a week showed a significant increase in both sLVD and dLVD. (Lee and Oh, 2016). However, physiological cardiac hypertrophy caused by strenuous exercise could be detrimental to cardiac function associated with increased risk of cardiac sudden death, reviewed by Lauschke and Maisch (2009). Therefore, exercise in diabetic patients, specifically, should be mild-moderate in intensity due to the maladaptive cardiac response.

An expected finding was that exercise and exercise/diet exchange groups had a decrease in resting heart rate with one explanation being the increase in left ventricular dimensions. DeMaria et al. (1979) found a negative linear correlation between sLVD, dLVD and the heart rate as an increase in the heart rate by atrial pacing was accompanied by a decrease in sLVD and dLVD. Moreover, Reimers et al. (2018) concluded in their systematic review that aerobic exercise decreases resting heart rate which supports our finding. The effect of exercise on

cardiac parameters reported here are mostly in agreement with human studies highlighting that the swimming model used in this study is a good surrogate model of human exercise.

4.4.6 Upregulation of fusion protein Mfn2 in exercise group.

While weight loss and cardiac function have been investigated in patients there is very little known about mitochondrial function, in particular mitochondrial dynamics. Fusion proteins were not changed in the HFD (DIO) model and remained the same in diet exchange and exercise/diet exchange groups. However, there was un upregulation of Mfn2 in exercise group. Stress-induced mitochondrial fusion was reported to be associated with a high production of mitochondrial ATP (Tondera et al., 2009).

The increase in Mfn2, despite no increase in other fusion proteins, might promote fusion to form bigger mitochondria. Cartoni et al. (2005) reported an increase in Mfn2 mRNA level, but not protein level, in human skeletal muscle after acute exercise (cycling). Kang et al. (2020) also showed an increase in Mfn2 levels in skeletal muscle of male Sprague-Dawley (SD) rats fed 45% HFD (DIO) and underwent at the same time low-intensity treadmill exercise for 6 weeks. Male C57BL/6 mice fed normal chow diet and swim trained for 8 weeks also showed an upregulation of Mfn2 in skeletal muscle (Ju et al., 2016). Further, Cartoni et al. (2005) found an increase in Mfn2 transcript expression in human skeletal muscle after 24 hours of the exercise. These results confirm the association between Mfn2 and exercise. However, there was no increase in Mfn2 in our exercise/diet exchange group. A possible explanation for this might be that the exercise group was on a HFD (DIO) while the exercise/diet exchange group were on chow diet after week 12. Thus, different body weights might affect the intensity of exercise together with the high fat in the diet could affect the outcome. Interestingly, the exercise group was insulin resistant which could have a link to Mfn2 level. These results reflect those of Sebastian et al. (2012) who also found that using a liver-specific Mfn2 KO mice, the insulin level in the plasma was increased and Western blotting showed a decreased expression of insulin receptor substrate 1 (IRS1) and IRS2. Therefore, Mfn2 upregulation could be a compensatory mechanism to restore normal insulin signalling.

Mfn2 also has a role in tethering ER and mitochondria which allows calcium transportation from ER/SR to the mitochondria to induce heart contractility (Merkwirth and Langer, 2008). Papanicolaou et al. (2011) found an impaired Ca^{2+} signalling and deterioration in LV contractility in genetically ablated Mfn2 in the heart. It could be therefore assumed that the

increase of Mfn2 expression in our exercise group was an adaptation mechanism to increased cardiac contractility. In future investigations, it might be possible to use Langendorff hearts to study the effect of Mfn2 on cardiac contractility.

Mfn2 has been studied as a therapeutic target for DCM. Hu et al. (2019) suggested that overexpression of Mfn2 restored mitochondrial function and prevented the development of DCM. Using *db/db* mice, model of T2DM, Ni et al. (2020) found that Icariin, an anti-atherosclerotic drug, enhanced the function of the mitochondria as well as the cardiac function (increased in EF% and FS%). Western blotting showed an increase in Mfn2 expression in *db/db* mice after Icariin treatment. These studies highlight the importance of Mfn2 in quality control of the mitochondria.

A natural progression of this work is to investigate whether the increase in Mfn2 led to increased fusion by assessing mitochondrial ultrastructure using SBF-SEM or was involved in different non-canonical pathway. As Mfn2 is upregulated at protein level but not at transcript level the data suggest that it is not being degraded. We showed for the first time that exercise training while on HFD (DIO) can increase Mfn2 level in the myocardium and suggest that it may be a compensatory mechanism contributing towards restoration of cardiac function.

4.4.7 The fission protein Drp1 was unchanged in exercise, diet exchange and exercise/diet exchange groups.

There was an increase in the total Drp1 expression in the myocardium of the HFD (DIO) model in our study with a decrease in the phosphorylated form at Serine 637 to the total Drp1 ratio. These changes were returned to normal in all groups after exercise and/or diet exchange to chow diet. However, the decrease in the mRNA level of Drp1 in the HFD (DIO) model remained the same in the exercise group and returned to normal in diet exchange and exercise/diet exchange groups. This suggest that Drp1 is not being turned over in the HFD (DIO) and this is process is not amended in the exercise group.

Mitochondrial fission proteins have been reported to be perturbed after exercise. Konopka et al. (2014) reported an increase in Fis1 protein level in skeletal muscles of young and old individuals after 12 weeks of cycling training, 3-4 sessions per week, 20-45 minutes per session, associated with better aerobic capacity. The paper does not quantify Drp1 protein and its isoforms. Givvimani et al. (2015) observed a decrease in Drp1 expression in the myocardium of treadmill trained *db/db* mice for 8 weeks associated with decreased blood

pressure (BP), interstitial fibrosis, apoptosis (decrease cytochrome c leakage) and improvement of left ventricular function. The Givvimani did not compare changes in mitochondrial dynamics before and after exercise. However, Yoo et al. (2019) found that single-bout treadmill exercise did not alter Drp1 level in rats heart tissue.

Coronado et al. (2018) reported an increase in Drp1 and S616 Drp1 and fragmented mitochondria by transmission electron microscopy (TEM) immediately after exercise. These changes returned to normal after an hour of recovery from exercise. In addition, a single high intensity exercise in rats increased transcript levels of Fis1 after 24 hours of the onset of exercise in skeletal muscle and was associated with an increase in ROS (Ding et al., 2010). These experiments highlight the importance of the time between harvesting tissue post-exercise and how that may be a factor which could lead to conflicting reports. Changes within 24-48 hours can be transient changes to recover from damages caused by exercise and does not represent the long-term changes. In our model, we were interested in long term changes and that is why we harvested the tissue after 48 hours of the last exercise. Interestingly, Drp1 level and P-Drp1 (S637) returned to normal in all groups associated with improvement in diastolic dysfunction highlighting that Drp1 is an important therapeutic target. To our knowledge, this is the first study assess the reversible effect of exercise on mitochondrial dynamics in the setting of early-stage diabetic cardiomyopathy.

Although Drp1 expression returned to normal in all groups, there were changes in its receptors. Mff returned to normal in diet exchange and exercise/diet exchange groups and remained downregulated in the exercise group. The exercise group was on HFD (DIO) and remained insulin resistant indicating the potential link between Mff and insulin signalling pathway. The decrease in Mff and the increase in Mfn2 in the exercise group may favour mitochondrial fusion. On the other hand, MID49 returned to normal in exercise group and remained upregulated in diet exchange and exercise/diet exchange groups. These finding support the idea that Drp1 receptors are involved in non-canonical pathways within the mitochondria. Otera et al. (2016) have found a role of MID49 in cristae remodelling during apoptosis using MID49 knockout HeLa cell lines by using transmission electron microscopy. It has been suggested that MID49 recruits the inactive form of Drp1 and has been shown to inhibit fission by inhibiting the GTPase activity of Drp1 (Osellame et al., 2016). The expression of MID49 was induced in mouse embryonic fibroblasts and shown to lead to elongated mitochondria using fluorescence microscopy (Palmer et al., 2013). Thus, upregulation of MID49 in diet exchange and exercise/diet exchange groups might be a

defensive mechanism indicating stabilisation of mitochondrial cristae and inhibiting fission. However, there remains controversy surrounding the role of MID49 role in fission and fusion. There are also still many unanswered questions about the role of Drp1 receptors when there is no change to Drp1. This study lays the groundwork for future research into Drp1 receptors.

4.4.8 Mitophagy still upregulated in the exercise group.

The main regulators of mitophagy PINK1 and Parkin were investigated in all groups. Both transcript and protein levels of PINK1 and Parkin returned to normal in diet exchange and exercise/diet exchange groups. These data indicate that mitophagy has returned to normal level in these groups. However, both PINK1 and Parkin mRNA remained upregulated in exercise group. At the protein level PINK1 expression was increased in the exercise group whereas Parkin expression returned to normal. These finding could suggest that mitophagy process is still upregulated in exercise group. The increase in Parkin transcript expression, but not protein level, indicates an increase in the protein turnover. Koyano et al. (2014) reported that PINK1 phosphorylates Parkin at Serine65 to activate it. A natural progression of this work is to analyse phosphorylated form of Parkin. It has been suggested that mitophagy needs to be preceded by fission (Arnoult et al., 2005, Gomes and Scorrano, 2008). However, some studies reported that Drp1 is not necessary for mitophagy (Mendl et al., 2011, Song et al., 2015, Yamashita et al., 2016). For example, Drp1 knockout in MEF led to an increase in Parkin-mediated mitophagy concomitant with co-localisation of lysosomes and mitochondria confirmed through fluorescent images of MitoTracker (Song et al., 2015). Therefore, although Drp1 has returned to normal in the exercise group, mitophagy might still be activated. Instead, there might be mitochondrial fusion represented by Mfn2 upregulation. Additionally, Mfn2 is a critical mediator of mitophagy. Mfn2 enhances the recruitment and phosphorylation of Parkin as a marker to degrade damaged mitochondria (Chen and Dorn, 2013) and as described in the main Introduction (section 1.5). Xiong et al. (2019) stimulated neonatal rat cardiomyocytes with angiotensin II inducing injury, ROS and apoptosis were increased together with decreased expression of Mfn2. Overexpressing Mfn2 in the same cells using recombinant adenovirus attenuated ROS and apoptosis. Authors also reported an increase in mitophagy by translocation of Parkin to mitochondria using MitoTracker fluorescence images associated with an increase in PINK1/Parkin expression. An increase in Mfn2, as well as PINK1/Parkin, could be indicative of mitophagy was still activated in exercise group. However, further investigation is needed to confirm activation of mitophagy.

To develop a full picture of mitochondrial structure, SBF-SEM will be needed to assess the size of mitochondrial subpopulations.

Unchanged PGC1α transcript level in the HFD (DIO) model remained the same in all groups, whereas upregulation of TFAM transcript level in the HFD (DIO) model returned to normal. TFAM and PGC1α were within normal levels across all groups indicating no increase in mitochondrial biogenesis. These data suggest that the alteration in molecular analysis is unrelated to mitochondrial number.

4.5 Conclusion

The purpose of the current study was to determine the reversible effect of exercise and/or diet exchange on cardiac mitochondrial dynamics identified in the 12-week HFD (DIO) model. The findings of this study suggest that maximum benefits were gained in the combination of exercise and healthy diet. Normal blood glucose, triglyceride and diastolic function were restored in all groups, except insulin resistance which remained in the exercise group only. This study has shown for the first time the effectiveness of exercise and/or diet exchange on the reversibility of normalisation of mitochondrial fission/fusion axis, highlighting Drp1 as a potential therapeutic target in the early-stage diabetic cardiomyopathy. This Chapter has provided a deeper insight into the reversible effect of exercise and diet on mitochondrial dynamics. It was not feasible to assess mitochondrial size within the time frame of this research; therefore, it is unknown if restoring mitochondrial fission/fusion axis reversed the formation of smaller PNM reported in Chapter 3.

Chapter 5 Mechanistic pathways regulating mitochondrial dynamics and role of Sirt5

5.1 Introduction

Mitochondrial fission/fusion has been reported to be regulated by different mechanisms including Prohibitins, ER stress and Sirtuins pathways. Prohibitins, PHB1 and PHB2, form a ring-like structure in the inner mitochondrial protein; deletion of PHBs in mouse embryonic fibroblasts leads to a decrease in L-Opa1 associated with mitochondrial fission (Merkwirth et al., 2008). Another study illustrated that miR-361 induces mitochondrial fission by decreasing PHB1 translation (Wang et al., 2015b). However, much uncertainty still exists about the relation between PHBs and mitochondrial dynamics in the heart.

In addition, there is some research linking ER stress pathway to mitochondrial fission and fusion proteins. For example, ablation of Mfn2 in mouse cardiomyocyte has been reported to be associated with ER stress and apoptosis (Ngoh et al., 2012). In the same study, induction of ER stress was associated with overexpression of Mfn2 in mouse embryonic fibroblasts (MEF). Further, an increase in Drp1 and a decrease in Mfn2 expression has been reported in tunicamycin-induced ER stress mouse (Prola et al., 2019). Details of ER stress pathways are described in the main Introduction section 1.7. There has been no detailed investigation of activation of ER stress in the early-stage DCM.

Mitochondrial sirtuins have been shown to be associated with mitochondrial dynamics. For example, Sirt3 targets OPA1 to stimulate mitochondrial fusion (Samant et al., 2014). Sirt5 is linked to the down regulation of Drp1, Fis1 and MID51, resulting in a reduction of mitochondrial fragmentation (Guedouari et al., 2017). Sirt5 knock-out mouse embryonic fibroblasts showed an increase in Drp1, MID51 and Fis1 associated with mitochondrial fission (Guedouari et al., 2017). A comprehensive overview of Sirt5 in cardiac physiology and pathology can be found in Bugger et al. (2016). Despite these studies, there is a gap in the knowledge about Sirt5 and its involvement in mitochondrial fission/fusion in the heart. Therefore, we investigated whether Prohibitins, ER stress pathways and Sirt5 level were altered in the myocardium of our model of HFD (DIO) feeding. To develop these studies, we employed an H9c2 cardiac myoblast cell line.

Different cell lines have been used in cardiovascular research including primary neonatal cardiomyocytes and immortalised cells, *i.e.*, HL-1 (Claycomb et al., 1998) and H9c2 cardiac myoblasts (Kimes and Brandt, 1976). The advantage of primary cells is that they come

directly from the heart. For this reason, they exhibit comparable phenotypes. However, isolating cells can be costly and time-consuming. They are difficult to culture and have a short lifetime (Peter et al., 2016). For example, the cell shape changes and the density of the t-tubule in primary cardiomyocytes decreases within 96 hours of culture (Leach et al., 2005). Rat neonatal cardiomyocytes are also commonly used, although they are also costly, requiring the use of animals. However, in terms of mitochondrial investigations, rat neonatal cardiomyocytes may not be suitable, depending upon the research question posed, because they are neonatal and, thus, use glucose rather than FFA as an energy source (Cao et al., 2019). The use of an immortal cell line, on the other hand, is much more convenient and affordable to generate.

HL-1 cells are derived from atrial tumours in mice and have been used to study atrial fibrillation successfully. (Rao et al., 2009). H9c2 cells were originally derived from embryonic rat ventricular tissue. Even though H9c2 cells are not able to beat and have been manipulated to proliferate, they still show many common features of primary cardiomyocytes, including electrophysiological characteristics, membrane morphology and G-signalling protein expression (Sipido and Marban, 1991, Hescheler et al., 1991). In particular, H9c2 cells have similar properties in terms of mitochondrial function and morphology to primary cardiomyocytes (Kuznetsov et al., 2015). This makes them a viable alternative for the primary cardiomyocytes and hence were employed here in this study.

The aims of this Chapter were:

1) Assess the ER stress in the HFD (DIO) model.
2) Study the link between IR and mitochondrial dynamics.
3) Measure PHBs level in the HFD (DIO) model.
4) Quantify levels of Sirtuins in the HFD (DIO) model.
5) Explore a mechanistic pathway regulating mitochondrial dynamics.

5.2 Methods

5.2.1 Cell culture

H9c2 rat heart myoblasts were purchased from Sigma and cultured in Dulbecco's Modified Eagle Medium (DMEM, 25 mM glucose, Gibco) containing 1% (v/v) penicillin/streptomycin, 1% (v/v) non-essential amino acids and 10% (v/v) foetal bovine serum. H9c2 were seeded onto (Grenier) tissue culture flasks and incubated at 37°C in 5% CO2 and were passaged when they reached approximately 70-80% confluency. Cells were used from passages 10-20. All experiments were conducted in triplicate with data averaged from 3 technical replicates. Cell culture work was done in class II cabinets.

5.2.2 Protein extraction from cells

H9c2 cells were washed with cold phosphate-buffered saline (PBS) twice after removing the media. RIPA buffer containing protease inhibitors was added to the cells and incubated on ice for 20 minutes before the cells were scraped with a cell scraper. Lysates were then centrifuged at 4°C for 5 minutes at 8,000 rcf to remove non-lysed cells. The supernatant was transferred into new tubes to quantify total protein concentration by Bradford assay as described in section 2.2.3.1.

5.2.3 RNA extraction from cells

RNA isolation from H9c2s was as follows: Cells were washed with PBS (Sigma). One millilitre of Trizol was added to cells and scraped to collect the lysate in an RNase free tube before incubating the tube for 5 minutes in the room temperature. 200 µl chloroform was added to each tube before shaking the tubes vigorously for 15 seconds and incubating them at room temperature for 3 minutes. After the incubation, tubes were spun at 13,225 rcf at 4°C for 5 minutes. Top layer was transferred to new tubes and 500 µl isopropanol were added prior to mixing the tubes. Tubes were incubated at -20°C for 30 minutes after which the tubes were spun at 13,225 rcf for 10 minutes at 4°C. The supernatant was discarded, and the pellet was washed with 1 ml 75% (v/v) ethanol before gently agitating the tubes. After that, the tubes were spun 9184 rcf at 4°C for 10 minutes and supernatants were discarded. RNA pellets were air-dried for 15 minutes prior to resuspending it with 50 µl RNase-free water.

5.2.4 Insulin resistant H9c2 cells

H9c2 cells were made resistant to insulin using a previously published protocol (Ha and Pak, 2005). In brief, cells were grown in a 6-well cell culture plate. Cells were starved for 4 hours in a medium containing low glucose level (5.5 mM glucose and 0.5% (w/v) BSA) and a final concentration of 100nM insulin was added to the wells and incubated for 24 hours.

To validate the protocol, a glucose uptake assay kit from Abcam (ab136955) was used. This kit uses the glucose analogue 2-DG to be taken up by the cells and metabolized to 2-DG6P, which oxidized in the cells to generate NADPH, the latter entering a multiple oxidation reaction producing a colour at 412 nm as illustrated in Figure 5.1.

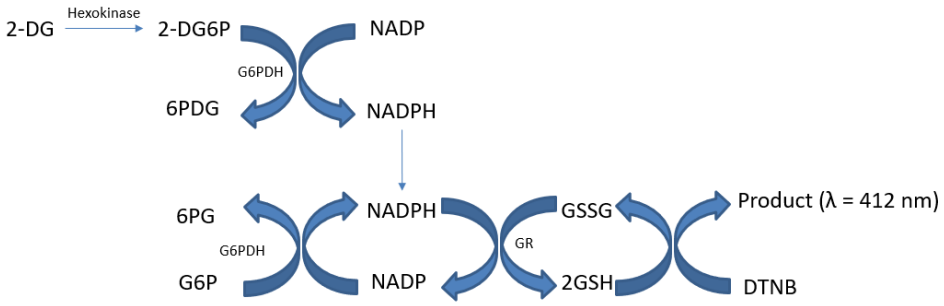

Figure 5.1: Glucose uptake assay chemical interactions.
A final product measured at 412 nm is proportional to 2-DG (glucose) taken up by cells.

The uptake of Glucose (2-DG) into the cells is directly proportional to the quantity of NADPH. Following the protocol to generate insulin resistant cells, wells were washed with PBS 3 times. 2-DG was added to insulin-treated and untreated cells and incubated for 20 minutes. After 20 minutes, cells were washed again with PBS for 3 times. 80 µl of extraction buffer was added to cells then scraped using a cell scraper and transferred to tubes. Samples were frozen/thawed and heated for 40 minutes at 85°C. Before neutralizing the samples by neutralizing buffer, samples were cooled on ice for 5 minutes. Samples were mixed properly by spinning briefly. 50 µl of diluted sample (1:10), standard dilution, background control was added to 96-well plates. 10 µl of mixture A (assay buffer and enzyme mix) was added to each well and incubated for 1 hour at 37°C. After that, 90 µl extraction buffer was added to each well and the plate was heated for 40 minutes at 90°C. Plate was cooled on ice ad neutralized by neutralizing buffer. 38 µl of mixture B (Glutathione Reductase, Substrate, Recycling Mix) were added to each well. Optimal density at 412 nm was then measured using FLUOstar® Omega microplate reader (BMG Labtech) every 2 minutes for 14 minutes. Glucose concentration were interpolated from the standard curve of 2-DG6P.

5.2.5 siRNA knockdown

Knockdown of Sirt5 gene using siRNA was achieved with "ON-TARGETplus smart pool rat (Dharmacon)" and "non-targeting pool control (Dharmacon)" as a control. H9c2 cells were seeded into different density for various plate sizes as listed in Table 5.1.

Table 5.1: H9c2 cardiac myoblasts seeding density.

Plate	Density
6-well plate	300,000
24-well plate	100,000
96-well plate	30,000

After the seeding, plates were incubated overnight at 37°C in 5% CO_2. 25 nM of siRNA per well (diluted with penicillin-free and serum-free medium OPTI-MEM) was used to transfect cells using 4 µl of DharmaFECT (Dharmacon). After that, the plate was incubated for 48 hours before harvesting for different assays. The validation of Sirt5 knockdown was confirmed by Western blotting and RT-qPCR.

5.2.6 qPCR and western blotting

Primary and secondary antibodies used in this Chapter are summarised in Table 5.2. Mitochondrial fission/fusion proteins antibodies used were the same as listed in section 2.2. Western blotting technique was carried out as detailed in section 2.2.

Table 5.2: List of primary and secondary antibodies for ER stress and sirtuin5 pathways.

Primary Antibody	Dilution	Manufacturer	Secondary Antibody	Dilution	Manufacturer
ATF6	1:1000	Abcam	Anti-Rabbit HRP	1:3000	Bio-Rad
Xbp1	1:200	Proteintech	Anti-Rabbit HRP	1:3000	Bio-Rad
ATF4	1:500	Proteintech	Anti-Rabbit HRP	1:3000	Bio-Rad
AMPK	1:1000	Cell signalling	Anti-Rabbit HRP	1:3000	Bio-Rad
Sirt5	1:1000	cell signalling	Anti-Rabbit HRP	1:3000	Bio-Rad

Quantitative PCR was used to identify the changes in the transcript expression. A specific primer was used to amplify a targeted gene, summarized in Table 5.3. Mouse mitochondrial fission/fusion proteins primers used were the same as listed in section 2.2. qPCR was conducted as described in section 2.2.

Table 5.3: List of primer assay for ER stress, sirtuin5, prohibitins and mitochondrial dynamics.

Species	Target gene	Primer	Supplier	Catalogue number
Mouse	Sirt3	Mm_Sirt3_1_SG	Qiagen	QT00147280
	Sirt4	Mm_Sirt4_1_SG	Qiagen	QT00312536
	Sirt5	Mm_Sirt5_1_SG	Qiagen	QT00494725
	PHB1	Mm_Phb_1_SG	Qiagen	QT00152992
	PHB2	Mm_Phb2_1_SG	Qiagen	QT01057161
	BiP	Mm_Hspa5_1_SG	Qiagen	QT00172361
Rat	Sirt5	Rn_Sirt5_1_SG	Qiagen	QT01577317
	Drp1	Rn_dnm1l_1_SG	Qiagen	QT05214855
	Mfn1	Rn_Mfn1_1_SG	Qiagen	QT03621452
	Mfn2	Rn_Mfn2_1_SG	Qiagen	QT00254863
	Opa1	Rn_Opa1_1_SG	Qiagen	QT07854412
	Gapdh	Rn_Gapdh_1_SG	Qiagen	QT06214459

5.2.7 Reactive oxygen species dihydroethidium assay

A Dihydroethidium (DHE) assay (Abcam) was carried out to ascertain whether Sirt5 knockdown affects reactive oxygen species (ROS). In this assay, DHE is used as a fluorescent probe to detect ROS. Cells were treated as prescribed in section 5.2.5. Culture media was aspirated and 150 µl cell-based assay buffer was added. 130 µl of ROS staining buffer was added to each well after aspirating most of the cell-based assay buffer. N-acetyl cysteine reagent (antioxidant) was added to negative control wells before incubation at 37°C for 30 minutes protected from light. After that, antimycin A (ROS generator) was added to positive control wells and incubated for another hour. ROS staining buffer was aspirated, and cell-based assay buffer was then added to all wells. The plate was placed on a FLUOstar® Omega microplate reader (BMG Labtech) to measure the fluorescence excitation wavelength at 480-520 and emission wavelength at 570-600 nm.

5.2.8 Mitochondrial membrane potential

A tetramethylrhodamine ethyl ester (TMRE) mitochondrial membrane potential assay kit (Abcam) was used to assess changes in mitochondrial membrane potential. In this assay, TMRE (red-orange dye) is used to label active mitochondria. Depolarized mitochondria will have less staining. Carbonyl cyanide-4-(trifluoromethoxy)phenylhydrazone (FCCP) is a mitochondrial uncoupler used as a depolarization control. Cells were seeded and pre-treated with sirt5 SiRNA in 96-well plate as mentioned in section 5.2.5. FCCP (20 µM) was added then incubated for 10 minutes. 1000 nM TMRE was added to all wells then incubated for 30

minutes. After that, wells were washed twice with PBS. FLUOstar® Omega microplate reader (BMG Labtech) was then used to read fluorescence at excitation/emission wavelengths = 549/575 nm.

5.2.9 Statistical analysis

All data are displayed as the mean ± standard error of the mean (mean ± SEM), assessed for normality using Shapiro-Wilk test. Comparison of two groups were performed using unpaired t-test. P value <0.05 was considered statistically significant. Statistical analysis was done by GraphPad Prism (version 7, California, USA).

5.3 Results

5.3.1 Sirtuins and Prohibitins level in the 12-week high-fat diet (DIO) model

Mitochondrial Sirtuins expression was first investigated in the HFD (DIO) model characterised in Chapter 2 due to previous studies highlighting the association between Sirtuins and mitochondrial fission/fusion proteins (Section 5.1). We found that transcript expression of Sirt5, but not Sirt3 and Sirt4, was significantly decreased in the HFD (DIO) model compared to control (Figure 5.2).

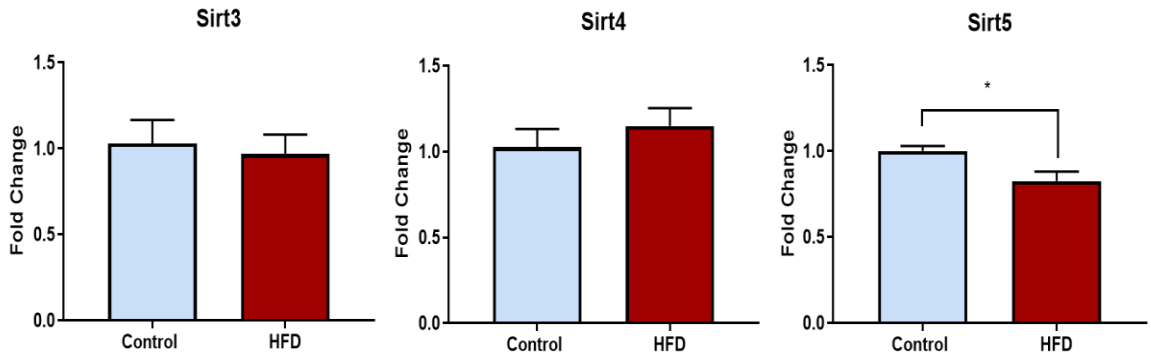

Figure 5.2: The transcript expression of Sirtuin5 was decreased in the HFD (DIO) mice model.

Sirtuin3 and Sirtuin4 transcript expression showed no significant difference, while sirtuin 5 showed a significant decrease in the HFD (DIO) model (n=8) compared to control (n=5-6). Data are expressed as mean ± SEM. *P≤0.05

As discussed above Prohibitins (PHBs) are involved in the mitochondrial apoptosis, mitophagy, mitochondrial biogenesis and mitochondrial networks (Signorile et al., 2019). However, PHB1 and PHB2 mRNA level was not changed in the HFD (DIO) model compared to control (Figure 5.3). Therefore, we excluded the link between prohibitins and fission/fusion proteins changes in early DCM.

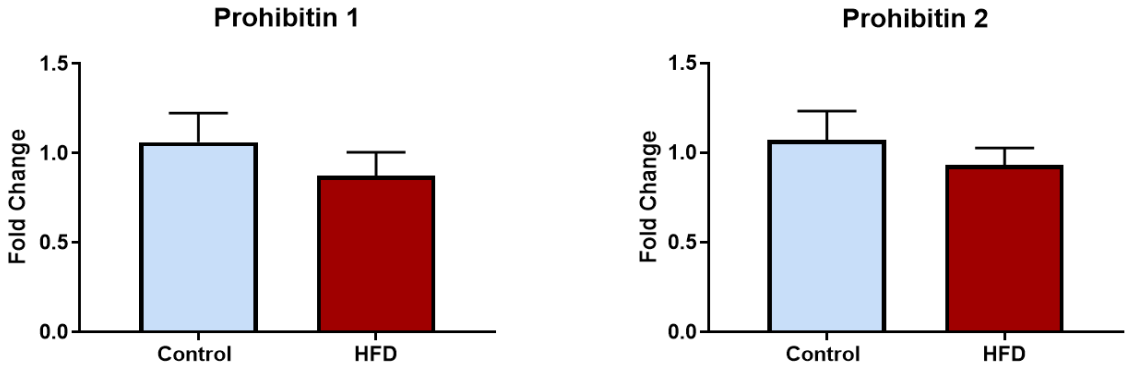

Figure 5.3: No change in the transcript expression of prohibitins in the high fat diet (DIO) model.

There were no significant changes detected in transcript expression of prohibitin 1 and 2 in HFD (DIO) model (n=7-8) compared to control (n=6). Data are expressed as mean ± SEM.

5.3.2 Endoplasmic reticulum stress in high-fat diet

We also assessed ER stress activation in our HFD (DIO) model as a potential regulator of fission/fusion proteins by investigating the main ER stress pathway proteins. Binding immunoglobulin protein (BiP) is an essential regulator for ER stress but there was no change at the mRNA level in the HFD (DIO) model compared to control (Figure 5.4A). ATF6, Xbp1 and ATF4 proteins also form the main pathways in ER stress; however, none of these proteins at the transcript level were affected by the HFD (DIO) (Figure 5.4B). Therefore, it was concluded that there was no evidence that ER stress being activated by 12 weeks high fat feeding.

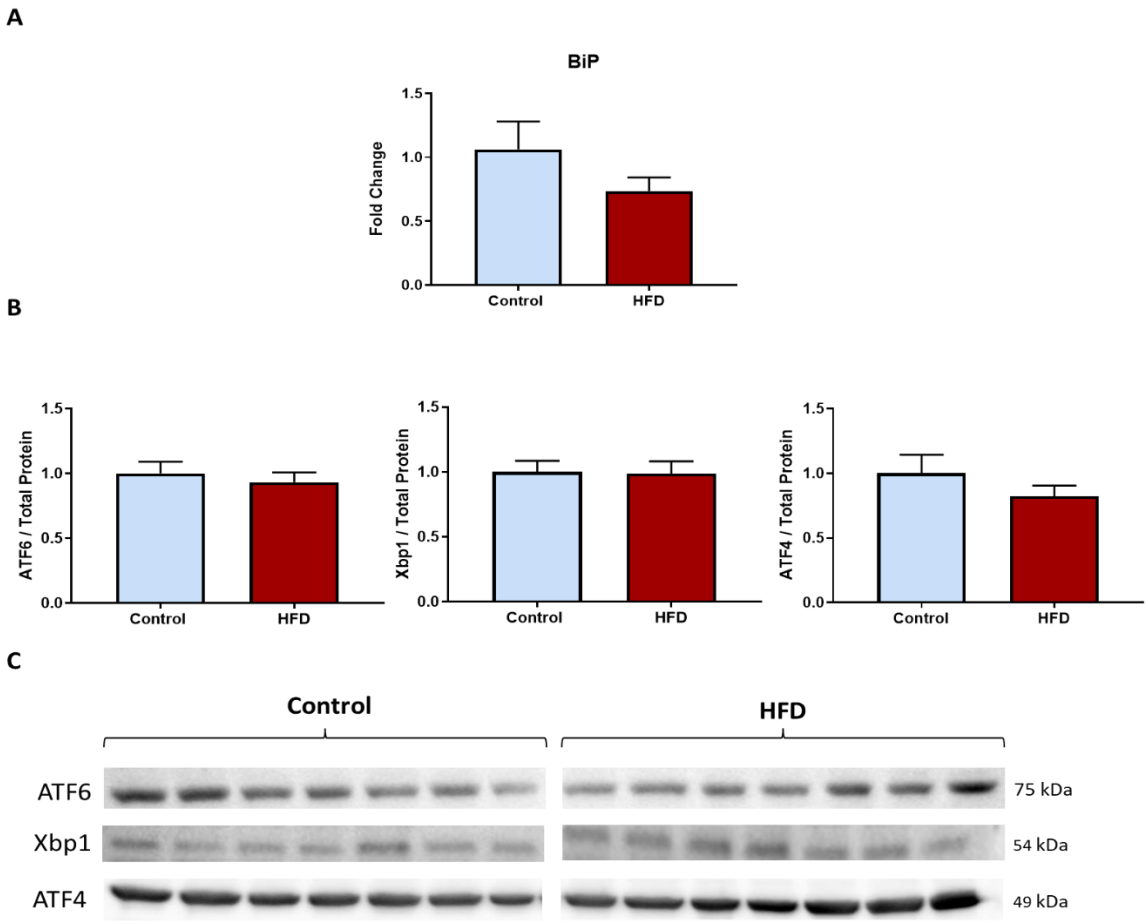

Figure 5.4: proteins involved in endoplasmic reticulum stress were not changed in the high-fat diet (DIO) model.

A. Binding immunoglobulin protein (BiP) transcript expression showed no significant change in HFD compared to control. B. No change in the expression of ATF6, Xbp1 and ATF4 was detected. C. Representative blots of ATF6, Xbp1 and ATF4 in control and HFD. Data are expressed as mean ± SEM (n=7).

5.3.3 Investigation of the effect of insulin resistance upon expression levels of mitochondrial fission-fusion proteins

We treated H9c2 cells according to the method described by Ha and Pak (2005) to render them insulin resistant. We next confirmed that H9c2 cells were insulin resistant using the glucose uptake assay. The figure below shows that 2-DG (glucose) uptake in treated H9c2 (100 nM insulin) cells were significantly decreased compared to untreated cells confirming cells became insulin resistant (Figure 5.5). However, RT-qPCR and western blotting showed that expression of the fission/fusion proteins were unchanged in response to IR (Figure 5.6).

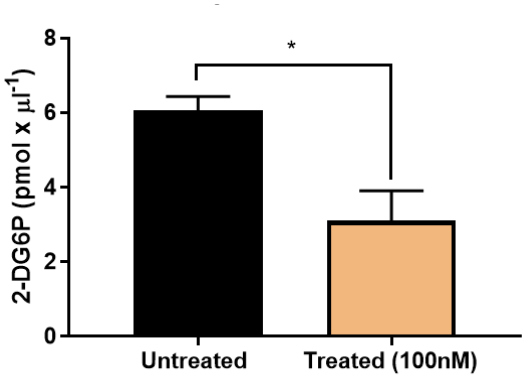

Figure 5.5: A decrease in 2-DG uptake in H9c2 treated with 100nM insulin.
2-DG uptake is significantly decreased in treated cells (100nM insulin) using glucose uptake assay. Data are expressed as mean ± SEM (n=3 technical replicates from 3 different passages). * P≤0.05

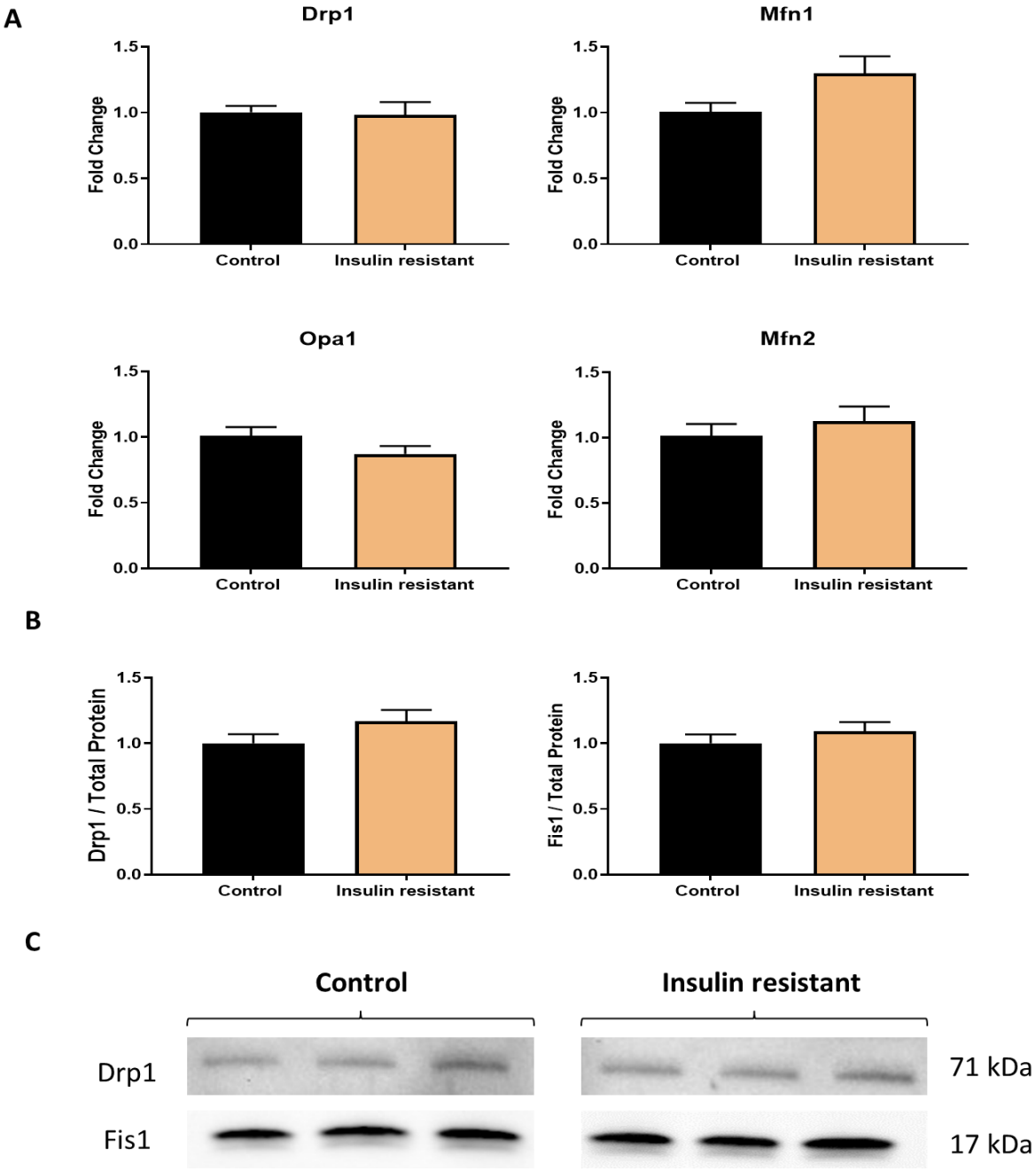

Figure 5.6: Proteins involved in mitochondrial dynamic remain unchanged in insulin resistant H9c2 cells.

A. The transcript levels of the main fission/fusion proteins showed no significant changes compared to control. B. No differences were detected in the fission proteins level. C. Representative blots of Drp1 and Fis1 in insulin resistant H9c2 cells and control. Data are expressed as mean ± SEM (n=3 technical replicates from 3 different passages).

5.3.5. Expression of mitochondrial fission and fusion proteins following siRNA mediated Sirt5 knockdown in vitro

Based upon the above data revealing that levels of Sirt5 are reduced in the HFD (DIO) model we next focussed upon exploring the link between Sirt5 and mitochondrial fission-fusion by undertaking experiments to knock-down Sirt5 in H9c2 cells using siRNA methods. As shown below this approach led to a decrease by approximately 72-74% in Sirt5 mRNA and protein expression levels after the siRNA transfection (Figure 5.7). These results show that the siRNA-mediated knockdown of Sirt5 is effective for decreasing both the Sirt5 gene and the protein expression.

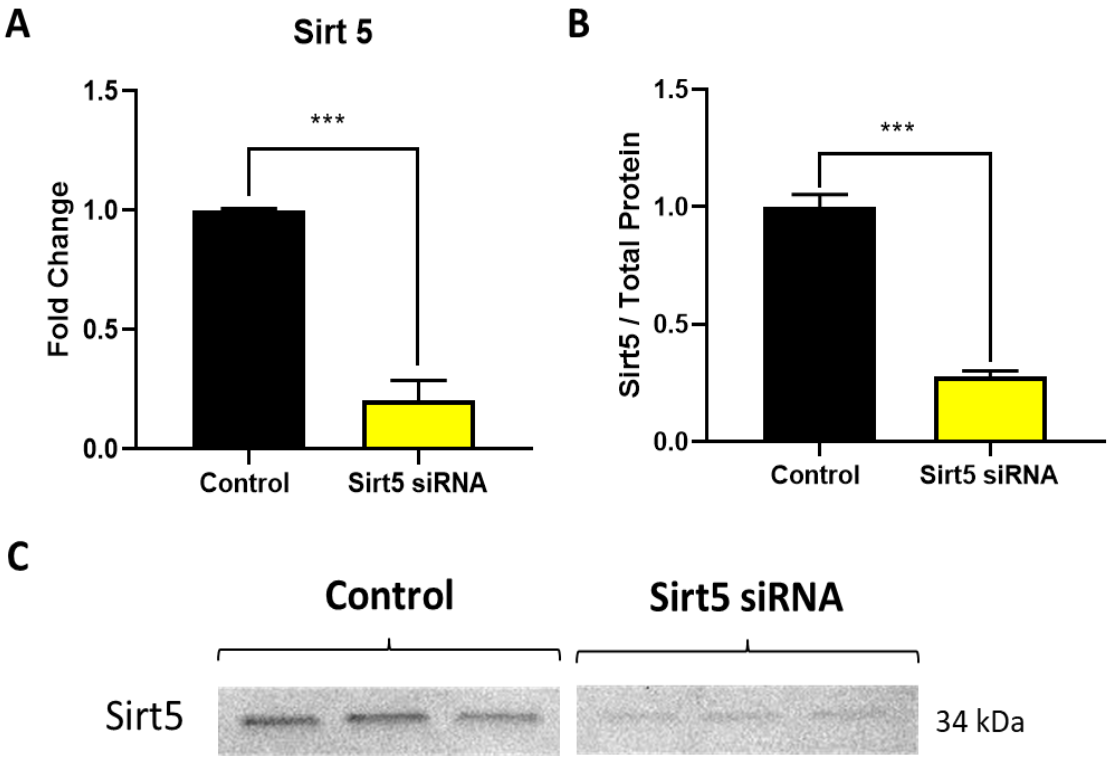

Figure 5.7: mRNA expression and protein level of Sirt5 decreased after Sirt5 siRNA-mediated knockdown.

Validation of Sirt5 knockdown by Western blotting and RT-qPCR showed a significant decrease in Sirt5 transcript expression (A) and Sirt5 protein level (B). C. Representative blot of Sirt5 protein in Sirt5 knockdown H9c2 cells and non-targeted cells (control). Data are expressed as mean ± SEM (n=3 technical replicates from 3 different passages). ***P≤0.001.

5.3.6 Analysis of mitochondrial fission/fusion proteins following Sirt5 knockdown

After the validation of Sirt5 siRNA-mediated knockdown, we investigated the changes in mitochondrial fission/fusion proteins. Opa1 transcript expression was not significantly changed between Sirt5 knockdown cells and control (Figure 5.8A), but Western blotting

showed at the protein level Opa1 was increased. Analysis of both isoforms showed that the short isoform (S-Opa1) enhancing fission was upregulated, while the long isoform (L-Opa1) enhancing fusion was not changed (Figure 5.8B).

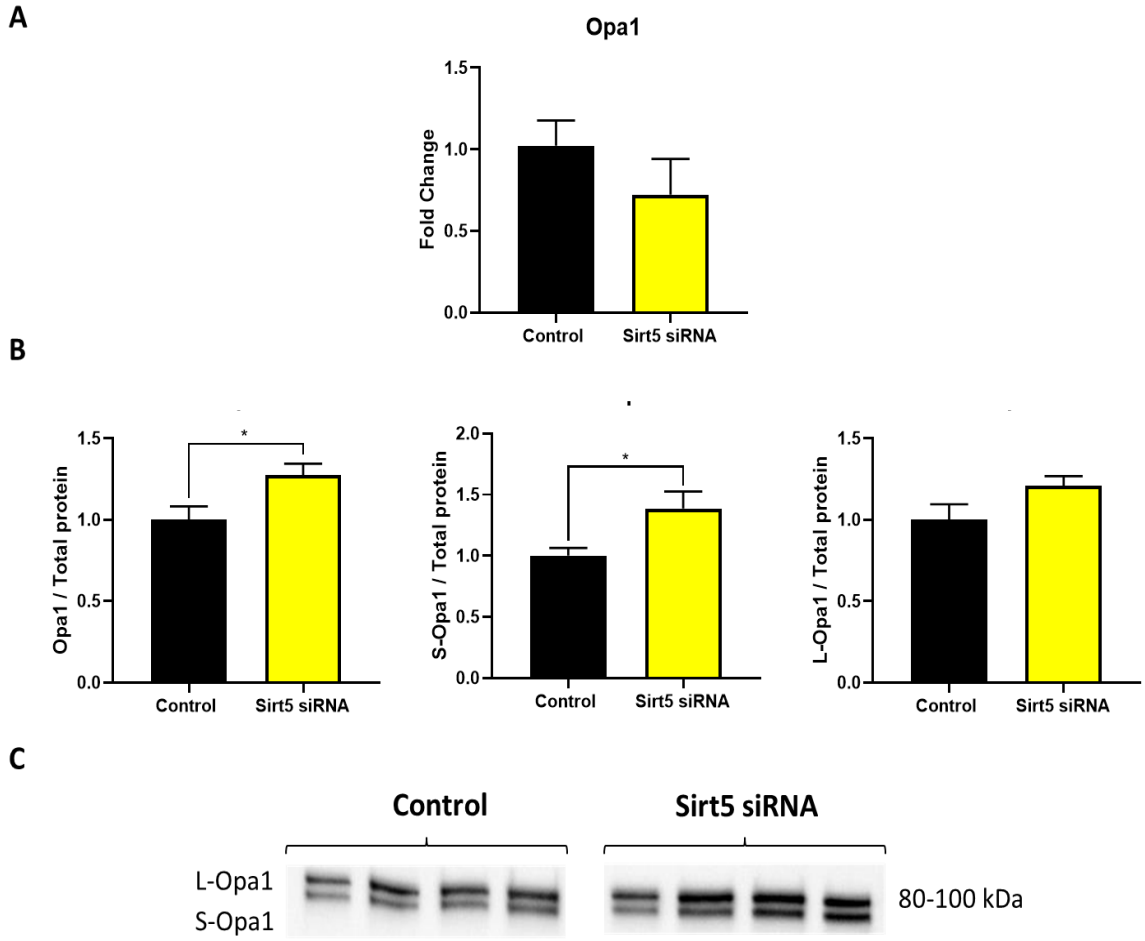

Figure 5.8: An increase in the total Opa1 and S-opa1 expression following Sirt5 siRNA-mediated knockdown.
A. mRNA of Opa1 showed no significant change compared to control in Sirt5 siRNA. B. Significant elevation in the Opa1 level, specifically S-Opa1 in Sirt5 knockdown cells. C. Representative blots of L-Opa1 and S-Opa1 in control and Sirt5 siRNA mediated knockdown. Data are expressed as mean ± SEM (n=3 technical replicates from 4 different passages). *P≤0.05

Other fusion proteins (Mfns) were studied. Mfn1 mRNA level, but not protein expression, was significantly decreased in Sirt5 knocked down cells compared to control. No changes were detected in both Mfn2 transcript and protein expressions between Sirt5 knockdown and control (Figure 5.9).

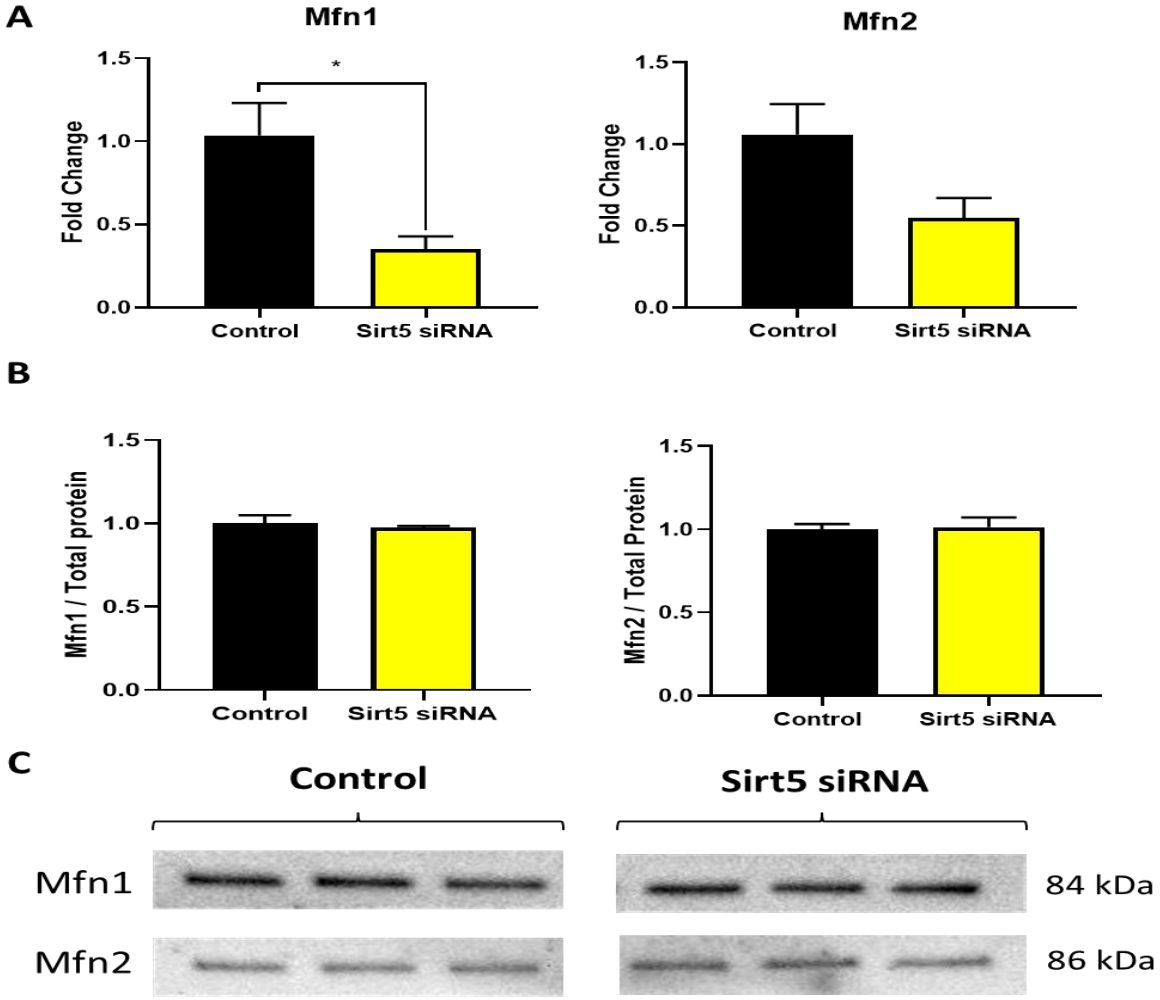

Figure 5.9: A decrease in Mfn1 transcript expression following Sirt5 siRNA-mediated knockdown.

A. Mfn1, but not Mfn2, mRNA level was downregulated in Sirt5 siRNA compared to control. B. Both Mfn1 and Mfn2 showed no significant difference in expression between control and Sirt5 siRNA. C. Representative blots showing Mfn1 and Mfn2 expression level in control and Sirt5 siRNA H9c2 cells. Data are expressed as mean ± SEM (n=3 technical replicates from 3 different passages). *P≤0.05

The phosphorylation state of Drp1 determine the function i.e. P-Drp1 at position S616 stimulates fission whereas P-Drp1 at S637 inhibits fission. There was a significant upregulation of total Drp1 in Sirt5 knockdown cells compared to control. This change was associated with a reduction to the phosphorylated form of Drp1 at Serine 637 (Figure 5.10B). Interestingly, these results are identical to the findings seen in our HFD (DIO) model. Therefore, these data suggest a potential link between changes in Sirt5 expression and alteration to the fission/fusion axis.

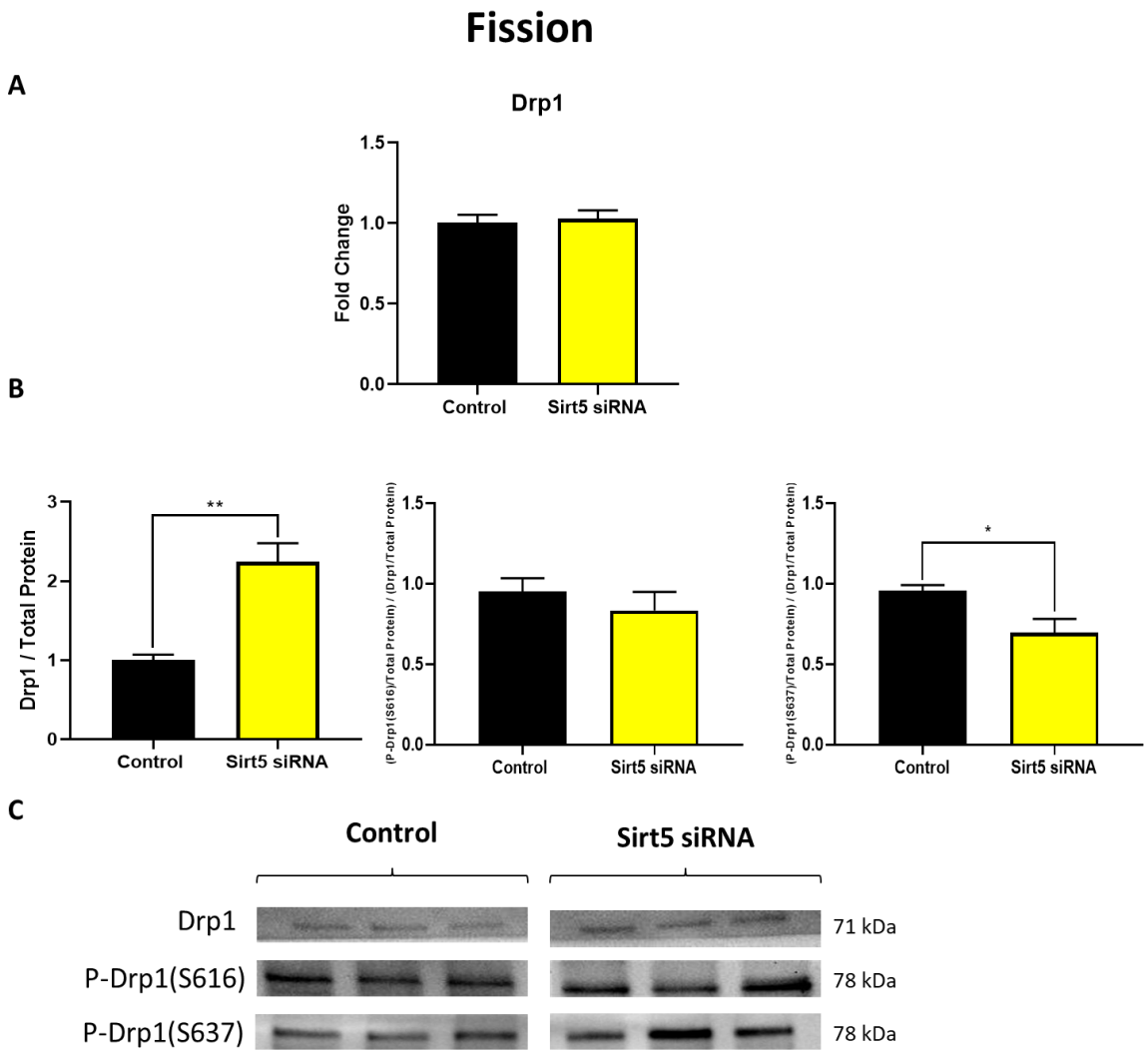

Figure 5.10: A decrease in the phosphorylated Drp1 at S637 following Sirt5 siRNA-mediated knockdown.

A. No change was detected in Drp1 transcript expression between control and Sirt5 siRNA cells. B. A significant increase in Drp1 expression in Sirt5 knockdown cells compared to control was associated with a significant decrease of the phosphorylated form of Drp1 (S637) in Sirt5 knockdown cells compared to control. C. Representative blots of total and phosphorylated forms of Drp1 expression in control and Sirt5 siRNA. Data are expressed as mean ± SEM (n=3 technical replicates from 3 different passages). *P≤0.05, **P≤0.01.

However, none of the Drp1 receptors includes MID51, Mff and Fis1 was significantly changed in Sirt5 knocked down cells compared to control (Figure 5.11).

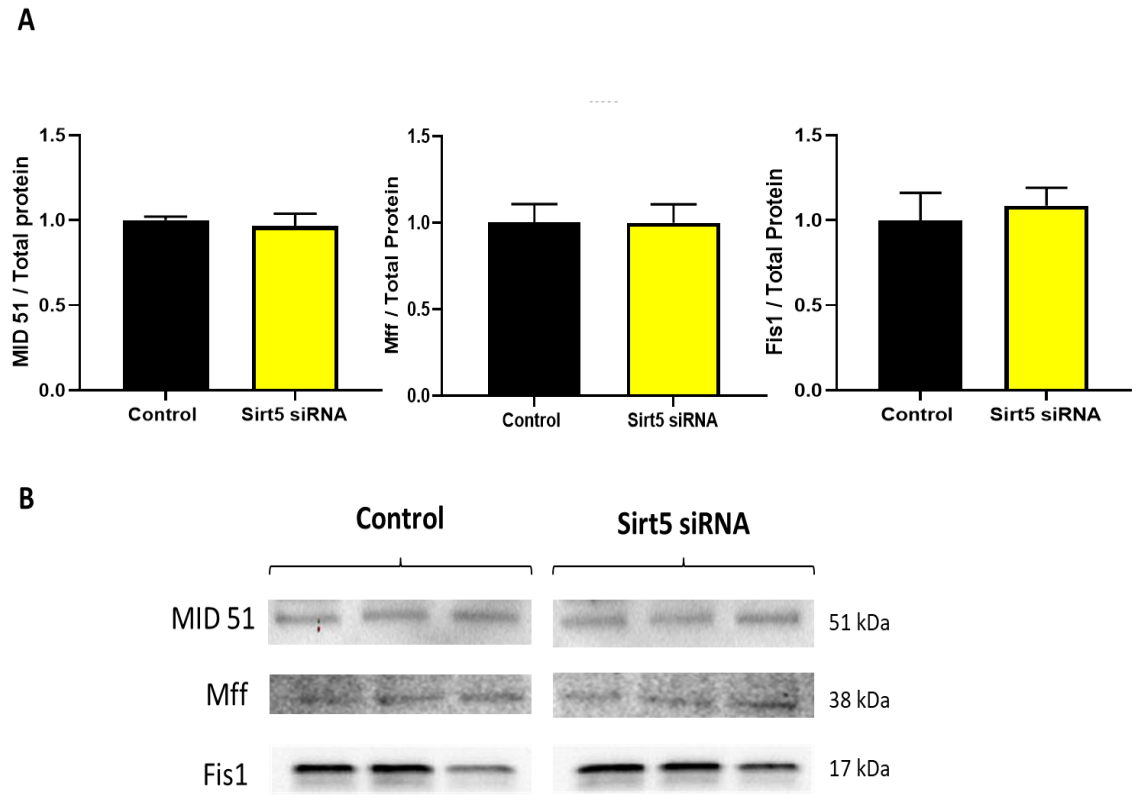

Figure 5.11: No change in the expression of Drp1 receptors following Sirt5 siRNA-mediated knockdown.
A. All Drp1 receptors level showed no significant difference in control and Sirt5 knockdown cells. B. Representative blots of MID 51, Mff and Fis1 expressions. Data are expressed as mean ± SEM (n=3 technical replicates from 3 different passages).

The enzyme 5' adenosine monophosphate-activated protein kinase (AMPK) is involved in cellular energy homeostasis and has been reported to regulate Sirt5 and mitochondrial fission/fusion proteins (Zhang et al., 2019, Li et al., 2015). To exclude the effect of AMPK on Sirt5 and vice versa, we assessed AMPK level in Sirt5 siRNA-mediated knockdown. We found that AMPK expression was not statistically changed (Figure 5.12). This result excludes that changes in mitochondrial fission proteins seen in the Sirt5 knockdown were due to changes in AMPK.

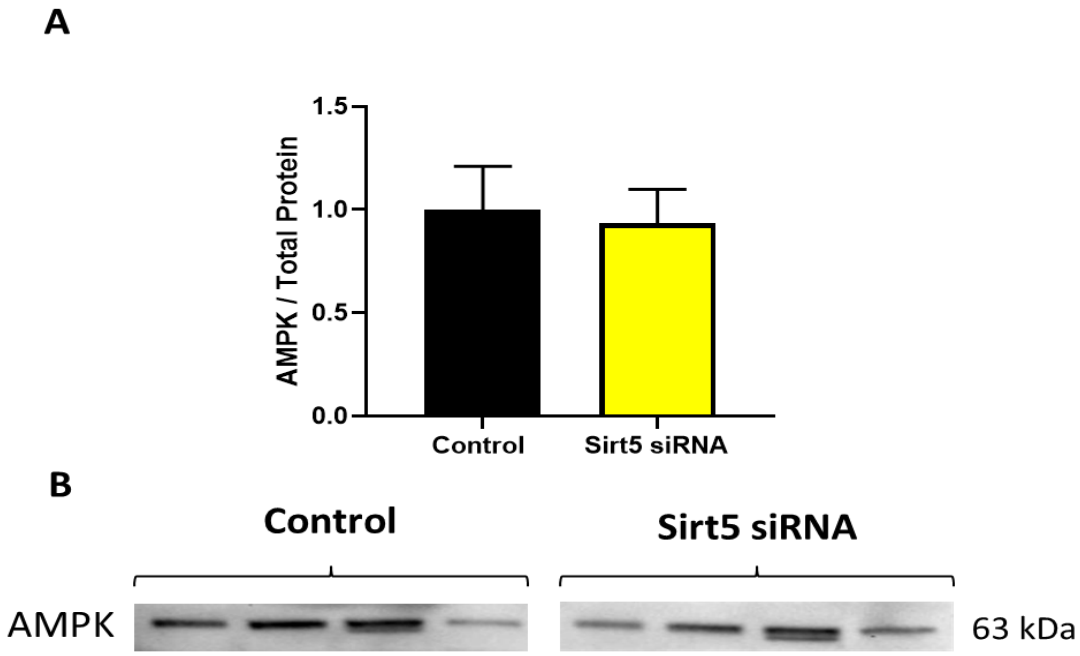

Figure 5.12: Level of AMPK protein was not changed in H9c2 cells after Sirt5 siRNA-mediated knockdown.
A. There was no difference in AMPK level between control and Sirt5 siRNA. B. Representative blot showing AMPK level in control and Sirt5 knockdown H9c2 cells. Data are expressed as mean ± SEM (n=3 technical replicates from 3 different passages).

5.3.7 Assessment of reactive oxygen species levels and membrane potential following Sirt5 siRNA mediated knockdown

To evaluate if the mitochondrial function has been affected following Sirt5 siRNA-mediated knockdown, mitochondrial membrane potential and mitochondrial ROS were assessed.

Mitochondrial membrane potential detects depolarized and damaged mitochondria by a decrease in the membrane potential. FCCP is a mitochondrial uncoupler of oxidative phosphorylation. It was used for two reasons, as a positive control, and to assess mitochondrial membrane potential in uncoupled respiration. As shown in Figure 5.13A, no significant change in mitochondrial membrane potential was detected in Sirt5 knockdown compared to control in both conditions i.e. with and without FCCP.

Reactive oxygen species were measured to assess oxidative stress. The level of ROS in Sirt5 knockdown cells showed no significant changes to control (Figure 5.13B). These results suggest that a decrease in Sirt5 does not affect mitochondrial function.

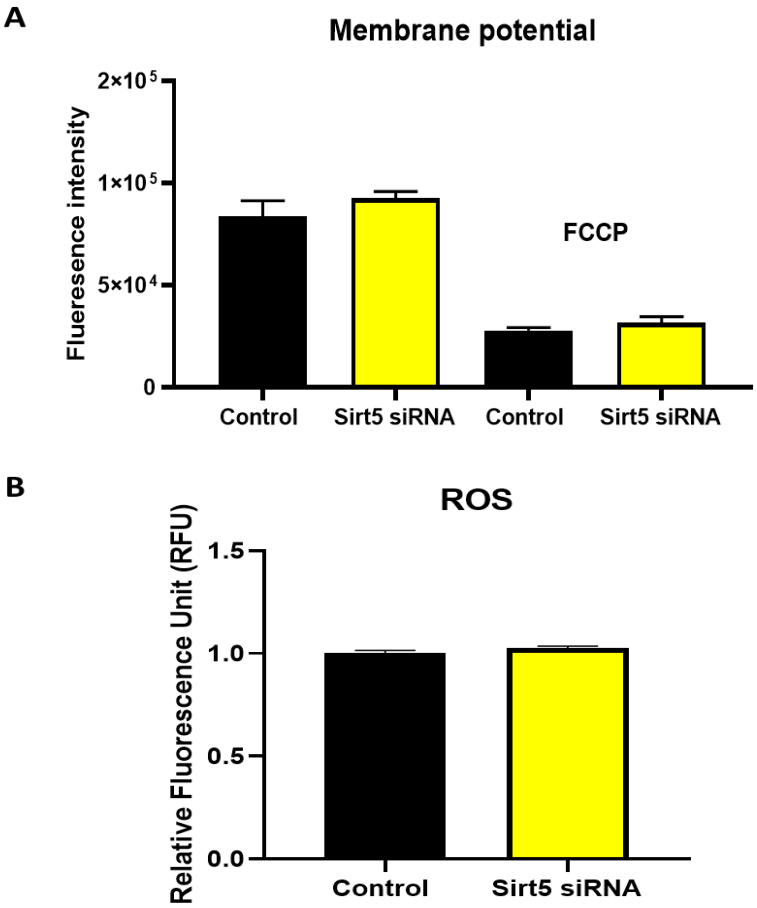

Figure 5.13: Mitochondrial membrane potential and reactive oxygen species level were not changed after Sirt5 siRNA-mediated knockdown.
A. Measurement of membrane potential with nothing added (left side) and with FCCP added, uncoupled, (right side) in Sirt5 knockdown cells. B. Reactive oxygen species level in both Sirt5 siRNA and control showed no difference. Data are expressed as mean ± SEM (n=3).

5.3.8 Summary of results

In order to elucidate mechanistic pathway affecting mitochondrial fission/fusion protein in our HFD (DIO) model which represent an early mild phenotype of DCM, we investigated if multiple regulatory pathways were activated due to IR, ER stress and expression levels of Prohibitins and Sirtuins. The main findings of this Chapter are

- Sirt5, but not Sirt3 and Sirt4, is downregulated in our HFD (DIO) model
- There is no evidence that ER stress pathways are activated in the HFD (DIO) model.
- In-vitro studies indicate that IR alone does not alter expression levels of the fission-fusion proteins.

- Our data suggest there is no link between mitochondrial fission and PHB1/2 proteins in the HFD (DIO) model.
- I have shown for the first time (to our knowledge) that Sirt5 knockdown in H9c2 cells shifts mitochondrial dynamics towards fission, but this has not led to changes to mitochondrial membrane potential or ROS levels.

5.4 Discussion

5.4.1 ER stress is not activated in HFD (DIO) model (early DCM)

Mitochondria and ER are highly connected, a requirement for healthy cardiac function (Murley and Nunnari, 2016). Mitochondrial fission/fusion proteins are an important factor in the tethering and interactions between mitochondria and ER (Gordaliza-Alaguero et al., 2019). ER stress is induced by obesity and diabetes in several organs including the muscles liver, pancreatic cells, adipose tissues and hypothalamus (Cnop et al., 2012).

Many studies suggest that DCM is associated with ER stress (Yang et al., 2015). For example, Lakshmanan et al. (2013) found an activation of ER stress by increased expression of some ER stress proteins in spontaneously diabetic torii rat (non-obese model of T2DM) compared to control (Sprague-Dawley rat), associated with multiple complications i.e. ocular complications, nephropathy, neuropathy and immunodeficiency. The activation of ER stress is likely to be related to the severity of diabetes, as it has been reported that the spontaneously diabetic torii rat typically presents with severe diabetic complications (Sasase et al., 2013). In our HFD (DIO) model, which represents an early stage of DCM, no signs of ER stress were found as assessed by expression levels of key proteins regulating the ER stress pathway. However, levels of proteins do not necessarily indicate the formation of unfolded proteins in the endoplasmic reticulum. Other methods can directly assess ER stress. For example, in ER stress, there is significant widening of the ER lumen, detectable by electron microscopy (Riggs et al., 2005). Another method is to measure real-time redox state by an oxidation reporter, green fluorescent proteins (GFP) to evaluate ER stress (Merksamer et al., 2008). As an oxidizing environment is required to facilitate the forming of disulphide bonds in new proteins. These methods should be considered in future work.

Several reports focused on reducing ER stress as a potential treatment of diabetic cardiomyopathy although since we show here that is not activated in the early stage of disease it may make it a less attractive target. Given that we determined an imbalance towards fission in the HFD (DIO) it would suggest that ER stress is not directly linked. However, a caveat to this conclusion is if Drp1 upregulation in the early stages of DCM is a cardioprotective mechanism to remove damaged mitochondria rather than a pathological development. Future studies could focus upon testing if in-vitro activation of ER stress pathways (e.g. treating H9c2 cells with tunicamycin and dithiothreitol) impacts upon mitochondrial dynamics.

5.4.2 Insulin resistance has no effect on mitochondrial fission/fusion axis

Given that our HFD (DIO) model was insulin resistant and that both diet exchange and exercise/diet exchange groups showed insulin levels returning to normal but not in the exercise alone group, it highlighted the association between insulin resistance (IR) and HFD (DIO) and the possible effect on mitochondrial dynamics. Currently, there is little in the literature on the association between IR and fission/fusion proteins in the heart. For example, Jheng et al. (2012) suggested that mitochondrial fission can cause insulin resistance in skeletal muscle and that inhibition of mitochondrial fission protected muscle cells from insulin resistance. In addition, Lin et al. (2018) reported that overexpression of Mfn1 and Mfn2 ameliorate IR while overexpression of Drp1 and Fis1 deteriorate IR by assessing insulin receptor substrate 1 (IRS-1) phosphorylation of Tyr-896 and the translocation of GLUT1 and GLUT4 to plasma membrane in diabetes-susceptible cybrid cells. Parra et al. (2014) demonstrated that an increase in mitochondrial fusion was linked to an increase in Opa1 levels after primary rat cardiomyocytes were treated with insulin for 3 hours (10 nmol/L). These studies suggest a relationship between IR and mitochondrial fission/fusion proteins. However, the data here indicate there is no change in mitochondrial fission/fusion proteins in the insulin-resistant cardiomyoblast cells. A possible explanation for these results may be the difference in the cell line. Another explanation might be the severity and the method used to induce insulin resistance in cells. The length of high insulin treatment could result in a different severity of insulin resistance (48-72 hours). Insulin resistance can be induced by different techniques including high insulin, dexamethasone, hypoxia, TNFα and free fatty acids (Lo et al., 2013). These methods could be explored further to investigate greater severity of insulin resistance.

5.4.3 Prohibitins has no effect on mitochondrial fission/fusion axis in vitro

Mitochondrial prohibitins (PHB1 and PHB2) are chaperone proteins. These two proteins form a complex in the inner mitochondrial membrane which has been found to stabilize mitochondrial respiratory enzymes (Nijtmans et al., 2000). Targeting prohibitins as a new therapeutic approach is discussed in the review by (Mishra et al., 2005). Several studies have indicated a relationship between PHBs and mitochondrial fission/fusion proteins. For example, Merkwirth et al. (2008) found the loss of PHB1/2 in mouse embryonic fibroblasts (MEFs) induced mitochondrial fission. Additionally, Wang et al. (2015b) suggested that overexpression of PHB1 attenuates mitochondrial fission and apoptosis caused by H_2O_2 treatment in isolated cardiomyocytes from mice. However, here we determined that there was no change to the expression of either isoform of PHB after HFD (DIO) feeding and thus we

suggest that the PHB-regulated pathways do not affect mitochondrial fission/fusion proteins in our early model of DCM.

5.4.4 The effect of Sirt5 on mitochondrial fission and fusion proteins

One of the key regulators of metabolism are Sirtuins. Sirtuins are capable of directly modulating the activity of various metabolic enzymes (Houtkooper et al., 2012). The current study found that only Sirt5 among the others, Sirt3 and Sirt4, is downregulated in the HFD (DIO) model. However, the influence of sirtuin 5 on mitochondrial dynamics is still unknown. Sirt5 is believed to act primarily as desuccinylase and demalonylase (Du et al., 2011). Hundreds of proteins include mitochondrial proteins can be succinylated in Sirt5 deletion models (Yu et al., 2013, Rardin et al., 2013, Park et al., 2013, Boylston et al., 2015).

Following Sirt5 knockdown, levels of S-Opa1 were significantly increased as was total Drp1 with a decrease P-Drp1 (S637) compared to non-targeted cells. Collectively, these protein changes would likely promote mitochondrial fission. Interestingly, the HFD (DIO) model showed the same significant decrease in P-Drp1 (S637) compared to control. These results highlighting the association between Sirt5 and the phosphorylation form of Drp1. These data broadly support the work of other studies in this area linking Sirt5 ablation with mitochondrial fission. For example, silenced Sirt5 human breast cancer cells showed a significant decrease in Mfn2 and Opa1 shifting towards mitochondrial fission (Polletta et al., 2015). In addition, Sirt5 ablation in mouse embryonic fibroblasts caused an increase in Fis1 and MID51 associated with mitochondrial fragmentation (Guedouari et al., 2017). However, they showed that the level of phosphorylated forms of Drp1 (S637) and (S616) did not change in the Sirt5 ablated cells compared to control. This differs from the findings presented here. A possible explanation for this might be the different cell type and that Sirt5 targets different mechanisms for mitochondrial fission. Future work could include EM analysis investigating the size of different subtypes of mitochondria and cristae morphology and stabilisation. Further experiments investigating mitophagy and apoptosis e.g. PINK1/Parkin expression levels, and TUNEL assay could provide a better indication of how Sirt5 impacts mitochondrial dynamics. As our Sirt5 knockdown studies showed an increase in Drp1 and S-Opa1, it will be interesting to explore the mechanism by which Sirt5 affects these proteins and highlight a potential therapeutic target to stall disease progression.

One of the mechanisms that a decrease in Sirt5 cause mitochondrial fission is through adenosine monophosphate-activated protein kinase (AMPK) which in turn activates Mff

during mitochondrial stress (Toyama et al., 2016). No activation of AMPK was found in our Sirt5 knockdown cells. Based upon these studies we would suggest that down-regulation of Sirt5 is an early event in the pathology of DCM (confirmed by our HFD (DIO) feeding model) with cell culture experiments indicating a direct link to mitochondrial fission.

Further work is required to identify whether Sirt5 can target mitochondrial fission proteins directly via deacylation or to target them indirectly via other signalling pathways. For example, target enzymes that affect the function of Drp1 through phosphorylation include; phosphorylation of Drp1 at Ser616 by cyclin dependant kinase 1 (CDK1-cyclin B) (Taguchi et al., 2007), Ser637 by protein kinase A (PKA), Ser600 by calcium/calmodulin-dependent protein kinase 1α (CamKIα) (Han et al., 2008) and dephosphorylation of Ser637 by calcineurin (Cereghetti et al., 2008). Little is known about Sirt5 regulation. The transcription level of Sirt5 was found to be regulated by miRNA-19b (Yang et al., 2018). In addition, overexpression of miRNA-195 was reported in diabetic cardiac tissues to regulate metabolism through Sirt1 and Sirt3 (Gollmer et al., 2020). It would be useful in future work to investigate expression levels of miRNA-19b and miRNA-195 in Sirt5 knockdown experiments to further explore this link. Another pathway involved in the regulation of Sirt5 is PGC1α-Sirt5 (Geng et al., 2011) which was unchanged in our HFD (DIO) model. It has been reported in the literature that Sirt3 deacetylates Opa1 and increases its activity (Samant et al., 2014). However, this is yet to be investigated in other sirtuins and Opa1 isoforms and therefore could be a basis for future work to explore how Sirt5 alters S-Opa1 and Drp1 expression.

5.4.5 The effect of Sirt5 knock out on mitochondrial function

To assess mitochondrial function in Sirt5 knockdown cells, mitochondrial membrane potential and ROS were measured and showed no significant changes. This finding was also reported by Guedouari et al. (2017) who illustrated that mitochondrial membrane potential is not affected by Sirt5 deletion in mouse embryonic fibroblasts (MEFs). This outcome is contrary to that of Li et al. (2019) who found a decrease in the mitochondrial membrane potential in Sirt5 knock down human kidney 2 (HK-2) cell line. This inconsistency may be due to different cell lines.

Several reports have shown that Sirt5 knockdown leads to a deterioration in mitochondrial function. For example, Sirt5 knockdown in HEK293 cells showed defects in mitochondrial complex I and complex II (Zhang et al., 2017). Another study showed that basal and

uncoupled cellular respiration, induced by FCCP, in $Sirt5^{-/-}$ was significantly decreased compared to $Sirt5^{+/+}$ mouse embryonic fibroblasts (Guedouari et al., 2017). A possible explanation for this inconsistency may be due to different levels of Sirt5 knockdown. Another explanation is that mitochondrial membrane potential and ROS do not reflect all aspects of mitochondrial function. Future experiments are needed to assess mitochondrial function further i.e. ATP synthesis, oxygen consumption rate and enzyme activity. Methods of assessing in vivo and in vitro mitochondrial function is reviewed in Lanza and Nair (2010).

Future investigations could implement the use of different cell lines, for example, human-induced pluripotent stem cell (iPSC)-derived cardiomyocytes (beating cardiac muscle cells), which better represent human cardiac cells than H9c2 cells; however, initial differentiated cells have more foetal characteristics which have a different main source of energy (glucose) which may impact mitochondrial metabolism and therefore the translational relevance to adult cardiomyocytes. Additional studies could also include adding other stressors e.g. fatty acids to Sirt5 knock down cells to investigate the link between Sirt5 and dyslipideamia, as in obesity/T2DM.

Targeting Sirt5 as a therapeutic target for improving diabetic cardiomyopathy has not been studied yet. However, activation of Sirt1 and Sirt3 has been shown to effectivity reduce mitochondrial dysfunction. For example, Ding et al. (2018) showed that melatonin inhibits diabetes-induced cardiac dysfunction by preventing Drp1-mediated mitochondrial fission in diabetic hearts via the Sirt1-PGC1α pathway. We found no change to PGC1α in the HFD (DIO) model (Chapter 2), suggesting involvement of other pathways. In addition, Ni et al. (2020) found that icariin ameliorated diabetic cardiomyopathy by preventing mitochondrial dysfunction via Apelin/Sirt3 pathway. A recent review by Gollmer et al. (2020) presented a proposed mechanism that impinges on mitochondrial dysfunction in DCM. However, these studies have have not yet included Sirt5. Figure 5.14 summarised the main findings in the HFD (DIO) model and Sirt5 siRNA knock down H9c2 cell line.

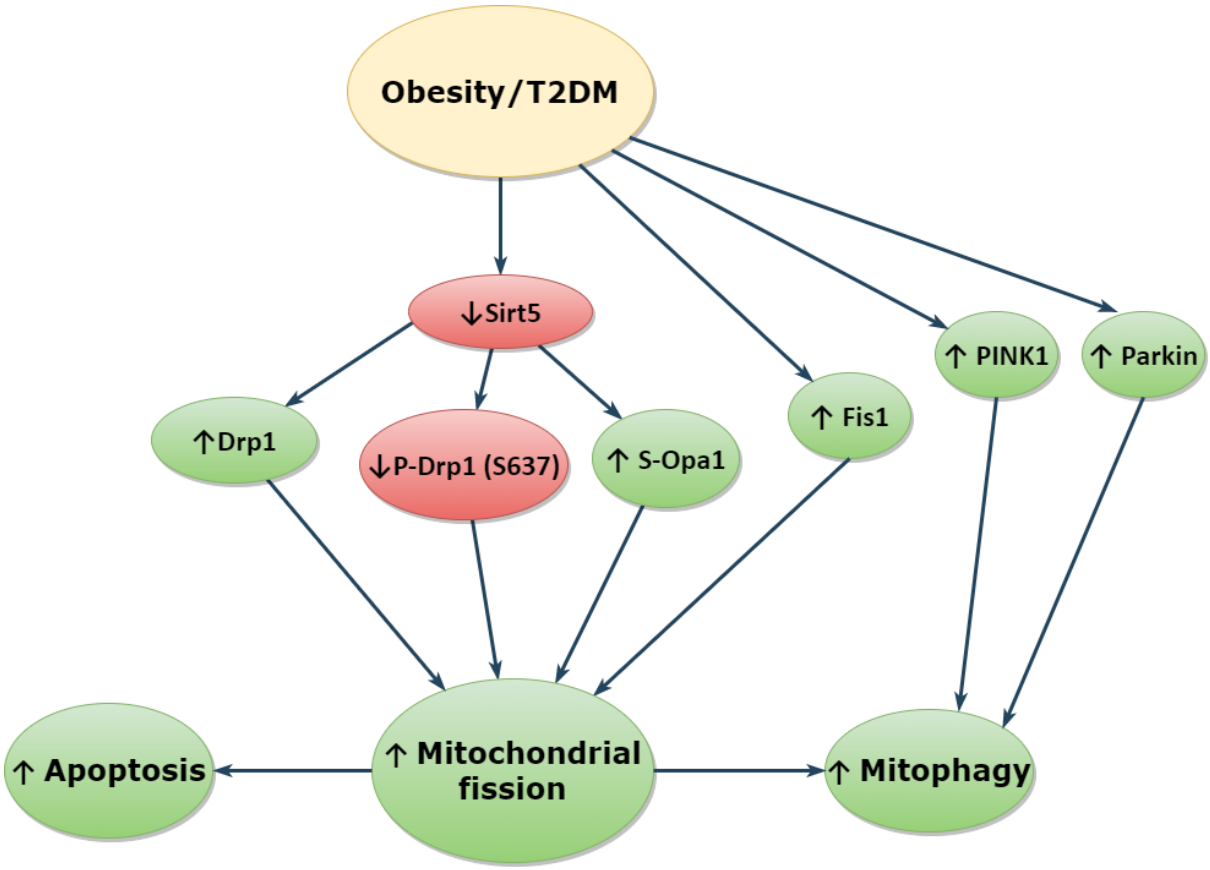

Figure 5.14: Summary of the finding in the HFD (DIO) model and Sirt5 knockdown H9c2 cells.
The red colour indicates down-regulated protein or mechanism, while the red colour indicates up-regulated protein or mechanism. Our HFD model shows a decrease mRNA level of Sirt5, with an increase in Fis1, PINK1 and Parkin expression. Sirt5 siRNA knock down in H9c2 cells was found to lead to increased Drp1 and S-Opa1 expression.

5.5 Conclusion

The main goal of this Chapter was to determine a mechanistic pathway regulating mitochondrial dynamics. There was no activation of ER stress and no change in the expression of prohibitins in our HFD (DIO) model. Using cell culture, we found no link between insulin resistance and mitochondrial dynamics. The high-fat diet model which represents an early stage of DCM showed a significant decrease in Sirt5 associated with a decrease in P-Drp1 (S637). The same changes in Drp1 phosphorylation and an increase in S-Opa1 expression were found after siRNA mediated Sirt5 knockdown in H9c2 cells. The present study lays the groundwork for future research into exploring the regulation of Drp1 and S-Opa1 through Sirt5. Targeting Sirt5 could be a therapeutic target for early-stage diabetic cardiomyopathy.

Chapter 6 Proteomics analysis for HFD (DIO) model and exercise/weight loss regimens

6.1 Introduction

Proteomics is a high-throughput approach to large-scale protein analysis. The purpose of proteomics is to identify proteins within a sample type e.g. cell line, tissue or organelle and provide a comprehensive representation of the levels of each protein and if for example there is a change due to disease. Proteomic techniques mainly use mass spectrometry (MS) for the identification and quantification of proteins. Mass spectrometry (MS) is an analytical technique that provides a measurement of the mass-to-charge ratio (m/z) of the ionised protein/peptide. A plot of intensity vs m/z, known as the mass spectrum, is then generated. Proteins cover a wide range of sizes - ranging from the small protein histone H2A at 66 amino acids to the biggest titin at 34,350 amino acids in length with molecular mass of 3-megadaltons. Proteins are usually digested to small peptides by proteases, such as trypsin for MS analysis (Divan and Royds, 2013). Identification of peptide mix by MS is then matched to protein sequence by computational methods. To improve the analysis, two MS procedures done together in a process called tandem mass spectrometry (MS/MS), is commonly used in the study of biological molecules such as peptides. First, at the entry of each sample (MS1), the peptides are ionized and then separated by their m/z by quadrupoles mass filter consisting of four cylindrical rods. There are several ways to ionise molecules include 1) electron ionisation 2) electrospray ionisation 3) matrix-assisted laser ionisation. A second analysis phase (MS2) is required for the identification of peptides. At this stage, the chosen m/z peptides are fragmented by a collision with a gas to form smaller peptides. These sequences of peptides are then processed in a database for identification (Figure 6.1).

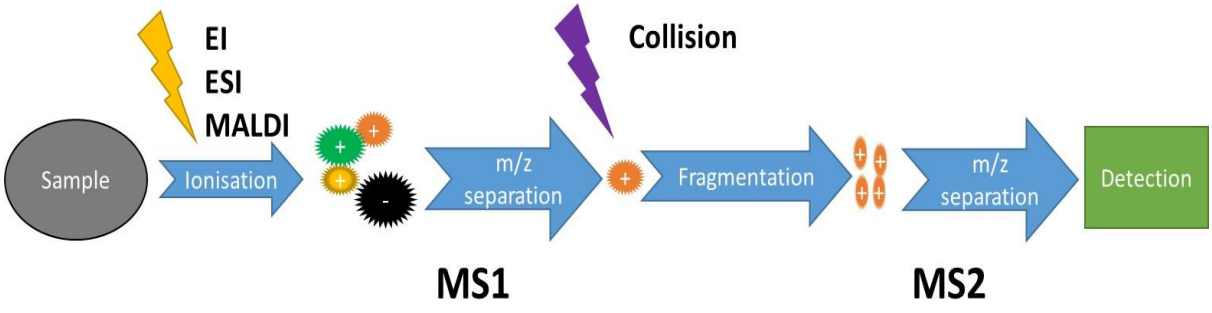

Figure 6.1: Tandem mass spectrometry principle.
EI: electron ionisation, ESI: electrospray ionisation, MALDI: matrix-assisted laser ionisation.

Another commonly used technique to separate proteins is High-Quality Liquid Chromatography (HPLC). The two techniques, HPLC and MS/MS have been combined to improve the sensitivity and efficiency, liquid chromatography with tandem mass spectrometry (LC-MS/MS). The HPLC separate the individual peptides in a mix before entering the mass analysis of MS/MS. In this case, the results are typically presented as a chromatogram, where the y-axis is the signal intensity, and the x-axis is the time in minutes (See Figure 6.2). LC-MS/MS is a robust analysis technique that integrates the separation efficiency of liquid chromatography with the high-sensitivity and selectivity power of the quadrupole mass spectrometry (Bantscheff et al., 2007). It has a wide dynamic range up to 6000 m/z which improves the recognition of single-charged small molecules.

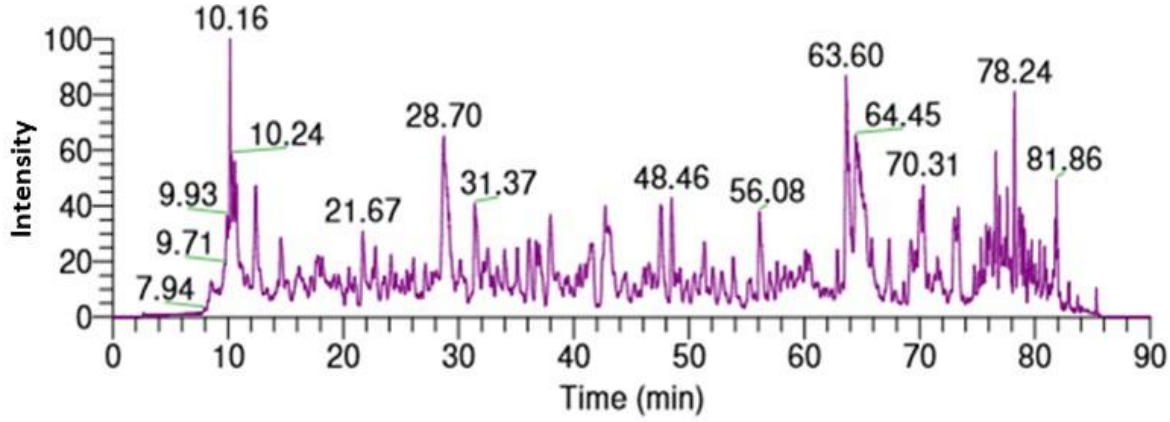

Figure 6.2: The total ion chromatogram of a control sample.
The y-axis represents the summed intensity of masses that have been detected. The x-axis represents the time in minutes.

Detection and quantifying proteins techniques include Western blot, mass spectrometry, protein arrays and ELISA. Each one of them has its advantages and disadvantages. For example, detection of pictograms levels of protein is one of the benefits for Western blotting (Coorssen et al., 2002), which make it usable as an early diagnostic tool (Bertoni et al., 2012). Some of the disadvantages of Western blotting include the molecular weight of a protein can only be approximate, instead of being quantified exactly as in mass spectrometry. Another downside is the limitation of proteins primary antibodies. Western blotting is focussed (one protein at a time), unlike mass spectrometry which will provide global proteins identification.

In MS, two techniques are used for proteins identification: top-down analysis and bottom-up analysis. Top-down analysis can be done in the form of intact proteins, while bottom-up

analysis digest proteins to peptide before mass spectrometry analysis. Bottom-up analysis is more sensitive than top-down analysis (Yates et al., 2009). However, the bottom-up analysis has its disadvantages: 1) the limitation of protein sequence coverage 2) cannot detect post-translational modifications and low abundance peptides of proteins. Top-down analysis has some advantages include better sequence coverage of proteins and preferable detection of posttranslational modifications. One of the drawbacks of top-down analysis is the separation difficulty of intact proteins. In addition, there are not yet any effective techniques for fragmenting bulk proteins. Because of these operational restrictions, the field of application of the top-down method has been narrowed down to the analysis of simple protein mixtures. Mass spectrometry needs highly specialized and costly equipment as well as technical skills that are not common in most laboratories. The use of both mass spectrometry and WB can be done to validate the specificity of antibodies and to detect PTM. Technologies and their applications in proteomics are reviewed by Aslam et al. (2017).

Examples of where proteomics have been applied in the cardiovascular setting include diabetic arteriopathy (Jullig et al., 2010), type 1 diabetic cardiomyopathy (Jullig et al., 2007, Turko and Murad, 2003). Turko and Murad (2003) demonstrated in the quantitative protein profiling of cardiac tissue lysate from STZ rats compared to controls that the TCA cycle was not changed but identified a shift towards fatty acid β-oxidation over glycolysis as a major source of energy. These changes were associated with a decrease in electron transport chain proteins. To our knowledge, there have been no proteomics analysis of the cardiac mitochondrial proteome in the early stage of type 2 diabetic cardiomyopathy. Around 46% of mitochondrial proteins may not be identified by MS due to the low abundance of mitochondrial proteins (Prokisch et al., 2004, Chaiyarit and Thongboonkerd, 2009). Therefore, rather than analyse the whole, the mitochondria were first isolated, as described in section 2.2. This Chapter reports the first large-scale protein profiling for cardiac mitochondrial proteins in the early stage of a mouse model of diabetic cardiomyopathy. Additionally, we have employed proteomics to investigate mitochondrial pathway alteration in our HFD (DIO) model. Moreover, we have used proteomics to study the reversible effects of an HFD (DIO) by 1) exercise alone, 2) diet exchange alone, and 3) combination of diet exchange and exercise.

6.2 Methods

Quantitative mass spectrometry was used to study cardiac mitochondrial proteins. Mitochondria were isolated from each group, as described in section 2.2.5. Sample preparation was conducted in the biological mass spectrometry facility at The University of Manchester. Sample processing was kindly performed by the facility team.

6.2.1 Sample lysis

An equal volume of 2x S-Trap lysis buffer (10% (w/v) SDS, 100 mM tetraethylammonium bromide "TEAB", PH = 7.5) was added to the mitochondrial isolate. The mixture was then added to the microTUBE AFA Fibre Pre-Slit Snap-Cap tube (Covaris). Covaris tubes were added to a steel rack (LE220_500282) and then placed in a LE220-plus focused ultrasonicator (Covaris) to lyse the samples by the following settings: Duration: 300 Sec, Peak power: 500, Duty factor: 40%, Cycles/Burst: 500 and AVG power: 200, and Sonolab 8.2 software.

6.2.2 Reduction and alkylation

A final concentration of 5 mM of dithiothreitol (DTT) was added to the lysates and the mixture was heated for 10 minutes at 60°C. Samples were then alkylated with 15 mM iodoacetamide (IAM) and incubated in the dark for 30 minutes at room temperature. The alkylation reaction was quenched by adding the same amount of DTT again. An Eppendorf 5430R centrifuge was used to spin the lysates at 14,000 rcf for 10 minutes. The supernatants were transferred to clean tubes.

6.2.3 Quantification of extracted proteins

Protein concentration was measured using a Direct Detect® Infrared Spectrometer. Two microliters of the pooled sample, which consisted of 2 µl of each sample combined, was loaded onto Millipore Direct Detect® Assay-free Cards (Merck). S-Trap buffer containing 10 mM DTT and 15 mM IAM was used as a blank.

6.2.4 S-Trap sample digestion

S-Trap digestion was used to digest proteins into peptides. A final concentration of 1.2% aqueous phosphoric acid was added to the lysates along with S-Trap binding buffer (100 mM Tetraethylammonium bicarbonate (TEAB), PH= 7.1, 90% (v/v) aqueous methanol). The solution was then added to S-Trap plate on top of a 96 well plate. The plate was then centrifuged at 1,500 rcf for 2 minutes using a Megafuge™ 16 centrifuge (ThermoFisher). The trapped proteins were then washed three times with S-Trap binding buffer with centrifugation at 1,500 rcf for 2 minutes. 125 microliters of digestion buffer (50 mM TEAB) containing 5

µg trypsin were added to the trapped proteins to digest them. The mixture was then placed in a thermomixer (Eppendorf) for 1 hour at 47°C. For elution, 80 µl of digestion buffer (50 mM TEAB) was added, followed by centrifugation at 1,500 rcf for 2 minutes. Further elution with 80 µl of 0.1% (v/v) aqueous formic acid was conducted, with centrifugation again at 1,500 rcf for 2 minutes. Last elution used 40 µl of 30% (v/v) aqueous acetonitrile containing 0.1% (v/v) formic acid and another centrifugation at 1,500 rcf for 2 minutes. All flow-through from elution steps was collected for further processing.

6.2.5 Sample desalting

Ten microliters POROS R3 beads were added to each well in a FiltrEX filter plate. Following this, the filter plate and the beads were washed with 200 µl of 0.1% (v/v) formic acid in acetonitrile, followed by centrifugation at 200 rcf for 1 minute (Thermo Megafuge). Then the beads were washed twice by 0.1% (v/v) formic acid in water. Samples were added to the wells, followed by incubation on the thermomixer (Eppendorf) at 800 rpm for 5 minutes. The plate was then centrifuged at 200 rcf for 1 minute. Next, the plate was washed twice with 200 µl of 0.1 formic acid, followed by centrifugation at 200 rcf for 1 minute. For elution, 50 µl of 0.1% (v/v) formic acid in 30% (v/v) acetonitrile was added and the solution incubated for 2 minutes on the thermomixer (Eppendorf) at 800 rpm, followed by centrifugation at 200 rcf for 1 minute. This step was repeated once and all flow-through was collected and transferred to LC-MS sample vials. Samples were then dried in a Heto vacuum centrifuge, and stored at 4°C.

6.2.6 Sample processing

Samples were loaded into liquid chromatography with tandem mass spectrometry (LC-MS/MS) (Q Exactive™ Hybrid Quadrupole-Orbitrap™ Mass Spectrometer, ThermoFisher) by members of staff at Bio-MS research core facility at The University of Manchester, prior to checking sufficient peptides number and a good sample quality. The analysis of the obtained MS data was performed using Progenesis QI (v3.0, Non-linear Dynamics). Resulting peak lists were searched against the Uniprot Mouse database (version 2018) by Mascot (version 2.4, Matrix Science). The results of included samples were then analysed using the Ingenuity Pathway Analysis (IPA) software (Qiagen) and STRING. Inclusion of a sample in the study required the identification of at least two unique peptides, based on previous published paper (Higdon and Kolker, 2007). In certain forms of IPA analysis, Z-score was used to predict upstream (positive values) or downstream (negative values)

processes. Z-score more than 2 or less than -2 and P value<0.05 were considered significant. Log_2 ratio was used to simplify the interpretation of the fold change.

6.3 Results

For a more comprehensive understanding of how mitochondria are impaired in the HFD (DIO) mice compared to control, we applied quantitative proteomics of isolated mitochondria, HFD (DIO) (n=5) and control (n=5). We identified a total of 1502 proteins in HFD (DIO) model, 75 (5%) proteins were significantly changed. Of these significantly changed proteins, 41 (54.7%) were upregulated, 34 (45.3%) were downregulated in HFD (DIO) compared to control (Figure 6.3A). Analysis of the proteins that were either up or downregulated by String showed that multiple pathways are potentially perturbed as shown in Figure 6.3B.

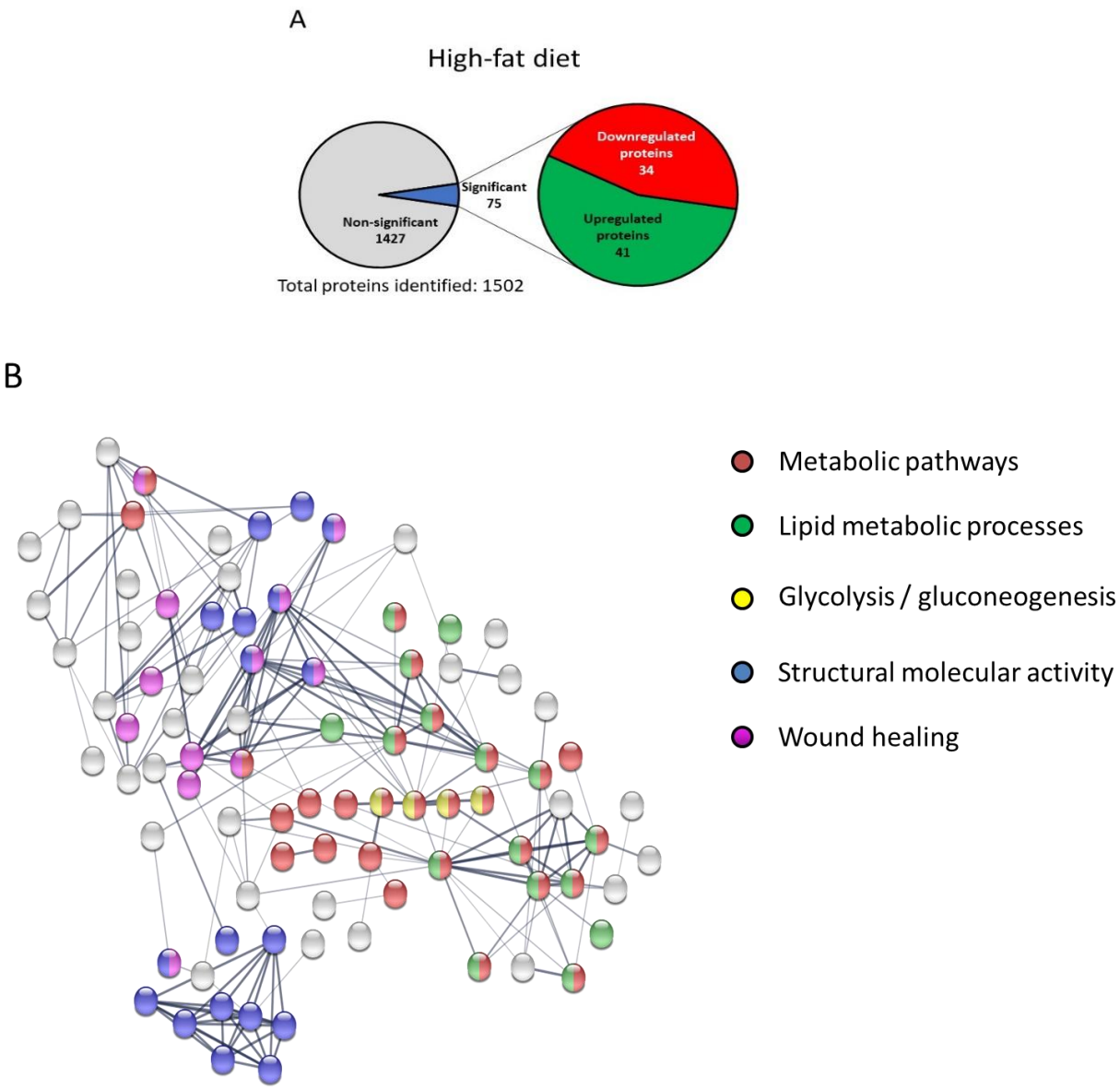

Figure 6.3: Percentage of upregulated and downregulated mitochondrial proteins in the high-fat diet mice and the mechanisms perturbed compared to control by mass spectrometry.
A. Pie chart showing that of the 1502 proteins identified, about 5% is significantly changed, with most proteins upregulated (≈55%). B. Significant altered proteins networks analysed by STRING network analysis.

6.3.1 Ingenuity Pathway Analysis of canonical pathways altered in the HFD (DIO) model

IPA analysis indicated that the significantly altered proteins in HFD (DIO) were involved in many canonical pathways and molecular function. Canonical pathways that have been changed in HFD (DIO) include acute phase response signalling, IL-7 signalling and GP6 signalling (Figure 6.4A); proteins in these pathways were all upregulated. The acute phase

response signalling was activated in HFD (DIO) model (Z-Score=2.236) with around 20% of total proteins in the pathway being upregulated. IPA analysis additionally revealed a significant alteration in two pathways of the interleukin family, IL-7 and IL-12 signalling, a group of cytokines in HFD (DIO) compared to control. On the other hand, proteins involved in apelin cardiomyocyte signalling were all downregulated. A combination between proteins upregulation and downregulation were found in IL-12 signalling, atherosclerosis signalling, production of ROS, ketogenesis and glucocorticoid receptor signalling pathways. Ketogenesis includes the D-β-hydroxybutyrate dehydrogenase (BDH1) protein which was upregulated and 3-hydroxy-3-methylglutaryl-CoA synthase 2 (HMGCS2) which was downregulated.

Significantly changed molecular functions in HFD (DIO) include cell death, lipid metabolism, energy production, carbohydrate metabolism, molecular transport, protein synthesis, amino acid metabolism and free radical scavenging, as summarised in Figure 6.4B, of which the most significantly changed function was cell death and survival, with more than 80% of proteins being upregulated. Most of these proteins were associated with apoptosis which may suggest an increase in cell death rate. These data are supported by our previous finding of increased apoptosis as assessed using the TUNEL assay (Section 2.3). Free radical scavenging showed 7 significantly downregulated proteins including UCP1, UCP3 and catalase. IPA analysis also indicated that the quantity of ROS is increased (Z-score = 2.14). The majority (≈75%) of carbohydrate metabolism proteins were downregulated in HFD (DIO). Most of these proteins were associated with the concentration of D-glucose. Our HFD (DIO) model was insulin resistant (section 2.3) which could explain these changes. Upstream regulator analysis in IPA can identify potential upstream regulators by the analysis of protein expression changes and showed that one of the inhibited upstream regulators in HFD (DIO) is PPARA (Z-score = -4.039).

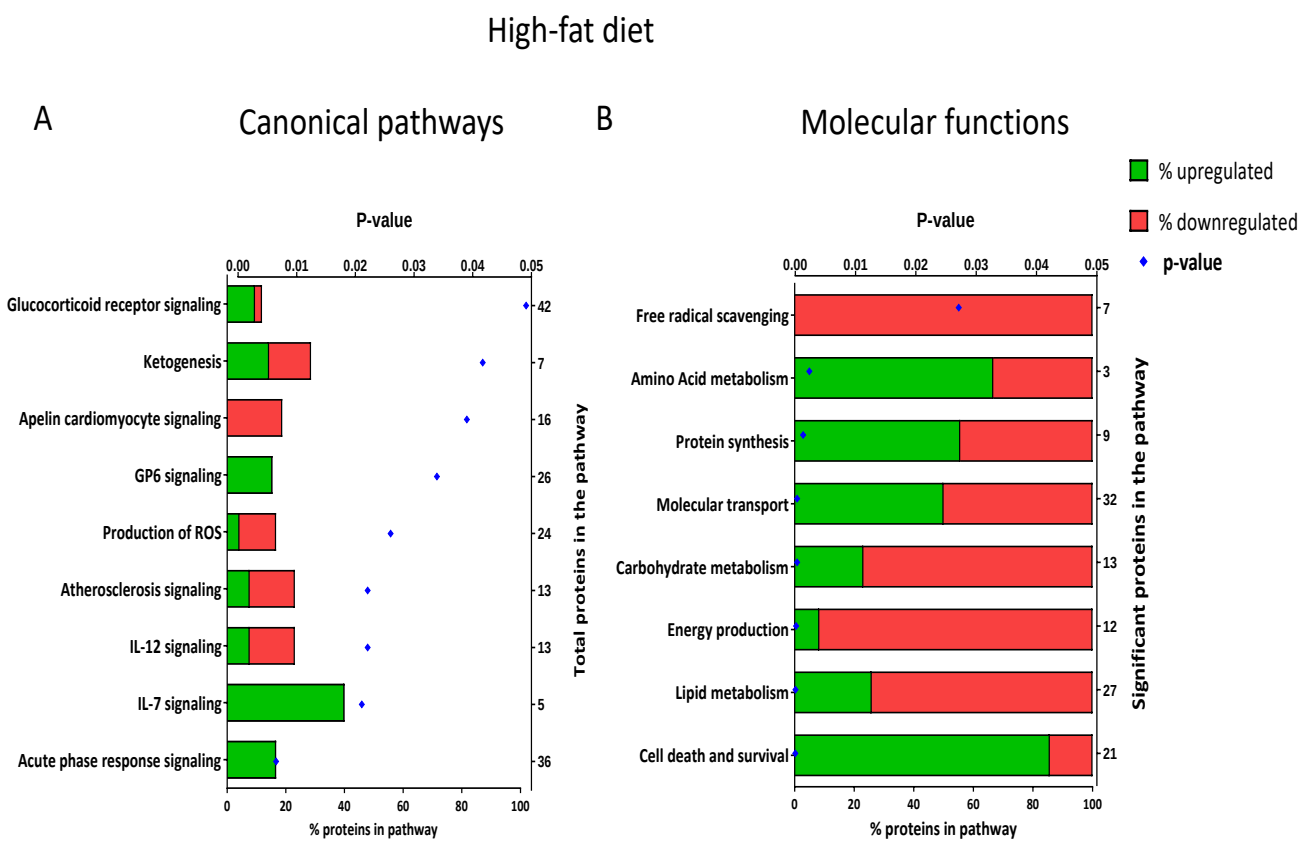

Figure 6.4: Alteration of canonical pathways in the high-fat diet (DIO) mice cardiac mitochondria using proteomic analysis.
A. Significant canonical pathways altered in HFD (DIO) compared to control. Total protein number in each pathway is shown on the right-hand y-axis. B. Significant molecular functions altered in HFD (DIO) compared to control. The significant protein number in each pathway is shown on the right-hand y-axis. The bars in both A and B illustrate the protein percentage within each pathway that are upregulated (green) or downregulated (red). Pathways were listed by highest to lowest P value (top x-axis).

6.3.2 Ingenuity Pathway Analysis of canonical pathways altered in the exercise model

To build upon the data in Chapter 4 quantitative proteomics of isolated mitochondria was conducted in control (n=4), exercise (n=5), diet exchange (n=5) and exercise/diet exchange (n=4). A total of 1706 proteins were identified in the exercise group, with 122 (7.2%) proteins significantly changed. Interestingly, the majority of proteins (111 proteins, 91%) were downregulated and only 11 (9%) proteins were upregulated in the exercise group compared to control. In the diet exchange group, we identified a total of 1709 proteins and 81 (4.7%) proteins were significantly changed; 48 (59.3%) proteins were upregulated, and 33 (40.7%) proteins were downregulated in diet exchange group compared to control. The total number of proteins identified in the exercise/diet exchange group were 1704; 118 (6.9%) proteins were significantly changed, and 86 (72.9%) proteins were upregulated, and 32 (27.1%) proteins were downregulated compared to control. Interestingly, lipid metabolism pathways were not affected in the exercise/diet exchange group. String analysis in Figure

6.5B, D and F show the functionally associated networks between significantly changed proteins in all groups. Most of the altered proteins in both exercise groups (exercise and exercise/diet exchange) were associated with cardiac muscle development and actin-filament-based processes.

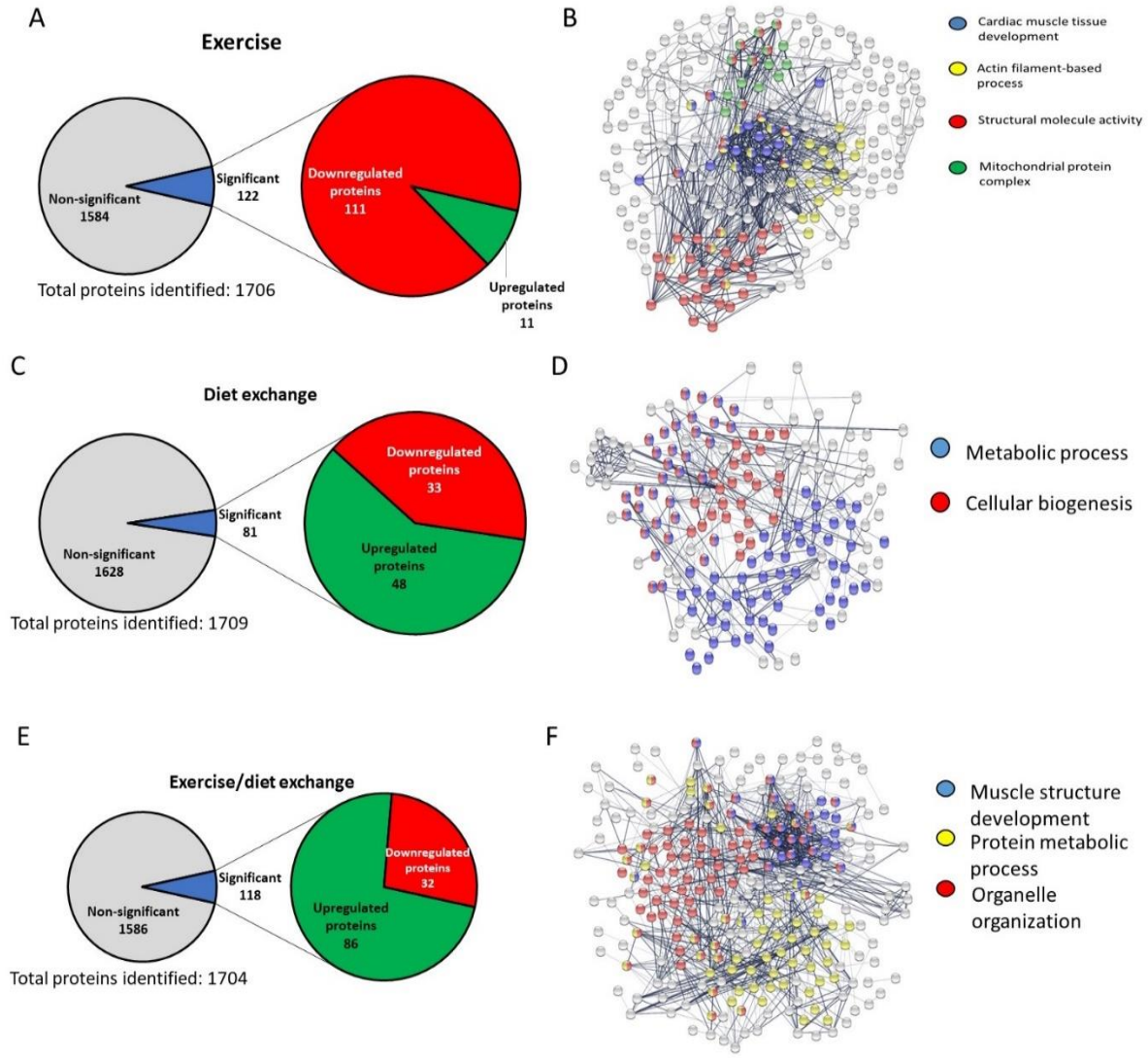

Figure 6.5: Mass spectrometry analysis of exercise, diet exchange and exercise/diet exchange groups compared to control.
A. Pie chart showing that 7% of total proteins identified in the exercise group were altered, with the majority being downregulated (≈91%). B. STRING analysis of exercise group. C. Eighty one out of 1709 proteins were significantly changed in the diet exchange group and are mostly upregulated. D. Diet exchange group STRING network analysis. E. Seven per cent of exercise/diet exchange group proteins identified were significantly altered, with an increase to the vast majority proteins. F. STRING network analysis in exercise/diet exchange group.

The reversible effect of exercise, diet exchange and exercise/diet exchange groups in pathways were additionally assessed using IPA analysis, Control (n=4), exercise (n=5), diet exchange (n=5), exercise/diet exchange (n=4). The analysis showed a significant alteration in

the GP6 signalling pathway in the exercise group with downregulation of all proteins (Figure 6.6A). Changed proteins were either collagen (COL15A1, COL1A1, COL1A2, COL3A1, COL4A2, COL6A1, COL6A2, COL6A3) or laminin (LAMA2, LAMA5, LAMB1, LAMB2, LAMC1). The second most impacted canonical pathway is calcium signalling with proteins being downregulated being either actin (ACTA1, ACTA2), myosin (MYH6, MYH13, MYL2, MYL3, MYL4) or troponin (TNNC1, TNNI3, TNNT2). One of the categories of cellular development (Figure 6.6B) affected were differentiation of muscle cells which were significantly decreased (Z-score = -2.382). All proteins identified in the differentiation of muscle cells were downregulated in the exercise group (DES, LAMA2, LAMC1, LMNA, MYL2, NPPA and TTN).

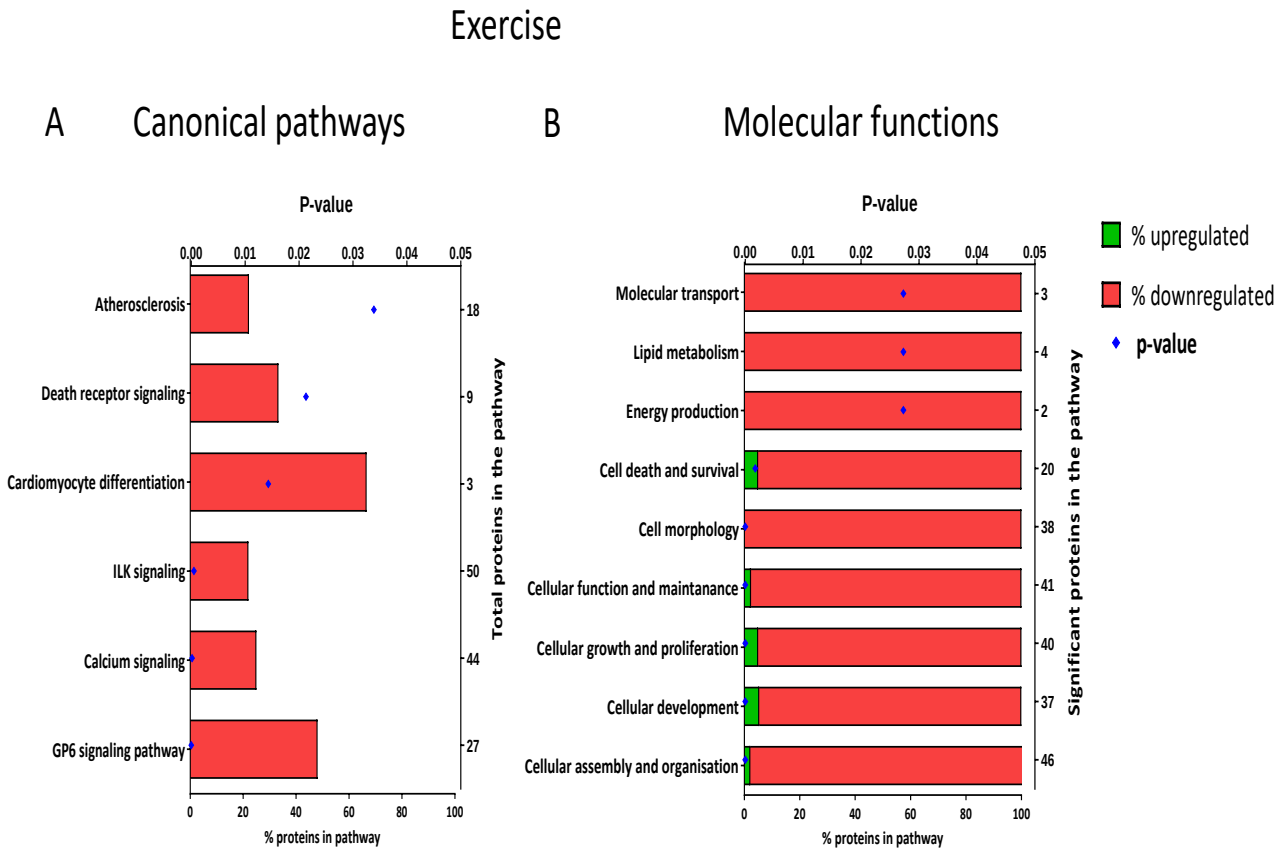

Figure 6.6: Down regulation of proteins involved in the most common altered canonical pathways in the cardiac mitochondria of the exercise group.
A. Significant canonical pathways altered in the exercise group compared to control. Total protein number in each pathway is shown on the right-hand y-axis. B. Significant molecular functions altered in exercise compared to control. The protein number affected in each pathway is shown on the right-hand y-axis. The bars in both A and B illustrate the protein percentage within each pathway are displayed in green (upregulated) or red (downregulated). Pathways were listed by the least to most significant "lowest P value" (top x-axis).

6.3.3 Ingenuity Pathway Analysis of canonical pathways altered in the diet exchange model

The changed canonical pathways in diet exchange group are summarized in Figure 6.7A; pathways identified with proteins being downregulated were IL-7, EGF, IL17A and FGF signalling. Interestingly, free radical scavenging was altered in the diet exchange group (Figure 6.7B) with the majority of proteins being upregulated (CA3, DPP4, FCGRT, MGST3, TXN, UCP1) with the downregulation of only one protein (exog) suggestive of increased antioxidant mechanisms. The quantity of ROS is predicted by IPA to be decreased (Z-score= -1.016). IPA analysis revealed the cell death in the diet exchange group was decreased (Z-score= -1.4). Although lipid and carbohydrate metabolism were significantly altered, as shown in Figure 6.7B, none of the proteins were associated with either β-oxidation of fatty acid or glycolysis/gluconeogenesis.

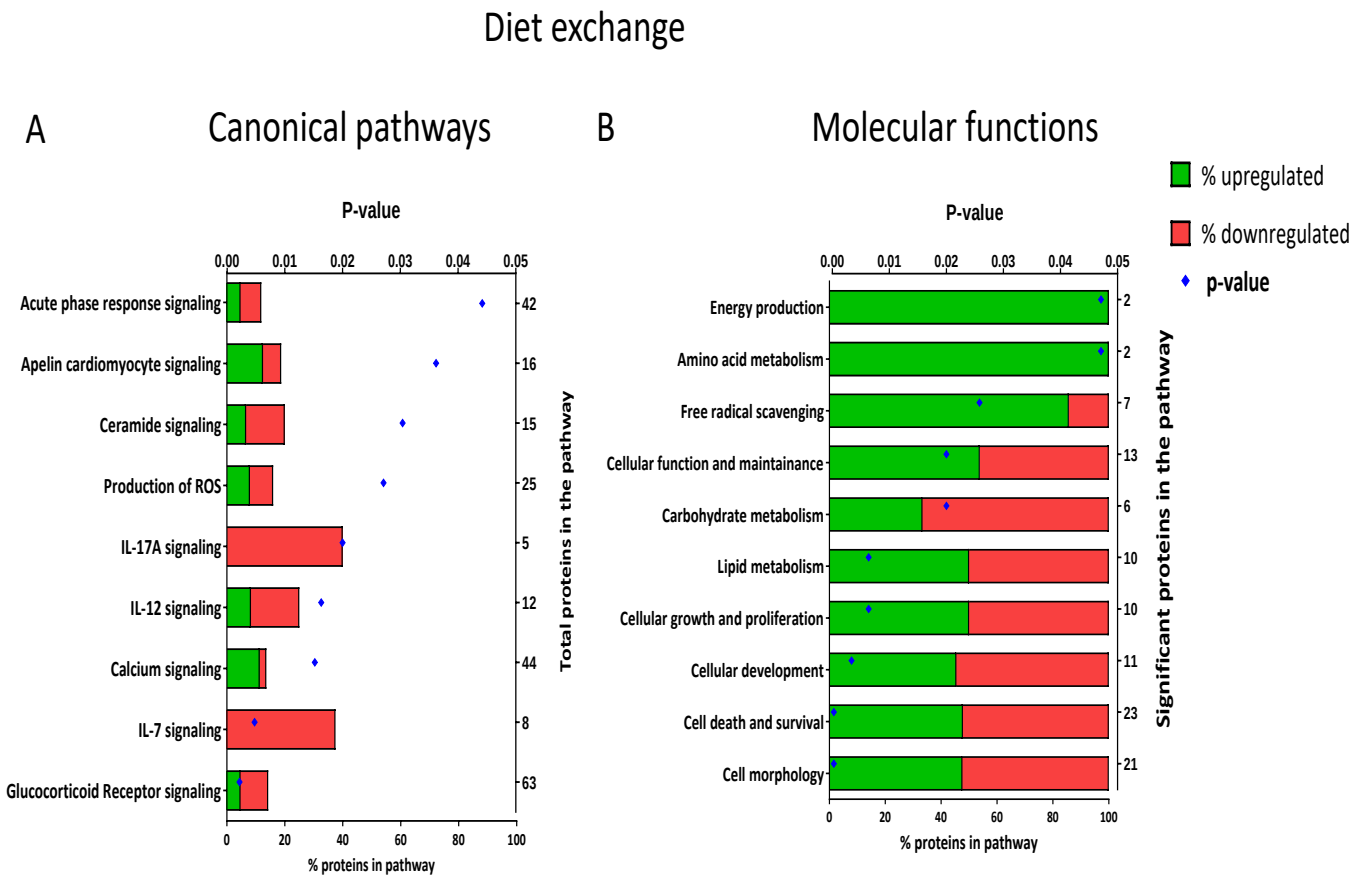

Figure 6.7: Alteration of canonical pathways in the cardiac mitochondria of diet exchange group.

A. Canonical pathways significantly altered in diet exchange group than that of control. The right-hand y-axis shows the total proteins number in each pathway. B. Molecular functions of proteins significantly changed in diet exchange group compared to control. The number of significant proteins in each pathway is shown on the y-axis (right-hand). The bars in both A and B represents the proteins percentage within each pathway that are green (upregulated) or red (downregulated). Pathways were ordered by P value "highest to lowest" (top x-axis).

6.3.4 Ingenuity Pathway Analysis of canonical pathways altered in the exercise/diet exchange model

Canonical pathways that have been changed in the exercise/diet exchange group are summarised in Figure 6.8A. Muscle contraction proteins in calcium signalling pathway were upregulated including actin (ACTA1, ACTA2) myosin (MYH6, MYH13, MYL2, MYL3, MYL4, MYL7) and troponin (TNNC1, TNNI3, TNNT2, TPM1). The GP6 signalling pathway was activated (Z-score=2.236); all proteins in the pathway affected were collagen types and were upregulated (COL1A2, COL3A1, COL6A1, COL6A2, COL6A3). The majority of apelin cardiomyocyte signalling pathway proteins were upregulated (MYL2, MYL3, MYL4, MYL7). All the changed proteins in cardiomyocyte differentiation were upregulated (MYL2, NPPA). In addition, the death receptor signalling proteins were all upregulated (ACTA1, ACTA2, and LMNA). Most of the proteins in cell death and survival were upregulated (LMNB1, LMNB2, LMNA, MYH6, DES, SAA1, TF, and OBSCN). Figure 6B summarises the molecular functions with proteins that are either up or downregulated.

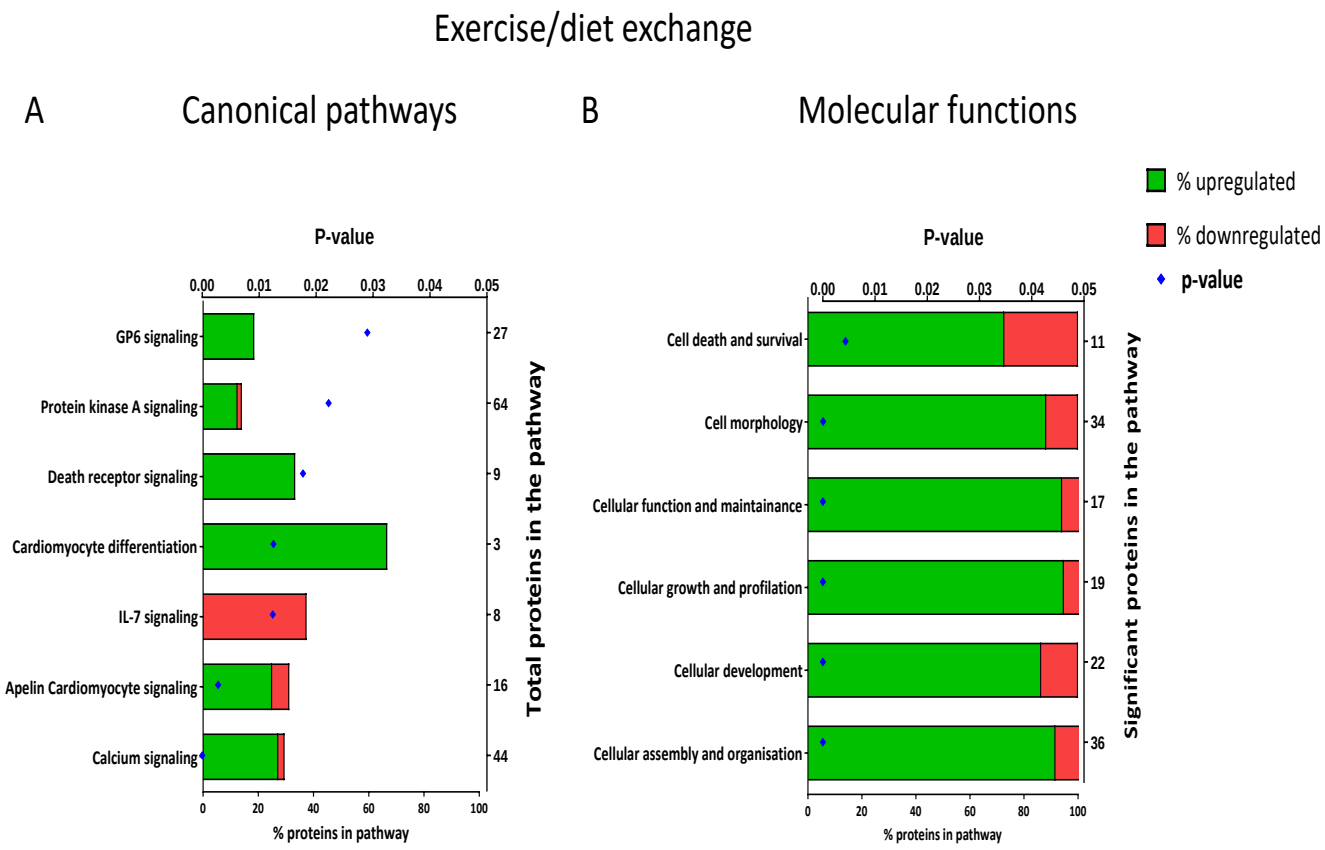

Figure 6.8: Alteration of canonical pathways in the cardiac mitochondria of exercise/diet exchange group.

A. Significant alteration of canonical pathways in the exercise/diet exchange group compared to control. The y-axis on the right hand illustrates the number of the total proteins in each pathway. B. Molecular functions of proteins significantly changed in the exercise/diet exchange group compared to control. The number of proteins in each pathway is shown on the right hand of the y-axis. The bars in both A and B represents the protein percentage within each pathway that are affected displayed as either green (upregulated) or red (downregulated). Pathways were sorted by the P value "highest to lowest" (top x-axis).

6.3.5 Proteomic analysis of metabolism

This comprehensive, unfocused screen has provided new details about the specific pathways affected under each condition and how they connect. Since the proteomics identified in the HFD (DIO) that there was alteration of the metabolism's pathways (Carbohydrate, Lipid and amino acid) and energy production, therefore we next examined these pathways, including glycolysis, TCA cycle, β-oxidation of fatty acid and oxidative phosphorylation, in each of the models. Log_2 fold change and P value of proteins in each pathway were displayed as a heat map. Proteins forming each pathway were obtained from the KEGG pathway database. Figure 6.9 illustrates the glycolysis pathway showing that Aldolase B was significantly upregulated which plays a major role in glycolysis/gluconeogenesis and is encoded by ALDOB in the HF feeding model. Aldolase B catalyses the reversible metabolism of fructose-1-phosphate to glyceraldehyde and dihydroxyacetone phosphate. A pattern of decreased expression of glycolysis proteins in exercise group is noted.

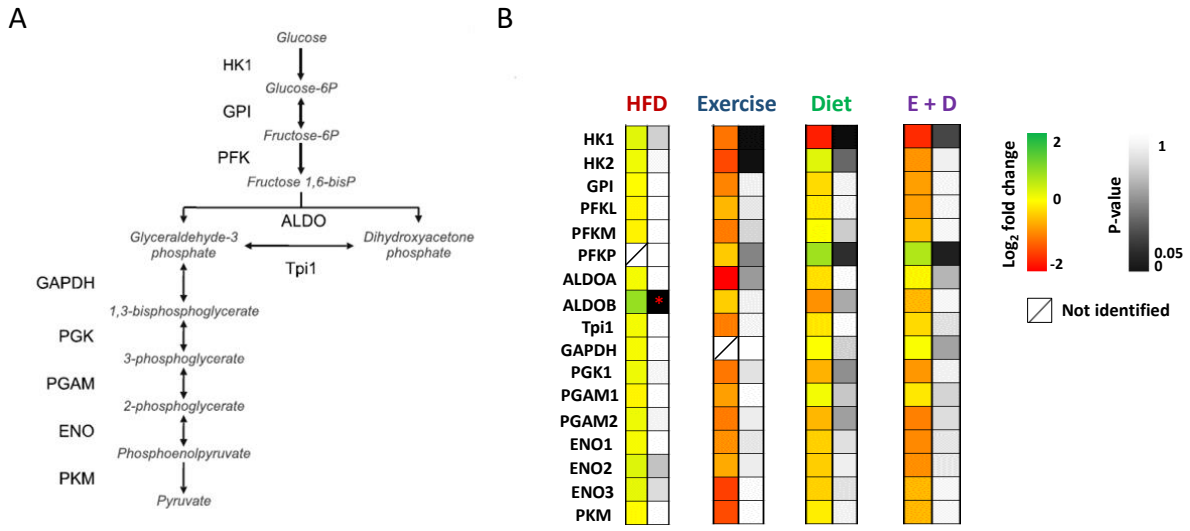

Figure 6.9: Upregulation of glycolysis in the high-fat diet mice, but not in the exercise, diet exchange and exercise/diet exchange mice.

A. The glycolysis pathway showing the conversion of glucose to pyruvate. Unidirectional arrows indicate irreversible reactions, while bidirectional arrows represent the reversible reactions. B. Glycolysis pathway proteins that were quantified in each of the four groups – high-fat diet (n=5), exercise (n=5), diet exchange (n=5) and exercise/diet exchange (E + D) (n=4) are presented. Log_2 fold change of proteins were represented by colour scale from green (+2) to red (-2). The significance was presented by colour scale from 1 (white) to 0.05 (black). Significant changes (P value<0.05) in proteins were marked by red asterisk.

The TCA cycle is illustrated in Figure 6.10A with panel B showing that none of the proteins involved in the TCA cycle were significantly changed. However, there was a significant decrease in PDK4 and PDK3 in HFD (DIO) compared to control. Pyruvate dehydrogenase

kinase (PDK) an enzyme inhibits pyruvate dehydrogenase (PDH). Interestingly, PDK3 and PDK4 were no longer significantly changed in exercise, diet exchange and exercise/diet exchange groups. A pattern of decreased expression of proteins in the TCA cycle in exercise groups is noticed.

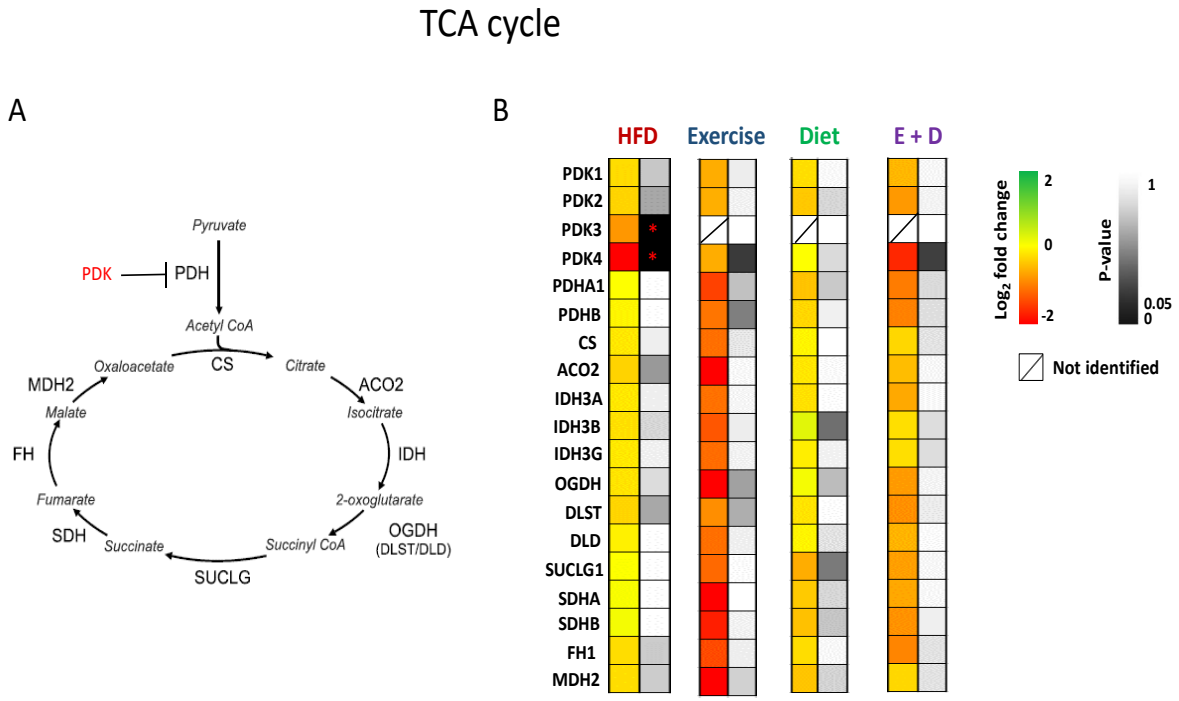

Figure 6.10: Down-regulation of PDK in the high-fat diet (DIO) mice.
A. A series of chemical reactions in the tricarboxylic acid cycle (TCA). Pyruvate dehydrogenase kinase (PDK) is an inhibitory enzyme (in red colour). B. TCA pathways proteins that were quantified in each of the four groups – high-fat diet (n=5), exercise (n=5), diet exchange (n=5) and exercise/diet exchange (E + D) (n=4) are presented. The left-coloured box of each group is a colour scale from +2 (green) to -2 (red) were represented of the Log_2 fold change of each protein identified. The right coloured box is representative of P value from 1 (white) to 0.05 (black). Significant P value <0.05 were marked by red asterisk.

The fatty acid beta-oxidation pathway proteins were investigated in detail, as shown in Figure 6.11. There was a significant decrease in ACOX1, a protein in the beta-oxidation of fatty acid pathway in the HFD (DIO) model (P value=0.004). A pattern of a decrease in fold change with no significant changes in the exercise group. Proteins' expression returned to the normal level in diet exchange and exercise/diet exchange groups.

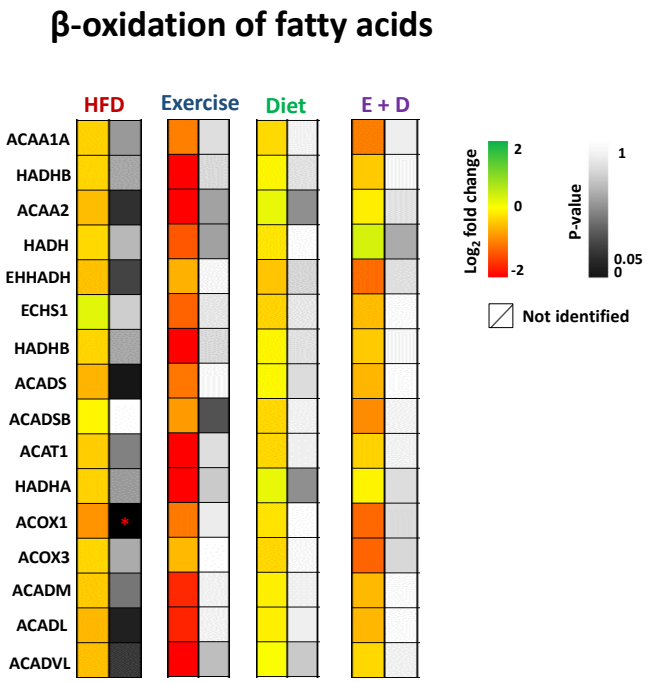

Figure 6.11: Decrease expression of ACOX1 in the high fat diet (DIO) model.
β-oxidation of fatty acid proteins that were quantified in each of the four groups – high-fat diet (DIO) (n=5), exercise (n=5), diet exchange (n=5) and exercise/diet exchange (E + D) (n=4) are presented. A heat map for Log_2 fold change of the protein expression represented by green (2), yellow (0) and red (-2). Two colour scale black and white represent the P value. Significant P value <0.05 were marked by red asterisk.

Additionally, IPA analysis showed that β-oxidation of fatty acid in 12-weeks HFD (DIO) was significantly decreased (P value=0.004, Z-score = -2.1) with identifying proteins linked to the pathway; 5 proteins significantly decreased (ABCD3, ACOX1, HMGCS2, LONP2, PLIN5) and only 1 protein significantly increased (HSD11B1). Two of the downregulated proteins (HMGCS2 and PLIN5) were still downregulated in the exercise group with other proteins returned to the normal level. Interestingly, all these proteins return to normal level in diet exchange and exercise/diet exchange group. Figure 6.12 shows proteins associated with electron transport chains. In the electron transport chain, there are five complexes, with the first 4 (I-IV) electrons are passed from electron donor to electron acceptors. The electrochemical gradient is utilized by Complex V to produce ATP. We identified 53 proteins from all complexes in the HFD (DIO) (Figure 6.12). None of the proteins were significantly changed in any of the groups with no notable changes in the expression as illustrated by the heat map (Figure 6.12). Although there were no significant protein changes in the exercise group, a pattern of decreased proteins expression is noticed. This pattern returns partially to

normal in the diet exchange and exercise/diet exchange groups. Unexpectedly, there was a significant decrease in COX6A2 and COX7C located in Complex IV and a significant increase in ATP6 located in Complex V.

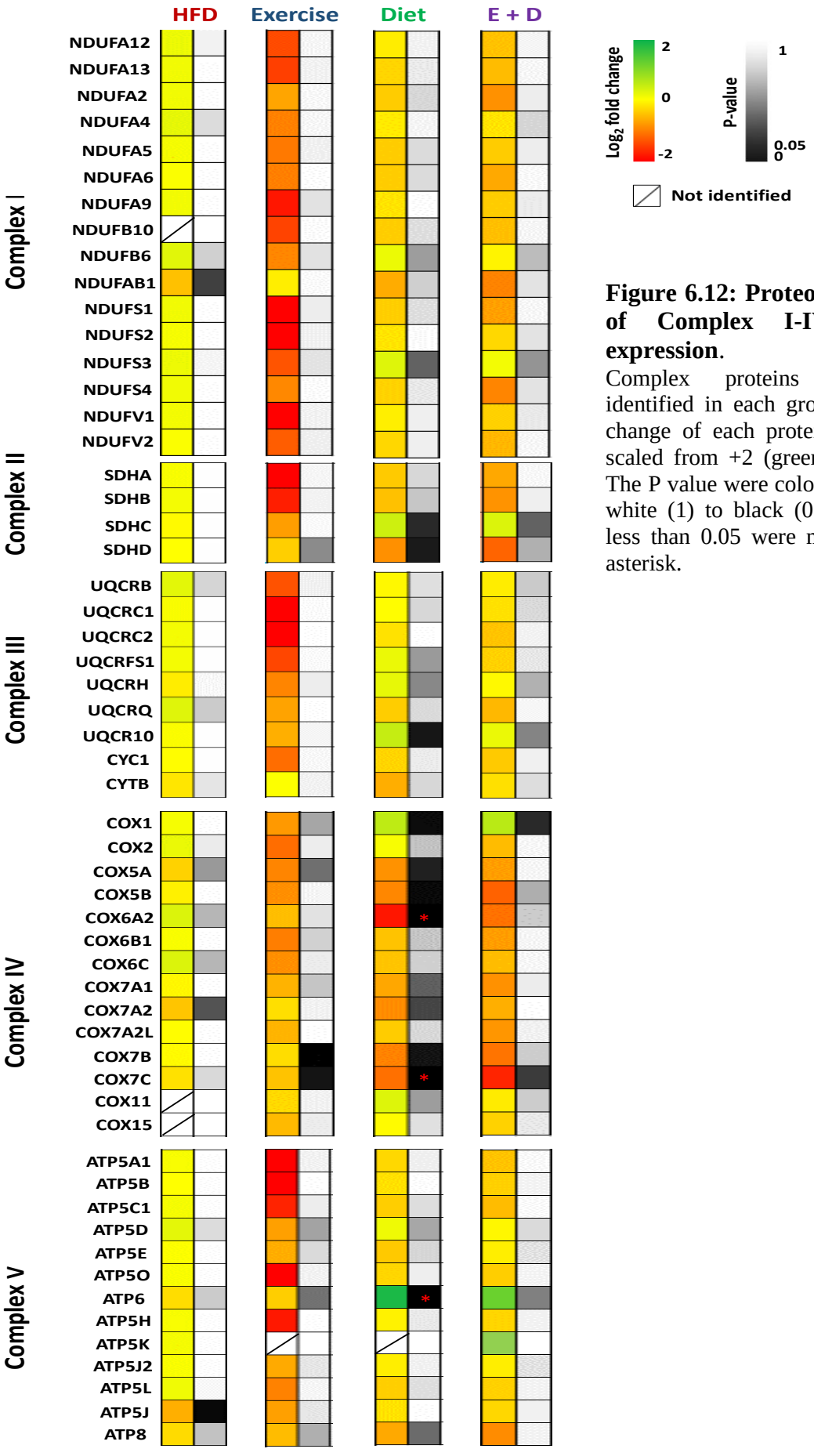

Figure 6.12: Proteomic analysis of Complex I-IV proteins expression.

Complex proteins that were identified in each group. Log_2 fold change of each protein was colour scaled from +2 (green) to -2 (red). The P value were colour scaled from white (1) to black (0.05). P values less than 0.05 were marked by red asterisk.

6.3.6 Quantitative mass spectrometry of mitochondrial dynamic proteins

Table 6.1 presents the proteomic analysis of mitochondrial dynamic proteins. In contrary to Western blotting data in Chapter 2, the fission protein Drp1 and receptor Mff showed no significant changes in HFD (DIO) and exercise groups compared to control. Other mitochondrial fission and fusion proteins in HFD (DIO) and exercise groups agreed with the Western blotting data. All mitochondrial fission and fusion proteins in diet exchange and exercise/diet exchange are consistent with earlier results with no changes. Proteins associated with mitochondrial motility were not significantly changed in all groups. Unlike qPCR results, Sirt5 showed no significant difference in HFD (DIO) compared to control. Interestingly, Sirt5 was trending down (P value= 0.056, Log_2 fold change = -1.1) in the diet exchange group with unchanged levels in other groups.

Table 6.1: Quantitative analysis of mitochondrial dynamic proteins expression changes in HFD (DIO) group, exercise, diet exchange and exercise/diet exchange groups.

Role	Protein	HFD (Log_2 fold change, P value)	Exercise (Log_2 fold change, P value)	Diet exchange (Log_2 fold change, P value)	E+D (Log_2 fold change, P value)
Fusion	Mfn1	(0.1, 0.9)	(-0.88, 0.9)	(-0.29, 0.9)	(-0.63, 0.9)
	Mfn2	(-0.04, 0.9)	(-0.77, 0.9)	(-0.25, 0.9)	(-0.65, 0.9)
	Opa1	(0.07, 0.9)	(-3.31, 0.9)	(-0.03, 0.8)	(-0.49, 0.9)
Fission	Drp1	(-0.03, 0.9)	(-0.48, 0.7)	(-0.88, 0.2)	(-1.04, 0.8)
	Fis1	(0.03, 0.9)	(-0.78, 0.9)	(-0.83, 0.1)	(-1.04, 0.8)
	Mff	(0.05, 0.9)	(-0.56, 0.9)	(0.04, 0.8)	(-0.25, 0.9)
Motility	Miro1	(-0.04, 0.9)	(-0.88, 0.9)	(-0.36, 0.8)	(-0.85, 0.9)
	Miro2	(-0.18, 0.9)	(-0.77, 0.9)	(-0.11, 0.9)	(-0.44, 0.9)
	KIF5B	(-0.03, 0.9)	(-0.65, 0.9)	(-0.21, 0.9)	(-0.53, 0.9)
	TRAK1	(-0.01, 0.9)	(-0.42, 0.6)	(-0.24, 0.9)	(-0.97, 0.8)
Sirtuins	Sirt5	(-0.1, 0.9)	(-0.74, 0.9)	(-1.1, 0.056)	(-1.33, 0.6)

6.3.7 Summary of results

Global protein study for cardiac mitochondrial pathways in HFD (DIO) model along with exercise and/or diet exchange trials has been studied in this Chapter using LC-MS/MS. The key findings of this chapter were:

- There is a perturbed inflammatory pathway in HFD (DIO) model.
- A decrease in oxidative stress defence network proteins in HFD (DIO) which return to basal levels in all exercise and/or diet exchange experimental groups.
- There is alteration to cardiac contraction signalling in HFD (DIO) model.
- In the HFD (DIO) myocardium there is a shift of the main source of energy from β-oxidation of fatty acids to glycolysis.
- One of the main inhibited upstream regulators in HFD (DIO) is Peroxisome proliferator-activated receptor alpha (PPARA).
- Many of the proteins associated with oxidative stress defence network returned to basal levels in all exercise and/or diet exchange experimental groups.
- The upstream regulator PPARA returned to control levels in exercise and exercise/diet exchange groups, and was activated in diet exchange group.

A summary of mitochondrial fission/fusion proteins changes in all mice groups studied are shown in Table 6.2.

Table 6.2: Summary of mitochondrial dynamic proteins expression in the HFD (DIO), Exercise, diet exchange and exercise and diet exchange mice models.
NS, non-significant, *P≤0.05, **P≤0.01, ***P≤0.001, ****P≤0.0001

Protein	HFD	Exercise	Diet exchange	Exercise + diet exchange
Mfn1	NS	NS	NS	NS
Mfn2	NS	↑*	NS	NS
Total Opa1	NS	NS	NS	NS
S-Opa1	NS	NS	NS	NS
L-Opa1	NS	NS	NS	NS
Total Drp1	↑**	NS	NS	NS
P-Drp1(Ser637)/total Drp1	↓*	NS	NS	NS
P-Drp1(Ser616)/total Drp1	NS	NS	NS	NS
Fis1	↑*	NS	NS	NS
MID49	↑**	NS	↑****	↑****
MID51	NS	NS	NS	NS
Mff	↓***	↓**	NS	NS
PINK1	↑***	↑***	NS	NS
Parkin	↑*	NS	NS	NS

6.4 Discussion

6.4.1 Activation of inflammatory signalling in HFD (DIO) model

An activation of acute-phase response signalling in HFD (DIO) suggests an early inflammatory response (Baumann and Gauldie, 1994). The acute phase response leads to release of inflammatory cytokines. More commonly studied interleukins in diabetic cardiomyopathy e.g. IL-1B, IL-18, IL-6 and TNF-alpha were not detected (Westermann et al., 2007). IL-7 and IL-12 signalling networks were also altered. Both cytokines (IL-7 and IL-12) have an anti-inflammatory response (Willis et al., 2012, Chang and Radbruch, 2007). While most IL-12 signalling proteins were downregulated. All those changed in the IL-7 pathway were upregulated including immunoglobulin heavy constant gamma 2B and immunoglobulin heavy constant gamma 2C. According to these data, we can infer that inflammation is activated in our HFD (DIO) model. IL-7 expression has been previously reported to be increased in the adipose tissue of obese individuals (Maury et al., 2007). Lucas et al. (2012) demonstrated that IL-7 could contribute to the progression of metabolic pathologies by the modulation of adipose tissue, with impaired insulin sensitivity in IL-7 overexpressed transgenic C57BL/6J mice. IL-12 has been reported to be increased in cardiovascular diseases including coronary artery disease, atrial fibrillation, cardiac ischemia-reperfusion injury and autoimmune cardiomyopathy as recently reviewed by Ye et al. (2020). One study has reported that lowering IL-12 activity improves cardiac function in psoriasis patients (Ikonomidis et al., 2017). Here we determined that the IL-12 signalling pathway was not altered in exercise and exercise/diet exchange group but was affected in the diet exchange group (majority being downregulated). Interestingly, proteins in IL-7 signalling in diet exchange and exercise/diet exchange groups were downregulated (40% of total proteins in the pathway) whereas there was no change to the pathway in the exercise group. The role of IL-7 and IL-12 in developing diabetic cardiomyopathy in the myocardium is not currently understood; the data here indicate that future work may be warranted.

6.4.2 Increased oxidative stress in HFD (DIO) model by quantitative mass spectrometry analysis

Proteins associated with the oxidative stress defence network were downregulated in the 12-week HFD (DIO) model. For example, catalase is an antioxidant enzyme that protects the cell from oxidative stress by decomposition of hydrogen peroxide. In a cardiac-specific catalase overexpressing mouse model, there was a decrease in ROS associated with prevention of pathological abnormalities (Cong et al., 2015). Cong and colleagues showed that the suppression of inflammatory responses by catalase protected the heart of mice from DCM.

Interestingly, levels of catalase returned to normal levels in exercise, diet exchange and exercise/diet exchange groups consistent with lifestyle changes leading to reduced body mass and hyperglycaemia being beneficial.

Uncoupling proteins (UCPs) play a major role in limiting ROS production, as reviewed by Mailloux and Harper (2011). Further, Jastroch (2017) found a significant reduction of ROS production in the brown fat mitochondrial inner membrane by UCP1 activity. UCP1 and UCP3 were identified in our proteomic analysis showing a significant downregulation in HFD (DIO) by log_2 fold change -4.5 and -1, respectively. In the exercise group, UCP1 remained downregulated, unlike UCP3, which showed no change. Interestingly, in the diet exchange group, UCP1 was upregulated (Log_2 fold change = 1.32) but the level of UCP3 was not affected. The exercise/diet exchange group showed no differences in both UCPs. Increased levels of mitochondrial uncoupling proteins (UCPs) have been reported to be linked to increased free fatty acid levels (Murray et al., 2008). Apolipoprotein E and apolipoprotein A4 which were involved in multiple pathways in HFD (DIO) were both significantly downregulated. They have roles in atherosclerosis and production of ROS. A study used apolipoprotein E knockout mice found an increase levels of oxidized LDL (Kato et al., 2009). Apolipoprotein A4 shows anti-atherogenic and antioxidant properties. Both these proteins returned to control levels in exercise, diet exchange and exercise/diet exchange groups. Oxidative modification of LDL by reactive oxygen species produces oxidized LDL which is widely studied as a potential risk factor for cardiovascular disease due to its association with the progression of atherosclerosis (Stocker and Keaney, 2004). Seven proteins were significantly downregulated in free radical scavenging which also suggest an increase in ROS production.

Although obesity/T2DM is linked to oxidative stress, most antioxidant proteins were downregulated. It was reported in the early stage of obesity there was an increase in antioxidants which decreased after fat accumulation (Alcala et al., 2015, Alcala et al., 2017, Alcala et al., 2018). This could be explained by the imbalance of free radicals and antioxidants which could lead to cell death. Twenty-one proteins were significantly changed in the cell death pathway in the HFD (DIO) with more than 80% being upregulated. This is further supported by our previous finding illustrated an increase in apoptosis by the TUNEL assay in HFD (DIO) (see section 2.3). Interestingly, level of antioxidants returned to normal after exercise, diet exchange and exercise/diet exchange.

6.4.3 Proteomics revealed alteration to cardiac contraction signalling in HFD (DIO) model

Apelin is one of the regulators of cardiac contractility (Szokodi et al., 2002). Apelin cardiomyocyte signalling is altered in HFD (DIO), with all proteins downregulated including myosin light chain 4 and 7 (MYL4 and MYL7); both MYL4 and MYL7 have been reported to improve contractile parameters in the heart (Abdelaziz et al., 2004, Grimm et al., 2005). Peng et al. (2017) reported that MYL4 knockout mice developed atrial cardiomyopathy. Other cardiac muscle contraction proteins identified in this proteomics analysis include both isoforms of myosin heavy chains (MYH6 and MYH7); with unchanged level of MYH6 and downregulation of MYH7 in the HFD (DIO) model (Warkman et al., 2012). This finding is contrary to that of Nakao et al. (1997) who found a decrease in MYH6 mRNA expression in end-stage heart failure. This contradictory result is likely to be related to the different stage of heart failure.

Although some contractile proteins were downregulated, ejection fraction was within normal parameters in our HFD (DIO) model (Section 2.3), therefore one explanation may be that the changes are linked to diastolic dysfunction. Liu et al. (1997) found a decrease in the total myosin light chain (40-45%) in the diabetic rat heart. However, the authors did not quantify the different isoforms of myosin light chain. In general, there have been few studies been published about myosin light and heavy chains in the heart tissue in diabetic cardiomyopathy and therefore the data here provides new information as to how contractile dysfunction may develop in response to a high-fat diet.

MYL7 and MYH7 returned to normal levels in the exercise group but not MYL4 which was still significantly downregulated. The downregulation in MYL4 alone might not cause any cardiac dysfunction, supported by normal function earlier (Section 3.3), but can cause dysfunction with additional stress i.e. bacterial infection, psychological stress, etc. Interestingly, MYL4 and MYL7 were both significantly upregulated in diet exchange group and exercise/diet exchange group with restoration of MYH7 normal level which suggests improvement in cardiac contractility function. This support previous results of normal diastolic function seen in diet exchange and exercise/diet exchange group (Section 3.3).

6.4.4 Proteomics analysis shows changes to energy production pathways in HFD (DIO)

One of the major enzymes in regulating glycolysis and gluconeogenesis is ALDOB (aldolase B) which was significantly upregulated in HFD (DIO). Aldolase B is responsible for the metabolism of fructose. It is involved in the reversible break down of fructose 1,6-

bisphosphate into glyceraldehyde 3-phosphate and dihydroxyacetone phosphate. An alteration in its expression can indicate an effect on its catalytic activity in the metabolism of glucose.

Pyruvate dehydrogenase kinase has 4 isoforms which are encoded by PDK1, PDK2, PDK3 and PDK4. PDK4, inhibits pyruvate dehydrogenase, and was downregulated in the HFD (DIO) model. This suggests increased generation of acetyl CoA from pyruvate produced by glycolysis and a decrease of fatty acid β-oxidation. Park et al. (2013) found an increase in pyruvate dehydrogenase complex activity in Sirt5 knockdown human embryonic kidney (HEK) cells. The authors also demonstrated that Sirt5 inhibits pyruvate dehydrogenase complex by desuccinylation of multiple subunits of the complex. Our finding of decrease Sirt5 mRNA level in the HFD (DIO) model support the idea of increasing the activity of pyruvate dehydrogenase.

To further support this concept, β-oxidation of fatty acid was decreased in HFD (DIO) (P value = 0.004, Z-score= -2.1). Five proteins in the pathway were downregulated (ABCD3, ACOX1, HMGCS2, LONP2, and PLIN5) . Two of these proteins remained downregulated in the exercise group (HMGCS2 and PLIN5). Interestingly, all the changes in proteins associated with β-oxidation of fatty acid seen in HFD (DIO) return to normal level in diet exchange and exercise/diet exchange groups.

Normally, 60-80% of the heart's ATP is generated by mitochondrial fatty acid oxidation. The rest comes from carbohydrates (glucose and lactate) and to a lesser extent from the oxidation of the ketone body (Aubert et al., 2013). The heart functions optimally when it oxidizes glucose and fatty acid at the same time (Taegtmeyer, 2000). The myocardial energy supply in heart failure switches from fatty acids to glucose (Razeghi et al., 2001b). The shift of substrate preference in the failing heart from fatty acids towards glucose metabolism has been reported to protect against further deterioration and enhance contractile function (Stanley et al., 2005). However, cardiac diabetics cannot make full use of glucose due to insulin resistance and may have to increase the usage of fatty acids as a source of energy (Boudina and Abel, 2007). Our data suggest an increase in glycolysis which could be explained by the mild insulin resistance in our model. Uncontrolled diabetes will lead to deterioration of insulin sensitivity which could increase the fatty acid β-oxidation as a compensatory mechanism. However, the oxygen required for fatty acid metabolism is more than glucose

and therefore leads to the production of more reactive oxygen species (Janardhan et al., 2011).

Mizuno et al. (2017) reported a decrease in myocardial uptake of glucose, lactate and pyruvate in diabetic patients compared to non-diabetics, associated with an increase myocardial uptake of ketone bodies, β-hydroxybutyrate and acetoacetate. Here we also identified changes to the ketogenesis pathway in the HFD (DIO) model. Notably, proteomics revealed an increase in D-β-hydroxybutyrate dehydrogenase (BDH1), a mitochondrial enzyme that catalyses the reversible reaction of β-hydroxybutyrate to acetoacetate, the two main ketone bodies generated by break down of fatty acid. Further, HMGCS2 which catalyses the first reaction in ketogenesis was significantly decreased in HFD (DIO). D-lactate dehydrogenase (LDHD) catalyses the reversible conversion of pyruvate to D-lactate also found to be significantly decreased in HFD (DIO).

One of the predicted inhibited upstream regulators in HFD (DIO) model is PPARA, as it is linked to the downregulation of 15 different proteins (APOA4, APOE, APOC3, CAT, DBI, ECH1, HMGCS2, HSD17B11, PDK4, PLIN5, UCP1, UCP3, ABCD3, ACOT2, and ACOX1). PPARA is an important lipid metabolism regulator as it regulates fatty acid catabolism, utilization and uptake (Kersten, 2014). This finding is consistent with that of Depre et al. (2000) who reported a decrease in PPARA expression in the cardiac tissue of STZ chronic type I diabetic rats. Similar results have been found in other diabetic models. For example, obese Zucker Diabetic Fatty (ZDF) rats had lower expression of PPARA compared to controls associated with lower fatty acid oxidation which agrees with the results shown in this Chapter (Zhou et al., 2000). This reduction could be a response to oxidative stress, as heart muscle of rat model of hypoxia has been shown to have decreased PPARA expression (Razeghi et al., 2001a). Similarly, downregulation of PPARA has been reported in the failing human heart and can be linked to the decreased utilisation of free fatty acids seen in heart failure (Karbowska et al., 2003).

Conversely, PPARA upregulation has been reported in type I diabetes. For example, it has been shown that in STZ diabetic mouse hearts there is an activation of PPARA (Finck et al., 2002). Moreover, Finck and his colleagues found that upregulation of PPARA has induced a phenotype similar to the diabetic heart, highlighting the role of PPARA in DCM pathogenesis. The variation in the expression of PPARA in diabetic models can be caused by various factors influencing the pathogenicity of diabetes. Another possibility is that age is an

essential factor in regulating PPARA, as expression in the diabetic heart has been observed to decrease with time (Depre et al., 2000).

Interestingly, upstream regulator (PPARA) was activated in the diet exchange group (Z-score=2.148), unlike exercise and exercise/diet exchange groups. Fibrates drugs (class of amphipathic carboxylic acids) are used to treat patients with high cholesterol level (Kersten, 2008). Interestingly, these drugs are classified as PPARA agonists. This highlights the importance of dietary habits. Although exercise/diet exchange group had similar phenotype and molecular changes to diet exchange group, PPARA was not activated in exercise/diet exchange group.

Many of the proteins linked to energy production were downregulated, in the HFD (DIO) model, highlighting the importance of measuring ATP level in the future work. Luptak et al. (2018) studied the association between ATP production and metabolic heart disease by feeding the mice high fat, high sucrose (HFHS) diet. The concentration of myocardial ATP, ADP and the rate of ATP production were quantified. ADP concentration was significantly increased associated with unchanged ATP levels. The authors demonstrated that the impairment in energy production may contribute to diastolic dysfunction in obesity-related cardiomyopathy. It may be useful in the future to quantify ATP/ADP levels in our study to determine if it may be a factor responsible for the diastolic dysfunction and mitochondrial dysfunction in the HFD (DIO) myocardium.

The electron transport chain produces ATP by electrons transfer through the inner mitochondrial membrane by creating an electrochemical proton gradient. None of the proteins associated with mitochondrial respiratory complexes were changed in HFD (DIO) model. Unexpectedly, COX6A2 one of the proteins located in complex IV was significantly downregulated in diet exchange group. Interestingly, it was found that mice deficient in this protein were protected against HFD (DIO) and IR and reported its role in regulating respiratory uncoupling (Quintens et al., 2013). There was an increase in ATP6 located in complex V in diet exchange group could be as a compensatory mechanism to the downregulation of COX6A2. Moreover, it is known that the complexes interact with each other to form structures of a higher order, called super complexes (Wittig and Schagger, 2008). Complexes IV and V can form dimers and oligomers. These complexes contribute to the stability of the mitochondrial membrane (Signes and Fernandez-Vizarra, 2018). An increase in ATP6 in complex V might be a compensatory mechanism to the decrease of

COX6A2 protein in complex IV to stabilise the bonds between both complexes. The proteomics data showing no change to the Complex subunits in the HFD (DIO) model is consistent with the biochemical data in Chapter 2.

6.4.5 Quantitative mass spectrometry analysis of mitochondrial dynamic proteins

Quantification of the mitochondrial fission/fusion proteins in mass spectrometry analysis was not consistent with Western blotting and qPCR. The reason for this is could be that the detection of protein depends on its abundance. Low-abundance proteins are dominated by high-abundance proteins; one of the disadvantages of bottom-up analysis used in this study. The analysis time of LC-MS/MS could be an important factor. In our study, we ran the samples for three hours, while other studies run samples for 2 weeks (Piehowski et al., 2013), as complex peptide mixtures required a long run time. Liu and Chan (2015) reported that Drp1 is recruited to Mff forming a higher molecular weight Drp-Mff complex. This could explain the inconsistency in Drp1 and Mff expression between proteomics and Western blotting where total lysate was employed rather than isolated mitochondria. Another downside is the loss of labile post-translational modification (PTM). For example, the function of Drp1 could not be detected because such a technique does not determine the phosphorylation status of a protein which could determine the protein function (although there are MS techniques to measure PTMs e.g. phosphoproteomics). However, bottom-up analysis is more sensitive than top-down analysis. Advantages and disadvantages of each method are reviewed in (Gregorich et al., 2014).

Limitations of proteomics studies include the reliance of the protein turnover rate on a specific protein half-life which is a key factor in measuring protein abundance (Belle et al., 2006). It is also important to note that multiple proteins can be translated from a single transcript by alternative RNA splicing. In addition, the activity of proteins can be affected by post-translational modifications including phosphorylation and glycation; protein function is not always correlated with protein level. Therefore, it is worth considering metabolomics work in the future. Moreover, the properties of a peptide such as length, mass, amino acid composition, solubility and net charge may affect peptide detection. This variability in peptide detection can result in inaccuracies in the assessment of the abundance of the protein (Braisted et al., 2008). It has been reported that the coefficient of variation in LC-MS/MS peptide intensity level in two samples under the same conditions from different cultures was 25% (Piehowski et al., 2013). Furthermore, the expense of an LC-MS/MS device in

combination with the cost of collecting data is a substantial disadvantage (Bereman, 2015). For further evaluation of the proteomics technique see Gupta and Kumar (2014).

6.5 Conclusion

In this investigation, the aim was to assess mitochondrial pathways changes in our HFD (DIO)model and whether effects were reversed by exercise and/or diet exchange. Most altered pathways in HFD (DIO) were associated with metabolism, while most proteins changes in exercise and exercise/diet exchange group were associated with cardiac muscle contractility. The analysis of exercise group has shown that the majority of proteins (91%) altered were downregulated. The study has shown that inflammation pathways were significantly altered in HFD (DIO) model but not after exercise training suggesting that the inflammatory response can be adaptive. A major enzyme in regulating the source of energy (PDK) was significantly downregulated in HFD (DIO), suggesting a shift toward glucose metabolism. One of the key findings to emerge from this study is that the upstream lipid metabolism regulator PPARA was inhibited in HFD (DIO), which changed after the diet exchange highlighting the effect of dietary habits. Overall, the results of this chapter strengthen the idea that exercise and/or diet exchange is beneficial in reversing pathological processes but also highlights that certain pathways are not reversible. In conclusion, this research has provided a new insight into mitochondrial pathway alterations occurring in early-stage diabetic cardiomyopathy. A limitation of this study include that some proteins were not identified. A natural progression of this work is to confirm some of the main changed proteins by other techniques such as qPCR and western blotting and also functional assays to investigate whether changes to protein expression levels translate into reduced or overactive activity.

Chapter 7 General discussion

7.1 Main findings

Obesity due to a high-fat diet is one of the most common causes of T2DM. Here, employing a mouse model of diet-induced obesity we assessed cardiac and mitochondrial function, specifically mitochondrial fission and fusion, an alteration of which is believed to be one of the developmental causes of diabetic cardiomyopathy. Understanding changes in the early stages of the disease is a major factor for preventing disease progression. For this purpose, the project also integrated global proteomic analysis with molecular biology, measurement of mitochondrial bioenergetics properties and morphological investigations using 3D electron microscopy.

The main findings from this research were that C57BL/6J mice fed HFD (DIO) for 12 weeks exhibit signs of diastolic dysfunction, concentric remodelling and at the cellular level has changes to mitochondrial fission/fusion proteins as well as mitochondrial bioenergetics and evidence of inflammation. Physiological measurements revealed insulin resistance, hyperglycaemia and hyperlipidaemia. Significantly, the echocardiography data with normal ejection fraction and signs of early diastolic dysfunction indicate a type of heart failure known as heart failure with preserved ejection fraction (HFpEF). HFpEF represents about half of all cases of heart failure (Nanayakkara et al., 2018). Although the growing prevalence of HFpEF, the effect of treatment on functional outcomes has not been successful (Zheng et al., 2018). Hence, early diabetic cardiomyopathy patients may have limited therapeutic options preventing the progression of the disease. There was an association between proteins regulating mitochondrial dynamics in the HFD (DIO) model favouring fission and the ultrastructure of the cardiac mitochondria by SBF-SEM showing smaller PNM compared to control. These data show that a relatively short period of high-fat feeding results in mild diastolic dysfunction and alteration in mitochondrial dynamics.

The mechanistic pathways regulating mitochondrial fission/fusion proteins remain poorly understood. Therefore, the next aim was to investigate the regulator of mitochondrial dynamics, activation of Drp1 which was upregulated in the HFD (DIO) model, by exploring the role of insulin resistance, ER stress, prohibitins and Sirt5. It was determined that there is no link between insulin resistance and levels of fission/fusion proteins. This result using H9c2 cells was supported by our exercise model which shows that Drp1 levels returned to normal whilst the animals remained insulin resistant. Previous work from our group had shown that the concentration of glucose in the culture medium (5.5 mM or 25 mM) had no

effect upon the expression of fission or fusion proteins (Lucy Murfitt, PhD Thesis). Due to the close contact between mitochondria and endoplasmic reticulum and known communication between the two organelles, we investigated endoplasmic reticulum stress in our HFD (DIO) model; however, there was no evidence of activation of the ER stress pathways which would imply that molecular remodelling of these pathways does not occur in the early stage of the disease. Based upon some reports in the literature linking prohibitins to Drp1 expression we also measured levels of prohibitin 1 and 2 but found that these were unchanged (Raut et al., 2019). However, we did identify a decrease in expression of mitochondrial Sirt5 (regulator of cellular homeostasis) mRNA level in our HFD (DIO) model. By knocking down Sirt5 *in vitro* using a cardiomyoblast cell line (H9c2), we showed a novel finding that Sirt5 expression is connected to the mitochondrial structure through an increase in S-Opa1 and total Drp1 associated with a decrease in P-Drp1 (S637). Future work will investigate the mechanistic link between Sirt5 and Drp1 activation.

The most important management of obesity/T2DM is weight loss through a low-calorie diet and exercise, which is why the second aspect of this project focused on the investigating reversible effect of exercise and a low-fat diet both in terms of gross cardiac function and at the cellular and molecular level. The best outcome in terms of cardiac function was in the diet exchange group and the combination of both exercise and diet exchange group. This is illustrated by the reversal of insulin resistance, hyperglycaemia, hyperlipidaemia, and fission/fusion proteins. Interestingly, one of the Drp1 receptors remained upregulated which may be involved in a different mechanism. The exercise group, while on HFD (DIO), showed the least weight loss and remained insulin resistant. Although some of the fission proteins returned to normal level in the exercise group, the fusion protein Mfn2 became upregulated.

Proteomic analysis revealed more extensive changes to mitochondrial function with a shift in fuel energetics to glucose, disturbance in inflammatory pathways, a downregulation of cardiac contractility proteins and inhibition of the upstream regulator of fatty acid, PPARA. We also reported the activation of mitophagy and evidence of apoptosis. Interestingly, significant downregulation of beta-oxidation of fatty acid in the HFD (DIO) model was not changed in exercise, diet exchange and exercise/diet exchange groups. Another interesting finding was that PPARA, an upstream regulator of fatty acid, was significantly increased in the diet exchange group, unlike exercise and exercise/diet exchange groups.

Therefore, these data indicate that in young obese mice gross cardiac function may be restored through a combination and diet with the fission-fusion axis largely rebalanced. However, proteomics revealed that some mitochondrial pathways remained perturbed. Whether these discrete molecular level changes would leave the mice more vulnerable to any future stress would be an interesting area to investigate in future studies.

7.2 Methodological considerations

7.2.1 Model of obesity and exercise

The use of animal models is often employed to study obesity. Although human tissue may offer a better understanding of human physiology, availability for study is understandably limited. As lifestyle and eating habits are the most common cause of obesity in humans, HFD (DIO) feeding is physiologically the best relevant to the animal model of obesity. A high-fat diet was chosen over a high-glucose diet because fat has more calories (one gram of fat has nine calories while one gram of carbohydrates has four calories) which is important in a calorie surplus to gain weight. For example, Tang et al. (2014) reported obesity in 20 weeks of HFD (DIO) on C57BL/6J and no significant change in body weight in 20 weeks of the high-glucose diet. Obesity in rodents is classified as moderate obesity when there is a 10-25% increase in body weight compared to control and severe obesity if it exceeded a 40% increase in body weight compared to control (Hariri and Thibault, 2010). Therefore, it was decided, before starting the HFD (DIO) trial, to exclude all HFD (DIO) mice with a bodyweight increase of under 10% when compared to controls. Our mice were moderately obese. The behaviour of the mouse is also to be considered; we have found that in each cage there is a hierarchy determined by mice fighting. Typically, there is an alpha mouse who gains the most weight, and a mouse at the lower end of the hierarchy gaining the least weight. We were able to eliminate these mice according to the 10% exclusion criteria. The differences in obesity-related cardiovascular diseases between human genders are well known (Cordero et al., 2009). Nevertheless, in the process of this research, male mice were included only. The reason for this was to exclude the hormonal fluctuations associated with the female oestrus cycle. However, the ranges of blood glucose level in diagnosis diabetes in laboratory mice are not known. Therefore, the severity of hyperglycaemia was difficult to interpret and so the prediabetes or borderline diabetes could not be determined.

Our HFD (DIO) model was a surrogate model to human obesity as it develops a similar phenotype to obese humans include weight gain, hyperglycaemia, hyperinsulinemia and

hyperlipidaemia. Although exercise and weight loss are the first-line management of obesity, patient noncompliance is one of the challenges. The opposite is in the murine model as you can organise the exercise protocol as well as the dietary regime. We understand that swimming can be stressful to mice if they have never experienced it before. Thus, one week of introducing mice to water and gradually increased the duration of swimming was performed. Additionally, any mouse showing signs of distress was excluded from the study. However, physiological changes to our exercise (swimming) model i.e. eccentric remodelling and bradycardia were comparable to humans which strengthen the interpretation of our results to humans. Future work could include validating the results with other types of aerobic exercise, with different intensity and different duration. Further research could also be conducted to determine the distribution of body fat and its effect on cardiac complications. As it is known that different fat distribution would lead to a different outcome. For example, obese individuals with visceral obesity develop a worse outcome of metabolic dysfunction (Koster et al., 2010).

7.2.2 Cell culture

Cell culture using an immortal H9c2 rat cardiomyoblast cell line was used to study the effect of Sirt5 on mitochondrial dynamics. The cell culture techniques allow better control of the culture environment and reveal more information on the development of molecular diseases, especially in T2DM pathogenesis. The use of H9c2 cells offers a powerful benefit of having an unlimited supply of cells available, thus negating the ethical concerns, such as those for murine model studies. However, attention is drawn to the fact that an extensive passage of cell lines like H9c2 would lead to the variation of primary cell phenotypes and was taken into consideration while performing this work. This was overcome by using new cell lines when they reach passage 20. In the case of primary cell lines, they have slow cell growth and more susceptible to contamination. Therefore, optimization of the culture condition is required. For cardiac research, it is not a trivial task to isolate primary cardiomyocytes at every phase of the experiment. Neonatal rat cardiomyocytes (NRCMs) display a downside in the assessment of mitochondrial function, since their major source of energy is glucose, while fatty acid oxidation takes place in mature cardiomyocyte. Overall, neither of these cell models offers a complete solution and the choice of either option has its pros and cons. As a validating method, it could be assessed in the future whether the findings in this project could be reproduced in primary adult cardiomyocytes.

7.3 Limitations

7.3.1 SBF-SEM

The novel technique SBF-SEM produces three-dimensional high-resolution images from fixed tissue. In this project, SBF-SEM was successfully performed to assess the mitochondrial size of the HFD (DIO) cardiac mitochondria. By doing so it was feasible to develop a better understanding of the alteration of mitochondrial dynamics proteins and the link to mitochondrial ultrastructure. This technique, however, has different limitations such as each mitochondrion has to be segmented manually with high accuracy through the stack to form the 3D structure which takes a huge amount of laborious work at least three months. The resolution also is limited as cristae formation is not visible. Alternative techniques such as focussed ion-beam scanning electron microscopy (FIB-SEM) based on the same concept as SBF-SEM can produce higher resolution images up to 9.4 nm in the X-Y plane and 20 nm in the Z plane (Xiao et al., 2018) which may facilitate details of the cristae to be resolved. There is currently much effort in the community to develop automated methods for organelle segmentation which as well as making the process more towards high throughput (manual segmentation can take several months) it will also remove selection bias.

7.3.2 Mitochondrial oxygen consumption rate

To investigate whether functional changes occur in the mitochondria, an Instech (based on the fibre optics) was used to measure the oxygen consumption rate (OCR). Since this machine is relatively new in the research laboratory and the protocols are still being optimized, an enormous amount of time was spent on optimisation. In the future we can develop this technique to measure the activity of each complex by using a combination of substrates and inhibitors.

7.4 Future direction

7.4.1 The age factor

A possible major influencing factor on the outcome of this study is the age of the mice at the start of the HFD (DIO) feeding, as we started the HFD (DIO) feeding at the age of 8 weeks old which approximately matches a human age of 14-18 years old. Laboratory mice have an average lifespan of about 24 months (Wilkinson et al., 2012). On average, mice reach puberty at about 6 weeks (Hagenauer et al., 2009, Kercmar et al., 2014). The estimations for maturity in C57BL/6J mice are a mature adult (13–26 weeks old), middle-aged (43-65 weeks old), and old (78-104 weeks old) (Liu et al., 2016). So, our HFD (DIO) model corresponds to an

adolescent, the transition between childhood and adulthood. After the 12-week HFD (DIO) feeding, mice aged 20 weeks were at the stage of a mature adult, as well as exercise and/or diet exchange models (25 weeks). A study on overweight and obese adolescents showed an increase in LV mass as compensation to the high hemodynamic load in overweight adolescents, while the increase in LV mass in obese adolescents exceeded the demand leading to a decrease in ejection fraction and cardiac contractility (Chinali et al., 2006). Therefore, beginning HF feeding at 8 weeks old can mean that most of the compensatory mechanisms are active against disease progression. Interestingly, another study within our group with mice between 13 and 17 weeks, considered as mature adult (Liu et al., 2016) being fed HFD (DIO) for 12 weeks, showed a significant impairment of cardiac function and a significant decrease in mitochondrial complexes activity; but it may be an additional factor that a different strain of mice was used. However, these data may be important in the context of childhood and adolescence obesity, given that almost a third of the population in the UK between 2 and 15 years of age are overweight or obese in government statistics (Health Survey for England, 2018). Accordingly, future work could investigate the potential different results of starting the HFD (DIO) at an older age (13-26 weeks). Research questions that could be asked include changes to mitochondrial fission/fusion proteins in extended HFD (DIO) duration (severe obesity), as we mentioned before our model represented a moderate obesity, and whether these changes are still reversible by exercise and weight loss. Therefore, longitudinal study of increasing the HFD (DIO) duration is also an important consideration for future studies.

7.4.2 Phosphorylation of Drp1

The main regulator of mitochondrial fission is Drp1. PTMs including phosphorylation, ubiquitination, S-nitrosylation and SUMOylation are applied to Drp1. Of these, the best studied is phosphorylation. For example, phosphorylation of Drp1 in Ser616 by cyclin dependent kinase 1 (CDK1-cyclin B) is reported to enhance its GTPase activity leads to fragmentation of mitochondria (Taguchi et al., 2007). Furthermore, phosphorylation of Drp1 in Ser637 by protein kinase A (PKA) reduces its activity (Cribbs and Strack, 2007). This can be antagonized by dephosphorylation of Ser637 by calcineurin (Cereghetti et al., 2008). Another phosphorylation site that has not been studied in this thesis is Ser600 which can be phosphorylated by calcium/calmodulin-dependent protein kinase 1α (CamKIα) to induce mitochondrial fission (Han et al., 2008). The multiple phosphorylation sites with different functions highlight the complexity and importance of this protein. Further research should be

undertaken to investigate the enzyme levels in our models; phosphoproteomics may be a useful approach. Similarly, given the link between Sirt5 and Drp1 shown here exploring changes to protein post-translational modifications will also be important. Additionally, investigating how Sirt5 may be associated with the upstream regulator PPARA (identified in the proteomics analysis) may also be an area for development. Purushotham et al. (2009) reported that Sirt1 activates PPARA to increase fatty acid beta-oxidation by deacetylation in hepatocytes. This is linked to our study as we found an inhibition of the PPARA pathway in our HFD (DIO) as well as a decrease in mRNA of Sirt5 which may be linked. The deacetylation activity of Sirt2 is inhibited by nicotinamide (vitamin B3), which is considered a non-competitive inhibitor of Sirtuins (Avalos et al., 2005); it has been reported to inhibit Sirt1 in vitro (Hwang and Song, 2017), as well as other isoforms include Sirt3,4,5 and 6 (Hu et al., 2014). Nicotinamide has been used to treat niacin deficiency, acne and skin cancer.

Activation of Sirt5 is potentially essential for the protection of obesity-related cardiovascular complications. So, rather than directly focussing on the fission and fusion proteins, a strategy we are considering in future work will be how we can target Sirt5 to manipulate Drp1. There is a lot of interest in regulating sirtuins in the literature with a number of agonists and antagonists, reviewed in (Dai et al., 2018). However, the disadvantage of targeting Sirt5 as a therapeutic target is that it could have multiple off-target effects as there are vast array of proteins substrates regulated by its deacetylation and desuccinylation activity.

7.5 Conclusion

Combining a variety of experimental techniques, this PhD thesis explored early changes in mitochondrial fission proteins linked to the pathogenesis of early-stage diabetic cardiomyopathy, using a mouse model of HFD (DIO) feeding for 12 weeks. In summary, our new data show that relatively short periods of high fat feeding lead to cardiac complications and with an imbalance in mitochondrial fission/fusion processes, providing insights into potential regulatory pathways. Additionally, we have reported that a combination of diet and exercise is most beneficial for the return of cardiac function to a healthy phenotype, consistent with clinical practice. Further, we have described for the first time that the fission-fusion axis can also be restored, although proteomics identified some mitochondrial proteins that did not exhibit this plasticity. There is a lot of interest in the therapeutic applications of in targeting fission and fusion, mainly for promoting fusion, for a recent review see (Kalkhoran et al., 2020), since small and fragmented mitochondria have been reported in patients and animal models of diabetes, as discussed in Chapter 3. However, future work is required to

ascertain whether the increased fission that is occurring after 12 weeks high fat feeding is a cardioprotective reaction to remove damaged mitochondria with increased expression of the mitophagy proteins PINK1 and Parkin. A detailed understanding of the mitochondrial dynamics and the morphological changes mediated by these proteins will be important for future translational into strategies for therapeutic intervention in the treatment of progression of early-stage diabetic cardiomyopathy.

Appendices:

Appendix 7.1

Table 7.1: Masson's trichrome staining protocol.

Step	Solution	Time
1.	Pure xylene	15 minutes
2.	100% IMS	3 minutes
3.	90%IMS	3 minutes
4.	70% IMS	3 minutes
5.	Wash in distilled water	4 minutes
6.	Bouin's solution (water bath =56˚C)	120 minutes
7.	Wash in tap water	7 minutes
8.	Filtered haematoxylin	5 minutes
9.	Wash in tap water	7 minutes
10.	Acid alcohol	10 seconds
11.	Wash in tap water	30 seconds
12.	Biebrich scarlet-acid fuchsin solution (0.9% Biebrich scarlet, 0.1% Ponceau Fuchsin in 1% acetic acid)	5 minutes
13.	Wash in distilled water	30 seconds
14.	2.5% phosphomolybdic acid solution	15 minutes
15.	Aniline blue	60 minutes
16.	Distilled water	10 seconds
17.	1% acetic acid	2 minutes
18.	Distilled water	10 seconds
19.	90% IMS	1 minute
20.	95%IMS	1 minute
21.	100% IMS	1 minute
22.	Xylene	2 minutes
23.	Xylene	2 minutes
24.	Xylene	2 minutes

References

ABDELAZIZ, A. I., SEGARIC, J., BARTSCH, H., PETZHOLD, D., SCHLEGEL, W. P., KOTT, M., SEEFELDT, I., KLOSE, J., BADER, M., HAASE, H. & MORANO, I. 2004. Functional characterization of the human atrial essential myosin light chain (hALC-1) in a transgenic rat model. *J Mol Med (Berl),* 82**,** 265-74.

ABDURRACHIM, D., CIAPAITE, J., WESSELS, B., NABBEN, M., LUIKEN, J. J., NICOLAY, K. & PROMPERS, J. J. 2014. Cardiac diastolic dysfunction in high-fat diet fed mice is associated with lipotoxicity without impairment of cardiac energetics in vivo. *Biochim Biophys Acta,* 1842**,** 1525-37.

ABOUASSI, H., SLENTZ, C. A., MIKUS, C. R., TANNER, C. J., BATEMAN, L. A., WILLIS, L. H., SHIELDS, A. T., PINER, L. W., PENRY, L. E., KRAUS, E. A., HUFFMAN, K. M., BALES, C. W., HOUMARD, J. A. & KRAUS, W. E. 2015. The effects of aerobic, resistance, and combination training on insulin sensitivity and secretion in overweight adults from STRRIDE AT/RT: a randomized trial. *J Appl Physiol (1985),* 118**,** 1474-82.

AIZAWA, N., HOMMA, Y. & IGAWA, Y. 2013. Influence of High Fat Diet Feeding for 20 Weeks on Lower Urinary Tract Function in Mice. *Low Urin Tract Symptoms,* 5**,** 101-8.

AL-MEHDI, A. B., PASTUKH, V. M., SWIGER, B. M., REED, D. J., PATEL, M. R., BARDWELL, G. C., PASTUKH, V. V., ALEXEYEV, M. F. & GILLESPIE, M. N. 2012. Perinuclear mitochondrial clustering creates an oxidant-rich nuclear domain required for hypoxia-induced transcription. *Sci Signal,* 5**,** ra47.

ALCALA, M., CALDERON-DOMINGUEZ, M., SERRA, D., HERRERO, L., RAMOS, M. P. & VIANA, M. 2017. Short-term vitamin E treatment impairs reactive oxygen species signaling required for adipose tissue expansion, resulting in fatty liver and insulin resistance in obese mice. *PLoS One,* 12**,** e0186579.

ALCALA, M., GUTIERREZ-VEGA, S., CASTRO, E., GUZMAN-GUTIERREZ, E., RAMOS-ALVAREZ, M. P. & VIANA, M. 2018. Antioxidants and Oxidative Stress: Focus in Obese Pregnancies. *Front Physiol,* 9**,** 1569.

ALCALA, M., SANCHEZ-VERA, I., SEVILLANO, J., HERRERO, L., SERRA, D., RAMOS, M. P. & VIANA, M. 2015. Vitamin E reduces adipose tissue fibrosis, inflammation, and oxidative stress and improves metabolic profile in obesity. *Obesity (Silver Spring),* 23**,** 1598-606.

ALLEMAN, R. J., STEWART, L. M., TSANG, A. M. & BROWN, D. A. 2015. Why Does Exercise "Trigger" Adaptive Protective Responses in the Heart? *Dose-Response,* 13.

AMARAL, N. & OKONKO, D. O. 2015. Metabolic abnormalities of the heart in type II diabetes. *Diab Vasc Dis Res,* 12**,** 239-48.

AMERICAN DIABETES ASSOCIATION 2017. Classification and Diagnosis of Diabetes.

AN, D. & RODRIGUES, B. 2006. Role of changes in cardiac metabolism in development of diabetic cardiomyopathy. *Am J Physiol Heart Circ Physiol,* 291**,** H1489-506.

ANAND, R., WAI, T., BAKER, M. J., KLADT, N., SCHAUSS, A. C., RUGARLI, E. & LANGER, T. 2014. The i-AAA protease YME1L and OMA1 cleave OPA1 to balance mitochondrial fusion and fission. *J Cell Biol,* 204**,** 919-29.

ANDERSON, E. J., RODRIGUEZ, E., ANDERSON, C. A., THAYNE, K., CHITWOOD, W. R. & KYPSON, A. P. 2011. Increased propensity for cell death in diabetic human heart is mediated by mitochondrial-dependent pathways. *Am J Physiol Heart Circ Physiol,* 300**,** H118-24.

ANDRES, A. M., HERNANDEZ, G., LEE, P., HUANG, C. Q., RATLIFF, E. P., SIN, J., THORNTON, C. A., DAMASCO, M. V. & GOTTLIEB, R. A. 2014. Mitophagy Is Required for Acute Cardioprotection by Simvastatin. *Antioxidants & Redox Signaling,* 21**,** 1960-1973.

ANDRES, A. M., STOTLAND, A., QUELICONI, B. B. & GOTTLIEB, R. A. 2015. A time to reap, a time to sow: mitophagy and biogenesis in cardiac pathophysiology. *J Mol Cell Cardiol,* 78**,** 62-72.

ANEJA, A., TANG, W. H. W., BANSILAL, S., GARCIA, M. J. & FARKOUH, M. E. 2008. Diabetic cardiomyopathy: Insights into pathogenesis, diagnostic challenges, and therapeutic options. *American Journal of Medicine,* 121**,** 748-757.

ANTONIOLI, L., PELLEGRINI, C., FORNAI, M., TIROTTA, E., GENTILE, D., BENVENUTI, L., GIRON, M. C., CAPUTI, V., MARSILIO, I., ORSO, G., BERNARDINI, N., SEGNANI, C., IPPOLITO, C., CSOKA, B., NEMETH, Z. H., HASKO, G., SCARPIGNATO, C., BLANDIZZI, C. & COLUCCI, R. 2017. Colonic motor dysfunctions in a mouse model of high-fat diet-induced obesity: an involvement of A2B adenosine receptors. *Purinergic Signal*.

ARNOULT, D., RISMANCHI, N., GRODET, A., ROBERTS, R. G., SEEBURG, D. P., ESTAQUIER, J., SHENG, M. & BLACKSTONE, C. 2005. Bax/Bak-dependent release of DDP/TIMM8a promotes Drp1-mediated mitochondrial fission and mitoptosis during programmed cell death. *Curr Biol,* 15**,** 2112-8.

ARSENAULT, B. J., RANA, J. S., STROES, E. S., DESPRES, J. P., SHAH, P. K., KASTELEIN, J. J., WAREHAM, N. J., BOEKHOLDT, S. M. & KHAW, K. T. 2009. Beyond low-density lipoprotein cholesterol: respective contributions of non-high-density lipoprotein cholesterol levels, triglycerides, and the total cholesterol/high-density lipoprotein cholesterol ratio to coronary heart disease risk in apparently healthy men and women. *J Am Coll Cardiol,* 55**,** 35-41.

ARSENIJEVIC, D., ONUMA, H., PECQUEUR, C., RAIMBAULT, S., MANNING, B. S., MIROUX, B., COUPLAN, E., ALVES-GUERRA, M. C., GOUBERN, M., SURWIT, R., BOUILLAUD, F., RICHARD, D., COLLINS, S. & RICQUIER, D. 2000. Disruption of the uncoupling protein-2 gene in mice reveals a role in immunity and reactive oxygen species production. *Nat Genet,* 26**,** 435-9.

ARTAL-SANZ, M. & TAVERNARAKIS, N. 2009. Prohibitin couples diapause signalling to mitochondrial metabolism during ageing in C. elegans. *Nature,* 461**,** 793-7.

ASCENSAO, A., LUMINI-OLIVEIRA, J., MACHADO, N. G., FERREIRA, R. M., GONCALVES, I. O., MOREIRA, A. C., MARQUES, F., SARDAO, V. A., OLIVEIRA, P. J. & MAGALHAES, J. 2011. Acute exercise protects against calcium-induced cardiac mitochondrial permeability transition pore opening in doxorubicin-treated rats. *Clin Sci (Lond),* 120**,** 37-49.

ASLAM, B., BASIT, M., NISAR, M. A., KHURSHID, M. & RASOOL, M. H. 2017. Proteomics: Technologies and Their Applications. *J Chromatogr Sci,* 55**,** 182-196.

AUBERT, G., VEGA, R. B. & KELLY, D. P. 2013. Perturbations in the gene regulatory pathways controlling mitochondrial energy production in the failing heart. *Biochim Biophys Acta,* 1833**,** 840-7.

AVALOS, J. L., BEVER, K. M. & WOLBERGER, C. 2005. Mechanism of sirtuin inhibition by nicotinamide: altering the NAD(+) cosubstrate specificity of a Sir2 enzyme. *Mol Cell,* 17**,** 855-68.

AVOGARO., A., KREUTZENBERG., S. V. D., NEGUT., C., TIENGO., A. & SCOGNAMIGLIO., R. 2004. Diabetic cardiomyopathy: A metabolic perspective. 93**,** 13–16.

AWA, W. L., FACH, E., KRAKOW, D., WELP, R., KUNDER, J., VOLL, A., ZEYFANG, A., WAGNER, C., SCHÜTT, M., BOEHM, B., SOUZA, M. D. & HOLL, R. W. 2012. Type 2 diabetes from pediatric to geriatric age: analysis of gender and obesity among 120183 patients from the German/Austrian DPV database.
BANDO, Y. K. & MUROHARA, T. 2014. Diabetes-related heart failure. *Circ J,* 78**,** 576-83.
BANTSCHEFF, M., SCHIRLE, M., SWEETMAN, G., RICK, J. & KUSTER, B. 2007. Quantitative mass spectrometry in proteomics: a critical review. *Anal Bioanal Chem,* 389**,** 1017-31.
BASELER, W. A., DABKOWSKI, E. R., WILLIAMSON, C. L., CROSTON, T. L., THAPA, D., POWELL, M. J., RAZUNGUZWA, T. T. & HOLLANDER, J. M. 2011. Proteomic alterations of distinct mitochondrial subpopulations in the type 1 diabetic heart: contribution of protein import dysfunction. *Am J Physiol Regul Integr Comp Physiol,* 300**,** R186-200.
BAUMANN, H. & GAULDIE, J. 1994. The acute phase response. *Immunol Today,* 15**,** 74-80.
BAYOT, A., GAREIL, M., ROGOWSKA-WRZESINSKA, A., ROEPSTORFF, P., FRIGUET, B. & BULTEAU, A. L. 2010. Identification of novel oxidized protein substrates and physiological partners of the mitochondrial ATP-dependent Lon-like protease Pim1. *J Biol Chem,* 285**,** 11445-57.
BELKE, D. D., SWANSON, E. A. & DILLMANN, W. H. 2004. Decreased sarcoplasmic reticulum activity and contractility in diabetic db/db mouse heart. *Diabetes,* 53**,** 3201-8.
BELLE, A., TANAY, A., BITINCKA, L., SHAMIR, R. & O'SHEA, E. K. 2006. Quantification of protein half-lives in the budding yeast proteome. *Proc Natl Acad Sci U S A,* 103**,** 13004-9.
BEREMAN, M. S. 2015. Tools for monitoring system suitability in LC MS/MS centric proteomic experiments. *Proteomics,* 15**,** 891-902.
BERS, D. M. 2002. Cardiac excitation-contraction coupling. *Nature,* 415**,** 198-205.
BERTONI, T. A., PERENHA-VIANA, M. C., PATUSSI, E. V., CARDOSO, R. F. & SVIDZINSKI, T. I. 2012. Western blotting is an efficient tool for differential diagnosis of paracoccidioidomycosis and pulmonary tuberculosis. *Clin Vaccine Immunol,* 19**,** 1887-8.
BETTERIDGE, D. J. 2000. What is oxidative stress? *Metabolism-Clinical and Experimental,* 49**,** 3-8.
BHAMRA, G. S., HAUSENLOY, D. J., DAVIDSON, S. M., CARR, R. D., PAIVA, M., WYNNE, A. M., MOCANU, M. M. & YELLON, D. M. 2008. Metformin protects the ischemic heart by the Akt-mediated inhibition of mitochondrial permeability transition pore opening. *Basic Res Cardiol,* 103**,** 274-84.
BILLIA, F., HAUCK, L., KONECNY, F., RAO, V., SHEN, J. & MAK, T. W. 2011. PTEN-inducible kinase 1 (PINK1)/Park6 is indispensable for normal heart function. *Proc Natl Acad Sci U S A,* 108**,** 9572-7.
BLEICH, S. N., CUTLER, D., MURRAY, C. & ADAMS, A. 2008. Why Is the Developed World Obese? *http://dx.doi.org/10.1146/annurev.publhealth.29.020907.090954*.
BODEN, G. 2009. Endoplasmic Reticulum Stress: Another Link Between Obesity and Insulin Resistance/Inflammation? *Diabetes,* 58**,** 518-519.
BORBELY, A., PAPP, Z., EDES, I. & PAULUS, W. J. 2009. Molecular determinants of heart failure with normal left ventricular ejection fraction. *Pharmacol Rep,* 61**,** 139-45.
BOUDINA, S. & ABEL, E. D. 2006. Mitochondrial uncoupling: a key contributor to reduced cardiac efficiency in diabetes. *Physiology (Bethesda),* 21**,** 250-8.

BOUDINA, S. & ABEL, E. D. 2007. Diabetic cardiomyopathy revisited. *Circulation,* 115**,** 3213-23.
BOUDINA, S., SENA, S., O'NEILL, B. T., TATHIREDDY, P., YOUNG, M. E. & ABEL, E. D. 2005. Reduced mitochondrial oxidative capacity and increased mitochondrial uncoupling impair myocardial energetics in obesity. *Circulation,* 112**,** 2686-95.
BOUDINA, S., SENA, S., THEOBALD, H., SHENG, X., WRIGHT, J. J., HU, X. X., AZIZ, S., JOHNSON, J. I., BUGGER, H., ZAHA, V. G. & ABEL, E. D. 2007. Mitochondrial energetics in the heart in obesity-related diabetes: direct evidence for increased uncoupled respiration and activation of uncoupling proteins. *Diabetes,* 56**,** 2457-66.
BOYLSTON, J. A., SUN, J., CHEN, Y., GUCEK, M., SACK, M. N. & MURPHY, E. 2015. Characterization of the cardiac succinylome and its role in ischemia-reperfusion injury. *J Mol Cell Cardiol,* 88**,** 73-81.
BRADLEY, U., SPENCE, M., COURTNEY, C. H., MCKINLEY, M. C., ENNIS, C. N., MCCANCE, D. R., MCENENY, J., BELL, P. M., YOUNG, I. S. & HUNTER, S. J. 2009. Low-fat versus low-carbohydrate weight reduction diets: effects on weight loss, insulin resistance, and cardiovascular risk: a randomized control trial. *Diabetes,* 58**,** 2741-8.
BRAISTED, J. C., KUNTUMALLA, S., VOGEL, C., MARCOTTE, E. M., RODRIGUES, A. R., WANG, R., HUANG, S. T., FERLANTI, E. S., SAEED, A. I., FLEISCHMANN, R. D., PETERSON, S. N. & PIEPER, R. 2008. The APEX Quantitative Proteomics Tool: generating protein quantitation estimates from LC-MS/MS proteomics results. *BMC Bioinformatics,* 9**,** 529.
BRAND, M. D., AFFOURTIT, C., ESTEVES, T. C., GREEN, K., LAMBERT, A. J., MIWA, S., PAKAY, J. L. & PARKER, N. 2004. Mitochondrial superoxide: production, biological effects, and activation of uncoupling proteins. *Free Radic Biol Med,* 37**,** 755-67.
BRINI, M., CALI, T., OTTOLINI, D. & CARAFOLI, E. 2013. Intracellular calcium homeostasis and signaling. *Met Ions Life Sci,* 12**,** 119-68.
BRYONY BUTLAND, S. J., PETER KOPELMAN, KLIM MCPHERSON, SANDY THOMAS, JANE MARDELL, VIVIENNE PARRY 2007. Tackling Obesities: Future Choices. *In:* FORESIGHT (ed.).
BUCHANAN, J., MAZUMDER, P. K., HU, P., CHAKRABARTI, G., ROBERTS, M. W., YUN, U. J., COOKSEY, R. C., LITWIN, S. E. & ABEL, E. D. 2005. Reduced cardiac efficiency and altered substrate metabolism precedes the onset of hyperglycemia and contractile dysfunction in two mouse models of insulin resistance and obesity. *Endocrinology,* 146**,** 5341-9.
BUCK, D. W., 2ND, JIN, D. P., GERINGER, M., HONG, S. J., GALIANO, R. D. & MUSTOE, T. A. 2011. The TallyHo polygenic mouse model of diabetes: implications in wound healing. *Plast Reconstr Surg,* 128**,** 427e-437e.
BUGGER, H. & ABEL, E. D. 2009. Rodent models of diabetic cardiomyopathy. *Dis Model Mech,* 2**,** 454-66.
BUGGER, H. & ABEL, E. D. 2010. Mitochondria in the diabetic heart. *Cardiovasc Res,* 88**,** 229-40.
BUGGER, H. & ABEL, E. D. 2014. Molecular mechanisms of diabetic cardiomyopathy. *Diabetologia,* 57**,** 660-71.
BUGGER, H., BOUDINA, S., HU, X. X., TUINEI, J., ZAHA, V. G., THEOBALD, H. A., YUN, U. J., MCQUEEN, A. P., WAYMENT, B., LITWIN, S. E. & ABEL, E. D. 2008. Type 1 diabetic akita mouse hearts are insulin sensitive but manifest

structurally abnormal mitochondria that remain coupled despite increased uncoupling protein 3. *Diabetes,* 57**,** 2924-32.
BUGGER, H., WITT, C. N. & BODE, C. 2016. Mitochondrial sirtuins in the heart. *Heart Fail Rev,* 21**,** 519-28.
CAI, L., LI, W., WANG, G., GUO, L., JIANG, Y. & KANG, Y. J. 2002. Hyperglycemia-induced apoptosis in mouse myocardium: mitochondrial cytochrome C-mediated caspase-3 activation pathway. *Diabetes,* 51**,** 1938-48.
CAMACHO, A., RODRIGUEZ-CUENCA, S., BLOUNT, M., PRIEUR, X., BARBARROJA, N., FULLER, M., HARDINGHAM, G. E. & VIDAL-PUIG, A. 2012. Ablation of PGC1 beta prevents mTOR dependent endoplasmic reticulum stress response. *Exp Neurol,* 237**,** 396-406.
CAO, J., SINGH, S. P., MCCLUNG, J. A., JOSEPH, G., VANELLA, L., BARBAGALLO, I., JIANG, H., FALCK, J. R., ARAD, M., SHAPIRO, J. I. & ABRAHAM, N. G. 2017. EET intervention on Wnt1, NOV, and HO-1 signaling prevents obesity-induced cardiomyopathy in obese mice. *Am J Physiol Heart Circ Physiol,* 313**,** H368-H380.
CAO, T., LICCARDO, D., LACANNA, R., ZHANG, X., LU, R., FINCK, B. N., LEIGH, T., CHEN, X., DROSATOS, K. & TIAN, Y. 2019. Fatty Acid Oxidation Promotes Cardiomyocyte Proliferation Rate but Does Not Change Cardiomyocyte Number in Infant Mice. *Front Cell Dev Biol,* 7**,** 42.
CARTONI, R., LEGER, B., HOCK, M. B., PRAZ, M., CRETTENAND, A., PICH, S., ZILTENER, J. L., LUTHI, F., DERIAZ, O., ZORZANO, A., GOBELET, C., KRALLI, A. & RUSSELL, A. P. 2005. Mitofusins 1/2 and ERRalpha expression are increased in human skeletal muscle after physical exercise. *J Physiol,* 567**,** 349-58.
CEREGHETTI, G. M., STANGHERLIN, A., MARTINS DE BRITO, O., CHANG, C. R., BLACKSTONE, C., BERNARDI, P. & SCORRANO, L. 2008. Dephosphorylation by calcineurin regulates translocation of Drp1 to mitochondria. *Proc Natl Acad Sci U S A,* 105**,** 15803-8.
CHAAR, L. J., COELHO, A., SILVA, N. M., FESTUCCIA, W. L. & ANTUNES, V. R. 2016. High-fat diet-induced hypertension and autonomic imbalance are associated with an upregulation of CART in the dorsomedial hypothalamus of mice. *Physiol Rep,* 4.
CHAIYARIT, S. & THONGBOONKERD, V. 2009. Comparative analyses of cell disruption methods for mitochondrial isolation in high-throughput proteomics study. *Anal Biochem,* 394**,** 249-58.
CHANDRASEKARAN, K., ANJANEYULU, M., INOUE, T., CHOI, J., SAGI, A. R., CHEN, C., IDE, T. & RUSSELL, J. W. 2015. Mitochondrial transcription factor A regulation of mitochondrial degeneration in experimental diabetic neuropathy. *Am J Physiol Endocrinol Metab,* 309**,** E132-41.
CHANG, C. R. & BLACKSTONE, C. 2010. Dynamic regulation of mitochondrial fission through modification of the dynamin-related protein Drp1. *Mitochondrial Research in Translational Medicine,* 1201**,** 34-39.
CHANG, H. D. & RADBRUCH, A. 2007. The pro- and anti-inflammatory potential of interleukin-12. *Ann N Y Acad Sci,* 1109**,** 40-6.
CHAVALI, V., TYAGI, S. C. & MISHRA, P. K. 2013. Predictors and prevention of diabetic cardiomyopathy. *Diabetes Metab Syndr Obes,* 6**,** 151-60.
CHEN, D., LI, X., ZHANG, L., ZHU, M. & GAO, L. 2018. A high-fat diet impairs mitochondrial biogenesis, mitochondrial dynamics, and the respiratory chain complex in rat myocardial tissues. *J Cell Biochem,* 119**,** 9602.

CHEN, H., ZHENG, C., ZHANG, X., LI, J., LI, J., ZHENG, L. & HUANG, K. 2011a. Apelin alleviates diabetes-associated endoplasmic reticulum stress in the pancreas of Akita mice. *Peptides,* 32**,** 1634-9.
CHEN, L., GONG, Q., STICE, J. P. & KNOWLTON, A. A. 2009. Mitochondrial OPA1, apoptosis, and heart failure. *Cardiovasc Res,* 84**,** 91-9.
CHEN, Y. & DORN, G. W., 2ND 2013. PINK1-phosphorylated mitofusin 2 is a Parkin receptor for culling damaged mitochondria. *Science,* 340**,** 471-5.
CHEN, Y., LIU, Y. Q. & DORN, G. W. 2011b. Mitochondrial Fusion is Essential for Organelle Function and Cardiac Homeostasis. *Circulation Research,* 109**,** 1327-U36.
CHENG, S., KEYES, M. J., LARSON, M. G., MCCABE, E. L., NEWTON-CHEH, C., LEVY, D., BENJAMIN, E. J., VASAN, R. S. & WANG, T. J. 2009. Long-term outcomes in individuals with prolonged PR interval or first-degree atrioventricular block. *JAMA,* 301**,** 2571-7.
CHINALI, M., DE SIMONE, G., ROMAN, M. J., LEE, E. T., BEST, L. G., HOWARD, B. V. & DEVEREUX, R. B. 2006. Impact of obesity on cardiac geometry and function in a population of adolescents: the Strong Heart Study. *J Am Coll Cardiol,* 47**,** 2267-73.
CHRISTOFFERSEN, C., BOLLANO, E., LINDEGAARD, M. L., BARTELS, E. D., GOETZE, J. P., ANDERSEN, C. B. & NIELSEN, L. B. 2003. Cardiac lipid accumulation associated with diastolic dysfunction in obese mice. *Endocrinology,* 144**,** 3483-90.
CIPOLAT, S., MARTINS DE BRITO, O., DAL ZILIO, B. & SCORRANO, L. 2004. OPA1 requires mitofusin 1 to promote mitochondrial fusion. *Proc Natl Acad Sci U S A,* 101**,** 15927-32.
CLAUDE, A. & FULLAM, E. F. 1945. An Electron Microscope Study of Isolated Mitochondria : Method and Preliminary Results. *J Exp Med,* 81**,** 51-62.
CLAYCOMB, W. C., LANSON, N. A., JR., STALLWORTH, B. S., EGELAND, D. B., DELCARPIO, J. B., BAHINSKI, A. & IZZO, N. J., JR. 1998. HL-1 cells: a cardiac muscle cell line that contracts and retains phenotypic characteristics of the adult cardiomyocyte. *Proc Natl Acad Sci U S A,* 95**,** 2979-84.
CLEE, S. M. & ATTIE, A. D. 2007. The genetic landscape of type 2 diabetes in mice. *Endocr Rev,* 28**,** 48-83.
CNOP, M., FOUFELLE, F. & VELLOSO, L. A. 2012. Endoplasmic reticulum stress, obesity and diabetes. *Trends Mol Med,* 18**,** 59-68.
CONG, W., RUAN, D., XUAN, Y., NIU, C., TAO, Y., WANG, Y., ZHAN, K., CAI, L., JIN, L. & TAN, Y. 2015. Cardiac-specific overexpression of catalase prevents diabetes-induced pathological changes by inhibiting NF-kappaB signaling activation in the heart. *J Mol Cell Cardiol,* 89**,** 314-25.
COORSSEN, J. R., BLANK, P. S., ALBERTORIO, F., BEZRUKOV, L., KOLOSOVA, I., BACKLUND, P. S., JR. & ZIMMERBERG, J. 2002. Quantitative femto- to attomole immunodetection of regulated secretory vesicle proteins critical to exocytosis. *Anal Biochem,* 307**,** 54-62.
CORDERO, A., LEON, M., ANDRES, E., ORDONEZ, B., LACLAUSTRA, M., GRIMA, A., PASCUAL, I., LUENGO, E., CIVEIRA, F., POCOVI, M., ALEGRIA, E., CASASNOVAS, J. A. & INVESTIGATORS, M. R. 2009. Gender differences in obesity related cardiovascular risk factors in Spain. *Prev Med,* 48**,** 134-9.
CORONADO, M., FAJARDO, G., NGUYEN, K., ZHAO, M., KOOIKER, K., JUNG, G., HU, D. Q., REDDY, S., SANDOVAL, E., STOTLAND, A., GOTTLIEB, R. A. & BERNSTEIN, D. 2018. Physiologic Mitochondrial Fragmentation Is a Normal Cardiac Adaptation to Increased Energy Demand. *Circ Res,* 122**,** 282-95.

CRIBBS, J. T. & STRACK, S. 2007. Reversible phosphorylation of Drp1 by cyclic AMP-dependent protein kinase and calcineurin regulates mitochondrial fission and cell death. *EMBO Rep,* 8**,** 939-44.
CROCHEMORE, C., MEKKI, M., CORBIÈRE, C., KAROUI, A., NOËL, R., VENDEVILLE, C., VAUGEOIS, J.-M. & MONTEIL, C. 2015. Subsarcolemmal and interfibrillar mitochondria display distinct superoxide production profiles. *http://dx.doi.org/10.3109/10715762.2015.1006212*.
CROSTON, T. L., THAPA, D., HOLDEN, A. A., TVETER, K. J., LEWIS, S. E., SHEPHERD, D. L., NICHOLS, C. E., LONG, D. M., OLFERT, I. M., JAGANNATHAN, R. & HOLLANDER, J. M. 2014. Functional deficiencies of subsarcolemmal mitochondria in the type 2 diabetic human heart. *Am J Physiol Heart Circ Physiol,* 307**,** H54-65.
D'SOUZA, A., BUCCHI, A., JOHNSEN, A. B., LOGANTHA, S. J., MONFREDI, O., YANNI, J., PREHAR, S., HART, G., CARTWRIGHT, E., WISLOFF, U., DOBRYZNSKI, H., DIFRANCESCO, D., MORRIS, G. M. & BOYETT, M. R. 2014. Exercise training reduces resting heart rate via downregulation of the funny channel HCN4. *Nat Commun,* 5**,** 3775.
DABKOWSKI, E. R., BASELER, W. A., WILLIAMSON, C. L., POWELL, M., RAZUNGUZWA, T. T., FRISBEE, J. C. & HOLLANDER, J. M. 2010. Mitochondrial dysfunction in the type 2 diabetic heart is associated with alterations in spatially distinct mitochondrial proteomes. *American Journal of Physiology-Heart and Circulatory Physiology,* 299**,** H529-H540.
DABKOWSKI, E. R., WILLIAMSON, C. L., BUKOWSKI, V. C., CHAPMAN, R. S., LEONARD, S. S., PEER, C. J., CALLERY, P. S. & HOLLANDER, J. M. 2009. Diabetic cardiomyopathy-associated dysfunction in spatially distinct mitochondrial subpopulations. *Am J Physiol Heart Circ Physiol,* 296**,** H359-69.
DAGHISTANI, H. M., RAJAB, B. S. & KITMITTO, A. 2019. Three-dimensional electron microscopy techniques for unravelling mitochondrial dysfunction in heart failure and identification of new pharmacological targets. *Br J Pharmacol,* 176**,** 4340-4359.
DAI, H., SINCLAIR, D. A., ELLIS, J. L. & STEEGBORN, C. 2018. Sirtuin activators and inhibitors: Promises, achievements, and challenges. *Pharmacol Ther,* 188**,** 140-154.
DAMASO, A. R., DA SILVEIRA CAMPOS, R. M., CARANTI, D. A., DE PIANO, A., FISBERG, M., FOSCHINI, D., DE LIMA SANCHES, P., TOCK, L., LEDERMAN, H. M., TUFIK, S. & DE MELLO, M. T. 2014. Aerobic plus resistance training was more effective in improving the visceral adiposity, metabolic profile and inflammatory markers than aerobic training in obese adolescents. *J Sports Sci,* 32**,** 1435-45.
DANIELS, A., LINZ, D., VAN BILSEN, M., RUTTEN, H., SADOWSKI, T., RUF, S., JURETSCHKE, H. P., NEUMANN-HAEFELIN, C., MUNTS, C., VAN DER VUSSE, G. J. & VAN NIEUWENHOVEN, F. A. 2012. Long-term severe diabetes only leads to mild cardiac diastolic dysfunction in Zucker diabetic fatty rats. *Eur J Heart Fail,* 14**,** 193-201.
DAVIES, K. M., DAUM, B., GOLD, V. A., MUHLEIP, A. W., BRANDT, T., BLUM, T. B., MILLS, D. J. & KUHLBRANDT, W. 2014. Visualization of ATP synthase dimers in mitochondria by electron cryo-tomography. *J Vis Exp***,** 51228.
DE BRITO, O. M. & SCORRANO, L. 2008. Mitofusin 2: a mitochondria-shaping protein with signaling roles beyond fusion. *Antioxid Redox Signal,* 10**,** 621-33.
DE CASTRO, U. G., DOS SANTOS, R. A., SILVA, M. E., DE LIMA, W. G., CAMPAGNOLE-SANTOS, M. J. & ALZAMORA, A. C. 2013. Age-dependent

effect of high-fructose and high-fat diets on lipid metabolism and lipid accumulation in liver and kidney of rats. *Lipids Health Dis,* 12**,** 136.

DE LAS FUENTES, L., WAGGONER, A. D., MOHAMMED, B. S., STEIN, R. I., MILLER, B. V., 3RD, FOSTER, G. D., WYATT, H. R., KLEIN, S. & DAVILA-ROMAN, V. G. 2009. Effect of moderate diet-induced weight loss and weight regain on cardiovascular structure and function. *J Am Coll Cardiol,* 54**,** 2376-81.

DE VOS, K. J., ALLAN, V. J., GRIERSON, A. J. & SHEETZ, M. P. 2005. Mitochondrial function and actin regulate dynamin-related protein 1-dependent mitochondrial fission. *Curr Biol,* 15**,** 678-83.

DEEDS, M. C., ANDERSON, J. M., ARMSTRONG, A. S., GASTINEAU, D. A., HIDDINGA, H. J., JAHANGIR, A., EBERHARDT, N. L. & KUDVA, Y. C. 2011. Single dose streptozotocin-induced diabetes: considerations for study design in islet transplantation models. *Lab Anim,* 45**,** 131-40.

DELETTRE, C., GRIFFOIN, J. M., KAPLAN, J., DOLLFUS, H., LORENZ, B., FAIVRE, L., LENAERS, G., BELENGUER, P. & HAMEL, C. P. 2001. Mutation spectrum and splicing variants in the OPA1 gene. *Hum Genet,* 109**,** 584-91.

DEMARIA, A. N., NEUMANN, A., SCHUBART, P. J., LEE, G. & MASON, D. T. 1979. Systematic correlation of cardiac chamber size and ventricular performance determined with echocardiography and alterations in heart rate in normal persons. *Am J Cardiol,* 43**,** 1-9.

DENK, W. & HORSTMANN, H. 2004. Serial block-face scanning electron microscopy to reconstruct three-dimensional tissue nanostructure. *PLoS Biol,* 2**,** e329.

DEPRE, C., YOUNG, M. E., YING, J., AHUJA, H. S., HAN, Q., GARZA, N., DAVIES, P. J. & TAEGTMEYER, H. 2000. Streptozotocin-induced changes in cardiac gene expression in the absence of severe contractile dysfunction. *J Mol Cell Cardiol,* 32**,** 985-96.

DI ANGELANTONIO, E., KAPTOGE, S., WORMSER, D., WILLEIT, P., BUTTERWORTH, A. S., BANSAL, N., O'KEEFFE, L. M., GAO, P., WOOD, A. M., BURGESS, S., FREITAG, D. F., PENNELLS, L., PETERS, S. A., HART, C. L., HAHEIM, L. L., GILLUM, R. F., NORDESTGAARD, B. G., PSATY, B. M., YEAP, B. B., KNUIMAN, M. W., NIETERT, P. J., KAUHANEN, J., SALONEN, J. T., KULLER, L. H., SIMONS, L. A., VAN DER SCHOUW, Y. T., BARRETT-CONNOR, E., SELMER, R., CRESPO, C. J., RODRIGUEZ, B., VERSCHUREN, W. M., SALOMAA, V., SVARDSUDD, K., VAN DER HARST, P., BJORKELUND, C., WILHELMSEN, L., WALLACE, R. B., BRENNER, H., AMOUYEL, P., BARR, E. L., ISO, H., ONAT, A., TREVISAN, M., D'AGOSTINO, R. B., SR., COOPER, C., KAVOUSI, M., WELIN, L., ROUSSEL, R., HU, F. B., SATO, S., DAVIDSON, K. W., HOWARD, B. V., LEENING, M. J., ROSENGREN, A., DORR, M., DEEG, D. J., KIECHL, S., STEHOUWER, C. D., NISSINEN, A., GIAMPAOLI, S., DONFRANCESCO, C., KROMHOUT, D., PRICE, J. F., PETERS, A., MEADE, T. W., CASIGLIA, E., LAWLOR, D. A., GALLACHER, J., NAGEL, D., FRANCO, O. H., ASSMANN, G., DAGENAIS, G. R., JUKEMA, J. W., SUNDSTROM, J., WOODWARD, M., BRUNNER, E. J., KHAW, K. T., WAREHAM, N. J., WHITSEL, E. A., NJOLSTAD, I., HEDBLAD, B., WASSERTHEIL-SMOLLER, S., ENGSTROM, G., ROSAMOND, W. D., SELVIN, E., SATTAR, N., THOMPSON, S. G. & DANESH, J. 2015. Association of Cardiometabolic Multimorbidity With Mortality. *JAMA,* 314**,** 52-60.

DIAZ, B., FUENTES-MERA, L., TOVAR, A., MONTIEL, T., MASSIEU, L., MARTINEZ-RODRIGUEZ, H. G. & CAMACHO, A. 2015. Saturated lipids decrease mitofusin 2

leading to endoplasmic reticulum stress activation and insulin resistance in hypothalamic cells. *Brain Res,* 1627**,** 80-9.
DING, H., JIANG, N., LIU, H., LIU, X., LIU, D., ZHAO, F., WEN, L., LIU, S., JI, L. L. & ZHANG, Y. 2010. Response of mitochondrial fusion and fission protein gene expression to exercise in rat skeletal muscle. *Biochim Biophys Acta,* 1800**,** 250-6.
DING, M., FENG, N., TANG, D., FENG, J., LI, Z., JIA, M., LIU, Z., GU, X., WANG, Y., FU, F. & PEI, J. 2018. Melatonin prevents Drp1-mediated mitochondrial fission in diabetic hearts through SIRT1-PGC1alpha pathway. *J Pineal Res,* 65**,** e12491.
DIVAN, A. & ROYDS, J. 2013. *Tools and techniques in biomolecular science,* Oxford, Oxford University Press.
DORN, G. W., 2ND 2016. Parkin-dependent mitophagy in the heart. *J Mol Cell Cardiol,* 95**,** 42-9.
DRAZNER, M. H. 2011. The progression of hypertensive heart disease. *Circulation,* 123**,** 327-34.
DU, J., ZHOU, Y., SU, X., YU, J. J., KHAN, S., JIANG, H., KIM, J., WOO, J., KIM, J. H., CHOI, B. H., HE, B., CHEN, W., ZHANG, S., CERIONE, R. A., AUWERX, J., HAO, Q. & LIN, H. 2011. Sirt5 Is an NAD-Dependent Protein Lysine Demalonylase and Desuccinylase*. *Science,* 334**,** 806-9.
DUMKE, C. L., MARK DAVIS, J., ANGELA MURPHY, E., NIEMAN, D. C., CARMICHAEL, M. D., QUINDRY, J. C., TRAVIS TRIPLETT, N., UTTER, A. C., GROSS GOWIN, S. J., HENSON, D. A., MCANULTY, S. R. & MCANULTY, L. S. 2009. Successive bouts of cycling stimulates genes associated with mitochondrial biogenesis. *Eur J Appl Physiol,* 107**,** 419-27.
DUNCAN, J. G., BHARADWAJ, K. G., FONG, J. L., MITRA, R., SAMBANDAM, N., COURTOIS, M. R., LAVINE, K. J., GOLDBERG, I. J. & KELLY, D. P. 2010. Rescue of cardiomyopathy in peroxisome proliferator-activated receptor-alpha transgenic mice by deletion of lipoprotein lipase identifies sources of cardiac lipids and peroxisome proliferator-activated receptor-alpha activators. *Circulation,* 121**,** 426-35.
DZEJA, P. P., BORTOLON, R., PEREZ-TERZIC, C., HOLMUHAMEDOV, E. L. & TERZIC, A. 2002. Energetic communication between mitochondria and nucleus directed by catalyzed phosphotransfer. *Proc Natl Acad Sci U S A,* 99**,** 10156-61.
EISINGER, K., LIEBISCH, G., SCHMITZ, G., ASLANIDIS, C., KRAUTBAUER, S. & BUECHLER, C. 2014. Lipidomic analysis of serum from high fat diet induced obese mice. *Int J Mol Sci,* 15**,** 2991-3002.
FANG, C. X., DONG, F., THOMAS, D. P., MA, H., HE, L. & REN, J. 2008. Hypertrophic cardiomyopathy in high-fat diet-induced obesity: role of suppression of forkhead transcription factor and atrophy gene transcription. *Am J Physiol Heart Circ Physiol,* 295**,** H1206-H1215.
FANG, Z. Y., PRINS, J. B. & MARWICK, T. H. 2004. Diabetic cardiomyopathy: evidence, mechanisms, and therapeutic implications. *Endocr Rev,* 25**,** 543-67.
FEALY, C. E., MULYA, A., LAI, N. & KIRWAN, J. P. 2014. Exercise training decreases activation of the mitochondrial fission protein dynamin-related protein-1 in insulin-resistant human skeletal muscle. *Journal of Applied Physiology,* 117**,** 239-245.
FENG, R., WANG, L., LI, Z., YANG, R., LIANG, Y., SUN, Y., YU, Q., GHARTEY-KWANSAH, G., SUN, Y., WU, Y., ZHANG, W., ZHOU, X., XU, M., BRYANT, J., YAN, G., ISAACS, W., MA, J. & XU, X. 2019. A systematic comparison of exercise training protocols on animal models of cardiovascular capacity. *Life Sci,* 217**,** 128-140.

FERNSTROM, M., TONKONOGI, M. & SAHLIN, K. 2004. Effects of acute and chronic endurance exercise on mitochondrial uncoupling in human skeletal muscle. *Journal of Physiology-London,* 554**,** 755-763.

FERREIRA, R., VITORINO, R., PADRAO, A. I., ESPADAS, G., MANCUSO, F. M., MOREIRA-GONCALVES, D., CASTRO-SOUSA, G., HENRIQUES-COELHO, T., OLIVEIRA, P. A., BARROS, A. S., DUARTE, J. A., SABIDO, E. & AMADO, F. 2014. Lifelong exercise training modulates cardiac mitochondrial phosphoproteome in rats. *J Proteome Res,* 13**,** 2045-55.

FINCK, B. N., LEHMAN, J. J., LEONE, T. C., WELCH, M. J., BENNETT, M. J., KOVACS, A., HAN, X., GROSS, R. W., KOZAK, R., LOPASCHUK, G. D. & KELLY, D. P. 2002. The cardiac phenotype induced by PPARalpha overexpression mimics that caused by diabetes mellitus. *J Clin Invest,* 109**,** 121-30.

FISCHER, F., GERTZ, M., SUENKEL, B., LAKSHMINARASIMHAN, M., SCHUTKOWSKI, M. & STEEGBORN, C. 2012. Sirt5 Deacylation Activities Show Differential Sensitivities to Nicotinamide Inhibition. *PLoS One.*

FRANKLIN, B. A., THOMPSON, P. D., AL-ZAITI, S. S., ALBERT, C. M., HIVERT, M. F., LEVINE, B. D., LOBELO, F., MADAN, K., SHARRIEF, A. Z., EIJSVOGELS, T. M. H., AMERICAN HEART ASSOCIATION PHYSICAL ACTIVITY COMMITTEE OF THE COUNCIL ON, L., CARDIOMETABOLIC, H., COUNCIL ON, C., STROKE, N., COUNCIL ON CLINICAL, C. & STROKE, C. 2020. Exercise-Related Acute Cardiovascular Events and Potential Deleterious Adaptations Following Long-Term Exercise Training: Placing the Risks Into Perspective-An Update: A Scientific Statement From the American Heart Association. *Circulation,* 141**,** e705-e736.

FRANZ, M. J., VANWORMER, J. J., CRAIN, A. L., BOUCHER, J. L., HISTON, T., CAPLAN, W., BOWMAN, J. D. & PRONK, N. P. 2007. Weight-loss outcomes: a systematic review and meta-analysis of weight-loss clinical trials with a minimum 1-year follow-up. *J Am Diet Assoc,* 107**,** 1755-67.

FREZZA, C., CIPOLAT, S., DE BRITO, O. M., MICARONI, M., BEZNOUSSENKO, G. V., RUDKA, T., BARTOLI, D., POLISHUCK, R. S., DANIAL, N. N., DE STROOPER, B. & SCORRANO, L. 2006. OPA1 controls apoptotic cristae remodeling independently from mitochondrial fusion. *Cell,* 126**,** 177-189.

FRIEDMAN, J. R., LACKNER, L. L., WEST, M., DIBENEDETTO, J. R., NUNNARI, J. & VOELTZ, G. K. 2011. ER tubules mark sites of mitochondrial division. *Science,* 334**,** 358-62.

FUJIOKA, H., TANDLER, B. & HOPPEL, C. L. 2012. Mitochondrial division in rat cardiomyocytes: an electron microscope study. *Anat Rec (Hoboken),* 295**,** 1455-61.

GAO, Q., WANG, X. M., YE, H. W., YU, Y., KANG, P. F., WANG, H. J., GUAN, S. D. & LI, Z. H. 2012. Changes in the expression of cardiac mitofusin-2 in different stages of diabetes in rats. *Mol Med Rep,* 6**,** 811-4.

GARDNER, D. G., SHOBACK, D. M. & GREENSPAN, F. S. 2011. *Greenspan's Basic & Clinical Endocrinology,* New York, McGraw-Hill Medical.

GENG, Y. Q., LI, T. T., LIU, X. Y., LI, Z. H. & FU, Y. C. 2011. SIRT1 and SIRT5 activity expression and behavioral responses to calorie restriction. *J Cell Biochem,* 112**,** 3755-61.

GERBER, L. K., ARONOW, B. J. & MATLIB, M. A. 2006. Activation of a novel long-chain free fatty acid generation and export system in mitochondria of diabetic rat hearts. *Am J Physiol Cell Physiol,* 291**,** C1198-207.

GIVVIMANI, S., VEERANKI, S., PUSHPAKUMAR, S., KUNDU, S., WINCHESTER, L., METREVELI, N. & TYAGI, S. 2015. Exercise Mitigates Aberrant Mitophagy and Cardiovascular Remodeling in Diabetes. *Faseb Journal,* 29.

GLEMBOTSKI, C. C. 2012. Roles for the sarco-/endoplasmic reticulum in cardiac myocyte contraction, protein synthesis, and protein quality control. *Physiology (Bethesda),* 27**,** 343-50.

GOLBIDI, S. & LAHER, I. 2012. Exercise and the cardiovascular system. *Cardiol Res Pract,* 2012**,** 210852.

GOLLMER, J., ZIRLIK, A. & BUGGER, H. 2020. Mitochondrial Mechanisms in Diabetic Cardiomyopathy. *Diabetes Metab J,* 44**,** 33-53.

GOMES, L. C. & SCORRANO, L. 2008. High levels of Fis1, a pro-fission mitochondrial protein, trigger autophagy. *Biochim Biophys Acta,* 1777**,** 860-6.

GONG, S., MIAO, Y. L., JIAO, G. Z., SUN, M. J., LI, H., LIN, J., LUO, M. J. & TAN, J. H. 2015. Dynamics and correlation of serum cortisol and corticosterone under different physiological or stressful conditions in mice. *PLoS One,* 10**,** e0117503.

GORDALIZA-ALAGUERO, I., CANTO, C. & ZORZANO, A. 2019. Metabolic implications of organelle-mitochondria communication. *EMBO Rep,* 20**,** e47928.

GREGORICH, Z. R., CHANG, Y. H. & GE, Y. 2014. Proteomics in heart failure: top-down or bottom-up? *Pflugers Arch,* 466**,** 1199-209.

GRIMM, M., HAAS, P., WILLIPINSKI-STAPELFELDT, B., ZIMMERMANN, W. H., RAU, T., PANTEL, K., WEYAND, M. & ESCHENHAGEN, T. 2005. Key role of myosin light chain (MLC) kinase-mediated MLC2a phosphorylation in the alpha 1-adrenergic positive inotropic effect in human atrium. *Cardiovasc Res,* 65**,** 211-20.

GUEDOUARI, H., DAIGLE, T., SCORRANO, L. & HEBERT-CHATELAIN, E. 2017. Sirtuin 5 protects mitochondria from fragmentation and degradation during starvation. *Biochim Biophys Acta Mol Cell Res,* 1864**,** 169-176.

GUO, S., HUANG, Y., ZHANG, Y., HUANG, H., HONG, S. & LIU, T. 2020. Impacts of exercise interventions on different diseases and organ functions in mice. *J Sport Health Sci,* 9**,** 53-73.

GUPTA, A. & KUMAR, A. 2014. Pros and cons of the proteomics. *Biomed J,* 37**,** 163-4.

GURTLER, A., KUNZ, N., GOMOLKA, M., HORNHARDT, S., FRIEDL, A. A., MCDONALD, K., KOHN, J. E. & POSCH, A. 2013. Stain-Free technology as a normalization tool in Western blot analysis. *Analytical Biochemistry,* 433**,** 105-111.

HA, H. & PAK, Y. 2005. Modulation of the caveolin-3 and Akt status in caveolae by insulin resistance in H9c2 cardiomyoblasts. *Exp Mol Med,* 37**,** 169-78.

HAFSTAD, A. D., LUND, J., HADLER-OLSEN, E., HOPER, A. C., LARSEN, T. S. & AASUM, E. 2013. High- and moderate-intensity training normalizes ventricular function and mechanoenergetics in mice with diet-induced obesity. *Diabetes,* 62**,** 2287-94.

HAGENAUER, M. H., PERRYMAN, J. I., LEE, T. M. & CARSKADON, M. A. 2009. Adolescent changes in the homeostatic and circadian regulation of sleep. *Dev Neurosci,* 31**,** 276-84.

HAN, X. J., LU, Y. F., LI, S. A., KAITSUKA, T., SATO, Y., TOMIZAWA, K., NAIRN, A. C., TAKEI, K., MATSUI, H. & MATSUSHITA, M. 2008. CaM kinase I alpha-induced phosphorylation of Drp1 regulates mitochondrial morphology. *J Cell Biol,* 182**,** 573-85.

HARE, J. L., HORDERN, M. D., LEANO, R., STANTON, T., PRINS, J. B. & MARWICK, T. H. 2011. Application of an exercise intervention on the evolution of diastolic dysfunction in patients with diabetes mellitus: efficacy and effectiveness. *Circ Heart Fail,* 4**,** 441-9.

HARIRI, N. & THIBAULT, L. 2010. High-fat diet-induced obesity in animal models. *Nutr Res Rev,* 23**,** 270-99.
HARJUTSALO, V., LAMMI, N., KARVONEN, M. & GROOP, P. H. 2010. Age at Onset of Type 1 Diabetes in Parents and Recurrence Risk in Offspring. *Diabetes,* 59**,** 210-214.
HATANO, A., OKADA, J., WASHIO, T., HISADA, T. & SUGIURA, S. 2015. Distinct Functional Roles of Cardiac Mitochondrial Subpopulations Revealed by a 3D Simulation Model. *Biophysical Journal,* 108**,** 2732-2739.
HEALTH SURVEY FOR ENGLAND. 2015. *Health, social care and lifestyles* [Online]. NHS. Available: http://www.content.digital.nhs.uk/catalogue/PUB22610 [Accessed].
HEALTH SURVEY FOR ENGLAND 2018. Adult and child overweight and obesity. *NHS digital*.
HERRERO, P., PETERSON, L. R., MCGILL, J. B., MATTHEW, S., LESNIAK, D., DENCE, C. & GROPLER, R. J. 2006. Increased myocardial fatty acid metabolism in patients with type 1 diabetes mellitus. *J Am Coll Cardiol,* 47**,** 598-604.
HESCHELER, J., MEYER, R., PLANT, S., KRAUTWURST, D., ROSENTHAL, W. & SCHULTZ, G. 1991. Morphological, biochemical, and electrophysiological characterization of a clonal cell (H9c2) line from rat heart. *Circ Res,* 69**,** 1476-86.
HIGA TS, SPINOLA AV, FONSECA-ALANIZ MH & FS, E. 2014. Comparison between cafeteria and high-fat diets in the induction of metabolic dysfunction in mice. *Int J Physiol Pathophysiol Pharmacol*.
HIGDON, R. & KOLKER, E. 2007. A predictive model for identifying proteins by a single peptide match. *Bioinformatics,* 23**,** 277-80.
HIRSCHEY, M. D. & ZHAO, Y. 2015. Metabolic Regulation by Lysine Malonylation, Succinylation, and Glutarylation. *Mol Cell Proteomics,* 14**,** 2308-15.
HOLLANDER, J. M., THAPA, D. & SHEPHERD, D. L. 2014. Physiological and structural differences in spatially distinct subpopulations of cardiac mitochondria: influence of cardiac pathologies. *Am J Physiol Heart Circ Physiol,* 307**,** H1-14.
HOLMUHAMEDOV, E. L., OBERLIN, A., SHORT, K., TERZIC, A. & JAHANGIR, A. 2012. Cardiac subsarcolemmal and interfibrillar mitochondria display distinct responsiveness to protection by diazoxide. *PLoS One,* 7**,** e44667.
HOOD, D. A. 2001. Invited Review: contractile activity-induced mitochondrial biogenesis in skeletal muscle. *J Appl Physiol (1985),* 90**,** 1137-57.
HOOD, D. A. 2009. Mechanisms of exercise-induced mitochondrial biogenesis in skeletal muscle. *Appl Physiol Nutr Metab,* 34**,** 465-72.
HOSHINO, A., MITA, Y., OKAWA, Y., ARIYOSHI, M., IWAI-KANAI, E., UEYAMA, T., IKEDA, K., OGATA, T. & MATOBA, S. 2013. Cytosolic p53 inhibits Parkin-mediated mitophagy and promotes mitochondrial dysfunction in the mouse heart. *Nat Commun,* 4**,** 2308.
HOUTKOOPER, R. H., PIRINEN, E. & AUWERX, J. 2012. Sirtuins as regulators of metabolism and healthspan. *Nature Reviews Molecular Cell Biology,* 13**,** 225-238.
HOW, O. J., AASUM, E., SEVERSON, D. L., CHAN, W. Y., ESSOP, M. F. & LARSEN, T. S. 2006. Increased myocardial oxygen consumption reduces cardiac efficiency in diabetic mice. *Diabetes,* 55**,** 466-73.
HSU, C. C., OU, H. C. & LEE, S. D. 2010. Effects of exercise training on cardiac mitochondrial apoptosis in ovariectomized rats. *Faseb Journal,* 24.
HSU, H. C., CHEN, C. Y., LEE, B. C. & CHEN, M. F. 2016. High-fat diet induces cardiomyocyte apoptosis via the inhibition of autophagy. *Eur J Nutr,* 55**,** 2245-54.
HU, J., JING, H. & LIN, H. 2014. Sirtuin inhibitors as anticancer agents. *Future Med Chem,* 6**,** 945-66.

HU, L., DING, M., TANG, D., GAO, E., LI, C., WANG, K., QI, B., QIU, J., ZHAO, H., CHANG, P., FU, F. & LI, Y. 2019. Targeting mitochondrial dynamics by regulating Mfn2 for therapeutic intervention in diabetic cardiomyopathy. *Theranostics,* 9**,** 3687-3706.

HU, S., WANG, L., YANG, D., LI, L., TOGO, J., WU, Y., LIU, Q., LI, B., LI, M., WANG, G., ZHANG, X., NIU, C., LI, J., XU, Y., COUPER, E., WHITTINGTON-DAVIES, A., MAZIDI, M., LUO, L., WANG, S., DOUGLAS, A. & SPEAKMAN, J. R. 2018. Dietary Fat, but Not Protein or Carbohydrate, Regulates Energy Intake and Causes Adiposity in Mice. *Cell Metab,* 28**,** 415-431 e4.

HUANG, B., BATES, M. & ZHUANG, X. 2009. Super-resolution fluorescence microscopy. *Annu Rev Biochem,* 78**,** 993-1016.

HWANG, E. S. & SONG, S. B. 2017. Nicotinamide is an inhibitor of SIRT1 in vitro, but can be a stimulator in cells. *Cell Mol Life Sci,* 74**,** 3347-3362.

HWANG, S. J. & KIM, W. 2013. Mitochondrial dynamics in the heart as a novel therapeutic target for cardioprotection. *Chonnam Med J,* 49**,** 101-7.

IKEDA, H. 1994. KK mouse. *Diabetes Res Clin Pract,* 24 Suppl**,** S313-6.

IKONOMIDIS, I., PAPADAVID, E., MAKAVOS, G., ANDREADOU, I., VAROUDI, M., GRAVANIS, K., THEODOROPOULOS, K., PAVLIDIS, G., TRIANTAFYLLIDI, H., MOUTSATSOU, P., PANAGIOTOU, C., PARISSIS, J., ILIODROMITIS, E., LEKAKIS, J. & RIGOPOULOS, D. 2017. Lowering Interleukin-12 Activity Improves Myocardial and Vascular Function Compared With Tumor Necrosis Factor-a Antagonism or Cyclosporine in Psoriasis. *Circ Cardiovasc Imaging,* 10.

INTERNATIONAL DIABETES FEDERATION 2015.

ISHIHARA, N., EURA, Y. & MIHARA, K. 2004. Mitofusin 1 and 2 play distinct roles in mitochondrial fusion reactions via GTPase activity. *J Cell Sci,* 117**,** 6535-46.

ISHIHARA, N., FUJITA, Y., OKA, T. & MIHARA, K. 2006. Regulation of mitochondrial morphology through proteolytic cleavage of OPA1. *EMBO J.*

JANARDHAN, A., CHEN, J. & CRAWFORD, P. A. 2011. Altered systemic ketone body metabolism in advanced heart failure. *Tex Heart Inst J,* 38**,** 533-8.

JASTROCH, M. 2017. Uncoupling protein 1 controls reactive oxygen species in brown adipose tissue. *Proc Natl Acad Sci U S A,* 114**,** 7744-7746.

JEDERSTROM, G., GRASJO, NORDIN, A., SJOHOLM, I. & ANDERSSON, A. 2005. Blood glucose-lowering activity of a hyaluronan-insulin complex after oral administration to rats with diabetes. *Diabetes Technol Ther,* 7**,** 948-57.

JEPPESEN, J., FACCHINI, F. S. & REAVEN, G. M. 1998. Individuals with high total cholesterol/HDL cholesterol ratios are insulin resistant. *J Intern Med,* 243**,** 293-8.

JEPPESEN, T. D., SCHWARTZ, M., OLSEN, D. B., WIBRAND, F., KRAG, T., DUNO, M., HAUERSLEV, S. & VISSING, J. 2006. Aerobic training is safe and improves exercise capacity in patients with mitochondrial myopathy. *Brain,* 129**,** 3402-3412.

JHENG, H. F., TSAI, P. J., GUO, S. M., KUO, L. H., CHANG, C. S., SU, I. J., CHANG, C. R. & TSAI, Y. S. 2012. Mitochondrial fission contributes to mitochondrial dysfunction and insulin resistance in skeletal muscle. *Mol Cell Biol,* 32**,** 309-19.

JIANG, H. K., WANG, Y. H., SUN, L., HE, X., ZHAO, M., FENG, Z. H., YU, X. J. & ZANG, W. J. 2014. Aerobic interval training attenuates mitochondrial dysfunction in rats post-myocardial infarction: roles of mitochondrial network dynamics. *Int J Mol Sci,* 15**,** 5304-22.

JIN, S. M. & YOULE, R. J. 2012. PINK1- and Parkin-mediated mitophagy at a glance.

JU, J. S., JEON, S. I., PARK, J. Y., LEE, J. Y., LEE, S. C., CHO, K. J. & JEONG, J. M. 2016. Autophagy plays a role in skeletal muscle mitochondrial biogenesis in an endurance exercise-trained condition. *J Physiol Sci,* 66**,** 417-30.

JULLIG, M., CHEN, X., MIDDLEDITCH, M. J., VAZHOOR, G., HICKEY, A. J., GONG, D., LU, J., ZHANG, S., PHILLIPS, A. R. & COOPER, G. J. 2010. Illuminating the molecular basis of diabetic arteriopathy: a proteomic comparison of aortic tissue from diabetic and healthy rats. *Proteomics,* 10**,** 3367-78.

JULLIG, M., HICKEY, A. J., MIDDLEDITCH, M. J., CROSSMAN, D. J., LEE, S. C. & COOPER, G. J. 2007. Characterization of proteomic changes in cardiac mitochondria in streptozotocin-diabetic rats using iTRAQ isobaric tags. *Proteomics Clin Appl,* 1**,** 565-76.

KALKHORAN, S. B., HERNANDEZ-RESENDIZ, S., ONG, S. G., RAMACHANDRA, C. J. A. & HAUSENLOY, D. J. 2020. Mitochondrial shaping proteins as novel treatment targets for cardiomyopathies. *Cond Med,* 3**,** 216-226.

KANAMARU, Y., SEKINE, S., ICHIJO, H. & TAKEDA, K. 2012. The phosphorylation-dependent regulation of mitochondrial proteins in stress responses. *J Signal Transduct,* 2012**,** 931215.

KANG, K. W., KIM, O. S., CHIN, J. Y., KIM, W. H., PARK, S. H., CHOI, Y. J., SHIN, J. H., JUNG, K. T., LIM, D. S. & LEE, S. K. 2015. Diastolic Dysfunction Induced by a High-Fat Diet Is Associated with Mitochondrial Abnormality and Adenosine Triphosphate Levels in Rats. *Endocrinol Metab (Seoul),* 30**,** 557-68.

KANG, Y. S., SEONG, D., KIM, J. C. & KIM, S. H. 2020. Low-Intensity Exercise Training Additionally Increases Mitochondrial Dynamics Caused by High-Fat Diet (HFD) but Has No Additional Effect on Mitochondrial Biogenesis in Fast-Twitch Muscle by HFD. *Int J Environ Res Public Health,* 17.

KAPLAN, M. L., CHESLOW, Y., VIKSTROM, K., MALHOTRA, A., GEENEN, D. L., NAKOUZI, A., LEINWAND, L. A. & BUTTRICK, P. M. 1994. Cardiac adaptations to chronic exercise in mice. *Am J Physiol,* 267**,** H1167-73.

KARBOWSKA, J., KOCHAN, Z. & SMOLENSKI, R. T. 2003. Peroxisome proliferator-activated receptor alpha is downregulated in the failing human heart. *Cell Mol Biol Lett,* 8**,** 49-53.

KARBOWSKI, M., NORRIS, K. L., CLELAND, M. M., JEONG, S. Y. & YOULE, R. J. 2006. Role of Bax and Bak in mitochondrial morphogenesis. *Nature,* 443**,** 658-62.

KARIMIAN, S., STEIN, J., BAUER, B. & TEUPE, C. 2017. Improvement of impaired diastolic left ventricular function after diet-induced weight reduction in severe obesity. *Diabetes Metab Syndr Obes,* 10**,** 19-25.

KATO, R., MORI, C., KITAZATO, K., ARATA, S., OBAMA, T., MORI, M., TAKAHASHI, K., AIUCHI, T., TAKANO, T. & ITABE, H. 2009. Transient increase in plasma oxidized LDL during the progression of atherosclerosis in apolipoprotein E knockout mice. *Arterioscler Thromb Vasc Biol,* 29**,** 33-9.

KAVAZIS, A. N., MCCLUNG, J. M., HOOD, D. A. & POWERS, S. K. 2008. Exercise induces a cardiac mitochondrial phenotype that resists apoptotic stimuli. *Am J Physiol Heart Circ Physiol,* 294**,** H928-35.

KELLEY, D. E., HE, J., MENSHIKOVA, E. V. & RITOV, V. B. 2002. Dysfunction of mitochondria in human skeletal muscle in type 2 diabetes. *Diabetes,* 51**,** 2944-50.

KEMI, O. J., LOENNECHEN, J. P., WISLOFF, U. & ELLINGSEN, O. 2002. Intensity-controlled treadmill running in mice: cardiac and skeletal muscle hypertrophy. *J Appl Physiol (1985),* 93**,** 1301-9.

KENCHAIAH, S., EVANS, J. C., LEVY, D., WILSON, P. W. F., BENJAMIN, E. J., LARSON, M. G., KANNEL, W. B. & VASAN, R. S. 2009. Obesity and the Risk of Heart Failure. *http://dx.doi.org/10.1056/NEJMoa020245*.

KERCMAR, J., TOBET, S. A. & MAJDIC, G. 2014. Social isolation during puberty affects female sexual behavior in mice. *Front Behav Neurosci,* 8**,** 337.

KERSTEN, S. 2008. Peroxisome proliferator activated receptors and lipoprotein metabolism. *PPAR Res,* 2008**,** 132960.
KERSTEN, S. 2014. Integrated physiology and systems biology of PPARalpha. *Mol Metab,* 3**,** 354-71.
KIM, J., PARK, Y. J., JANG, Y. & KWON, Y. H. 2011. AMPK activation inhibits apoptosis and tau hyperphosphorylation mediated by palmitate in SH-SY5Y cells. *Brain Res,* 1418**,** 42-51.
KIM, S. C., SPRUNG, R., CHEN, Y., XU, Y., BALL, H., PEI, J., CHENG, T., KHO, Y., XIAO, H., XIAO, L., GRISHIN, N. V., WHITE, M., YANG, X. J. & ZHAO, Y. 2006. Substrate and functional diversity of lysine acetylation revealed by a proteomics survey. *Mol Cell,* 23**,** 607-18.
KIMES, B. W. & BRANDT, B. L. 1976. Properties of a clonal muscle cell line from rat heart. *Exp Cell Res,* 98**,** 367-81.
KING, A. J. F. 2012. The use of animal models in diabetes research. *British Journal of Pharmacology,* 166**,** 877-894.
KITABCHI, A. E., UMPIERREZ, G. E., MILES, J. M. & FISHER, J. N. 2009. Hyperglycemic crises in adult patients with diabetes. *Diabetes Care,* 32**,** 1335-43.
KONOPKA, A. R., SUER, M. K., WOLFF, C. A. & HARBER, M. P. 2014. Markers of human skeletal muscle mitochondrial biogenesis and quality control: effects of age and aerobic exercise training. *J Gerontol A Biol Sci Med Sci,* 69**,** 371-8.
KOSHIBA, T., DETMER, S. A., KAISER, J. T., CHEN, H., MCCAFFERY, J. M. & CHAN, D. C. 2004. Structural basis of mitochondrial tethering by mitofusin complexes. *Science,* 305**,** 858-62.
KOSTER, A., STENHOLM, S., ALLEY, D. E., KIM, L. J., SIMONSICK, E. M., KANAYA, A. M., VISSER, M., HOUSTON, D. K., NICKLAS, B. J., TYLAVSKY, F. A., SATTERFIELD, S., GOODPASTER, B. H., FERRUCCI, L., HARRIS, T. B. & HEALTH, A. B. C. S. 2010. Body fat distribution and inflammation among obese older adults with and without metabolic syndrome. *Obesity (Silver Spring),* 18**,** 2354-61.
KOTHARI, V., LUO, Y., TORNABENE, T., O'NEILL, A. M., GREENE, M. W., GEETHA, T. & BABU, J. R. 2017. High fat diet induces brain insulin resistance and cognitive impairment in mice. *Biochim Biophys Acta Mol Basis Dis,* 1863**,** 499-508.
KOYANO, F., OKATSU, K., KOSAKO, H., TAMURA, Y., GO, E., KIMURA, M., KIMURA, Y., TSUCHIYA, H., YOSHIHARA, H., HIROKAWA, T., ENDO, T., FON, E. A., TREMPE, J. F., SAEKI, Y., TANAKA, K. & MATSUDA, N. 2014. Ubiquitin is phosphorylated by PINK1 to activate parkin. *Nature,* 510**,** 162-6.
KREMER, J. R., MASTRONARDE, D. N. & MCINTOSH, J. R. 1996. Computer visualization of three-dimensional image data using IMOD. *J Struct Biol,* 116**,** 71-6.
KUBLI, D. A., QUINSAY, M. N. & GUSTAFSSON, A. B. 2013. Parkin deficiency results in accumulation of abnormal mitochondria in aging myocytes. *Commun Integr Biol,* 6**,** e24511.
KUZNETSOV, A. V., JAVADOV, S., SICKINGER, S., FROTSCHNIG, S. & GRIMM, M. 2015. H9c2 and HL-1 cells demonstrate distinct features of energy metabolism, mitochondrial function and sensitivity to hypoxia-reoxygenation. *Biochim Biophys Acta,* 1853**,** 276-84.
LAKSHMANAN, A. P., HARIMA, M., SUZUKI, K., SOETIKNO, V., NAGATA, M., NAKAMURA, T., TAKAHASHI, T., SONE, H., KAWACHI, H. & WATANABE, K. 2013. The hyperglycemia stimulated myocardial endoplasmic reticulum (ER) stress contributes to diabetic cardiomyopathy in the transgenic non-obese type 2

diabetic rats: a differential role of unfolded protein response (UPR) signaling proteins. *Int J Biochem Cell Biol,* 45**,** 438-47.

LANG, A., ANAND, R., ALTINOLUK-HAMBUCHEN, S., EZZAHOINI, H., STEFANSKI, A., IRAM, A., BERGMANN, L., URBACH, J., BOHLER, P., HANSEL, J., FRANKE, M., STUHLER, K., KRUTMANN, J., SCHELLER, J., STORK, B., REICHERT, A. S. & PIEKORZ, R. P. 2017. SIRT4 interacts with OPA1 and regulates mitochondrial quality control and mitophagy. *Aging (Albany NY),* 9**,** 2163-2189.

LANZA, I. R. & NAIR, K. S. 2010. Mitochondrial metabolic function assessed in vivo and in vitro. *Curr Opin Clin Nutr Metab Care,* 13**,** 511-7.

LASHIN, O. M., SZWEDA, P. A., SZWEDA, L. I. & ROMANI, A. M. 2006. Decreased complex II respiration and HNE-modified SDH subunit in diabetic heart. *Free Radic Biol Med,* 40**,** 886-96.

LAU, D. C. W., DOUKETIS, J. D., MORRISON, K. M., HRAMIAK, I. M., SHARMA, A. M., UR, E. & PANEL, F. M. O. T. O. C. C. P. G. E. 2007. 2006 Canadian clinical practice guidelines on the management and prevention of obesity in adults and children [summary].

LAUER, M. S., ANDERSON, K. M., KANNEL, W. B. & LEVY, D. 1991. The impact of obesity on left ventricular mass and geometry. The Framingham Heart Study. *Jama,* 266**,** 231-6.

LAUSCHKE, J. & MAISCH, B. 2009. Athlete's heart or hypertrophic cardiomyopathy? *Clin Res Cardiol,* 98**,** 80-8.

LAVIE, C. J., MILANI, R. V. & VENTURA, H. O. 2009. Obesity and Cardiovascular Disease.

LEACH, R. N., DESAI, J. C. & ORCHARD, C. H. 2005. Effect of cytoskeleton disruptors on L-type Ca channel distribution in rat ventricular myocytes. *Cell Calcium,* 38**,** 515-26.

LEBOUCHER, G. P., TSAI, Y. C., YANG, M., SHAW, K. C., ZHOU, M., VEENSTRA, T. D., GLICKMAN, M. H. & WEISSMAN, A. M. 2012. Stress-induced phosphorylation and proteasomal degradation of mitofusin 2 facilitates mitochondrial fragmentation and apoptosis. *Mol Cell,* 47**,** 547-57.

LEE, B. A. & OH, D. J. 2016. The effects of long-term aerobic exercise on cardiac structure, stroke volume of the left ventricle, and cardiac output. *J Exerc Rehabil,* 12**,** 37-41.

LEE, H., SMITH, S. B. & YOON, Y. 2017a. The short variant of the mitochondrial dynamin OPA1 maintains mitochondrial energetics and cristae structure. *J Biol Chem,* 292**,** 7115-7130.

LEE, J. H., COLLEGE OF PHARMACY AND RESEARCH INSTITUTE OF PHARMACEUTICAL SCIENCES, S. N. U., SEOUL, GASTROENTEROLOGY AND METABOLISM PRODUCTS DIVISION, P. S. B., KOREA FOOD & DRUG ADMINISTRATION, SEOUL, SOUTH KOREA, YANG, S. H., COLLEGE OF PHARMACY AND RESEARCH INSTITUTE OF PHARMACEUTICAL SCIENCES, S. N. U., SEOUL, OH, J. M., COLLEGE OF PHARMACY AND RESEARCH INSTITUTE OF PHARMACEUTICAL SCIENCES, S. N. U., SEOUL, LEE, M. G. & COLLEGE OF PHARMACY AND RESEARCH INSTITUTE OF PHARMACEUTICAL SCIENCES, S. N. U., SEOUL 2010. Pharmacokinetics of drugs in rats with diabetes mellitus induced by alloxan or streptozocin: comparison with those in patients with type I diabetes mellitus. *Journal of Pharmacy and Pharmacology,* 62**,** 1-23.

LEE, L., SEAGER, R., NAKAMURA, Y., WILKINSON, K. A. & HENLEY, J. M. 2019. Parkin-mediated ubiquitination contributes to the constitutive turnover of mitochondrial fission factor (Mff). *PLoS One,* 14**,** e0213116.

LEE, M. Y., SHIM, M. S., KIM, B. H., HONG, S. W., CHOI, R., LEE, E. Y., NAM, S. M., KIM, G. W., SHIN, J. Y., SHIN, Y. G. & CHUNG, C. H. 2011. Effects of spironolactone and losartan on diabetic nephropathy in a type 2 diabetic rat model. *Diabetes Metab J,* 35**,** 130-7.

LEE, T. W., BAI, K. J., LEE, T. I., CHAO, T. F., KAO, Y. H. & CHEN, Y. J. 2017b. PPARs modulate cardiac metabolism and mitochondrial function in diabetes. *J Biomed Sci,* 24**,** 5.

LEE, T. W., LEE, T. I., CHANG, C. J., LIEN, G. S., KAO, Y. H., CHAO, T. F. & CHEN, Y. J. 2015. Potential of vitamin D in treating diabetic cardiomyopathy. *Nutr Res,* 35**,** 269-79.

LEITER, E. H. 2009. Selecting the "right" mouse model for metabolic syndrome and type 2 diabetes research. *Methods Mol Biol,* 560**,** 1-17.

LESNEFSKY, E. J., GUDZ, T. I., MOGHADDAS, S., MIGITA, C. T., IKEDA-SAITO, M., TURKALY, P. J. & HOPPEL, C. L. 2001. Aging decreases electron transport complex III activity in heart interfibrillar mitochondria by alteration of the cytochrome c binding site. *J Mol Cell Cardiol,* 33**,** 37-47.

LI, H., MIAO, W., MA, J., XV, Z., BO, H., LI, J., ZHANG, Y. & JI, L. L. 2016. Acute Exercise-Induced Mitochondrial Stress Triggers an Inflammatory Response in the Myocardium via NLRP3 Inflammasome Activation with Mitophagy. *Oxid Med Cell Longev,* 2016**,** 1987149.

LI, J., WANG, Y., WANG, Y., WEN, X., MA, X. N., CHEN, W., HUANG, F., KOU, J., QI, L. W., LIU, B. & LIU, K. 2015. Pharmacological activation of AMPK prevents Drp1-mediated mitochondrial fission and alleviates endoplasmic reticulum stress-associated endothelial dysfunction. *J Mol Cell Cardiol,* 86**,** 62-74.

LI, S. Y., YANG, X., CEYLAN-ISIK, A. F., DU, M., SREEJAYAN, N. & REN, J. 2006. Cardiac contractile dysfunction in Lep/Lep obesity is accompanied by NADPH oxidase activation, oxidative modification of sarco(endo)plasmic reticulum Ca2+-ATPase and myosin heavy chain isozyme switch. *Diabetologia,* 49**,** 1434-46.

LI, W., YANG, Y., LI, Y., ZHAO, Y. & JIANG, H. 2019. Sirt5 Attenuates Cisplatin-Induced Acute Kidney Injury through Regulation of Nrf2/HO-1 and Bcl-2. *Biomed Res Int,* 2019**,** 4745132.

LI, Z. H., ZHANG, T., DAI, H. Y., LIU, G. H., WANG, H. B., SUN, Y. Y., ZHANG, Y. & GE, Z. M. 2010. Endoplasmic reticulum stress is involved in myocardial apoptosis of streptozocin-induced diabetic rats (Retraction of vol 196, pg 565, 2008). *Journal of Endocrinology,* 207**,** 123-123.

LIN, H. Y., WENG, S. W., CHANG, Y. H., SU, Y. J., CHANG, C. M., TSAI, C. J., SHEN, F. C., CHUANG, J. H., LIN, T. K., LIOU, C. W., LIN, C. Y. & WANG, P. W. 2018. The Causal Role of Mitochondrial Dynamics in Regulating Insulin Resistance in Diabetes: Link through Mitochondrial Reactive Oxygen Species. *Oxid Med Cell Longev,* 2018**,** 7514383.

LINDSTROM, P. 2007. The physiology of obese-hyperglycemic mice [ob/ob mice]. *ScientificWorldJournal,* 7**,** 666-85.

LIONETTI, L., MOLLICA, M. P., DONIZZETTI, I., GIFUNI, G., SICA, R., PIGNALOSA, A., CAVALIERE, G., GAITA, M., DE FILIPPO, C., ZORZANO, A. & PUTTI, R. 2014. High-Lard and High-Fish-Oil Diets Differ in Their Effects on Function and Dynamic Behaviour of Rat Hepatic Mitochondria. *Plos One,* 9.

LITTLE, J. P., SAFDAR, A., WILKIN, G. P., TARNOPOLSKY, M. A. & GIBALA, M. J. 2010. A practical model of low-volume high-intensity interval training induces mitochondrial biogenesis in human skeletal muscle: potential mechanisms. *J Physiol,* 588**,** 1011-22.

LITTLEJOHNS, PHILIPPE PASDOIS, SIMON DUGGAN, ANDREW R. BOND, KATE HEESOM, CHRISTOPHER L. JACKSON, GIANNI D. ANGELINI, ANDREW P. HALESTRAP & SULEIMAN, M.-S. 2014. Hearts from Mice Fed a Non-Obesogenic High-Fat Diet Exhibit Changes in Their Oxidative State, Calcium and Mitochondria in Parallel with Increased Susceptibility to Reperfusion Injury. *plos one*.

LIU, B., CHE, W., ZHENG, C., LIU, W., WEN, J., FU, H., TANG, K., ZHANG, J. & XU, Y. 2013. SIRT5: a safeguard against oxidative stress-induced apoptosis in cardiomyocytes. *Cell Physiol Biochem,* 32**,** 1050-9.

LIU, C.-Y., CHANG, C.-W., LEE, H.-C., CHEN, Y.-J., TSAI, T.-H., CHIAU, J.-S. C., WANG, T.-E., TSAI, M.-C., YEUNG, C.-Y. & SHIH, S.-C. 2016. Metabolic Damage Presents Differently in Young and Early-Aged C57BL/6 Mice Fed a High-Fat Diet. *International Journal of Gerontology,* 10**,** 105-111.

LIU, Q., WANG, S. & CAI, L. 2014. Diabetic cardiomyopathy and its mechanisms: Role of oxidative stress and damage. *J Diabetes Investig,* 5**,** 623-34.

LIU, R. & CHAN, D. C. 2015. The mitochondrial fission receptor Mff selectively recruits oligomerized Drp1. *Mol Biol Cell,* 26**,** 4466-77.

LIU, X., TAKEDA, N. & DHALLA, N. S. 1997. Myosin light-chain phosphorylation in diabetic cardiomyopathy in rats. *Metabolism,* 46**,** 71-5.

LO, K. A., LABADORF, A., KENNEDY, N. J., HAN, M. S., YAP, Y. S., MATTHEWS, B., XIN, X., SUN, L., DAVIS, R. J., LODISH, H. F. & FRAENKEL, E. 2013. Analysis of in vitro insulin-resistance models and their physiological relevance to in vivo diet-induced adipose insulin resistance. *Cell Rep,* 5**,** 259-70.

LOSON, O. C., SONG, Z., CHEN, H. & CHAN, D. C. 2013. Fis1, Mff, MiD49, and MiD51 mediate Drp1 recruitment in mitochondrial fission. *Mol Biol Cell,* 24**,** 659-67.

LOUWE, M. C., VAN DER HOORN, J. W., VAN DEN BERG, S. A., JUKEMA, J. W., ROMIJN, J. A., VAN DIJK, K. W., RENSEN, P. C., SMIT, J. W. & STEENDIJK, P. 2012. Gender-dependent effects of high-fat lard diet on cardiac function in C57Bl/6J mice. *Appl Physiol Nutr Metab,* 37**,** 214-24.

LU, X., THAI, P. N., LU, S., PU, J. & BERS, D. M. 2019. Intrafibrillar and perinuclear mitochondrial heterogeneity in adult cardiac myocytes. *J Mol Cell Cardiol,* 136**,** 72-84.

LUCAS, S., TARONT, S., MAGNAN, C., FAUCONNIER, L., DELACRE, M., MACIA, L., DELANOYE, A., VERWAERDE, C., SPRIET, C., SAULE, P., GOORMACHTIGH, G., HELIOT, L., KTORZA, A., MOVASSAT, J., POLAKOWSKA, R., AURIAULT, C., POULAIN-GODEFROY, O., DI SANTO, J., FROGUEL, P. & WOLOWCZUK, I. 2012. Interleukin-7 regulates adipose tissue mass and insulin sensitivity in high-fat diet-fed mice through lymphocyte-dependent and independent mechanisms. *PLoS One,* 7**,** e40351.

LUKYANENKO, V., CHIKANDO, A. & LEDERER, W. J. 2009. Mitochondria in cardiomyocyte Ca2+ signaling. *Int J Biochem Cell Biol,* 41**,** 1957-71.

LUMINI, J. A., MAGALHAES, J., OLIVEIRA, P. J. & ASCENSAO, A. 2008. Beneficial effects of exercise on muscle mitochondrial function in diabetes mellitus. *Sports Med,* 38**,** 735-50.

LUPTAK, I., SVERDLOV, A. L., PANAGIA, M., QIN, F., PIMENTEL, D. R., CROTEAU, D., SIWIK, D. A., INGWALL, J. S., BACHSCHMID, M. M., BALSCHI, J. A. &

COLUCCI, W. S. 2018. Decreased ATP production and myocardial contractile reserve in metabolic heart disease. *J Mol Cell Cardiol,* 116**,** 106-114.
MADALA, M. C., FRANKLIN, B. A., CHEN, A. Y., BERMAN, A. D., ROE, M. T., PETERSON, E. D., OHMAN, E. M., SMITH, S. C., JR., GIBLER, W. B., MCCULLOUGH, P. A. & INVESTIGATORS, C. 2008. Obesity and age of first non-ST-segment elevation myocardial infarction. *J Am Coll Cardiol,* 52**,** 979-85.
MAILLOUX, R. J. 2015. Teaching the fundamentals of electron transfer reactions in mitochondria and the production and detection of reactive oxygen species. *Redox Biol,* 4**,** 381-98.
MAILLOUX, R. J. & HARPER, M. E. 2011. Uncoupling proteins and the control of mitochondrial reactive oxygen species production. *Free Radic Biol Med,* 51**,** 1106-15.
MAKHLOUF, L., DUVIVIER-KALI, V. F., BONNER-WEIR, S., DIEPERINK, H., WEIR, G. C. & SAYEGH, M. H. 2003. Importance of hyperglycemia on the primary function of allogeneic islet transplants. *Transplantation,* 76**,** 657-64.
MAKINO, A., SCOTT, B. T. & DILLMANN, W. H. 2010. Mitochondrial fragmentation and superoxide anion production in coronary endothelial cells from a mouse model of type 1 diabetes. *Diabetologia,* 53**,** 1783-94.
MAKINO, A., SUAREZ, J., GAWLOWSKI, T., HAN, W., WANG, H., SCOTT, B. T. & DILLMANN, W. H. 2011. Regulation of mitochondrial morphology and function by O-GlcNAcylation in neonatal cardiac myocytes. *Am J Physiol Regul Integr Comp Physiol,* 300**,** R1296-302.
MARCIL, M., BOURDUAS, K., ASCAH, A. & BURELLE, Y. 2006. Exercise training induces respiratory substrate-specific decrease in Ca2+-induced permeability transition pore opening in heart mitochondria. *Am J Physiol Heart Circ Physiol,* 290**,** H1549-57.
MARKS, A. R. 2003. Calcium and the heart: a question of life and death. *J Clin Invest,* 111**,** 597-600.
MATHIAS, R. A., GRECO, T. M., OBERSTEIN, A., BUDAYEVA, H. G., CHAKRABARTI, R., ROWLAND, E. A., KANG, Y., SHENK, T. & CRISTEA, I. M. 2014. Sirtuin 4 is a lipoamidase regulating pyruvate dehydrogenase complex activity. *Cell,* 159**,** 1615-25.
MAURY, E., EHALA-ALEKSEJEV, K., GUIOT, Y., DETRY, R., VANDENHOOFT, A. & BRICHARD, S. M. 2007. Adipokines oversecreted by omental adipose tissue in human obesity. *Am J Physiol Endocrinol Metab,* 293**,** E656-65.
MAYER, C. M. & BELSHAM, D. D. 2010. Palmitate attenuates insulin signaling and induces endoplasmic reticulum stress and apoptosis in hypothalamic neurons: rescue of resistance and apoptosis through adenosine 5' monophosphate-activated protein kinase activation. *Endocrinology,* 151**,** 576-85.
MAZUMDER, P. K., O'NEILL, B. T., ROBERTS, M. W., BUCHANAN, J., YUN, U. J., COOKSEY, R. C., BOUDINA, S. & ABEL, E. D. 2004. Impaired cardiac efficiency and increased fatty acid oxidation in insulin-resistant ob/ob mouse hearts. *Diabetes,* 53**,** 2366-74.
MCLEOD, C. J., AZIZ, A., HOYT, R. F., JR., MCCOY, J. P., JR. & SACK, M. N. 2005. Uncoupling proteins 2 and 3 function in concert to augment tolerance to cardiac ischemia. *J Biol Chem,* 280**,** 33470-6.
MEDEIROS, D. M. 2008. Assessing mitochondria biogenesis. *Methods,* 46**,** 288-94.
MENDL, N., OCCHIPINTI, A., MULLER, M., WILD, P., DIKIC, I. & REICHERT, A. S. 2011. Mitophagy in yeast is independent of mitochondrial fission and requires the stress response gene WHI2. *J Cell Sci,* 124**,** 1339-50.

MERKSAMER, P. I., TRUSINA, A. & PAPA, F. R. 2008. Real-time redox measurements during endoplasmic reticulum stress reveal interlinked protein folding functions. *Cell,* 135**,** 933-47.
MERKWIRTH, C., DARGAZANLI, S., TATSUTA, T., GEIMER, S., LOWER, B., WUNDERLICH, F. T., VON KLEIST-RETZOW, J. C., WAISMAN, A., WESTERMANN, B. & LANGER, T. 2008. Prohibitins control cell proliferation and apoptosis by regulating OPA1-dependent cristae morphogenesis in mitochondria. *Genes Dev,* 22**,** 476-88.
MERKWIRTH, C. & LANGER, T. 2008. Mitofusin 2 builds a bridge between ER and mitochondria. *Cell,* 135**,** 1165-7.
MERKWIRTH, C., MARTINELLI, P., KORWITZ, A., MORBIN, M., BRONNEKE, H. S., JORDAN, S. D., RUGARLI, E. I. & LANGER, T. 2012. Loss of prohibitin membrane scaffolds impairs mitochondrial architecture and leads to tau hyperphosphorylation and neurodegeneration. *PLoS Genet,* 8**,** e1003021.
MICHALAK, M. & OPAS, M. 2009. Endoplasmic and sarcoplasmic reticulum in the heart. *Trends Cell Biol,* 19**,** 253-9.
MIHL, C., DASSEN, W. R. & KUIPERS, H. 2008. Cardiac remodelling: concentric versus eccentric hypertrophy in strength and endurance athletes. *Neth Heart J,* 16**,** 129-33.
MIKI, T., MIURA, T., HOTTA, H., TANNO, M., YANO, T., SATO, T., TERASHIMA, Y., TAKADA, A., ISHIKAWA, S. & SHIMAMOTO, K. 2009. Endoplasmic reticulum stress in diabetic hearts abolishes erythropoietin-induced myocardial protection by impairment of phospho-glycogen synthase kinase-3beta-mediated suppression of mitochondrial permeability transition. *Diabetes,* 58**,** 2863-72.
MIKI, T., YUDA, S., KOUZU, H. & MIURA, T. 2013. Diabetic cardiomyopathy: pathophysiology and clinical features. *Heart Fail Rev,* 18**,** 149-66.
MILLE-HAMARD, L., BREUNEVAL, C., ROUSSEAU, A. S., GRIMALDI, P. & BILLAT, V. L. 2015. Transcriptional modulation of mitochondria biogenesis pathway at and above critical speed in mice. *Mol Cell Biochem,* 405**,** 223-32.
MINAMINO, T. & KITAKAZE, M. 2010. ER stress in cardiovascular disease. *J Mol Cell Cardiol,* 48**,** 1105-10.
MISHRA, S., MURPHY, L. C., NYOMBA, B. L. & MURPHY, L. J. 2005. Prohibitin: a potential target for new therapeutics. *Trends Mol Med,* 11**,** 192-7.
MIZUNO, Y., HARADA, E., NAKAGAWA, H., MORIKAWA, Y., SHONO, M., KUGIMIYA, F., YOSHIMURA, M. & YASUE, H. 2017. The diabetic heart utilizes ketone bodies as an energy source. *Metabolism,* 77**,** 65-72.
MOCHIZUKI, K., FUKAYA, N., TANAKA, Y., FUCHIGAMI, M. & GODA, T. 2011. Treatment with the alpha-glucosidase inhibitor miglitol from the preonset stage in Otsuka Long-Evans Tokushima Fatty rats improves glycemic control and reduces the expression of inflammatory cytokine genes in peripheral leukocytes. *Metabolism,* 60**,** 1560-5.
MONTAIGNE, D., MARECHAL, X., COISNE, A., DEBRY, N., MODINE, T., FAYAD, G., POTELLE, C., EL ARID, J. M., MOUTON, S., SEBTI, Y., DUEZ, H., PREAU, S., REMY-JOUET, I., ZERIMECH, F., KOUSSA, M., RICHARD, V., NEVIERE, R., EDME, J. L., LEFEBVRE, P. & STAELS, B. 2014. Myocardial Contractile Dysfunction Is Associated With Impaired Mitochondrial Function and Dynamics in Type 2 Diabetic but Not in Obese Patients. *Circulation,* 130**,** 554-+.
MONTANI, J. P., CARROLL, J. F., DWYER, T. M., ANTIC, V., YANG, Z. & DULLOO, A. G. 2004. Ectopic fat storage in heart, blood vessels and kidneys in the pathogenesis of cardiovascular diseases. *Int J Obes Relat Metab Disord,* 28 Suppl 4**,** S58-65.

MOORE, A., SHINDIKAR, A., FOMISON-NURSE, I., RIU, F., MUNASINGHE, P. E., RAM, T. P., SAXENA, P., COFFEY, S., BUNTON, R. W., GALVIN, I. F., WILLIAMS, M. J., EMANUELI, C., MADEDDU, P. & KATARE, R. 2014. Rapid onset of cardiomyopathy in STZ-induced female diabetic mice involves the downregulation of pro-survival Pim-1. *Cardiovasc Diabetol,* 13**,** 68.

MORRISON, C. D., PISTELL, P. J., INGRAM, D. K., JOHNSON, W. D., LIU, Y., FERNANDEZ-KIM, S. O., WHITE, C. L., PURPERA, M. N., URANGA, R. M., BRUCE-KELLER, A. J. & KELLER, J. N. 2010. High fat diet increases hippocampal oxidative stress and cognitive impairment in aged mice: implications for decreased Nrf2 signaling. *J Neurochem,* 114**,** 1581-9.

MORTON, A. M., FURTADO, J. D., MENDIVIL, C. O. & SACKS, F. M. 2019. Dietary unsaturated fat increases HDL metabolic pathways involving apoE favorable to reverse cholesterol transport. *JCI Insight.*

MULLER, Y. D., GOLSHAYAN, D., EHIRCHIOU, D., WYSS, J. C., GIOVANNONI, L., MEIER, R., SERRE-BEINIER, V., YUNG, G. P., MOREL, P., BUHLER, L. H. & SEEBACH, J. D. 2011. Immunosuppressive Effects of Streptozotocin-Induced Diabetes Result in Absolute Lymphopenia and a Relative Increase of T Regulatory Cells. *Diabetes,* 60**,** 2331-2340.

MUNDY, A. L., HAAS, E., BHATTACHARYA, I., WIDMER, C. C., KRETZ, M., HOFMANN-LEHMANN, R., MINOTTI, R. & BARTON, M. 2007. Fat intake modifies vascular responsiveness and receptor expression of vasoconstrictors: implications for diet-induced obesity. *Cardiovasc Res,* 73**,** 368-75.

MUOIO, D. M. & NEWGARD, C. B. 2008. Mechanisms of disease:Molecular and metabolic mechanisms of insulin resistance and beta-cell failure in type 2 diabetes. *Nat Rev Mol Cell Biol,* 9**,** 193-205.

MURLEY, A. & NUNNARI, J. 2016. The Emerging Network of Mitochondria-Organelle Contacts. *Mol Cell,* 61**,** 648-653.

MURRAY, A. J., COLE, M. A., LYGATE, C. A., CARR, C. A., STUCKEY, D. J., LITTLE, S. E., NEUBAUER, S. & CLARKE, K. 2008. Increased mitochondrial uncoupling proteins, respiratory uncoupling and decreased efficiency in the chronically infarcted rat heart. *J Mol Cell Cardiol,* 44**,** 694-700.

MURRAY, A. J., PANAGIA, M., HAUTON, D., GIBBONS, G. F. & CLARKE, K. 2005. Plasma free fatty acids and peroxisome proliferator-activated receptor alpha in the control of myocardial uncoupling protein levels. *Diabetes,* 54**,** 3496-502.

NAKAO, K., MINOBE, W., RODEN, R., BRISTOW, M. R. & LEINWAND, L. A. 1997. Myosin heavy chain gene expression in human heart failure. *J Clin Invest,* 100**,** 2362-70.

NANAYAKKARA, S., PATEL, H. C. & KAYE, D. M. 2018. Hospitalisation in Patients With Heart Failure With Preserved Ejection Fraction. *Clin Med Insights Cardiol,* 12**,** 1179546817751609.

NARENDRA, D., WALKER, J. E. & YOULE, R. 2012. Mitochondrial quality control mediated by PINK1 and Parkin: links to parkinsonism. *Cold Spring Harb Perspect Biol,* 4.

NARESH, N. K., BUTCHER, J. T., LYE, R. J., CHEN, X., ISAKSON, B. E., GAN, L. M., KRAMER, C. M., ANNEX, B. H. & EPSTEIN, F. H. 2016. Cardiovascular magnetic resonance detects the progression of impaired myocardial perfusion reserve and increased left-ventricular mass in mice fed a high-fat diet. *J Cardiovasc Magn Reson,* 18**,** 53.

NGOH, G. A., PAPANICOLAOU, K. N. & WALSH, K. 2012. Loss of mitofusin 2 promotes endoplasmic reticulum stress. *J Biol Chem,* 287**,** 20321-32.

NI, T., LIN, N., HUANG, X., LU, W., SUN, Z., ZHANG, J., LIN, H., CHI, J. & GUO, H. 2020. Icariin Ameliorates Diabetic Cardiomyopathy Through Apelin/Sirt3 Signalling to Improve Mitochondrial Dysfunction. *Front Pharmacol,* 11**,** 256.

NIJTMANS, L. G., DE JONG, L., ARTAL SANZ, M., COATES, P. J., BERDEN, J. A., BACK, J. W., MUIJSERS, A. O., VAN DER SPEK, H. & GRIVELL, L. A. 2000. Prohibitins act as a membrane-bound chaperone for the stabilization of mitochondrial proteins. *EMBO J,* 19**,** 2444-51.

NILSSON, J., ERICSSON, M., JOIBARI, M. M., ANDERSON, F., CARLSSON, L., NILSSON, S. K., SJODIN, A. & BUREN, J. 2016. A low-carbohydrate high-fat diet decreases lean mass and impairs cardiac function in pair-fed female C57BL/6J mice. *Nutr Metab (Lond),* 13**,** 79.

NISHIDA, Y., RARDIN, M. J., CARRICO, C., HE, W., SAHU, A. K., GUT, P., NAJJAR, R., FITCH, M., HELLERSTEIN, M., GIBSON, B. W. & VERDIN, E. 2015. SIRT5 Regulates both Cytosolic and Mitochondrial Protein Malonylation with Glycolysis as a Major Target. *Mol Cell,* 59**,** 321-32.

NOGUEIRA-FERREIRA, R., MOREIRA-GONCALVES, D., SILVA, A. F., DUARTE, J. A., LEITE-MOREIRA, A., FERREIRA, R. & HENRIQUES-COELHO, T. 2016. Exercise preconditioning prevents MCT-induced right ventricle remodeling through the regulation of TNF superfamily cytokines. *Int J Cardiol,* 203**,** 858-66.

NOGUEIRA, P. A. S., PEREIRA, M. P., SOARES, J. J. G., FILHO, A. F. N., TANIMOTO, I. M. F., FONSECA, I. A. T., AVELAR, H. O., BOTELHO, F. V., ROEVER, L., VIEIRA, A. A. & ZANON, R. G. 2017. Physiological adaptations induced by swimming in mice fed a high fat diet. *J Exerc Rehabil,* 13**,** 284-291.

OKATSU, K., OKA, T., IGUCHI, M., IMAMURA, K., KOSAKO, H., TANI, N., KIMURA, M., GO, E., KOYANO, F., FUNAYAMA, M., SHIBA-FUKUSHIMA, K., SATO, S., SHIMIZU, H., FUKUNAGA, Y., TANIGUCHI, H., KOMATSU, M., HATTORI, N., MIHARA, K., TANAKA, K. & MATSUDA, N. 2012. PINK1 autophosphorylation upon membrane potential dissipation is essential for Parkin recruitment to damaged mitochondria. *Nat Commun,* 3**,** 1016.

OLIVEIRA, P. J., SEICA, R., COXITO, P. M., ROLO, A. P., PALMEIRA, C. M., SANTOS, M. S. & MORENO, A. J. 2003. Enhanced permeability transition explains the reduced calcium uptake in cardiac mitochondria from streptozotocin-induced diabetic rats. *FEBS Lett,* 554**,** 511-4.

ONG, S. B., KALKHORAN, S. B., HERNANDEZ-RESENDIZ, S., SAMANGOUEI, P., ONG, S. G. & HAUSENLOY, D. J. 2017. Mitochondrial-Shaping Proteins in Cardiac Health and Disease - the Long and the Short of It! *Cardiovasc Drugs Ther,* 31**,** 87-107.

ONG, S. B., SUBRAYAN, S., LIM, S. Y., YELLON, D. M., DAVIDSON, S. M. & HAUSENLOY, D. J. 2010. Inhibiting mitochondrial fission protects the heart against ischemia/reperfusion injury. *Circulation,* 121**,** 2012-22.

OSELLAME, L. D., SINGH, A. P., STROUD, D. A., PALMER, C. S., STOJANOVSKI, D., RAMACHANDRAN, R. & RYAN, M. T. 2016. Cooperative and independent roles of the Drp1 adaptors Mff, MiD49 and MiD51 in mitochondrial fission. *J Cell Sci,* 129**,** 2170-81.

OTERA, H., MIYATA, N., KUGE, O. & MIHARA, K. 2016. Drp1-dependent mitochondrial fission via MiD49/51 is essential for apoptotic cristae remodeling. *J Cell Biol,* 212**,** 531-44.

OZCAN, U., CAO, Q., YILMAZ, E., LEE, A. H., IWAKOSHI, N. N., OZDELEN, E., TUNCMAN, G., GORGUN, C., GLIMCHER, L. H. & HOTAMISLIGIL, G. S. 2004.

Endoplasmic reticulum stress links obesity, insulin action, and type 2 diabetes. *Science,* 306**,** 457-61.
PACHER, P., LIAUDET, L., SORIANO, F. G., MABLEY, J. G., SZABO, E. & SZABO, C. 2002. The role of poly(ADP-ribose) polymerase activation in the development of myocardial and endothelial dysfunction in diabetes. *Diabetes,* 51**,** 514-21.
PALIKARAS, K., LIONAKI, E. & TAVERNARAKIS, N. 2015. Coupling mitogenesis and mitophagy for longevity. *Autophagy,* 11**,** 1428-30.
PALMER, C. S., ELGASS, K. D., PARTON, R. G., OSELLAME, L. D., STOJANOVSKI, D. & RYAN, M. T. 2013. Adaptor proteins MiD49 and MiD51 can act independently of Mff and Fis1 in Drp1 recruitment and are specific for mitochondrial fission. *J Biol Chem,* 288**,** 27584-93.
PALMER, C. S., OSELLAME, L. D., LAINE, D., KOUTSOPOULOS, O. S., FRAZIER, A. E. & RYAN, M. T. 2011. MiD49 and MiD51, new components of the mitochondrial fission machinery. *EMBO Rep.*
PAPAKONSTANTINOU, E., TRIANTAFILLIDOU, D., PANAGIOTAKOS, D. B., KOUTSOVASILIS, A., SALIARIS, M., MANOLIS, A., MELIDONIS, A. & ZAMPELAS, A. 2010. A high-protein low-fat diet is more effective in improving blood pressure and triglycerides in calorie-restricted obese individuals with newly diagnosed type 2 diabetes. *Eur J Clin Nutr,* 64**,** 595-602.
PAPANICOLAOU, K. N., KHAIRALLAH, R. J., NGOH, G. A., CHIKANDO, A., LUPTAK, I., O'SHEA, K. M., RILEY, D. D., LUGUS, J. J., COLUCCI, W. S., LEDERER, W. J., STANLEY, W. C. & WALSH, K. 2011. Mitofusin-2 maintains mitochondrial structure and contributes to stress-induced permeability transition in cardiac myocytes. *Mol Cell Biol,* 31**,** 1309-28.
PARK, J., CHEN, Y., TISHKOFF, D. X., PENG, C., TAN, M., DAI, L., XIE, Z., ZHANG, Y., ZWAANS, B. M., SKINNER, M. E., LOMBARD, D. B. & ZHAO, Y. 2013. SIRT5-mediated lysine desuccinylation impacts diverse metabolic pathways. *Mol Cell,* 50**,** 919-30.
PARRA, V., VERDEJO, H. E., IGLEWSKI, M., DEL CAMPO, A., TRONCOSO, R., JONES, D., ZHU, Y., KUZMICIC, J., PENNANEN, C., LOPEZ-CRISOSTO, C., JANA, F., FERREIRA, J., NOGUERA, E., CHIONG, M., BERNLOHR, D. A., KLIP, A., HILL, J. A., ROTHERMEL, B. A., ABEL, E. D., ZORZANO, A. & LAVANDERO, S. 2014. Insulin stimulates mitochondrial fusion and function in cardiomyocytes via the Akt-mTOR-NFkappaB-Opa-1 signaling pathway. *Diabetes,* 63**,** 75-88.
PASCUAL, M., PASCUAL, D. A., SORIA, F., VICENTE, T., HERNÁNDEZ, A. M., TÉBAR, F. J. & VALDÉS, M. 2003. Effects of isolated obesity on systolic and diastolic left ventricular function.
PATTEN, D. A., WONG, J., KHACHO, M., SOUBANNIER, V., MAILLOUX, R. J., PILON-LAROSE, K., MACLAURIN, J. G., PARK, D. S., MCBRIDE, H. M., TRINKLE-MULCAHY, L., HARPER, M. E., GERMAIN, M. & SLACK, R. S. 2014. OPA1-dependent cristae modulation is essential for cellular adaptation to metabolic demand. *Embo Journal,* 33**,** 2676-2691.
PENG, C., LU, Z., XIE, Z., CHENG, Z., CHEN, Y., TAN, M., LUO, H., ZHANG, Y., HE, W., YANG, K., ZWAANS, B. M., TISHKOFF, D., HO, L., LOMBARD, D., HE, T. C., DAI, J., VERDIN, E., YE, Y. & ZHAO, Y. 2011. The first identification of lysine malonylation substrates and its regulatory enzyme. *Mol Cell Proteomics,* 10**,** M111 012658.
PENG, K., YANG, L., WANG, J., YE, F., DAN, G., ZHAO, Y., CAI, Y., CUI, Z., AO, L., LIU, J., ZOU, Z., SAI, Y. & CAO, J. 2016. The Interaction of Mitochondrial

Biogenesis and Fission/Fusion Mediated by PGC-1alpha Regulates Rotenone-Induced Dopaminergic Neurotoxicity. *Mol Neurobiol*.

PENG, W., LI, M., LI, H., TANG, K., ZHUANG, J., ZHANG, J., XIAO, J., JIANG, H., LI, D., YU, Y., SHAM, P. C., NATTEL, S. & XU, Y. 2017. Dysfunction of Myosin Light-Chain 4 (MYL4) Leads to Heritable Atrial Cardiomyopathy With Electrical, Contractile, and Structural Components: Evidence From Genetically-Engineered Rats. *J Am Heart Assoc,* 6.

PEREZ, L. J., RIOS, L., TRIVEDI, P., D'SOUZA, K., COWIE, A., NZIRORERA, C., WEBSTER, D., BRUNT, K., LEGARE, J. F., HASSAN, A., KIENESBERGER, P. C. & PULINILKUNNIL, T. 2017. Validation of optimal reference genes for quantitative real time PCR in muscle and adipose tissue for obesity and diabetes research. *Sci Rep,* 7**,** 3612.

PERRY, C. G., LALLY, J., HOLLOWAY, G. P., HEIGENHAUSER, G. J., BONEN, A. & SPRIET, L. L. 2010. Repeated transient mRNA bursts precede increases in transcriptional and mitochondrial proteins during training in human skeletal muscle. *J Physiol,* 588**,** 4795-810.

PETER, A. K., BJERKE, M. A. & LEINWAND, L. A. 2016. Biology of the cardiac myocyte in heart disease. *Mol Biol Cell,* 27**,** 2149-60.

PICATOSTE, B., RAMIREZ, E., CARO-VADILLO, A., IBORRA, C., ARES-CARRASCO, S., EGIDO, J., TUNON, J. & LORENZO, O. 2013. Sitagliptin reduces cardiac apoptosis, hypertrophy and fibrosis primarily by insulin-dependent mechanisms in experimental type-II diabetes. Potential roles of GLP-1 isoforms. *PLoS One,* 8**,** e78330.

PIEHOWSKI, P. D., PETYUK, V. A., ORTON, D. J., XIE, F., MOORE, R. J., RAMIREZ-RESTREPO, M., ENGEL, A., LIEBERMAN, A. P., ALBIN, R. L., CAMP, D. G., SMITH, R. D. & MYERS, A. J. 2013. Sources of technical variability in quantitative LC-MS proteomics: human brain tissue sample analysis. *J Proteome Res,* 12**,** 2128-37.

PINALI, C., BENNETT, H., DAVENPORT, J. B., TRAFFORD, A. W. & KITMITTO, A. 2013. Three-dimensional reconstruction of cardiac sarcoplasmic reticulum reveals a continuous network linking transverse-tubules: this organization is perturbed in heart failure. *Circ Res,* 113**,** 1219-30.

PINALI, C., BENNETT, H. J., DAVENPORT, J. B., CALDWELL, J. L., STARBORG, T., TRAFFORD, A. W. & KITMITTO, A. 2015. Three-dimensional structure of the intercalated disc reveals plicate domain and gap junction remodeling in heart failure. *Biophys J,* 108**,** 498-507.

PINALI, C. & KITMITTO, A. 2014. Serial block face scanning electron microscopy for the study of cardiac muscle ultrastructure at nanoscale resolutions. *J Mol Cell Cardiol,* 76**,** 1-11.

PISANO, A., CERBELLI, B., PERLI, E., PELULLO, M., BARGELLI, V., PREZIUSO, C., MANCINI, M., HE, L. P., BATES, M. G. D., LUCENA, J. R., DELLA MONICA, P. L., FAMILIARI, G., PETROZZA, V., NEDIANI, C., TAYLOR, R. W., D'AMATI, G. & GIORDANO, C. 2016. Impaired mitochondrial biogenesis is a common feature to myocardial hypertrophy and end-stage ischemic heart failure. *Cardiovascular Pathology,* 25**,** 103-112.

PODRINI, C., CAMBRIDGE, E. L., LELLIOTT, C. J., CARRAGHER, D. M., ESTABEL, J., GERDIN, A. K., KARP, N. A., SCUDAMORE, C. L., SANGER MOUSE GENETICS, P., RAMIREZ-SOLIS, R. & WHITE, J. K. 2013. High-fat feeding rapidly induces obesity and lipid derangements in C57BL/6N mice. *Mamm Genome,* 24**,** 240-51.

POLLETTA, L., VERNUCCI, E., CARNEVALE, I., ARCANGELI, T., ROTILI, D., PALMERIO, S., STEEGBORN, C., NOWAK, T., SCHUTKOWSKI, M., PELLEGRINI, L., SANSONE, L., VILLANOVA, L., RUNCI, A., PUCCI, B., MORGANTE, E., FINI, M., MAI, A., RUSSO, M. A. & TAFANI, M. 2015. SIRT5 regulation of ammonia-induced autophagy and mitophagy. *Autophagy,* 11**,** 253-70.

PONS, S., MARTIN, V., PORTAL, L., ZINI, R., MORIN, D., BERDEAUX, A. & GHALEH, B. 2013. Regular treadmill exercise restores cardioprotective signaling pathways in obese mice independently from improvement in associated co-morbidities. *J Mol Cell Cardiol,* 54**,** 82-9.

PROKISCH, H., SCHARFE, C., CAMP, D. G., 2ND, XIAO, W., DAVID, L., ANDREOLI, C., MONROE, M. E., MOORE, R. J., GRITSENKO, M. A., KOZANY, C., HIXSON, K. K., MOTTAZ, H. M., ZISCHKA, H., UEFFING, M., HERMAN, Z. S., DAVIS, R. W., MEITINGER, T., OEFNER, P. J., SMITH, R. D. & STEINMETZ, L. M. 2004. Integrative analysis of the mitochondrial proteome in yeast. *PLoS Biol,* 2**,** e160.

PROLA, A., NICHTOVA, Z., PIRES DA SILVA, J., PIQUEREAU, J., MONCEAUX, K., GUILBERT, A., GRESSETTE, M., VENTURA-CLAPIER, R., GARNIER, A., ZAHRADNIK, I., NOVOTOVA, M. & LEMAIRE, C. 2019. Endoplasmic reticulum stress induces cardiac dysfunction through architectural modifications and alteration of mitochondrial function in cardiomyocytes. *Cardiovasc Res,* 115**,** 328-342.

PUBLIC HEALTH ENGLAND 2015. Five million people at high risk of Type 2 diabetes.

PULINILKUNNIL, T., KIENESBERGER, P. C., NAGENDRAN, J., WALLER, T. J., YOUNG, M. E., KERSHAW, E. E., KORBUTT, G., HAEMMERLE, G., ZECHNER, R. & DYCK, J. R. 2013. Myocardial adipose triglyceride lipase overexpression protects diabetic mice from the development of lipotoxic cardiomyopathy. *Diabetes,* 62**,** 1464-77.

PURUSHOTHAM, A., SCHUG, T. T., XU, Q., SURAPUREDDI, S., GUO, X. & LI, X. 2009. Hepatocyte-specific deletion of SIRT1 alters fatty acid metabolism and results in hepatic steatosis and inflammation. *Cell Metab,* 9**,** 327-38.

QUINTENS, R., SINGH, S., LEMAIRE, K., DE BOCK, K., GRANVIK, M., SCHRAENEN, A., VROEGRIJK, I. O., COSTA, V., VAN NOTEN, P., LAMBRECHTS, D., LEHNERT, S., VAN LOMMEL, L., THORREZ, L., DE FAUDEUR, G., ROMIJN, J. A., SHELTON, J. M., SCORRANO, L., LIJNEN, H. R., VOSHOL, P. J., CARMELIET, P., MAMMEN, P. P. & SCHUIT, F. 2013. Mice deficient in the respiratory chain gene Cox6a2 are protected against high-fat diet-induced obesity and insulin resistance. *PLoS One,* 8**,** e56719.

RAO, F., DENG, C. Y., WU, S. L., XIAO, D. Z., YU, X. Y., KUANG, S. J., LIN, Q. X. & SHAN, Z. X. 2009. Involvement of Src in L-type Ca2+ channel depression induced by macrophage migration inhibitory factor in atrial myocytes. *J Mol Cell Cardiol,* 47**,** 586-94.

RARDIN, M. J., HE, W., NISHIDA, Y., NEWMAN, J. C., CARRICO, C., DANIELSON, S. R., GUO, A., GUT, P., SAHU, A. K., LI, B., UPPALA, R., FITCH, M., RIIFF, T., ZHU, L., ZHOU, J., MULHERN, D., STEVENS, R. D., ILKAYEVA, O. R., NEWGARD, C. B., JACOBSON, M. P., HELLERSTEIN, M., GOETZMAN, E. S., GIBSON, B. W. & VERDIN, E. 2013. SIRT5 regulates the mitochondrial lysine succinylome and metabolic networks. *Cell Metab,* 18**,** 920-33.

RAUH, D., FISCHER, F., GERTZ, M., LAKSHMINARASIMHAN, M., BERGBREDE, T., ALADINI, F., KAMBACH, C., BECKER, C. F., ZERWECK, J., SCHUTKOWSKI, M. & STEEGBORN, C. 2013. An acetylome peptide microarray reveals specificities and deacetylation substrates for all human sirtuin isoforms. *Nat Commun,* 4**,** 2327.

RAUT, G. K., CHAKRABARTI, M., PAMARTHY, D. & BHADRA, M. P. 2019. Glucose starvation-induced oxidative stress causes mitochondrial dysfunction and apoptosis via Prohibitin 1 upregulation in human breast cancer cells. *Free Radic Biol Med,* 145**,** 428-441.

RAZEGHI, P., YOUNG, M. E., ABBASI, S. & TAEGTMEYER, H. 2001a. Hypoxia in vivo decreases peroxisome proliferator-activated receptor alpha-regulated gene expression in rat heart. *Biochem Biophys Res Commun,* 287**,** 5-10.

RAZEGHI, P., YOUNG, M. E., ALCORN, J. L., MORAVEC, C. S., FRAZIER, O. H. & TAEGTMEYER, H. 2001b. Metabolic gene expression in fetal and failing human heart. *Circulation,* 104**,** 2923-31.

RECCHIA, F. A. & LIONETTI, V. 2007. Animal models of dilated cardiomyopathy for translational research. *Vet Res Commun,* 31 Suppl 1**,** 35-41.

REIMERS, A. K., KNAPP, G. & REIMERS, C. D. 2018. Effects of Exercise on the Resting Heart Rate: A Systematic Review and Meta-Analysis of Interventional Studies. *J Clin Med,* 7.

RESNICK, H. E., VALSANIA, P., HALTER, J. B. & LIN, X. 2000. Relation of weight gain and weight loss on subsequent diabetes risk in overweight adults. *J Epidemiol Community Health,* 54**,** 596-602.

RIGGS, A. C., BERNAL-MIZRACHI, E., OHSUGI, M., WASSON, J., FATRAI, S., WELLING, C., MURRAY, J., SCHMIDT, R. E., HERRERA, P. L. & PERMUTT, M. A. 2005. Mice conditionally lacking the Wolfram gene in pancreatic islet beta cells exhibit diabetes as a result of enhanced endoplasmic reticulum stress and apoptosis. *Diabetologia,* 48**,** 2313-21.

RIMBAUD, S., GARNIER, A. & VENTURA-CLAPIER, R. 2009. Mitochondrial biogenesis in cardiac pathophysiology. *Pharmacol Rep,* 61**,** 131-8.

RITOV, V. B., MENSHIKOVA, E. V., HE, J., FERRELL, R. E., GOODPASTER, B. H. & KELLEY, D. E. 2005. Deficiency of subsarcolemmal mitochondria in obesity and type 2 diabetes. *Diabetes,* 54**,** 8-14.

RIVA, A., TANDLER, B., LOFFREDO, F., VAZQUEZ, E. & HOPPEL, C. 2005. Structural differences in two biochemically defined populations of cardiac mitochondria. *Am J Physiol Heart Circ Physiol,* 289**,** H868-72.

RON, D. & WALTER, P. 2007. Signal integration in the endoplasmic reticulum unfolded protein response. *Nat Rev Mol Cell Biol,* 8**,** 519-29.

ROSSI, D., BARONE, V., GIACOMELLO, E., CUSIMANO, V. & SORRENTINO, V. 2008. The sarcoplasmic reticulum: an organized patchwork of specialized domains. *Traffic,* 9**,** 1044-9.

ROWLAND, A. A. & VOELTZ, G. K. 2012. Endoplasmic reticulum-mitochondria contacts: function of the junction. *Nat Rev Mol Cell Biol,* 13**,** 607-25.

RUBLER, S., DLUGASH, J., YUCEOGLU, Y. Z., KUMRAL, T., BRANWOOD, A. W. & GRISHMAN, A. 1972. New type of cardiomyopathy associated with diabetic glomerulosclerosis. *Am J Cardiol,* 30**,** 595-602.

RUIZ-MEANA, M., FERNANDEZ-SANZ, C. & GARCIA-DORADO, D. 2010. The SR-mitochondria interaction: a new player in cardiac pathophysiology. *Cardiovasc Res,* 88**,** 30-9.

SAMANT, S. A., ZHANG, H. J., HONG, Z., PILLAI, V. B., SUNDARESAN, N. R., WOLFGEHER, D., ARCHER, S. L., CHAN, D. C. & GUPTA, M. P. 2014. SIRT3 deacetylates and activates OPA1 to regulate mitochondrial dynamics during stress. *Mol Cell Biol,* 34**,** 807-19.

SANTEL, A., FRANK, S., GAUME, B., HERRIER, M., YOULE, R. J. & FULLER, M. T. 2003. Mitofusin-1 protein is a generally expressed mediator of mitochondrial fusion in mammalian cells. *Journal of Cell Science,* 116**,** 2763-2774.

SARWAR, N., GAO, P., SESHASAI, S. R., GOBIN, R., KAPTOGE, S., DI ANGELANTONIO, E., INGELSSON, E., LAWLOR, D. A., SELVIN, E., STAMPFER, M., STEHOUWER, C. D., LEWINGTON, S., PENNELLS, L., THOMPSON, A., SATTAR, N., WHITE, I. R., RAY, K. K. & DANESH, J. 2010. Diabetes mellitus, fasting blood glucose concentration, and risk of vascular disease: a collaborative meta-analysis of 102 prospective studies. *Lancet,* 375**,** 2215-22.

SASASE, T., OHTA, T., MASUYAMA, T., YOKOI, N., KAKEHASHI, A. & SHINOHARA, M. 2013. The spontaneously diabetic torii rat: an animal model of nonobese type 2 diabetes with severe diabetic complications. *J Diabetes Res,* 2013**,** 976209.

SAXTON, S. N. 2017. Effects of the sympathetic nervous system on perivascular adipose tissue in health and disease. *A thesis submitted to the University of Manchester.*

SCHENK, S., HARBER, M. P., SHRIVASTAVA, C. R., BURANT, C. F. & HOROWITZ, J. F. 2009. Improved insulin sensitivity after weight loss and exercise training is mediated by a reduction in plasma fatty acid mobilization, not enhanced oxidative capacity. *J Physiol,* 587**,** 4949-61.

SCHLICKER, C., GERTZ, M., PAPATHEODOROU, P., KACHHOLZ, B., BECKER, C. F. & STEEGBORN, C. 2008. Substrates and regulation mechanisms for the human mitochondrial sirtuins Sirt3 and Sirt5. *J Mol Biol,* 382**,** 790-801.

SCHUSTER, I., VINET, A., KARPOFF, L., STARTUN, A., JOURDAN, N., DAUZAT, M., NOTTIN, S. & PEREZ-MARTIN, A. 2012. Diastolic dysfunction and intraventricular dyssynchrony are restored by low intensity exercise training in obese men. *Obesity (Silver Spring),* 20**,** 134-40.

SCHWARZER, M., SCHREPPER, A., AMORIM, P. A., OSTERHOLT, M. & DOENST, T. 2013. Pressure overload differentially affects respiratory capacity in interfibrillar and subsarcolemmal mitochondria. *Am J Physiol Heart Circ Physiol,* 304**,** H529-37.

SEBASTIAN, D., HERNANDEZ-ALVAREZ, M. I., SEGALES, J., SORIANELLO, E., MUNOZ, J. P., SALA, D., WAGET, A., LIESA, M., PAZ, J. C., GOPALACHARYULU, P., ORESIC, M., PICH, S., BURCELIN, R., PALACIN, M. & ZORZANO, A. 2012. Mitofusin 2 (Mfn2) links mitochondrial and endoplasmic reticulum function with insulin signaling and is essential for normal glucose homeostasis. *Proc Natl Acad Sci U S A,* 109**,** 5523-8.

SEJERSTED, O. M. 2011. Calcium controls cardiac function--by all means! *J Physiol,* 589**,** 2919-20.

SENA, L. A. & CHANDEL, N. S. 2012. Physiological roles of mitochondrial reactive oxygen species. *Mol Cell,* 48**,** 158-67.

SEO, D. Y., KO, J. R., JANG, J. E., KIM, T. N., YOUM, J. B., KWAK, H. B., BAE, J. H., KIM, A. H., KO, K. S., RHEE, B. D. & HAN, J. 2019. Exercise as A Potential Therapeutic Target for Diabetic Cardiomyopathy: Insight into the Underlying Mechanisms. *Int J Mol Sci,* 20.

SHARMA, S., ADROGUE, J. V., GOLFMAN, L., URAY, I., LEMM, J., YOUKER, K., NOON, G. P., FRAZIER, O. H. & TAEGTMEYER, H. 2004. Intramyocardial lipid accumulation in the failing human heart resembles the lipotoxic rat heart. *FASEB J,* 18**,** 1692-700.

SHESHALA, R., PEH, K. K. & DARWIS, Y. 2009. Preparation, characterization, and in vivo evaluation of insulin-loaded PLA-PEG microspheres for controlled parenteral drug delivery. *Drug Dev Ind Pharm,* 35**,** 1364-74.

SIGNES, A. & FERNANDEZ-VIZARRA, E. 2018. Assembly of mammalian oxidative phosphorylation complexes I-V and supercomplexes. *Essays Biochem,* 62**,** 255-270.
SIGNORILE, A., SGARAMELLA, G., BELLOMO, F. & DE RASMO, D. 2019. Prohibitins: A Critical Role in Mitochondrial Functions and Implication in Diseases. *Cells,* 8.
SIPIDO, K. R. & MARBAN, E. 1991. L-type calcium channels, potassium channels, and novel nonspecific cation channels in a clonal muscle cell line derived from embryonic rat ventricle. *Circ Res,* 69**,** 1487-99.
SIRI-TARINO, P. W., SUN, Q., HU, F. B. & KRAUSS, R. M. 2010a. Saturated fat, carbohydrate, and cardiovascular disease1234. *Am J Clin Nutr.*
SIRI-TARINO, P. W., SUN, Q., HU, F. B. & KRAUSS, R. M. 2010b. Saturated fatty acids and risk of coronary heart disease: modulation by replacement nutrients. *Curr Atheroscler Rep,* 12**,** 384-90.
SOARES, D. D. S., PINTO, G. H., LOPES, A., CAETANO, D. S. L., NASCIMENTO, T. G., ANDRADES, M. E., CLAUSELL, N., ROHDE, L. E. P., LEITAO, S. A. T. & BIOLO, A. 2019. Cardiac hypertrophy in mice submitted to a swimming protocol: influence of training volume and intensity on myocardial renin-angiotensin system. *Am J Physiol Regul Integr Comp Physiol,* 316**,** R776-R782.
SOKOLOVA, M., SJAASTAD, I., LOUWE, M. C., ALFSNES, K., ARONSEN, J. M., ZHANG, L., HAUGSTAD, S. B., BENDIKSEN, B. A., OGAARD, J., BLIKSOEN, M., LIEN, E., BERGE, R. K., AUKRUST, P., RANHEIM, T. & YNDESTAD, A. 2019. NLRP3 Inflammasome Promotes Myocardial Remodeling During Diet-Induced Obesity. *Front Immunol,* 10**,** 1621.
SONG, M., MIHARA, K., CHEN, Y., SCORRANO, L. & DORN, G. W., 2ND 2015. Mitochondrial fission and fusion factors reciprocally orchestrate mitophagic culling in mouse hearts and cultured fibroblasts. *Cell Metab,* 21**,** 273-286.
SONG, Z., GHOCHANI, M., MCCAFFERY, J. M., FREY, T. G. & CHAN, D. C. 2009. Mitofusins and OPA1 mediate sequential steps in mitochondrial membrane fusion. *Mol Biol Cell,* 20**,** 3525-32.
SRINIVASAN, K. & RAMARAO, P. 2007. Animal models in type 2 diabetes research: an overview. *Indian J Med Res,* 125**,** 451-72.
ST-PIERRE, J., DRORI, S., ULDRY, M., SILVAGGI, J. M., RHEE, J., JAGER, S., HANDSCHIN, C., ZHENG, K., LIN, J., YANG, W., SIMON, D. K., BACHOO, R. & SPIEGELMAN, B. M. 2006. Suppression of reactive oxygen species and neurodegeneration by the PGC-1 transcriptional coactivators. *Cell,* 127**,** 397-408.
STANLEY, W. C., RECCHIA, F. A. & LOPASCHUK, G. D. 2005. Myocardial substrate metabolism in the normal and failing heart. *Physiol Rev,* 85**,** 1093-129.
STOCKER, R. & KEANEY, J. F., JR. 2004. Role of oxidative modifications in atherosclerosis. *Physiol Rev,* 84**,** 1381-478.
STRITZKE, J., MARKUS, M. R. P., DUDERSTADT, S., LIEB, W., LUCHNER, A., DOERING, A., KEIL, U., HENSE, H. W., SCHUNKERT, H. & INVESTIGATORS, M. K. 2009. The Aging Process of the Heart: Obesity Is the Main Risk Factor for Left Atrial Enlargement During Aging The MONICA/KORA (Monitoring of Trends and Determinations in Cardiovascular Disease/Cooperative Research in the Region of Augsburg) Study. *Journal of the American College of Cardiology,* 54**,** 1982-1989.
SUAREZ, J., SCOTT, B. & DILLMANN, W. H. 2008. Conditional increase in SERCA2a protein is able to reverse contractile dysfunction and abnormal calcium flux in established diabetic cardiomyopathy. *Am J Physiol Regul Integr Comp Physiol,* 295**,** R1439-45.

SUH, J. H., HEATH, S. H. & HAGEN, T. M. 2003. Two subpopulations of mitochondria in the aging rat heart display heterogenous levels of oxidative stress. *Free Radic Biol Med,* 35**,** 1064-72.

SUH, S., JEONG, I. K., KIM, M. Y., KIM, Y. S., SHIN, S., KIM, S. S. & KIM, J. H. 2011. Effects of resistance training and aerobic exercise on insulin sensitivity in overweight korean adolescents: a controlled randomized trial. *Diabetes Metab J,* 35**,** 418-26.

SULEIMAN, J. B., MOHAMED, M. & BAKAR, A. B. A. 2020. A systematic review on different models of inducing obesity in animals: Advantages and limitations. *J Adv Vet Anim Res,* 7**,** 103-114.

SUN, G. Z., LI, Y., ZHOU, X. H., GUO, X. F., ZHANG, X. G., ZHENG, L. Q., LI, Y., JIAO, Y. D. & SUN, Y. X. 2013. Association between obesity and ECG variables in children and adolescents: A cross-sectional study. *Experimental and Therapeutic Medicine,* 6**,** 1455-1462.

SUPALE, S., THOREL, F., MERKWIRTH, C., GJINOVCI, A., HERRERA, P. L., SCORRANO, L., MEDA, P., LANGER, T. & MAECHLER, P. 2013. Loss of prohibitin induces mitochondrial damages altering beta-cell function and survival and is responsible for gradual diabetes development. *Diabetes,* 62**,** 3488-99.

SUSKI, J. M., LEBIEDZINSKA, M., BONORA, M., PINTON, P., DUSZYNSKI, J. & WIECKOWSKI, M. R. 2012. Relation Between Mitochondrial Membrane Potential and ROS Formation. *Mitochondrial Bioenergetics: Methods and Protocols,* 810**,** 183-205.

SUTHERLAND, L. N., BOMHOF, M. R., CAPOZZI, L. C., BASARABA, S. A. & WRIGHT, D. C. 2009. Exercise and adrenaline increase PGC-1{alpha} mRNA expression in rat adipose tissue. *J Physiol,* 587**,** 1607-17.

SVENSSON, M., ROSVALL, P., BOZA-SERRANO, A., ANDERSSON, E., LEXELL, J. & DEIERBORG, T. 2016. Forced treadmill exercise can induce stress and increase neuronal damage in a mouse model of global cerebral ischemia. *Neurobiol Stress,* 5**,** 8-18.

SZOKODI, I., TAVI, P., FOLDES, G., VOUTILAINEN-MYLLYLA, S., ILVES, M., TOKOLA, H., PIKKARAINEN, S., PIUHOLA, J., RYSA, J., TOTH, M. & RUSKOAHO, H. 2002. Apelin, the novel endogenous ligand of the orphan receptor APJ, regulates cardiac contractility. *Circ Res,* 91**,** 434-40.

TAEGTMEYER, H. 2000. Metabolism--the lost child of cardiology. *J Am Coll Cardiol,* 36**,** 1386-8.

TAGUCHI, N., ISHIHARA, N., JOFUKU, A., OKA, T. & MIHARA, K. 2007. Mitotic phosphorylation of dynamin-related GTPase Drp1 participates in mitochondrial fission. *J Biol Chem,* 282**,** 11521-9.

TAKAHASHI, M., IKEMOTO, S. & EZAKI, O. 1999. Effect of the fat/carbohydrate ratio in the diet on obesity and oral glucose tolerance in C57BL/6J mice. *J Nutr Sci Vitaminol (Tokyo),* 45**,** 583-93.

TAN, M., PENG, C., ANDERSON, K. A., CHHOY, P., XIE, Z., DAI, L., PARK, J. S., CHEN, Y., HUANG, H., ZHANG, Y., RO, J., WAGNER, G. R., GREEN, M. F., MADSEN, A. S., SCHMIESING, J., PETERSON, B. S., XU, G., ILKAYEVA, O. R., MUEHLBAUER, M. J., BRAULKE, T., MÜHLHAUSEN, C., BACKOS, D. S., OLSEN, C. A., MCGUIRE, P. J., PLETCHER, S. D., LOMBARD, D. B., HIRSCHEY, M. D. & ZHAO, Y. 2014. Lysine Glutarylation Is a Protein Post-Translational Modification Regulated by SIRT5. *Cell Metab,* 19**,** 605-17.

TANG, L. L., TANG, X. H., LI, X., YU, H. B., XIE, Z. G., LIU, X. Y. & ZHOU, Z. G. 2014. Effect of high-fat or high-glucose diet on obesity and visceral adipose tissue in mice. *Zhongguo Yi Xue Ke Xue Yuan Xue Bao,* 36**,** 614-9.

TANG, T., MUNETA, T., JU, Y. J., NIMURA, A., MIYAZAKI, K., MASUDA, H., MOCHIZUKI, T. & SEKIYA, I. 2008. Serum keratan sulfate transiently increases in the early stage of osteoarthritis during strenuous running of rats: protective effect of intraarticular hyaluronan injection. *Arthritis Res Ther,* 10**,** R13.

THOMAS, D. M., BOUCHARD, C., CHURCH, T., SLENTZ, C., KRAUS, W. E., REDMAN, L. M., MARTIN, C. K., SILVA, A. M., VOSSEN, M., WESTERTERP, K. & HEYMSFIELD, S. B. 2012. Why do individuals not lose more weight from an exercise intervention at a defined dose? An energy balance analysis. *Obes Rev,* 13**,** 835-47.

TONDERA, D., GRANDEMANGE, S., JOURDAIN, A., KARBOWSKI, M., MATTENBERGER, Y., HERZIG, S., DA CRUZ, S., CLERC, P., RASCHKE, I., MERKWIRTH, C., EHSES, S., KRAUSE, F., CHAN, D. C., ALEXANDER, C., BAUER, C., YOULE, R., LANGER, T. & MARTINOU, J. C. 2009. SLP-2 is required for stress-induced mitochondrial hyperfusion. *EMBO J,* 28**,** 1589-600.

TONG, M., SAITO, T., ZHAI, P., OKA, S., MIZUSHIMA, W., NAKAMURA, M., IKEDA, S., SHIRAKABE, A. & SADOSHIMA, J. 2019. Mitophagy Is Essential for Maintaining Cardiac Function During High Fat Diet-Induced Diabetic Cardiomyopathy. *Circ Res,* 124**,** 1360-71.

TOYAMA, E. Q., HERZIG, S., COURCHET, J., LEWIS, T. L., JR., LOSON, O. C., HELLBERG, K., YOUNG, N. P., CHEN, H., POLLEUX, F., CHAN, D. C. & SHAW, R. J. 2016. Metabolism. AMP-activated protein kinase mediates mitochondrial fission in response to energy stress. *Science,* 351**,** 275-281.

TSUSHIMA, K., BUGGER, H., WENDE, A. R., SOTO, J., JENSON, G. A., TOR, A. R., MCGLAUFLIN, R., KENNY, H. C., ZHANG, Y., SOUVENIR, R., HU, X. X., SLOAN, C. L., PEREIRA, R. O., LIRA, V. A., SPITZER, K. W., SHARP, T. L., SHOGHI, K. I., SPARAGNA, G. C., ROG-ZIELINSKA, E. A., KOHL, P., KHALIMONCHUK, O., SCHAFFER, J. E. & ABEL, E. D. 2018. Mitochondrial Reactive Oxygen Species in Lipotoxic Hearts Induces Post-Translational Modifications of AKAP121, DRP1 and OPA1 That Promote Mitochondrial Fission. *Circ Res,* 122**,** 58-73.

TURKO, I. V. & MURAD, F. 2003. Quantitative protein profiling in heart mitochondria from diabetic rats. *J Biol Chem,* 278**,** 35844-9.

VAINSHTEIN, A., TRYON, L. D., PAULY, M. & HOOD, D. A. 2015. Role of PGC-1alpha during acute exercise-induced autophagy and mitophagy in skeletal muscle. *Am J Physiol Cell Physiol,* 308**,** C710-9.

VALERO, T. 2014. Mitochondrial biogenesis: pharmacological approaches. *Curr Pharm Des,* 20**,** 5507-9.

VARADI, A., JOHNSON-CADWELL, L. I., CIRULLI, V., YOON, Y., ALLAN, V. J. & RUTTER, G. A. 2004. Cytoplasmic dynein regulates the subcellular distribution of mitochondria by controlling the recruitment of the fission factor dynamin-related protein-1. *J Cell Sci,* 117**,** 4389-400.

VARANITA, T., SORIANO, M. E., ROMANELLO, V., ZAGLIA, T., QUINTANA-CABRERA, R., SEMENZATO, M., MENABO, R., COSTA, V., CIVILETTO, G., PESCE, P., VISCOMI, C., ZEVIANI, M., DI LISA, F., MONGILLO, M., SANDRI, M. & SCORRANO, L. 2015. The OPA1-dependent mitochondrial cristae remodeling pathway controls atrophic, apoptotic, and ischemic tissue damage. *Cell Metab,* 21**,** 834-44.

VAZQUEZ, E. J., BERTHIAUME, J. M., KAMATH, V., ACHIKE, O., BUCHANAN, E., MONTANO, M. M., CHANDLER, M. P., MIYAGI, M. & ROSCA, M. G. 2015.

Mitochondrial complex I defect and increased fatty acid oxidation enhance protein lysine acetylation in the diabetic heart. *Cardiovasc Res,* 107**,** 453-65.
VEERANKI, S., GIVVIMANI, S., KUNDU, S., METREVELI, N., PUSHPAKUMAR, S. & TYAGI, S. C. 2016. Moderate intensity exercise prevents diabetic cardiomyopathy associated contractile dysfunction through restoration of mitochondrial function and connexin 43 levels in db/db mice. *J Mol Cell Cardiol,* 92**,** 163-73.
VEGA, R. B., KONHILAS, J. P., KELLY, D. P. & LEINWAND, L. A. 2017. Molecular Mechanisms Underlying Cardiac Adaptation to Exercise. *Cell Metab,* 25**,** 1012-1026.
VETTOR, R., VALERIO, A., RAGNI, M., TREVELLIN, E., GRANZOTTO, M., OLIVIERI, M., TEDESCO, L., RUOCCO, C., FOSSATI, A., FABRIS, R., SERRA, R., CARRUBA, M. O. & NISOLI, E. 2014. Exercise training boosts eNOS-dependent mitochondrial biogenesis in mouse heart: role in adaptation of glucose metabolism. *Am J Physiol Endocrinol Metab,* 306**,** E519-28.
WALTON, J. 1979. Lead aspartate, an en bloc contrast stain particularly useful for ultrastructural enzymology. *J Histochem Cytochem,* 27**,** 1337-42.
WANAHITA, N., MESSERLI, F. H., BANGALORE, S., GAMI, A. S., SOMERS, V. K. & STEINBERG, J. S. 2008. Atrial fibrillation and obesity--results of a meta-analysis. *Am Heart J,* 155**,** 310-5.
WANG, H., BEI, Y., LU, Y., SUN, W., LIU, Q., WANG, Y., CAO, Y., CHEN, P., XIAO, J. & KONG, X. 2015a. Exercise Prevents Cardiac Injury and Improves Mitochondrial Biogenesis in Advanced Diabetic Cardiomyopathy with PGC-1alpha and Akt Activation. *Cell Physiol Biochem,* 35**,** 2159-68.
WANG, K., LIU, C. Y., ZHANG, X. J., FENG, C., ZHOU, L. Y., ZHAO, Y. & LI, P. F. 2015b. miR-361-regulated prohibitin inhibits mitochondrial fission and apoptosis and protects heart from ischemia injury. *Cell Death Differ,* 22**,** 1058-68.
WANG, Y., SHEN, L. & XU, D. 2019. Aerobic exercise reduces triglycerides by targeting apolipoprotein C3 in patients with coronary heart disease. *Clin Cardiol,* 42**,** 56-61.
WANG, Z., LI, L., ZHAO, H., PENG, S. & ZUO, Z. 2015c. Chronic high fat diet induces cardiac hypertrophy and fibrosis in mice. *Metabolism,* 64**,** 917-25.
WANG, Z. V., LI, D. L. & HILL, J. A. 2014. Heart failure and loss of metabolic control. *J Cardiovasc Pharmacol,* 63**,** 302-13.
WARKMAN, A. S., WHITMAN, S. A., MILLER, M. K., GARRIOCK, R. J., SCHWACH, C. M., GREGORIO, C. C. & KRIEG, P. A. 2012. Developmental expression and cardiac transcriptional regulation of Myh7b, a third myosin heavy chain in the vertebrate heart. *Cytoskeleton (Hoboken),* 69**,** 324-35.
WATANABE, T., SAOTOME, M., NOBUHARA, M., SAKAMOTO, A., URUSHIDA, T., KATOH, H., SATOH, H., FUNAKI, M. & HAYASHI, H. 2014. Roles of mitochondrial fragmentation and reactive oxygen species in mitochondrial dysfunction and myocardial insulin resistance. *Exp Cell Res,* 323**,** 314-25.
WATERSTON, R. H., LINDBLAD-TOH, K., BIRNEY, E., ROGERS, J., ABRIL, J. F., AGARWAL, P., AGARWALA, R., AINSCOUGH, R., ALEXANDERSSON, M., AN, P., ANTONARAKIS, S. E., ATTWOOD, J., BAERTSCH, R., BAILEY, J., BARLOW, K., BECK, S., BERRY, E., BIRREN, B., BLOOM, T., BORK, P., BOTCHERBY, M., BRAY, N., BRENT, M. R., BROWN, D. G., BROWN, S. D., BULT, C., BURTON, J., BUTLER, J., CAMPBELL, R. D., CARNINCI, P., CAWLEY, S., CHIAROMONTE, F., CHINWALLA, A. T., CHURCH, D. M., CLAMP, M., CLEE, C., COLLINS, F. S., COOK, L. L., COPLEY, R. R., COULSON, A., COURONNE, O., CUFF, J., CURWEN, V., CUTTS, T., DALY, M., DAVID, R., DAVIES, J., DELEHAUNTY, K. D., DERI, J., DERMITZAKIS, E. T., DEWEY, C., DICKENS, N. J., DIEKHANS, M., DODGE, S., DUBCHAK, I.,

DUNN, D. M., EDDY, S. R., ELNITSKI, L., EMES, R. D., ESWARA, P., EYRAS, E., FELSENFELD, A., FEWELL, G. A., FLICEK, P., FOLEY, K., FRANKEL, W. N., FULTON, L. A., FULTON, R. S., FUREY, T. S., GAGE, D., GIBBS, R. A., GLUSMAN, G., GNERRE, S., GOLDMAN, N., GOODSTADT, L., GRAFHAM, D., GRAVES, T. A., GREEN, E. D., GREGORY, S., GUIGO, R., GUYER, M., HARDISON, R. C., HAUSSLER, D., HAYASHIZAKI, Y., HILLIER, L. W., HINRICHS, A., HLAVINA, W., HOLZER, T., HSU, F., HUA, A., HUBBARD, T., HUNT, A., JACKSON, I., JAFFE, D. B., JOHNSON, L. S., JONES, M., JONES, T. A., JOY, A., KAMAL, M., KARLSSON, E. K., et al. 2002. Initial sequencing and comparative analysis of the mouse genome. *Nature,* 420**,** 520-62.

WENDE, A. R. & ABEL, E. D. 2010. Lipotoxicity in the heart. *Biochim Biophys Acta,* 1801**,** 311-9.

WESTERMANN, B. 2010. Mitochondrial fusion and fission in cell life and death. *Nat Rev Mol Cell Biol,* 11**,** 872-84.

WESTERMANN, D., VAN LINTHOUT, S., DHAYAT, S., DHAYAT, N., ESCHER, F., BUCKER-GARTNER, C., SPILLMANN, F., NOUTSIAS, M., RIAD, A., SCHULTHEISS, H. P. & TSCHOPE, C. 2007. Cardioprotective and anti-inflammatory effects of interleukin converting enzyme inhibition in experimental diabetic cardiomyopathy. *Diabetes,* 56**,** 1834-41.

WHILLIER, S. 2020. Exercise and Insulin Resistance. *Adv Exp Med Biol,* 1228**,** 137-150.

WILKINSON, J. E., BURMEISTER, L., BROOKS, S. V., CHAN, C. C., FRIEDLINE, S., HARRISON, D. E., HEJTMANCIK, J. F., NADON, N., STRONG, R., WOOD, L. K., WOODWARD, M. A. & MILLER, R. A. 2012. Rapamycin slows aging in mice. *Aging Cell,* 11**,** 675-82.

WILLIAMSON, C. L., DABKOWSKI, E. R., BASELER, W. A., CROSTON, T. L., ALWAY, S. E. & HOLLANDER, J. M. 2010. Enhanced apoptotic propensity in diabetic cardiac mitochondria: influence of subcellular spatial location. *Am J Physiol Heart Circ Physiol,* 298**,** H633-42.

WILLIS, C. R., SEAMONS, A., MAXWELL, J., TREUTING, P. M., NELSON, L., CHEN, G., PHELPS, S., SMITH, C. L., BRABB, T., IRITANI, B. M. & MAGGIO-PRICE, L. 2012. Interleukin-7 receptor blockade suppresses adaptive and innate inflammatory responses in experimental colitis. *J Inflamm (Lond),* 9**,** 39.

WITTIG, I. & SCHAGGER, H. 2008. Structural organization of mitochondrial ATP synthase. *Biochim Biophys Acta,* 1777**,** 592-8.

WORLD HEALTH ORGANIZATION 2004. OBESITY AND OVERWEIGHT.

WORLD HEALTH ORGANIZATION 2009. Mortality and burden of disease attributable to selected major risks.

WORLD HEALTH ORGANIZATION. 2014. *WHO | Obesity and overweight* [Online]. World Health Organization. Available: http://www.who.int/mediacentre/factsheets/fs311/en/ [Accessed].

WORLD HEALTH ORGANIZATION 2017. WHO | Overweight and obesity. *WHO*.

XIA, M., ZHANG, Y., JIN, K., LU, Z., ZENG, Z. & XIONG, W. 2019. Communication between mitochondria and other organelles: a brand-new perspective on mitochondria in cancer. *Cell Biosci,* 9**,** 27.

XIAO, C., CHEN, X., LI, W., LI, L., WANG, L., XIE, Q. & HAN, H. 2018. Automatic Mitochondria Segmentation for EM Data Using a 3D Supervised Convolutional Network. *Front Neuroanat,* 12**,** 92.

XIONG, W., MA, Z., AN, D., LIU, Z., CAI, W., BAI, Y., ZHAN, Q., LAI, W., ZENG, Q., REN, H. & XU, D. 2019. Mitofusin 2 Participates in Mitophagy and Mitochondrial Fusion Against Angiotensin II-Induced Cardiomyocyte Injury. *Front Physiol,* 10**,** 411.

XU, C., BAILLY-MAITRE, B. & REED, J. C. 2005. Endoplasmic reticulum stress: cell life and death decisions. *J Clin Invest,* 115**,** 2656-64.
XU, X., KOBAYASHI, S., CHEN, K., TIMM, D., VOLDEN, P., HUANG, Y., GULICK, J., YUE, Z., ROBBINS, J., EPSTEIN, P. N. & LIANG, Q. 2013. Diminished autophagy limits cardiac injury in mouse models of type 1 diabetes. *J Biol Chem,* 288**,** 18077-92.
YAMASHITA, S. I., JIN, X., FURUKAWA, K., HAMASAKI, M., NEZU, A., OTERA, H., SAIGUSA, T., YOSHIMORI, T., SAKAI, Y., MIHARA, K. & KANKI, T. 2016. Mitochondrial division occurs concurrently with autophagosome formation but independently of Drp1 during mitophagy. *J Cell Biol,* 215**,** 649-665.
YAN, W. J., ZHANG, H. F., LIU, P. L., WANG, H., LIU, J. Y., GAO, C., LIU, Y., LIAN, K., YANG, L., SUN, L., GUO, Y. P., ZHANG, L. J., DONG, L., LAU, W. B., GAO, E. H., GAO, F., XIONG, L. Z., WANG, H. C., QU, Y. & TAO, L. 2013. Impaired mitochondrial biogenesis due to dysfunctional adiponectin-AMPK-PGC-1 alpha signaling contributing to increased vulnerability in diabetic heart. *Basic Research in Cardiology,* 108.
YANG, L., ZHAO, D., REN, J. & YANG, J. 2015. Endoplasmic reticulum stress and protein quality control in diabetic cardiomyopathy. *Biochim Biophys Acta,* 1852**,** 209-18.
YANG, W., VAN DE VEN, R. A. H. & HAIGIS, M. C. 2018. Chapter 8 - Mitochondrial Sirtuins: Coordinating Stress Responses Through Regulation of Mitochondrial Enzyme Networks. *In:* GUARENTE, L., MOSTOSLAVSKY, R. & KAZANTSEV, A. (eds.) *Introductory Review on Sirtuins in Biology, Aging, and Disease.* Academic Press.
YANG, Y. & SANTAMARIA, P. 2006. Lessons on autoimmune diabetes from animal models. *Clin Sci (Lond),* 110**,** 627-39.
YATES, J. R., RUSE, C. I. & NAKORCHEVSKY, A. 2009. Proteomics by mass spectrometry: approaches, advances, and applications. *Annu Rev Biomed Eng,* 11**,** 49-79.
YE, G., METREVELI, N. S., DONTHI, R. V., XIA, S., XU, M., CARLSON, E. C. & EPSTEIN, P. N. 2004. Catalase protects cardiomyocyte function in models of type 1 and type 2 diabetes. *Diabetes,* 53**,** 1336-43.
YE, J., WANG, Y., WANG, Z., LIU, L., YANG, Z., WANG, M., XU, Y., YE, D., ZHANG, J., LIN, Y., JI, Q. & WAN, J. 2020. Roles and Mechanisms of Interleukin-12 Family Members in Cardiovascular Diseases: Opportunities and Challenges. *Front Pharmacol,* 11**,** 129.
YE, X., LI, M., HOU, T., GAO, T., ZHU, W. G. & YANG, Y. 2017. Sirtuins in glucose and lipid metabolism. *Oncotarget,* 8**,** 1845-1859.
YOO, S. Z., NO, M. H., HEO, J. W., PARK, D. H., KANG, J. H., KIM, J. H., SEO, D. Y., HAN, J., JUNG, S. J. & KWAK, H. B. 2019. Effects of Acute Exercise on Mitochondrial Function, Dynamics, and Mitophagy in Rat Cardiac and Skeletal Muscles. *Int Neurourol J,* 23**,** S22-31.
YOSHINARI, O. & IGARASHI, K. 2011. Anti-diabetic effect of pyroglutamic acid in type 2 diabetic Goto-Kakizaki rats and KK-Ay mice. *Br J Nutr,* 106**,** 995-1004.
YOULE, R. J. & NARENDRA, D. P. 2011. Mechanisms of mitophagy. *Nat Rev Mol Cell Biol,* 12**,** 9-14.
YU, J., NOVGORODOV, S. A., CHUDAKOVA, D., ZHU, H., BIELAWSKA, A., BIELAWSKI, J., OBEID, L. M., KINDY, M. S. & GUDZ, T. I. 2007. JNK3 signaling pathway activates ceramide synthase leading to mitochondrial dysfunction. *J Biol Chem,* 282**,** 25940-9.

YU, J., SADHUKHAN, S., NORIEGA, L. G., MOULLAN, N., HE, B., WEISS, R. S., LIN, H., SCHOONJANS, K. & AUWERX, J. 2013. Metabolic characterization of a Sirt5 deficient mouse model. *Sci Rep,* 3**,** 2806.

ZHANG, F., HARTNETT, S., SAMPLE, A., SCHNACK, S. & LI, Y. 2016a. High fat diet induced alterations of atrial electrical activities in mice. *Am J Cardiovasc Dis,* 6**,** 1-9.

ZHANG, M., WU, J., SUN, R., TAO, X., WANG, X., KANG, Q., WANG, H., ZHANG, L., LIU, P., ZHANG, J., XIA, Y., ZHAO, Y., YANG, Y., XIONG, Y., GUAN, K. L., ZOU, Y. & YE, D. 2019. SIRT5 deficiency suppresses mitochondrial ATP production and promotes AMPK activation in response to energy stress. *PLoS One,* 14**,** e0211796.

ZHANG, M., YU, W. Z., SHEN, X. T., XIANG, Q., XU, J., YANG, J. J., CHEN, P. P., FAN, Z. L., XIAO, J., ZHAO, Y. Z. & LU, C. T. 2016b. Advanced Interfere Treatment of Diabetic Cardiomyopathy Rats by aFGF-Loaded Heparin-Modified Microbubbles and UTMD Technique. *Cardiovasc Drugs Ther,* 30**,** 247-61.

ZHANG, P. L., LUN, M., TENG, J., HUANG, J., BLASICK, T. M., YIN, L., HERRERA, G. A. & CHEUNG, J. Y. 2004. Preinduced molecular chaperones in the endoplasmic reticulum protect cardiomyocytes from lethal injury. *Ann Clin Lab Sci,* 34**,** 449-57.

ZHANG, Y., BHARATHI, S. S., RARDIN, M. J., LU, J., MARINGER, K. V., SIMS-LUCAS, S., PROCHOWNIK, E. V., GIBSON, B. W. & GOETZMAN, E. S. 2017. Lysine desuccinylase SIRT5 binds to cardiolipin and regulates the electron transport chain. *J Biol Chem,* 292**,** 10239-10249.

ZHAO, X. Y., HU, S. J., LI, J., MOU, Y., CHEN, B. P. & XIA, Q. 2006. Decreased cardiac sarcoplasmic reticulum Ca2+ -ATPase activity contributes to cardiac dysfunction in streptozotocin-induced diabetic rats. *J Physiol Biochem,* 62**,** 1-8.

ZHENG, S. L., CHAN, F. T., NABEEBACCUS, A. A., SHAH, A. M., MCDONAGH, T., OKONKO, D. O. & AYIS, S. 2018. Drug treatment effects on outcomes in heart failure with preserved ejection fraction: a systematic review and meta-analysis. *Heart,* 104**,** 407-415.

ZHOU, Y. T., GRAYBURN, P., KARIM, A., SHIMABUKURO, M., HIGA, M., BAETENS, D., ORCI, L. & UNGER, R. H. 2000. Lipotoxic heart disease in obese rats: implications for human obesity. *Proc Natl Acad Sci U S A,* 97**,** 1784-9.